The University Of Sheffield.

Investigating a novel biological function of PGC-1[alpha]: a master transcriptional regulator implicated in neurodegeneration and ageing

By:

Simeon Rosenov Mihaylov

A thesis submitted in partial fulfilment of the requirements for the degree of Doctor of Philosophy

The University of Sheffield
Faculty of Medicine, Dentistry and Health
Department of Neuroscience
Sheffield Institute for Translational Neuroscience

September 2017

Abstract

Mitochondrial dysregulation is a pathophysiological hallmark of neurodegeneration. The transcriptional coactivator PGC-1[alpha] is a key regulator of mitochondrial biogenesis and maintenance. Its expression levels are reduced in several neurodegenerative diseases and also during physiological ageing of the brain. PGC-1[alpha] is functionally divided into three domains. The amino-terminal and central domains are involved in transcriptional activation. We set to uncover the biological role of the C-terminal region. *In silico* structure analysis revealed an Arginine/Serine-rich region flanked by a putative RNA-binding domain typical of splicing factors. We further identified structural similarities to mRNA export adaptors with putative TAP/NXF1-binding site(s).

My study shows for the first time that PGC-1[alpha] interacts with the transcription-export (TREX) complex by directly interacting with RNA and TAP/NXF1:p15 in different cell models. Overexpression of PGC-1[alpha] results in a specific block of bulk mRNA nuclear export and nuclear mRNA accumulation, a characteristic effect observed for other nuclear export adaptors. In addition, I have mapped the interacting domains of PGC-1[alpha] and TAP/NXF1. Both depletion of PGC-1[alpha] or selective RNA-binding impairment result in an inhibition of the nuclear export of some of the PGC-1[alpha]-activated target transcripts and impact mitochondrial homeostasis leading to decreased cell viability and reduced ATP levels. Moreover, failure of COX2 protein upregulation is observed under galactose condition as a mitochondrial stressor. This is in agreement with a potential inhibition of mRNA export of mitochondrial transcription factors. In addition, I created a novel cell model utilising cell reprogramming of HEK293 stable cell lines into induced neural progenitor cells. In summary, my results show a novel biological function of PGC-1[alpha] suggesting that it acts as a novel mRNA nuclear export adaptor in addition to its well-recognised roles as a master co-transcriptional regulator.

Acknowledgements

'You frequently state, and in your letter you imply, that I have developed a completely one-sided outlook and look at everything and think of everything in terms of science. Obviously my method of thought and reasoning is influenced by a scientific training – if that were not so my scientific training would have been a waste and a failure.'

- Rosalind Franklin

Table of Contents

List of Tables

List of Figures

List of Abbreviations

aa	Amino acid
AD	Alzheimer's disease
AF-2	Activation function 2 domain
Akt/PKB	Akt/Protein kinase B
ALS	Amyotrophic Lateral Sclerosis
AMPK	AMP-activated protein kinase
APP	Amyloid precursor protein
ATP	Adenosine triphosphate
ATXN2	Ataxin 2
Aβ	Amyloid beta
BAT	Brown adipose tissue
BDNF	Brain-derived neurotrophic factor
C-terminal	Carboxyl terminal
C9ORF72	Chromosome 9 open-reading frame 72 (protein)
CBP	CREB-binding protein
Ci	Control miRNA
COXII	Cytochrome *c* oxidase subunit 2
Cyt*c*	Cytochrome *c*
D1	Domain 1
DA neurons	Dopaminergic neurons

DM	Diabetes mellitus
ERα	Estrogen receptor alpha
ETC	Electron transport chain
FALS	Familial ALS
FGF-b	Fibroblast growth factor basal
FISH	Fluorescence *in situ* hybridisation
FUS	Fused in sarcoma
G6Pase	Glucose-6-Phosphatase
GLUT4	Glucose transporter type 4
GOI	Gene of interest
GR	Glucocorticoid receptor
HATs	Histone acetyl transferases
HD	Huntington's disease
HEK cells	Human embryonic kidney cells
HNF4α	Hepatocyte nuclear factor 4 alpha
Htt	Huntingtin (gene)
IDP	Intrinsically disordered protein
IL-1α	Interleukin 1
iNPC	Induced neural progenitor cells
KD	Knock-down
KO	Knock-out
LRR	Leucine-rich repeat

LRRK2	Leucine-rich repeat kinase 2
LXXLL	L-leucine X-any amino acid
mHTT	mutant Huntingtin protein
MPTP	1-methyl-4-phenyl-1,2,3,6-tetrahydropyridine
mtDNA	mitochondrial DNA
MTT	Methylthiazolyldiphenyl-tetrazolium bromide
mtTFA	Mitochondrial Transcription factor A
N-terminal	Amino terminal
NQO1	NAD(P)H dehydrogenase quinone 1
NRF-1	Nuclear respiratory factor-1
NTF2L	Nuclear transport factor 2-like
OXPHOS	Oxidative phosphorylation
p38 MAPK	p38 mitogen-activated protein kinase
PD	Parkinson's disease
PEPCK	Phosphoenylpyruvate carboxykinase
PGC-1[alpha]	Peroxisome proliferator-activated receptor gamma coactivator 1 alpha
PGCi	PGC-1[alpha] miRNA
PINK1	PTEN induced putative kinase 1
PSEN1	Presenilin 1
RBD	RNA-binding domain
ROS	Reactive oxygen species

RRM	RNA recognition motif
RXRα	Retinoid X receptor alpha
SALS	Sporadic ALS
Ser	Serine
SNpc	Substantia nigra pars compacta
SOD1	Superoxide dismutase 1
SR-region	Serine/Arginine-rich region
SRC-1	Steroid coactivator-1
SUMO1	Small ubiquitin-like modifier 1 protein
T2DM	Type 2 Diabetes
TARDP/TDP43	Transcription of RNA activating protein/TAR DNA binding protein
Tet	Tetracycline
TF	Transcription factor
Thr	Threonine
TNFα	Tumour necrosis factor α
TREX	Transcription-export
UBA	Ubiquitin-associated domain
UCP1	Uncoupling protein 1
VEGF	Vascular endothelial growth factor
WT	Wild-type
αSyn	Alpha Synuclein

1. Introduction

Both physiological ageing of the brain and neurodegenerative disorders are characterised by a significant decrease of cell metabolism and energy homeostasis. Another key feature is the great financial burden on society due to the ever-increasing life expectancy and cost of hospital care and treatment. Despite the complex pathogenesis of neurodegenerative diseases, great advances have been made in our understanding of these conditions and this research area has become one of the most exciting and most-cited in the field of biological sciences in the past 10 years (Fig. 1.1. and 1.2.). For comparison, cancer is still one of the most researched areas of biological sciences and ageing and neurodegeneration yield five times fewer articles. Nevertheless, the growth of number of research papers on ageing and neurodegeneration in the past decade has reached similar heights to cancer studies showing significant increase in interest correlating with increased appreciation amongst the scientific community.

Several of the most studied disorders in the group of neurodegenerative diseases include Huntington's disease (HD), Alzheimer's disease (AD), Amyotrophic Lateral Sclerosis (ALS), and Parkinson's disease (PD). Therefore this introduction will start by reviewing each of these diseases in addition to physiological ageing of the brain in order to draw attention to common underlying pathways of mitochondrial impairment. This will be then followed by presenting mitochondria and energy metabolism and their fundamental role in cellular homeostasis. Finally, the master mitochondrial regulator PGC-1[alpha] will be introduced detailing its known biological function(s), regulation and role in disease. In addition, a hypothesis about a novel biological role will be presented that will be experimentally confirmed in subsequent chapters.

Number of papers until 31/12/2016
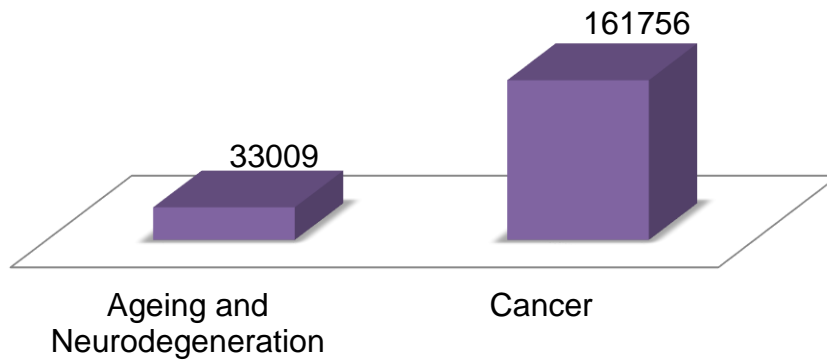
Figure 1.1 Statistical representation of number of articles until 2016.

Data were obtained from PubMed. Analysis carried out July, 2017.

Increase in articles in the past 10 years
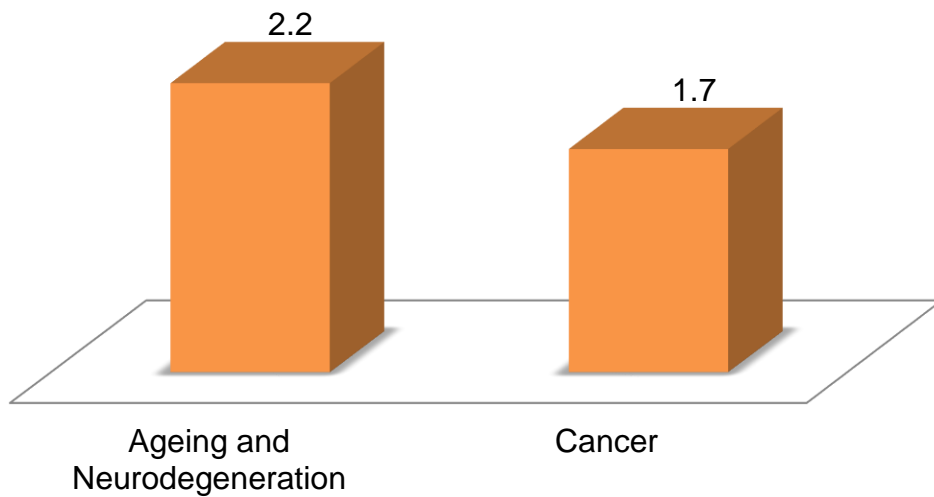
Figure 1.2 Statistical representation of increase in number of articles in the past decade.

Data were obtained from PubMed. Includes results until 31/12/2016. Analysis carried out July, 2017.

1.1. Physiological ageing of the brain and neurodegenerative diseases

1.1.1. Ageing

Ageing is a physiological process for all living organisms that is accompanied with changes in appearance, morphology, cellular homeostasis, cognition and many more (Bishop et al., 2010). A typical hallmark of normal ageing of the brain is progressive decline of cognitive ability. This is associated with structural changes of brain regions that account for diminished brain activity in relation to complex behaviour (Andrews-Hanna et al., 2007). Although there is no evidence of significant cell death of neurones during ageing, a proposed hypothesis is the loss of myelination of axons (Bishop et al., 2010). Degeneration of myelin sheets leads to less efficient neuronal signal transduction. Moreover, gene expression studies have found that levels of genes involved in synaptogenesis and synapse maintenance are decreased (Loerch et al., 2008; Lu et al., 2004). Another hallmark of ageing is genomic instability (López-Otín et al., 2013). This is caused in part by increase in toxic reactive oxygen species (ROS) leading to accumulation of nuclear (n) and/or mitochondrial (mt) DNA mutations. Examples come from studies with transgenic mice with progressive accumulation of mtDNA mutations (Kujoth et al., 2005; Trifunovic et al., 2004). mtDNA damage results in accelerated ageing and shortened lifespan.

The brain accounts for only 2% of the human body mass, however it uses 20% of all body energy required (Camandola and Mattson, 2017). Most of this energy is needed for the maintenance and correct function of neurones. Therefore, it is not surprising that neurones rely profoundly on mitochondrial respiration. Mitochondrial dysfunction is another typical feature of ageing. It has been characterised with reduced mitochondrial function correlated with decreased expression of genes involved in

energy homeostasis (Camandola and Mattson, 2017; López-Otín et al., 2013; Payne and Chinnery, 2015). Meta-analysis of proteomic studies of mitochondria during physiological ageing demonstrated reduced respiration and mitochondrial membrane potential (Ingram and Chakrabarti, 2016). In addition, expression levels of ETC complexes were reduced correlating with increase in ROS production. Finally, it has been shown that proteostasis dysregulation increases with advancement of age (Bishop et al., 2010; López-Otín et al., 2013; Löw, 2011; Martínez et al., 2017). Ageing is associated with the deposition of protein aggregates and oxidised proteins that are normally cleared. However, this process becomes impaired with age due to deregulation of ubiquitin-proteasomal pathways often resulting in cytotoxicity. These physiological changes have also been observed in neurodegenerative diseases where they are exacerbated and become pathological. Research on brain ageing and brain disorders is intricately connected and often interchangeable. Moreover, old age is a fundamental contributing factor to developing neurodegenerative disorders. Therefore, one cannot study ageing in isolation but needs to also focus on elucidating pathogenesis in conditions such as HD, AD, ALS and PD.

1.1.2. Huntington's disease (HD)

Huntington's disease is a debilitating and incurable brain disorder. It affects 4 to 10 individuals per 100,000 Caucasians. It is characterised by chorea, bradykinesia, rigidity, and gait impairment, often leading to psychiatric disorders, depression and dementia with the progression of the disease. HD typically manifests around the age of 40-50. Nevertheless, there are cases of juvenile forms of the disease albeit rare.

The key neuropathological hallmark of the disease is the progressive death of medium spiny neurones in the striatum, more specifically in the caudate and putamen (Gil and Rego, 2008; Jimenez-Sanchez et al., 2017; Reiner et al., 1988; Ross and Tabrizi,

2011). HD is a monogenic disorder inherited in an autosomal dominant manner. It is the result of a trinucleotide repeat expansion of CAG (which encodes for glutamine) in the Huntingtin gene (*Htt*). Healthy individuals carry glutamine repeats ranging up to 35, whereas repeat expansions exceeding 35 are pathological resulting in HD phenotype. Amongst its functions, wild-type HTT interacts with microtubules serving as a scaffolding protein; it acts as a transcriptional activator of brain-derived neurotrophic factor (BDNF) and other genes determining neuronal fate and has been implicated in the process of synaptogenesis (Fusco et al., 2003; Hoffner et al., 2002; McKinstry et al., 2014; Zuccato et al., 2003).

Pathological CAG expansions cause a structural dysregulation of the HTT protein leading to protein aggregation and often the formation of amyloid structures (DiFiglia, 1997; S. Li, 1998; McGowan et al., 2000). As a consequence, mutant HTT (mHTT) dysregulates key cellular pathways resulting in excitotoxicity, increase of reactive oxygen species (ROS), metabolic and mitochondrial dysfunction and transcriptional impairment (Jimenez-Sanchez et al., 2017; Ross and Tabrizi, 2011). The exact molecular mechanisms of mHTT pathogenicity remain elusive, however it has been proposed that mHTT aggregates sequester proteins bound to them such as molecular chaperones, ubiquitin and transcription factors (reviewed in Jimenez-Sanchez et al., 2017). In contrast, there is also evidence suggesting a neuroprotective nature of the aggregates (Arrasate et al., 2004).

HD differs from other neurodegenerative disorders in its genetic foundation. While HD is a monogenic disease, disorders like AD, ALS and PD are associated with several genes. Nevertheless, they frequently present with similar molecular phenotypes indicating a common pathological pathway. Therefore, studying each of these disorders would help elucidate common causes in all of them.

1.1.3. Alzheimer's disease (AD)

Alzheimer's disease is the most common neurodegenerative disease affecting 1.3% of the British population and over 2% of the world population. The age of onset is 60-65 and the disease risk increases dramatically after the age of 85.

AD manifests with memory loss and decline in cognition which results in devastating personality disturbances. These are direct consequences from the degeneration and death of neurones in areas of the brain responsible for memory and learning such as the frontal and temporal lobes. The two neuropathological hallmarks of the disease are extracellular amyloid beta (Aβ) plaques and intracellular tau tangles. They have been the primary focus of AD research for the past two decades.

Unlike Huntington's disease, Alzheimer's disease is typically a complex polygenic disorder that results from the intricate interplay between genetic and environmental risk factors. Current understanding of AD suggests that aggregation of Aβ plays a central role in the disease pathogenesis leading to neurotoxic gain of function (Bertram and Tanzi, 2012; Hardy, 2009; Kumar et al., 2015). Aβ is the product of the sequential cleavage of transmembrane amyloid precursor protein (APP) by β- and γ-secretase. According to the amyloid cascade hypothesis, Aβ species then aggregate resulting in cytotoxicity (Kumar et al., 2015). Moreover, mutations in the genes encoding for APP, and presenilin-1 and 2 (PSEN1, PSEN2; part of the γ-secretase complex) result in the rare autosomal dominant early-onset (before the age of 60) form of AD (Bertram et al., 2010; Bertram and Tanzi, 2012). This also coincides with elevated levels of aggregated Aβ. Studies from the common, sporadic form of the disease have identified risk factors such as APOEε4 (Coon et al., 2007; Holtzman et al., 2000). Nevertheless, evidence again suggests Aβ as a key player. Consequences

of its aggregation are disrupted synapses and death of neurones by stimulating excitotoxicity and increased levels of ROS as well as mitochondrial dysfunction (Kumar et al., 2015). Surprisingly, a recent study showed Aβ depositions in postmortem brain tissue of prion-infected individuals (Jaunmuktane et al., 2015). This indicated the possibility of Aβ transmission and further highlighted its pathogenicity. The exact biological role of Aβ remains elusive, however it was recently shown that Aβ impairs secretion of neuropeptides and neurotrophic factors affecting vesicle formation and processing (Plá et al., 2017).

1.1.4. Amyotrophic lateral sclerosis (ALS)

Amyotrophic lateral sclerosis is another progressive neurodegenerative disorder affecting approximately 2 people per 100,000 worldwide and typically at the age between 50 and 60.

ALS is characterised by the selective and progressive death of motor neurones in the spinal cord, brainstem and motor cortex (P. J. Shaw, 2005; Van Damme et al., 2017). The disease manifests with a range of devastating symptoms including muscle weakness and wasting. This eventually leads to progressive paralysis and respiratory failure which accounts for the most common cause of death 2-5 years from symptom onset (Rothstein, 2009; P. J. Shaw, 2005; Van Damme et al., 2017).

As with AD, ALS is a complex polygenic disorder. Only 5-10% of all cases are familial (FALS) and 90-95% are sporadic (SALS), however there is a reasonable number of evidence demonstrating common mechanisms and genes shared by FALS and SALS (Majounie et al., 2012; Saccon et al., 2013; Zarei et al., 2015). There is also increasing

evidence of the role of environmental factors such as smoking and high-intensity physical exercise in the disease pathology (reviewed in Zarei et al., 2015).

The most studied genes associated with ALS are copper-zinc superoxide dismutase (*SOD1*), TAR DNA-binding protein 43 (*TARDP; TDP-43*), fused in sarcoma (*FUS*), angiogenin (*ANG*), optineurin (*OPTN*), and *C9orf72* (chromosome 9, open reading frame 72) (Van Damme et al., 2017). Wild-type SOD1 is responsible for the conversion of ROS to hydrogen peroxide, however, its role in ALS remains unclear. Missense mutations resulting in gene silencing do not lead to ALS. However, functional studies involving pathological mutations in SOD1 indicate toxic gain of function (P. J. Shaw, 2005; Van Damme et al., 2017). TDP-43 and FUS are RNA-/DNA-binding proteins involved in RNA processing and energy homeostasis through regulation of mitochondrial gene expression (Lagier-Tourenne and Cleveland, 2009; W. Wang et al., 2013; 2016). Inclusion bodies containing aggregates of TDP-43 are present in most cases of ALS introducing the popular hypothesis of toxic protein aggregation cascade (Neumann et al., 2006). C9ORF72 was discovered only recently, in 2011 (Renton et al., 2011), and is the most common gene responsible for FALS accounting for as much as 50% in some populations such as Belgium (Cruts et al., 2013). Non-coding repeat expansion of GGGGCC in *C9orf72* is responsible for its pathogenic nature, however the exact number is less well defined. Repeats of magnitude >30 are thought to be pathogenic. Pathological *C9ORF72* repeat transcripts have also been associated with impairment of gene splicing positively correlating to disease severity and implicated in the process of autophagy (Cooper-Knock et al., 2015; Webster et al., 2016).

Research in the field of ALS thus far provides evidence for toxic gain-of-function of the genes involved in the pathology of the disease leading to impaired cellular

pathways that ultimately results in dysregulation of RNA processing, oxidative stress, excitotoxicity, mitochondrial dysfunction, and impairment of vesicle formation among others and to a lesser extent loss-of-function due to haploinsufficiency (Ling et al., 2013).

1.1.5. Parkinson's disease (PD)

Parkinson's disease is the second most common neurodegenerative disorder after Alzheimer's disease. 1-2% of the population worldwide or 1 in 500 people suffer with PD. It is a late-onset disorder manifesting in individuals at the age of 50-65. There are also rare forms of early-onset PD – under 40 years.

The symptomatology of Parkinson's disease typically encompasses movement-affected conditions such as bradykinesia, rigidity and resting tremor. However, there are also non-motor symptoms such as depression, insomnia, psychiatric disorders and in rare cases dementia. PD is a debilitating incurable disorder and available treatments target only symptoms such as tremors albeit effective only for several years before developing drug resistance.

A key feature of PD is the selective death of dopaminergic (DA) neurones in the substantia nigra pars compacta (SNpc) region of the midbrain (Ferreira and Massano, 2017; Lees et al., 2009; Poewe et al., 2017). The neuropathological hallmark of the disease is the presence of cytoplasmic inclusion bodies termed Lewy bodies. They contain aggregates of one of the main proteins associated with PD – alpha synuclein (αSyn). In addition, Lewy bodies stain also for ubiquitin.

Parkinson's disease is a progressive neurodegenerative disease, resulting from the complex cellular and molecular communication between environmental and genetic risk factors (Lees et al., 2009). As with ALS, 5-10% of all PD cases are familial and the remaining 90-95% - sporadic. Mutations in over ten genes have been reported as risk factors or disease causative (Ferreira and Massano, 2017; Poewe et al., 2017). The most studied pathogenic polymorphisms are in the genes encoding for αSyn, Leucine-rich repeat kinase 2 (LRRK2), parkin, DJ1, and PTEN-induced kinase 1 (PINK1) (Lees et al., 2009). Mutant αSyn and LRRK2 are inherited in an autosomal dominant manner, whereas parkin, DJ1 and PINK1 in an autosomal recessive fashion resulting in early-onset PD.

Understanding the genetic cause and mechanism of pathogenesis in familial cases will help elucidate key players in the sporadic forms of PD. Both, inherited and idiopathic PDs, share common pathogenic pathways such as toxic protein aggregation, autophagy-lysosomal dysfunction, mitochondrial impairments and increased oxidative stress.

Similarly to AD, protein depositions of aggregated αSyn in the substantia nigra of PD patients have been associated with cytotoxicity leading to dysregulation in proteostasis via impairments in lysosomal/chaperone-dependent autophagy pathways (Alvarez-Erviti et al., 2010; Anglade et al., 1997; Chu et al., 2009; Marin and Aguilar, 2011; Steele et al., 2013). The biological role of αSyn is largely unclear, however, there is evidence suggesting function in neuronal signalling via vesicle formation, release and docking (B.-K. Choi et al., 2013; Eguchi et al., 2017; Gaugler et al., 2012; Lou et al., 2017). It is apparent that any disturbances of αSyn would affect neuronal homeostasis often leading to impaired brain circuits, apoptosis and even motor dysfunction. However, the exact mechanism of action of most genes implicated

in PD is somewhat elusive. LRKK2-associated pathologies are often accompanied by neuroinflammation that has been observed to be the cause or consequence of synucleopathies in patients and cell models (Botta-Orfila et al., 2012; Brockmann et al., 2016; Volpicelli-Daley et al., 2016). Most importantly, central stage in the pathomechanisms of PD is taken by mitochondrial dysfunction. Dysregulation of energy homeostasis is a characteristic feature of PD. Impairments in mitochondrial biogenesis and maintenance have been a primary focus of research in the past decade. In addition, the crosstalk between PINK1 and parkin in the context of mitochondrial clearance has been implicated as an important contributor to disease progression (Lazarou et al., 2012; Pickrell and Youle, 2015). Moreover, mutations in DJ-1 lead to increase in oxidative stress (Di Nottia et al., 2017; Guzman et al., 2010). This could be explained by the fact that DJ-1 is a putative antioxidant and dysregulation in the pathway leads to oxidative damage and ultimately neuronal degeneration.

It is apparent that mitochondrial dysfunction is a common theme in physiological ageing and neurodegenerative diseases. Expanding our knowledge of the control of mitochondrial maintenance and the molecular mechanisms by which it is dysregulated would help uncover shared or novel pathways between the diseases and tailor better treatments. Nevertheless, to understand how mitochondrial impairments might arise, one needs to know how the organelle functions and appreciate its importance in the context of cellular homeostasis.

1.2. Mitochondrial homeostasis and dysfunction

Mitochondria are essential membrane-bound cellular organelles often referred to as the 'powerhouse' of cells. They are thought to have originated from prokaryotic endosymbionts in a eukaryotic cell and carry typical characteristics of bacteria such as two membranes and a circular genome (Nunnari and Suomalainen, 2012). Mitochondria house the electron transport chain (ETC) and ATP synthase machinery responsible for the process of cellular respiration. Their indispensable function in fatty acid oxidation, oxidative phosphorylation (OXPHOS) and ATP synthesis, lipid synthesis, Ca^{2+} storage, and stress responses ensures adequate cellular homeostasis.

Most eukaryotic cells, in particular neurones, are largely dependent on mitochondria to maintain energy homeostasis through the use of ATP (Ballard and Whitlock, 2004; Engl and Attwell, 2015; Nicholls and Budd, 2000). Consequently, there is an elaborate process of mitochondrial cycle in place. It includes biogenesis, maintenance and recycling as a countermeasure against mitochondrial dysregulation leading to apoptosis (Fig. 1.1.). The biogenesis of mitochondria is dependent on the discreet crosstalk between the nuclear and mitochondrial genomes (Attardi and Schatz, 1988). This is due to the fact that mitochondria possess over a thousand proteins, however their genome only encodes for 13. Nuclear respiratory factors comprise a general axis of mitochondrial biogenesis. Nuclear respiratory factor 1 and 2 (NRF-1, NRF-2) are nuclear-encoded transcription factors. They stimulate the expression of another nuclear gene, mitochondrial transcription factor A (mtTFA) (Medeiros, 2008). mtTFA is translocated to the mitochondrion and plays a key role in transcription and replication of mtDNA. In addition, there are other nuclear signalling axes resulting in mtDNA replication and biogenesis. These include nuclear hormone receptors,

transcription factors, co-transcriptional activators and sirtuins (Dominy and Puigserver, 2013). The organelle biogenesis is tightly linked to its DNA replication leading to division called fission.

The maintenance of mitochondria is accomplished by highly specialised control mechanisms. Mitochondrial molecular chaperones are a class of proteins responsible for the correct protein folding preventing the generation of toxic protein oligomers or misfolding resulting in aberrant functions (Dominy and Puigserver, 2013; Tatsuta and Langer, 2008). However, in the event of high protein misfolding, the proteasome cascade is activated during which proteins are degraded by enzymes such as ClpP-1 (Baker and Haynes, 2011; Haynes et al., 2007). This also results in retrograde mitochondrial signalling, where a transcription factor is activated and translocated to the nucleus resulting in increased expression of molecular chaperones such as mitochondrial heat-shock protein 70 (HSP70) (Haynes et al., 2010).

Another mechanism of circumventing mitochondrial dysfunction is their ability to fuse together with 'healthy-functioning' mitochondria creating highly-metabolic interconnected networks (Dominy and Puigserver, 2013; Tatsuta and Langer, 2008). Nevertheless, this quality-control surveillance can be evaded resulting in dysregulation and activation of the programmed cell death (apoptotic) cascade. In addition, cell loss could be detrimental for the specific tissue or ultimately for the whole organism by disrupting cellular networks in a non-autonomous manner. To prevent it, cells have evolved another level of quality-control which involves the fragmentation of affected mitochondria and their destruction by a specific type of autophagy termed mitophagy (Dominy and Puigserver, 2013; Kubli and Gustafsson, 2012). Mitophagy is mediated by the interplay of PINK1 and the E3 ubiquitin ligase parkin. They accumulate at damaged mitochondria and through ubiquitin-labelling activate the

degradation cascade resulting in clearance of mitochondria (Dominy and Puigserver, 2013). More recently, a novel complex has been implicated in the process of mitophagy. It is independent of parkin and involves the crosstalk between PINK1, synphilin-1 and SIAH-1 (Szargel et al., 2016). This is an alternative mechanism of mitophagy that might be utilised in diseases such as Parkinson's with mutated, inactive parkin. Finally, particularly in neurones, mitochondria are required for synaptic vesicle formation and neurotransmitter release, a process with high-energy demands. Mitochondrial trafficking along microtubules is an integral part of this event ensuring efficient and localised energy supply (Sheng, 2014).

The electron transport chain resides in the inner mitochondrial membrane (IMM). It is composed of four complexes (I, II, III, and IV) that are involved in the transport of electrons from donors such as NADH and FADH to acceptors – O_2 (Fig.1.3.). Along with this process of transport, complexes pump out protons (H^+) into the inter-membrane space (IMS), creating an electrochemical proton gradient. This gradient has an essential role in fueling the ATP synthase (complex V) that converts ADP to ATP. Apart from its main role in energy supply, the ETC is also a site of reactive oxygen species (ROS) production that increases upon inhibition of the complexes (Mortiboys et al., 2007). ROS lead to oxidative stress that could be deleterious for the cell by damaging the mitochondrial DNA. However, cells seem to be able to cope with such difficulties due to the redundancy of their mitochondrial genome and/or their mtDNA repair mechanisms, believed to be absent until recently (Alexeyev et al., 2013; Wisnovsky et al., 2016).

This, in short, is how mitochondria function to provide energy required for the maintenance of cellular homeostasis. However, impairment in any of the stages mentioned above could lead to mitochondrial dysfunction – mutations of nuclear-

encoded and mitochondrial-encoded proteins, dysregulation of genes and proteins important for the mitochondrial DNA replication and transcription, inhibition of ETC complexes and increased oxidative stress (Kwong et al., 2006). All of these pathogenic pathways have been reported in physiological ageing of the brain and neurodegeneration (Grimm and Eckert, 2017).
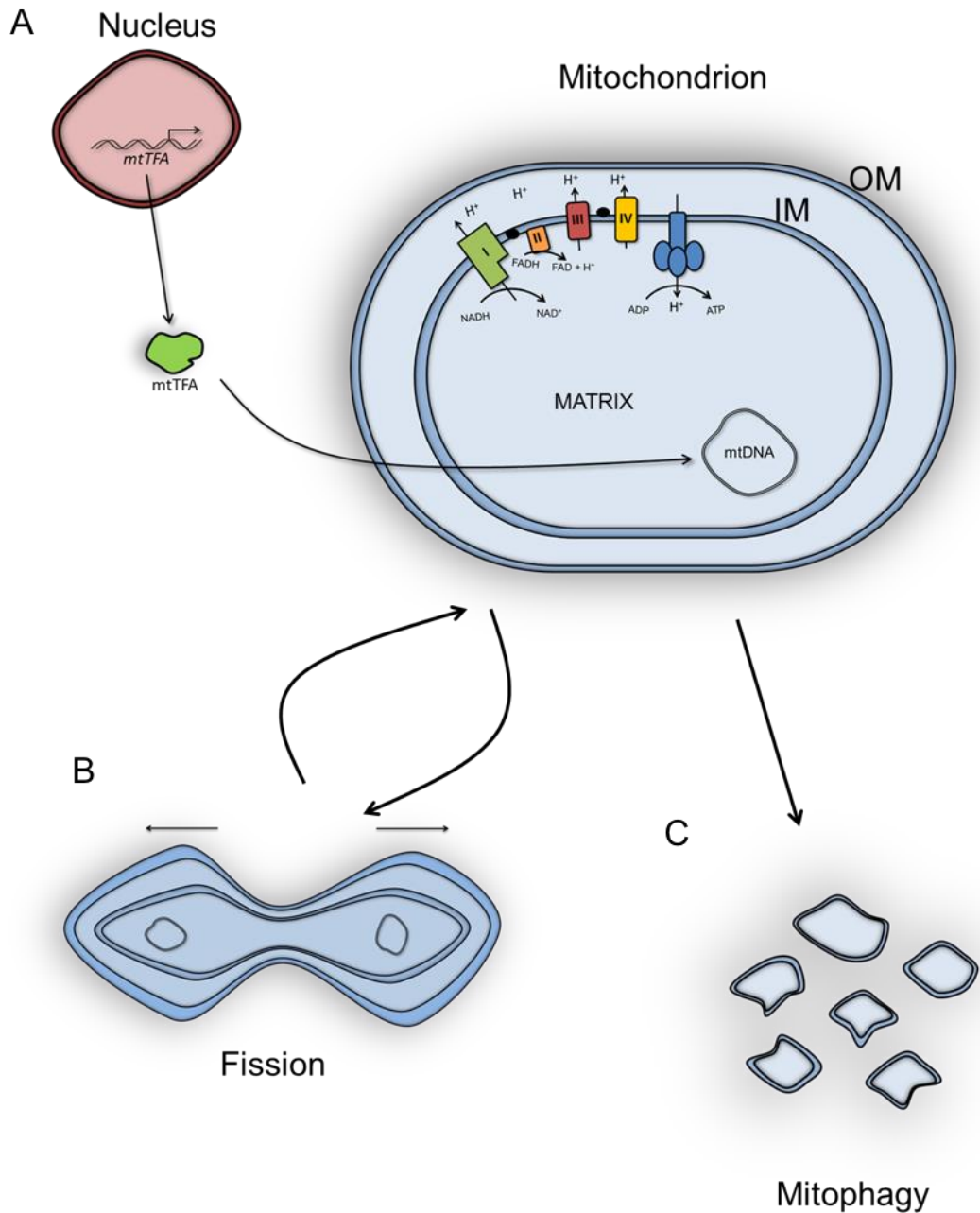
Figure 1.3 Mitochondrial cycle.

A) *mtTFA* is transcribed in the nucleus and translated in the cytoplasm. mtTFA stimulates the transcription of mitochondrial genes. Some of these genes code for proteins part of the complexes in the electron transport chain – Complex I (green), II (orange), III (red), IV (yellow). The ETC uses NADH (Complex I) or FADH (Complex II) as a source of electrons transferring them across the chain. This electron transport is coupled to the release of protons (H^+) creating an electrochemical gradient across the IM. Subsequently, this gradient fuels the ATP synthase (blue) and results in the formation of ATP. **B)** Mitochondria grow in number through the process of fission. mtDNA is replicated and the membranes separate in two, pulled in opposite directions. This is how mitochondria meet high cellular demands for energy. **C)** mtDNA polymorphisms or altered transcription/expression, ETC dysregulation, and fission impairments lead ultimately to mitochondrial dysfunction. Mitochondrial dysfunction poses danger of cell death. A specialised pathway of mitochondrial autophagy called mitophagy degrades mitochondria preventing them from inducing apoptosis. **IM** – inner membrane; **OM** – outer membrane.

16

As aforementioned, mitochondrial dysfunction is characteristic for brain ageing, AD, HD, ALS and PD. Ageing of the brain has long been associated with mitochondrial dysregulation (reviewed in Grimm and Eckert, 2017). Post-mortem and *in vivo* studies of aged individuals showed increase in oxidative insults and decrease the activity of antioxidant enzymes such as SOD and glutathione reductase (Mandal et al., 2012; Peskind et al., 2014; Venkateshappa et al., 2012). This is also accompanied by significant decrease of complex I activity. There is also increasing evidence for accumulation of mtDNA mutations during ageing (Bender et al., 2006; Kennedy et al., 2013; Kraytsberg et al., 2006). Some of these mutations specifically lead to decrease of mitochondrial respiration. In addition, mitophagy seems to decline with increase of age making neurones more prone to damage due to inability to clear impaired mitochondria (Diot et al., 2015). Morphological changes in mitochondria, decreased activity of complexes I and IV, and increase in ROS, along with impairment of axonal transport of mitochondria are some of the mitochondria-related molecular hallmarks observed in AD (Kwong et al., 2006; Morais and De Strooper, 2010; Moreira et al., 2010). Decrease in transcript levels of genes encoding for subunits of complex I and cytochrome c oxidase have been reported in post-mortem samples of AD human brain (Aksenov et al., 1999). This correlates with studies demonstrating significantly decreased activity of cytochrome *c* oxidase in patient platelets and brain compared to healthy elderly individuals (Mancuso et al., 2003; Mutisya et al., 1994; Valla et al., 2006; Verwer et al., 2000). This indicates the consequences of AD as opposed to typical differences observed during normal ageing. In addition, several studies in post-mortem AD brain or cell models have reported dysregulation of fusion/fission balance, where a downregulation of fusion genes was observed coinciding with upregulation of fission genes, decreased ATP levels and impaired mitochondrial transport (Calkins et al., 2011; Ju Gao et al., 2017; Hroudová et al., 2014; X. Wang et al., 2008). Similarly, patient samples, transgenic mice and cell models of HD show diminished activity of complex I of the ETC which correlates with increase in ROS and decrease

in ATP production (Kwong et al., 2006; Moreira et al., 2010). Decrease in complex II and III activity, impaired fusion/fission balance and reduced mitochondrial membrane potential in HD has also been reported (Cherubini and Ginés, 2017; Guedes-Dias et al., 2016; Liot et al., 2017). Degeneration of mitochondria due to impairment of ETC and increase of oxidative stress are also present in ALS (Kwong et al., 2006). Moreover, animal models carrying mutant SOD1 result in inhibition of complexes II and IV (Moreira et al., 2010). Reduced activity of all four complexes of the ETC has also been observed in spinal cord of patients. Recent evidence demonstrates the negative impact of mutant TDP-43 on mitochondrial dynamics and mtDNA transcription resulting in ETC impairments (W. Wang et al., 2016; 2013). In addition, dysregulation of mitochondrial respiration and axonal transport, among others, are part of the pathology of ALS (reviewed in E. F. Smith et al., 2017). Nevertheless, the exact temporal and overall implication of mitochondrial dysfunction in the pathogenesis of these neurodegenerative disorders is still elusive. It cannot simply be determined whether the observed mitochondrial dysfunction is a cause or consequence of primary, upstream disease-causing mechanisms (Kwong et al., 2006; Morais and De Strooper, 2010).

One of the best evidence-supported examples of a neurodegenerative disease where mitochondrial dysfunction has a central and direct role in the pathogenesis is Parkinson's disease (Ganguly et al., 2017; Morais and De Strooper, 2010). The first evidence for mitochondrial involvement in PD came from the discovery that 1-methyl-4-phenyl-1,2,3,6-tetrahydropyridine (MPTP) causes severe parkinsonism in humans (Giannoccaro et al., 2017; Langston et al., 1983; Santos and Cardoso, 2012). MPTP is a potent and specific inhibitor of complex I of the ETC. Furthermore, early studies involving sporadic PD patients have shown a decrease in complexes I and IV activity in post-mortem brain samples of the substantia nigra or blood cells (Benecke et al.,

1993; Giannoccaro et al., 2017; Santos and Cardoso, 2012; Schapira et al., 1990). Further evidence for the role of mitochondria in sporadic PD comes from mouse studies involving knock-out (KO) of mtTFA in dopaminergic neurones. Mitochondrial TFA is a key TF responsible for the transcription and replication of mtDNA and its deficiency results in cytoplasmic protein inclusions accompanied by movement dysregulation and selective death of DA neurones (Ekstrand et al., 2007).

Research on familial cases also supports an important role of mitochondrial dysfunction in PD. Parkin is a putative E3 ubiquitin ligase involved in protein quality-control or more specifically in the targeting of disrupted mitochondria for degradation by mitophagy (Santos and Cardoso, 2012). Mutations in the *parkin* gene lead to early-onset PD and mice lacking parkin show impaired function of complexes I and IV (Palacino et al., 2004). complex I dysregulation is also recapitulated in parkin-KD zebrafish (*Danio rerio)* models of PD and patient fibroblasts carrying mutations in this gene (Flinn et al., 2009; Mortiboys et al., 2008). Patient fibroblasts also demonstrate altered mitochondrial morphology, diminished membrane potential and reduced ATP production as a direct result of complex I impairment. Other studies account impairments of mitochondrial respiration to the increase of mutations in mtDNA and imbalance of mtDNA homeostasis (Bender et al., 2006; Dölle et al., 2016). These mutations were shown to affect complexes of the ETC.

PINK1 and αSyn have also been seen to associate with mitochondria. Mutations in either gene lead to changes in mitochondrial morphology and dysregulation of the ETC ultimately resulting in increased oxidative stress (Santos and Cardoso, 2012; Schapira, 2008). Loss of DJ-1 and aggregation of αSyn results in complex I activity deficiency, reduced ATP levels and reduced mitochondrial membrane potential (Devi et al., 2008; Heo et al., 2012; Reeve et al., 2015).

Another PD-related protein found in mitochondria is LRRK2. Mutations in the gene result in early-onset familial PD, as well as late-onset sporadic PD. Moreover, G2019S is of particular interest as it is the most common cause of PD (inherited and idiopathic). Recent studies on the involvement of LRRK2 in the pathophysiology of PD confirmed its importance in mitochondrial homeostasis (Mortiboys et al., 2010). Fibroblasts from patients carrying the pathologic mutation have diminished ATP production correlating with reduced ETC activity. Another interesting fact is the increase in mitochondrial fusion, which, as mentioned above, might be a survival event employing quality-control machinery from several mitochondria together. Other studies of mutant LRRK2 patient-derived fibroblasts and cell models demonstrate decreased mitochondrial membrane potential correlating with increased proton uncoupling and reduction in ATP production (Papkovskaia et al., 2012).

It is clear that mitochondria are essential and do play a key role in physiological ageing of the brain and in the pathogenesis of neurodegenerative diseases. However, current knowledge in the field is not able to answer key questions about the exact role of mitochondria in disease causation and progression and most molecular mechanisms remain largely unclear. The ever-growing appreciation of the importance of mitochondrial homeostasis has pushed research forward in the past decade. Greater understanding of mitochondrial biogenesis, maintenance and regulation would lead to the elucidation of novel pathways. This, in turn, would vastly improve current therapies and create new, more efficient and targeted approaches to tackling neurodegeneration.

Such promise holds the field of PGC-1[alpha] albeit neglected in the context of ageing and neurodegeneration. Peroxisome proliferator-activated receptor gamma, coactivator 1 alpha is a master regulator of mitochondrial biogenesis and

20

maintenance. Uncovering its elaborate biological function would lead to more detailed insight of mitochondrial homeostasis and dysfunction. The rest of this chapter will summarise our current knowledge about PGC-1[alpha] focusing on its structure, tissue-specific function and clinical relevance. In addition, a novel biological function of the protein will be proposed and the background to it reviewed.
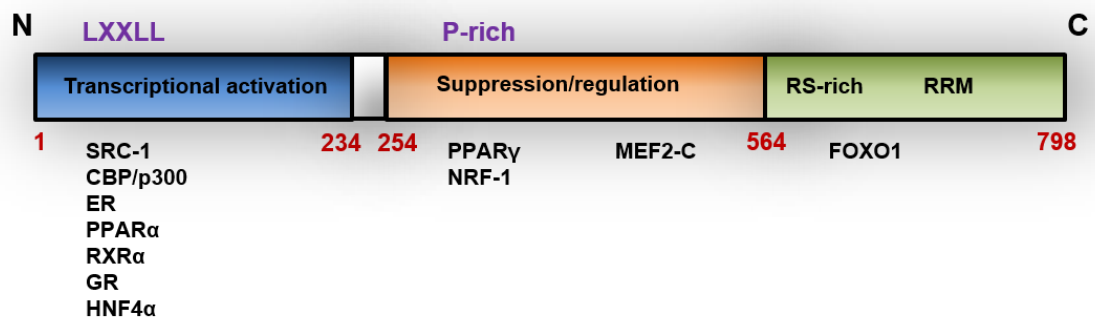
Figure 1.4 Schematic representation of the structure of PGC-1[alpha].
PGC-1[alpha] is schematically divided into three functional domains – N-terminal transcriptional activation domain (blue); Middle suppression domain (orange); and C-terminal domain (green) containing RNA-recognition motif (RRM) and a region rich in Arginine and Serine. Transcriptional (co)factors termed nuclear receptor factors (NRFs) are under the domain with which they interact. The C-terminal of most of the TFs interacting with the activation domain of PGC-1[alpha] bind a conserved consensus LXXLL sequence (L – lysine; X – any amino acid). The interactions between NRFs and the middle domain are not LXXLL-dependent but a Proline rich region in this domain seems to be involved in this binding. Lastly, the details of the binding to the C-terminal domain are unclear.

1.3. Peroxisome proliferator-activated receptor gamma, coactivator 1 alpha (PGC-1[alpha])

1.3.1. Structure and regulation of PGC-1[alpha]

The human gene encoding for PGC-1[alpha] is located on chromosome 4. It is a 798-amino-acid-long multidomain protein with a distinct structure of three different

functional domains – N-terminal, middle, and C-terminal domains respectively (Fig.1.4.).

1.3.1.1. N-terminal activation domain

The most prominent and typical characteristic of all nuclear receptor (NR) coactivators is a consensus amino acid sequence LXXLL (L-leucine, X-any amino acid) (Heery et al., 1997). Likewise, PGC-1[alpha] has an N-terminal class III LXXLL NR box consisting of three motifs (L1, L2 and L3) that interact with the C-terminal AF-2 (activation function 2 domain) of various nuclear receptors in a ligand-dependent manner (Puigserver et al., 1998; Savkur and Burris, 2004). Such transcription factors that bind PGC-1[alpha] include estrogen receptor alpha (ERα), steroid coactivator 1 (SRC-1), PPARα, retinoid X receptor alpha (RXRα), and glucocorticoid receptor (GR). Interestingly, the NR box of PGC-1[alpha] interacts with the AF-2 domain of hepatocyte nuclear factor 4 alpha (HNF4α) and results in its activation but does not require ligand binding to AF-2 (Puigserver, 2003). Moreover, the interaction is strengthened by the presence of all three LXXLL motifs (Rha et al., 2009). The mechanism of this interaction remains unclear. Contrary to that, several studies have shown that interaction with nuclear receptors requires only one LXXLL motif, predominantly L2 or L3 (Takacs et al., 2013).

Structurally, DNA is densely packed around histones resulting in the formation of supercoiled chromosomes that form heterochromatin. This spatial and structural conformation prevents genes from being transcribed and subsequently expressed. Therefore, there is an elaborate mechanism in place that unwinds DNA molecules. A special class of enzymes, referred to as histone acetyl transferases (HATs), acetylates the histones leading to DNA relaxation that provides access to TFs and

RNA polymerases. Unlike other nuclear receptor coactivators that have HAT activity located in their N-termini, PGC-1[alpha] lacks such intrinsic enzymatic capacity (Puigserver, 2003). Nevertheless, via its amino-terminal, PGC-1[alpha] is able to recruit proteins that are capable of histone acetylation such as SRC-1 and CREB-binding protein/p300 (CBP/p300).

The activation domain of PGC-1[alpha] gets its name due to the interaction with various transcription factors leading to their subsequent activation. This interaction results in the expression of specific target genes involved in processes such as gluconeogenesis. However, the actual mechanism of gene activation is somewhat elusive. There is supporting evidence from protein fusion studies that PGC-1[alpha] is capable of driving transcription initiation itself when directed to a gene promoter (Puigserver et al., 1998). This raises questions about the role of all PGC-1[alpha] TF partners, whether they are central for the process or they only provide specificity by directing the coactivator to the right gene promoter. Nevertheless, it is noteworthy that subsequent studies show that PGC-1[alpha] has only a low transcriptional activity that is greatly enhanced upon binding of nuclear receptors (Puigserver et al., 1999).

1.3.1.2. Middle repression/regulatory domain

The middle domain of PGC-1[alpha] encompasses the region between amino acids 254 and 564. It was characterised as a repression domain based upon fragment deletion studies showing that full-length PGC-1[alpha] has a diminished transcriptional activity compared to a form of the coactivator that lacks the middle region. Moreover, PGC-1[alpha]'s activity is vastly enhanced when bound to nuclear factors such as SRC-1 and CBP/p300 (as mentioned above). However, this interaction is regulated and mediated by binding of other TFs. PPARγ and NRF-1

(nuclear receptor factor 1) are involved in brown fat differentiation and mitochondrial biogenesis, respectively. Both nuclear receptors bind the middle domain of PGC-1[alpha] triggering a conformational change which results in the recruitment of SRC-1 and CBP/p300 (Puigserver et al., 1999). The crosstalk between TFs and coactivators presents an elaborate regulatory system that ensures efficient transcription initiation and docking at specific gene promoters.

Interestingly, the interaction with PPARγ and NRF-1 is ligand-independent (Puigserver, 2003). Furthermore, unlike other conventional coactivators that use the NR box to bind the AF-2 of TFs, here LXXLL is not required. Instead, a region rich in prolines binds the central hinge of both nuclear receptors (Fig.1.4.). This indicates that PGC-1[alpha] can orchestrate a variety of interactions with different proteins using alternative non-LXXLL regions.

1.3.1.3. C-terminal domain

Despite the great effort in determining the precise biological mechanisms of PGC-1[alpha], there is sparse understanding of the molecular functions of the carboxyl-terminal. Most of the research on PGC-1[alpha] has been concentrated on the first two domains leaving the C-terminus as the least studied region. Nonetheless, primary-structure prediction analysis reveals the presence of an RNA-recognition motif (RRM) and a region rich in arginines and serines (RS-region) (Puigserver et al., 1998). This indicates a putative interaction of PGC-1[alpha] with RNA molecules through its RRM. What is more intriguing is that PGC-1[alpha] has been found to be present in a complex together with RNA polymerase II (Charos et al., 2012; Monsalve et al., 2000; Puigserver, 2003). Moreover, this protein assembly is mediated by the presence of both RRM and RS-region in the C-terminus of the coactivator.

These characteristic motifs are often associated with proteins exhibiting splicing activity (Godin and Varani, 2007). Indeed, supporting evidence comes from studies showing that PGC-1[alpha] interacts with other splicing factors such as SC-35, and SRp75 (Monsalve et al., 2000; Puigserver, 2003).

Furthermore, PGC-1[alpha] plays a role in the RNA-processing of only those mRNA transcripts that are encoded by genes regulated by the coactivator. RNA-processing is critical for the correct gene expression and any dysregulation could lead to disease states (Walsh et al., 2015). However, screens for the exact mRNA targets of PGC-1[alpha], have not been conducted to date. Such information is essential and urgent and promises to elucidate new processes or molecular pathways in which PGC-1[alpha] might be central. This will lead to greater understanding of disease and improved therapeutics and treatments.

The C-terminal domain also binds to the N-terminus of FOXO1 transcription factor leading to its activation. FOXO1, in turn, stimulates the process of gluconeogenesis in liver (Puigserver et al., 2003).

1.3.1.4. Post-translational modifications

Unlike in many other diseases (ALS, HD, etc.), there are no known pathological mutations found in PGC-1[alpha] to date that lead to dramatic dysregulation of molecular pathways and contribute to the final state of a disease. Nevertheless, a polymorphism in PGC-1[alpha] (Gly482Ser) is associated with endurance ability during exercise, moderate susceptibility to type 2 diabetes and obesity, as well as

hypertension (Ahmetov et al., 2009; Fanelli et al., 2005; Gineviciene et al., 2016; Jemaa et al., 2015; Muller et al., 2003; Rojek et al., 2014). Of note, PGC-1[alpha]'s function is typically regulated at the expression level and by post-translational modifications. There is a growing body of evidence demonstrating epigenetic regulation of PGC-1[alpha]. Promoter methylation has been associated with mitochondrial homeostasis and diseases such as PD (Barrès et al., 2009; Su et al., 2015). More recently, an emerging field of research has concentrated on discovering new isoforms of PGC-1[alpha]. To date, there are 10 isoforms reported that arise from alternative splicing and the use of alternative promoters. Transcriptional activation from these promoters appears to be tissue-specific impacting on the structure and function of PGC-1[alpha]. There is an increasing appreciation of the different isoforms of PGC-1[alpha], however our understanding is still somewhat elusive. This doctoral work was solely focused on the full-length form of PGC-1[alpha], therefore it is beyond the scope of this section to review all isoforms in detail. However, it is worth noting that Martinez-Redondo *et al.* have produced the first and only comprehensive review detailing the reported isoforms of PGC-1[alpha] (Martínez-Redondo et al., 2015). They exclusively highlight the urgency of unified nomenclature in reporting novel isoforms of PGC-1[alpha] that has been an undeniable burden in the field.

On the other hand, post-translational modifications of PGC-1[alpha] have been well characterised. Such modifications include phosphorylation, acetylation, ubiquitinylation, methylation and sumoylation.

1.3.1.4.1. Phosphorylation

The first evidence supporting phosphorylation of PGC-1[alpha] came from studies on the so-called wasting syndrome (Puigserver et al., 2001). This disorder is characterised with increased expression of the immune-response signalling molecules – cytokines. Cytokines such as tumour necrosis factor alpha (TNFα), interleukin 1alpha and 1beta (IL-1α, IL-1β) stimulate the expression of NRF-1 resulting in increased cellular respiration in muscle cells. This interaction, however, is only possible in the presence of PGC-1[alpha]. The study showed that cytokines induce p38 mitogen-activated protein kinase (p38 MAPK), which in turn directly phosphorylates PGC-1[alpha] at residues Thr262, Ser265 and Thr298. This phosphorylation results in the stabilisation of PGC-1[alpha] by inhibiting its degradation.

Another protein kinase that directly interacts with PGC-1[alpha] is AMP-activated protein kinase (AMPK) (Jager et al., 2007). AMPK phosphorylates the coactivator at residues Thr177 and Ser538 in skeletal muscles. This interaction enhances the transcriptional activity of PGC-1[alpha] and results in elevated expression of glucose transporter 4 (GLUT4) and cytochrome *c* (Cyt*c*). Moreover, phosphorylated PGC-1[alpha] can also regulate its own expression by strongly binding to its promoter and increasing its transcription.

Studies on type 2 diabetes gave further insight on the post-translational modification of PGC-1[alpha]. Li et al (2007) showed that in T2D insulin inhibits the transcriptional coactivator through the stimulation of Akt/protein kinase B (Akt/PKB) (X. Li et al., 2007). Akt/PKB, in turn, interacts negatively with PGC-1[alpha] by phosphorylating Ser570 in its C-terminal domain, which results in impaired gluconeogenesis.

It seems that phosphorylation in the N-terminal or the middle domains of PGC-1[alpha] has a positive impact, stabilising the coactivator and upregulating its transcriptional activity and expression, whereas phosphorylation in the C-terminus results in its inhibition. This contributes towards disease pathogenesis by dysregulating essential downstream pathways.

1.3.1.4.2. Acetylation

Examples of regulation of the function of PGC-1[alpha] through acetylation come from studies on liver function, or more specifically – the production of glucose. PGC-1[alpha] has 13 lysine residues that are sites of acetylation (Rodgers et al., 2005). Most of them are located in the middle, suppression domain. SIRT1 is a deacetylase protein involved in nutrition regulation under conditions of low calorie intake. During fasting, its expression in liver is elevated (Rodgers et al., 2005). In addition, PGC-1[alpha] is also involved in the process of gluconeogenesis and its protein levels are increased upon fasting. This also correlates with the upregulation of genes involved in glucose production such as phosphoenylpyruvate carboxykinase (PEPCK). It appears that there might be a link between the increase of the levels of these proteins. Indeed, SIRT1 interacts directly with PGC-1[alpha] in liver by deacetylating it which results in its activation (Rodgers et al., 2005). This, in turn, stimulates HNF4α and the subsequent expression of PEPCK leading to glucose production and secretion. In contrast, acetylation by a PGC-1[alpha]-specific acetyltransferase called GCN5 leads to its repression in hepatocytes and *in vivo* (Lerin et al., 2006). Once inactive, PGC-1[alpha] is translocated into nuclear foci. The net result of this suppression is decrease in HNF4α and PEPCK expression and also genes involved in mitochondrial

maintenance such as Cyt*c*. These mechanisms of acetylation and deacetylation of PGC-1[alpha] provide a well-balanced mechanism of glucose regulation.

1.3.1.4.3. Methylation and sumoylation

Methylation and sumoylation of PGC-1[alpha] are the two least studied post-translational modifications.

Methylation of arginine residues occurs at the C-terminal of PGC-1[alpha] at residues 665, 667 and 669 (Teyssier et al., 2005). The process of methylation is mediated by protein arginine methyltransferase 1 (PRMT1) and results in the increase of PGC-1[alpha] activity. This, in turn, leads to stimulation of genes involved in mitochondrial homeostasis such as Cyt*c* and ERRα in cultured cells.

Methylation enhances the activity of PGC-1[alpha], whereas sumoylation is responsible for its diminished activity. Lysine 183 in the N-terminal domain gets sumoylated by the small ubiquitin-like modifier 1 protein (SUMO1) which recruits corepressor RIP140 leading to the functional attenuation of the transcriptional coactivator (Rytinki and Palvimo, 2009). In addition, the SUMO-specific protease 1 (SENP1) activates PGC-1[alpha] by desumoylating it, which ultimately results in upregulation of mitochondrial biogenesis (Cai et al., 2012).

1.3.1.4.4. Degradation of PGC-1[alpha] / ubiquitinylation

It is worth noting that PGC-1[alpha] has a short half-life (~30min). Most studies on the mechanism of degradation of PGC-1[alpha] so far were focused on the ubiquitin-dependent pathway (Jie Gao et al., 2015; Sano et al., 2007; Trausch-Azar et al., 2010). However, the mechanisms of ubiquitinylation are still somewhat unclear because of the contradiction between the results from the studies to date. There is

evidence that the C-terminal RS-region and RRM are important for the targeting of the protein for degradation (Sano et al., 2007). In contrast, another study showed that PGC-1[alpha] is degraded through ubiquitinylation of its N-terminus (Trausch-Azar et al., 2010). A more recent work shed light on the complex question about the degradation of PGC-1[alpha] (Adamovich et al., 2013). The group predicted that PGC-1[alpha] is an intrinsically-disordered protein (IDP) that lacks any defined secondary and/or tertiary structure and gets degraded by a novel pathway termed 'degradation by default'. Indeed, the coactivator gets ubiquitinated but most of the degradation takes place through this novel process. NADH quinone oxireductase 1 (NQO1) physically interacts with PGC-1[alpha] and protects it from degradation. Furthermore, the expression levels of NQO1 are similar to the basal protein levels of PGC-1[alpha] again indicating that the coactivator is likely to be mainly degraded by default (Adamovich et al., 2013). Further investigations into the regulation of PGC-1[alpha] stability might lead to promising new approaches of controlling disease factors where dysregulation of PGC-1[alpha] contributes to the pathological phenotype.

1.3.2. Tissue-specific functions

1.3.2.1. Brown fat

PGC-1[alpha] was first identified in mouse brown adipose tissue (BAT, brown fat) as a regulator of mitochondrial-specific proteins involved in adaptive thermogenesis (J. Lin et al., 2005; Puigserver et al., 1998). Adaptive thermogenesis is the process of body temperature regulation in response to weather changes (cold), stress stimuli and high-calorie intake (Bargut et al., 2016). It was shown that upon exposure to low temperatures, the protein levels of PGC-1[alpha] increase in cell models and *in vivo* in mouse (Fig.1.5 A) (Puigserver, 2003; Puigserver et al., 1998). Along with elevated

expression of PGC-1[alpha], increase in mitochondrial uncoupling protein 1 (UCP1) was also observed. UCP1 is brown-fat-specific protein which interacts directly with the ETC by dissipating the proton gradient to produce heat. The role of PGC-1[alpha] in thermogenesis and brown fat is further validated by ectopic expression experiments (Puigserver et al., 1998; Tiraby et al., 2003). Overexpression of PGC-1[alpha] in cultured mouse white fat cells leads to their differentiation to BAT. An identical result was observed also in human white cells (Bostrom et al., 2012). Furthermore, overexpression of PGC-1[alpha] in BAT results in increased amount of mtDNA and increased levels of ATP-synthase and NRF-1 (Puigserver, 2003; Puigserver et al., 1998). In addition, mouse model overexpressing SIRT1 results in increased function of BAT through regulation of PGC-1[alpha] (Boutant et al., 2015).

1.3.2.2. Skeletal muscle and heart

Skeletal and heart muscles have high demand for metabolic respiration and oxygen. They are also characterised by increased levels of PGC-1[alpha] compared to other tissues (e.g. kidney) (Lehman et al., 2000; Wu et al., 1999). Overexpression of PGC-1[alpha] in myotubes results in elevation of ETC-specific proteins such as cytochrome *c* oxidase subunits II and IV (COXII, COXIV) and cytochrome *c* indicating stimulation of oxidative phosphorylation (Wu et al., 1999). Moreover, increased PGC-1[alpha] also promotes mitochondrial biogenesis, and mtDNA transcription and replication as shown by upregulation of NRF-1 and mtTFA, and rise in mitochondrial count. Similar results are observed in neonatal cardiomyocytes upon overexpression of the coactivator in mice (Lehman et al., 2000).

There are two types of skeletal muscles based on their contractile function – type I (slow) and type II (fast). Type I muscle fibres are rich in mitochondria and show higher

oxidative rates compared to type II (J. Lin et al., 2002). Interestingly, PGC-1[alpha] expression is higher in type I slow-twitch muscle fibres. Fully-developed skeletal muscles have the ability to convert from type II to type I fatigue-resistant fibres when physically challenged with prolonged exercise (Fig.1.5 B). This also correlates with increase in the expression of PGC-1[alpha]. Accordingly, evidence for the function of PGC-1[alpha] in skeletal muscles comes from studies utilising its ectopic expression in type II fibres (J. Lin et al., 2002). These muscles start to express proteins characteristic of slow-twitch fibres indicating muscle fibre conversion. Moreover, PGC-1[alpha] directly interacts with calcineurin and Mef2, key proteins involved in the post-neuromuscular-junction response in type I skeletal muscles.
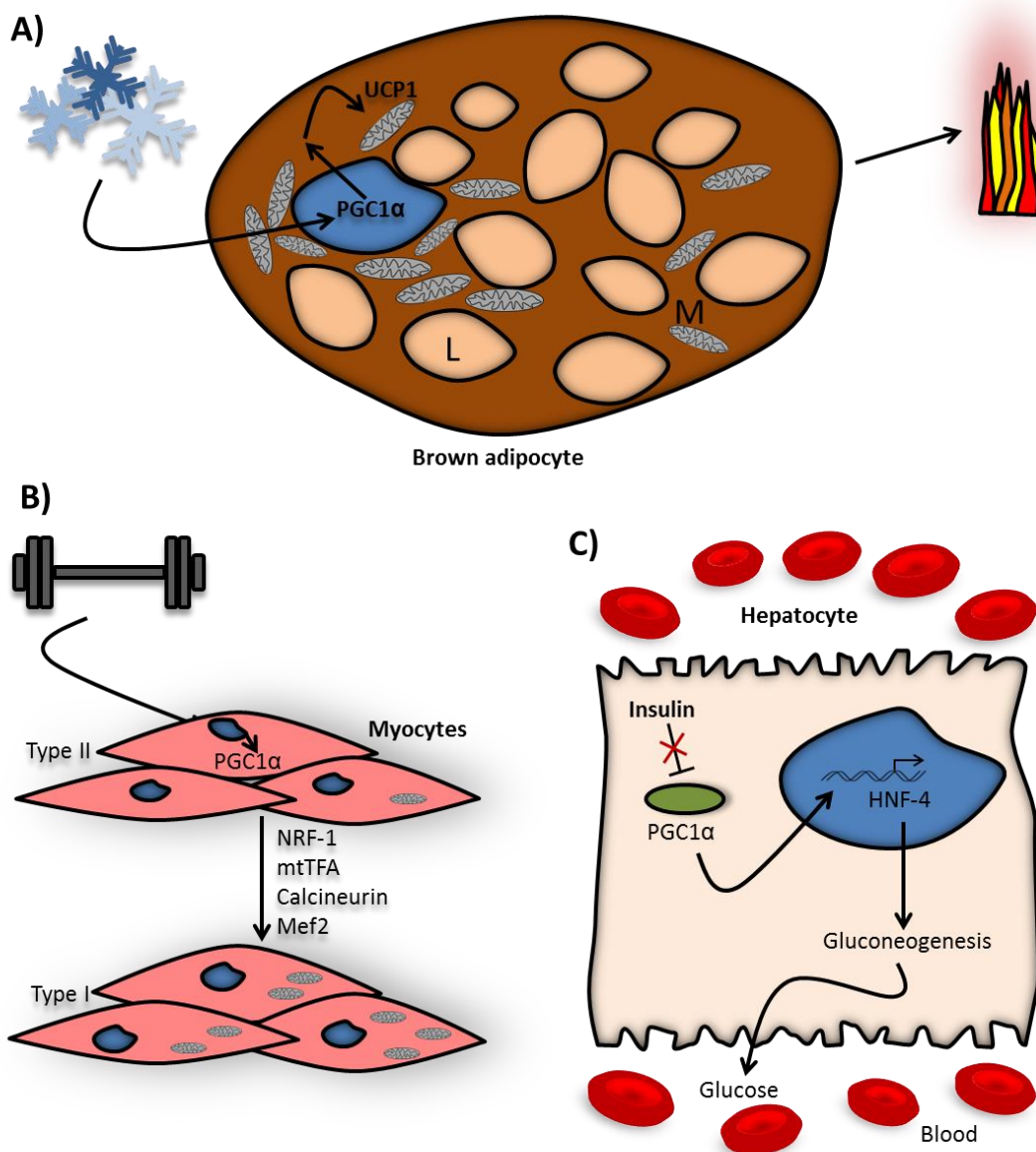
Figure 1.5 Tissue-specific function of PGC-1[alpha].

A) Upon exposure to cold, the transcription and expression of PGC-1[alpha] is upregulated in brown fat (BAT). This, in turn, stimulates the expression of UCP1. UCP1 is responsible for the dissipation of protons from the mitochondrial ETC ultimately resulting in the production of heat. **B)** Physically-challenged skeletal muscles upregulate the expression of PGC-1[alpha]. The transcriptional coactivator, in turn, induces the transcription of NRF-1 and mtTFA, and activates calcineurin and Mef2. This results in increased mitochondrial number and oxidative phosphorylation. As a consequence, fast-twitch fibre (type II) switches to slow-twitch fibre (type I). Type I fibres are fatigue-resistant and can withstand physical load. **C)** During periods of fasting, insulin levels decrease and it can no longer repress PGC-1[alpha] in liver resulting in the higher protein levels and activity of the coactivator. PGC-1[alpha] stimulates the transcription of HNF-4 which in turn upregulates genes involved in the process of gluconeogenesis – PEPCK and G6Pase. As a net result, glucose is synthesised in the liver and secreted into the blood. **L** – lipid droplet; **M** – mitochondrion; nucleus in blue.

Recent studies show that PGC-1[alpha] is not only involved in mitochondrial biogenesis and control of respiration in muscles and heart, but it has a rather versatile function even within the same tissue. In oxygen-deprived extracellular environment, the expression of PGC-1[alpha] is upregulated which in turn leads to angiogenesis through the stimulation of vascular endothelial growth factor (VEGF) *in vivo* (Arany et al., 2008). This is a protective mechanism preventing cellular 'suffocation' and death.

Furthermore, the functional repertoire of PGC-1[alpha] is not tissue-autonomous i.e. PGC-1[alpha] also provides links between different tissues ensuring highly elaborate control of cellular pathways. Exercise-induced expression of PGC-1[alpha] not only stimulates mitochondrial biogenesis and respiration in skeletal cells but also promotes the expression of a newly identified protein irisin in mice (Bostrom et al., 2012). Irisin, in turn, is secreted from skeletal muscles targeting white fat cells and driving brown-fat-like cell differentiation. The net result is exercise-induced thermogenesis which might be of great clinical importance giving insight into the link between physical activity and food breakdown i.e. calorie burning.

1.3.2.3. Liver

Glucose is the main source for energy production in liver. Glucose, in turn, is vital for the correct function of most cells but particularly important for red blood cells and brain cells. As mentioned before, neurones are highly-active cells that have high energy demand. Therefore, glucose production during prolonged periods of food deprivation (fasting) is of great importance for the cellular homeostasis. Glucose is mainly produced *de novo* by a process called gluconeogenesis. Gluconeogenesis is tightly controlled by PEPCK and glucose-6-phosphatase (G6Pase) in response to hormonal regulation (Yoon et al., 2001). Insulin is the principal hormone responsible for the

control of PEPCK and G6Pase expression by inhibiting their expression. During fasting, the levels of insulin are decreased, and the rate of gluconeogenesis increased, respectively (Fig.1.5 C). Interestingly, this correlates with elevated expression of PGC-1[alpha] in fasting and insulin-deficient mice indicating a role of PGC-1[alpha] in the process of gluconeogenesis (Yoon et al., 2001). Moreover, overexpression of the transcriptional coactivator in cultured hepatocytes and *in vivo* leads to increase of PEPCK and G6Pase resulting in elevated levels of glucose. Further evidence of the role of PGC-1[alpha] in the fasting response is the increase of HNF-4α expression. HNF-4α binds to and upregulates the protein synthesis of both gluconeogenic enzymes. This however, is mediated by the direct interaction of PGC-1[alpha] with the transcription factor as discussed earlier (section on structure and regulation of PGC-1[alpha]) (Yoon et al., 2001). This shows that PGC-1[alpha] is stimulated in response to food deprivation and in turn controls the glucose production pathway.

Another study using PGC-1[alpha] knock-out (KO) mice failed to show the role of PGC-1[alpha] in gluconeogenesis during fasting (Haase et al., 2011). Nevertheless, it is remarkable that the transcription coactivator regulates cellular respiration in liver in an exercise-induced manner. Wild-type mice showed elevated levels of CytC and COXI compared to PGC-1[alpha] KOs after prolonged physical challenge. This again shows that PGC-1[alpha] can serve different functions within the same tissue depending on the stimuli.

More recently, it has been shown that a typical cell-cycle regulator cyclin D1 is involved in inhibition of gluconeogenesis in liver (Bhalla et al., 2014). Cyclin D1 exerts its effect on gluconeogenesis via reduction of PGC-1[alpha] activity in the presence of CDK4 (cyclin-dependent kinase 4).

1.3.2.4. Brain

The role of PGC-1[alpha] in brain remains elusive although there is evidence for its involvement in neuronal homeostasis. Most of the research in this area has been undertaken using PGC-1[alpha] null mutant mice and observing their neuropathological phenotype. Alongside the expected changes in the tissues discussed above, several studies in null mutants showed vacuolisation of brain regions such as parietal cerebral cortex, hippocampus, basal ganglia, and cerebellum (Leone et al., 2005). Moreover, there is an apparent degeneration of neurones in the striatum, part of the basal ganglia (J. Lin et al., 2004). Furthermore, cultured striatal cells deficient for PGC-1[alpha] are unable to build complex networks due to reduced ability to form axons and dendrites. However, the underlying mechanism(s) for these brain structure malformations are unclear. Consequently, deducing the function of PGC-1[alpha] in brain is difficult. Synaptic formation requires transport of proteins from the soma to the axon ends and this is largely dependent on mitochondrial respiration. The function of PGC-1[alpha] in synaptogenesis is greatly supported by studies showing that overexpression of the transcription coactivator in cultured hippocampal cells leads to increased number of synapses (Cheng et al., 2012). Conversely, silencing of PGC-1[alpha] results in the loss of neuronal connections compared to controls. Moreover, null mutants also show aggregates of membranous material which might indicate mitochondrial dysfunction (Leone et al., 2005).

Interestingly, expression and secretion of irisin upon exercise challenge is not only apparent in skeletal muscles, but also in hippocampus *in vivo* (Wrann et al., 2013). This again is regulated by PGC-1[alpha] and results in the net increase of brain-derived neurotrophic factor (BDNF). This provides a link between exercise and brain

stimulation and homeostasis suggesting a role of PGC-1[alpha] in the transcription of brain-specific genes.

1.3.3. PGC-1[alpha] in physiological ageing of the brain and disease

Due to the plethora of biological functions in a tissue-specific manner, PGC-1[alpha] has been provoking great interest among scientists for over a decade now. Despite the rich body of articles (5890, PubMed, July 2017), little is known about the exact mechanism(s) of action of PGC-1[alpha]. Great effort has been put into understanding the tissue-specific role of the transcriptional activator. This also has been translated and studied in the context of diseases. However, most of the research so far has been conducted on non-neurological diseases such as type 2 diabetes, cancer and cardiomyopathies. The role of PGC-1[alpha] in physiological ageing and neurodegenerative disorders is a topic of only 6% of all papers published so far on the matter (Table 1.1.). Nevertheless, the identification of PGC-1[alpha]-linked pathomechanisms in other diseases may also provide insight into the role of this transcriptional coactivator in neurodegenerative disorders.

1.3.3.1. Type 2 Diabetes

Type 2 diabetes mellitus (T2DM) is a metabolic disease that accounts for as much as 90% of all diabetes cases. It is characterised with pancreatic beta-cell dysfunction, insulin resistance and elevated levels of blood glucose (Kahn et al., 2014; Stumvoll et al., 2005). T2DM is associated with obesity and sedentary lifestyle. Beta-cell dysregulation results in the downregulated production of insulin, a key regulator of

gluconeogenesis as discussed already. In addition, this leads to insulin-insensitive production of glucose in hepatic tissue.

Table 1.1 Statistical representation of published literature on PGC-1[alpha].

Studies	Number of Articles
Non-neurodegenerative	5890
Diabetes	1122
Cancer	679
Ageing and Neurodegenerative disorders	385
Huntington's disease	77
Parkinson's disease	64
Alzheimer's disease	57
Amyotrophic Lateral Sclerosis	42
Total: 6275	

Ageing/Neurode-generation 6%

Everything else 94%
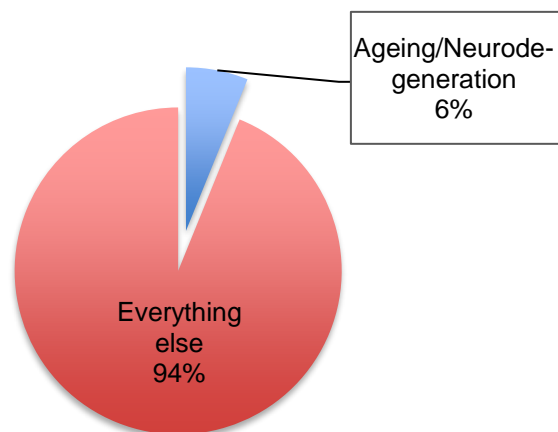
Online database used: PubMed (http://www.ncbi.nlm.nih.gov/pubmed)
Data are correct and up to date as of July 2017.

The pathophysiology of T2DM is also characterised by mitochondrial dysregulation in skeletal muscles with altered morphology and reduced activity of the ETC (Hernandez-Alvarez et al., 2010; Kelley et al., 2002). As discussed, the role of PGC-1[alpha] in skeletal muscles is tightly coupled with the maintenance of the ETC. In addition, the coactivator regulates the process of hepatic gluconeogenesis and is controlled by insulin. Therefore, it could be hypothesised that PGC-1[alpha] is involved in the molecular pathogenesis of T2DM. Indeed, early studies using Gene Set Enrichment Analysis (GSEA) of DNA microarray from patient skeletal muscles revealed a decrease in the expression of genes involved in oxidative phosphorylation (Mootha et al., 2003). This coincides with reduced mRNA levels of PGC-1[alpha]. Intriguingly, the dysregulated set of genes appears to be regulated by the coactivator demonstrating the role of PGC-1[alpha] in T2DM. Moreover, the authors showed that mitochondrial dysfunction takes place before the onset of the disease suggesting causative effect of the event. These findings were later replicated showing not only decreased expression of PGC-1[alpha] and genes involved in mitochondrial maintenance, but also a link between insulin and them (Hernandez-Alvarez et al., 2010). In early-onset T2DM where insulin-resistance is very high the stimulation of PGC-1[alpha] in skeletal muscles upon exercise fails to be initiated. This leads to the decrease of the target mitochondrial fusion protein mitofusin-2 (Mfn2) that is responsible for mitochondrial maintenance. Moreover, altered gene expression is also observed in non-diabetic individuals with history of T2DM in the family indicating hereditary predisposition (Patti et al., 2003). Identical results were seen in heart of transgenic mice recapitulating the disease phenotype (Duncan, 2011). Analysis of diabetic brains demonstrated a decrease in PINK1 and PGC-1[alpha] coinciding with diminished mitochondrial fatty acid oxidation (J. Choi et al., 2014). This further confirms the role of PGC-1[alpha] in diabetes and proposes an interaction with PINK1. Another hallmark of T2DM is impaired vasculogenesis of endothelial cells. This has been associated with elevated levels of PGC-1[alpha] in endothelium and silencing of

PGC-1[alpha] results in rescue of disease phenotype in mice and cultured endothelial cells (Sawada et al., 2014).

In addition, early genetic studies proposed the effect of polymorphisms, particularly Gly482Ser, in the gene of PGC-1[alpha] as a risk factor for T2DM (Hara et al., 2002). Such tendency was observed in Caucasian populations (Kunej et al., 2004). However, the results are debatable as other groups failed to find association between the risk polymorphism and T2DM. Nonetheless, recent meta-analysis studies support Gly482Ser as a moderate risk factor despite the wide heterogeneity in all data (Barroso et al., 2006; Yang et al., 2011). Similar correlation between the polymorphism Gly482Ser and T2DM was found recently in a Tunisian population (Jemaa et al., 2015). Another genetic study also showed significant link between the polymorphism and T2DM in Kurdish-Iranian subgroup (Shokouhi et al., 2015). In addition, they also identified Thr528Thr polymorphism as a risk factor.

1.3.3.2. Ageing and neurodegeneration

Much of the understanding of the role of PGC-1[alpha] in ageing comes from animal studies. Comparing PGC-1[alpha] expression in muscles of young and aged wild-type mice showed significant decrease during ageing (Sczelecki et al., 2014). This is accompanied by decrease of members of the mitochondrial electron transport chain. In another study, comparison of mice at different ages showed a decrease in PGC-1[alpha] and PGC-1[alpha]-regulated mitochondrial genes in old mice (Jiang et al., 2013). The same effect on mitochondrial respiration was observed in mice muscle-deficient for PGC-1[alpha] irrespective of their age. Another animal study involving *Drosophila* demonstrated the effect of PGC-1[alpha] on ageing and longevity (Rera et al., 2011). Ubiquitous overexpression of the transcriptional coactivator was

associated with increased mitochondrial biogenesis and metabolism. This was showed by the increased quantity of mtDNA, activity of citrate synthase, HSP60 (mitochondria-associated protein) and increase in the protein levels of ETC complexes. In addition, it was discovered that the expression of PGC-1[alpha] was decreased in the intestine of older flies and specific overexpression of PGC-1[alpha] in the digestive tract positively correlated with extended life span. PGC-1[alpha]-overexpressing flies show increased activity of complexes I and II, increased mitochondrial membrane potential and decreased ROS at advanced age. This was later confirmed in another study on mutant flies. Flies with diminished levels of *Indy* gene in their intestinal stem cells exhibit extended life span (Rogers and Rogina, 2014). This was associated with increased levels of PGC-1[alpha] and upregulated mitochondrial biogenesis and respiration. Contrary to that, human skin fibroblasts from aged individuals showed increased mRNA levels of PGC-1[alpha] that correlated with decreased SIRT1 and mitochondrial count (Kalfalah et al., 2014). This suggests an alternative mechanism and highlights the importance of SIRT1 regulation (also reviewed in Yuan et al., 2016). Moreover, stimulation of SIRT1 leads to extended lifespan in mice (S. J. Mitchell et al., 2014). More recently, a novel role of PGC-1[alpha] in ageing has been discovered. PGC-1[alpha]-deficient mice show typical characteristics of vascular ageing (Xiong et al., 2015). This was explained with telomere impairment and shortening and dysregulation of telomerase reverse transcriptase (TERT) activity. Interestingly, expression of PGC-1[alpha] results in upregulation of the expression and activity of TERT. This provides an exciting new axis of biological action of PGC-1[alpha] in the context of ageing and holds promise for anti-ageing therapies.

Mitochondrial dysfunction is also a common theme for most neurodegenerative disorders. Interestingly, reduced mRNA levels of PGC-1[alpha] in the striatum of

presymptomatic Huntington's disease patients correlate with diminished mitochondrial activity (Cui et al., 2006). Similar results were observed in PGC-1[alpha] KO mice and human HD brain. This appears to be the result of transcriptional repression of the coactivator by mutant huntingtin through interaction with PGC-1[alpha]'s promoter region. As with T2DM, this downregulation of PGC-1[alpha] expression is also characteristic for muscles of HD patients (Chaturvedi et al., 2009). However, overexpression of PGC-1[alpha] in mouse models of HD resulted in disease rescue by clearance of htt aggregates (Tsunemi et al., 2012). Another indication of the role of PGC-1[alpha] in the pathogenesis of HD is the association between polymorphisms in intron 2 and haplotypes in close vicinity of its gene and disease age of onset and progression (Taherzadeh-Fard et al., 2009; Weydt et al., 2009). Furthermore, a low-frequency polymorphism in the coding region of PGC-1[alpha] was associated with earlier age of onset of HD in the European population (Weydt et al., 2014). Interestingly, this correlation was observed only in males showing gender-specific mechanism of action.

The role of PGC-1[alpha] in the pathogenesis of Alzheimer's disease is less clear. No pathogenic polymorphisms in the gene have been found so far that are associated with increased risk of developing AD (Helisalmi et al., 2008). However, decreased levels of PGC-1[alpha] have been observed in the hippocampus of AD patients (Qin et al., 2009). Interestingly, this also coincides with increase in Aβ production suggesting key role of the coactivator in the disease phenotype. A recent study offered a novel pathway through which PGC-1[alpha] gets deregulated and potentially contributes towards the disease (A. Robinson et al., 2013). Mutations in *PSEN1* lead to decrease in expression of the coactivator. In contrast, wild-type PS1 stimulates the expression of PGC-1[alpha] with the help of APP and APP intracellular domain responsible for the increase of PGC-1[alpha] mRNA. In addition, studies conducted

with mouse models of insulin-resistant high-fat diet and obesity show decrease in PGC-1[alpha] mRNA levels which are concomitant with increased production of Aβ (Sajan et al., 2016).

Understanding the role of PGC-1[alpha] in Amyotrophic Lateral Sclerosis (ALS) is even more challenging. Mouse models of ALS carrying SOD1 G93A mutation show extended survival, enhanced motor abilities, and upregulation of mitochondrial genes involved in oxidative phosphorylation upon overexpression of PGC-1[alpha] (Zhao et al., 2011) and decreased mRNA expression of PGC-1[alpha] has been reported in the SOD1 G93A mouse model (Thau et al., 2012). However, the role of the transcriptional coactivator appears to be secondarily involved in the progression of the disease but not the cause of it in transgenic mice (Liang et al., 2011). Moreover, upregulation of PGC-1[alpha] in muscles of these transgenic mice results in attenuated muscle degeneration that does not lead to extended survival (Da Cruz et al., 2012). This suggests a novel symptomatic therapy target. In addition, polymorphisms in the brain-specific promoter of PGC-1[alpha] have been associated with earlier age of onset and shorter life-span in a male-specific manner (Eschbach et al., 2013). Results were obtained from ALS patients and later replicated in SOD1 G93A mouse models.

Undoubtedly, the importance of PGC-1[alpha] in neurodegeneration is most prominent in studies on Parkinson's disease. Mitochondrial dysfunction is a key pathway involved in the pathogenesis of PD and PGC-1[alpha] is a major regulator of mitochondrial biogenesis and maintenance, therefore the coactivator might have vital impact on the disorder. Fibroblasts from familial PD patients carrying parkin mutations exhibit a decrease in the expression of complexes of the ETC (Pacelli et al., 2011). In addition, expression of PGC-1[alpha] is upregulated and conversely, its targets such

as NRF-1 and COXII are downregulated. These findings not only indicate the involvement of the transcriptional regulator in the pathogenesis of PD but also suggest a novel pathway of dysregulation of PGC-1[alpha] – possibly through post-translational modifications. In contrast, another study showed reduction of gene expression in parkin-mutant PD mouse models through a novel pathway (Shin et al., 2011). The parkin interacting substrate termed PARIS appears to be a potent suppressor of PGC-1[alpha] expression by binding to its promoter. In healthy individuals the cellular levels of PARIS are regulated by parkin through the ubiquitin proteasome pathway targeting PARIS for degradation. However, mutant parkin is less capable of binding the suppressor *in vivo*, resulting in its increase followed by inhibition of PGC-1[alpha]. This ultimately leads to PD phenotype. More recently, these results were reproduced in rat models of PD carrying Q311X mutation in *parkin* (Siddiqui et al., 2015). Primary dopaminergic cells showed PARIS-mediated reduction in mitochondrial respiration and decreased levels of PGC-1[alpha].

Mice deficient for PGC-1[alpha] show increased sensitivity to MPTP, whereas overexpression in brain results in reduced neuronal death in the substantia nigra (Mudo et al., 2012; St-Pierre et al., 2006). This diminished sensitivity suggests a potential neuroprotective function of PGC-1[alpha] and moreover, it coincided with increase of antioxidant enzymes such as SOD2. Overexpression of the coactivator in neuronal-like cells (SH-SY5Y) overexpressing mutant alpha-Synuclein also appears to be neuroprotective by stimulating mitochondrial respiration (Zheng et al., 2010b). However, recent data are contradictory showing increased sensitivity to MPTP in transgenic mice with upregulated expression of PGC-1[alpha] (Clark et al., 2012). In fact, this suggests a fine-tuned balance of PGC-1[alpha] protein levels and any deviations from it might lead to its dysregulation and ultimately contribute towards disease pathogenesis. Other studies with transgenic mice carrying a pathogenic

A30P mutation in the alpha-synuclein gene showed decreased expression of PGC-1[alpha] (Eschbach et al., 2015). Reciprocally, mice deficient for PGC-1[alpha] showed increased oligomerisation of alpha-synuclein which is associated with cytotoxicity in the pathogenesis of PD.

More recently, further evidence has emerged demonstrating the impact of PGC-1[alpha] in PD. Substantia nigra samples from patients showed increased methylation of the brain-specific promoter of the coactivator. This resulted in downregulation of PGC-1[alpha] accompanied by decreased mitochondrial count (Su et al., 2015).

The role of PGC-1[alpha] in transcriptional activation has been well established. However, its putative function in RNA-binding has been neglected and requires more in depth investigation that might lead to fundamental answers about the exact role of PGC-1[alpha] in disease.

1.4. RNA dysregulation and mRNA nuclear export

Widespread dysregulation of RNA metabolism has more recently been implicated in the pathogenesis of many neurodegenerative diseases, including amyotrophic lateral sclerosis (ALS), spinal muscular atrophy (SMA), Huntington's disease (HD) and Alzheimer's disease (E. Y. Liu et al., 2017; Walsh et al., 2015). For example, overexpression of wild-type (WT) or mutant TDP-43 linked to familial ALS leads to neuronal degeneration that is rescued by deletion of the RNA-recognition motif (RRM) in *Drosophila* (Ihara et al., 2013). This suggests dysregulation in RNA binding as a pathological mechanism in neurodegeneration. In addition, stimulating the expression of TDP-43 in *Drosophila* models correlates with increased phosphorylation of eIF2α

leading to its inhibition (Hyung-Jun Kim et al., 2014). eIF2α is a translation initiation factor and its inactivation results in stalled protein synthesis. Mutations in RNA-processing proteins such as hnRNPA1 and hnRNPA2B1 result in increased mislocalisation of both proteins to cytoplasmic stress granules in *Drosophila* models and show muscle degeneration typical of ALS pathology (Hong Joo Kim et al., 2013). Dysregulation of RNA processing via alternative splicing (mis-splicing) of amyloid beta and tau has been implicated as a potential pathogenic mechanism in Alzheimer's disease (Love et al., 2015). More recently, it was shown that G2019S LRRK2 protein results in excessive phosphorylation of RPS15 (40S ribosomal protein subunit 15) leading to upregulated mRNA translation resulting in disease pathology (Martin et al., 2014). This suggests RNA-mediated gene expression dysregulation in the pathogenesis of Parkinson's disease. Ultimately, increasing evidence suggests RNA dysregulation as a common theme in many diseases including neurodegenerative disorders.

RNA biogenesis and processing are central events ensuring cell homeostasis and survival. They take place in the nucleus of the cell and include various coupled steps such as transcription, splicing, capping, cleavage/polyadenylation and mRNA nuclear export (Fig. 1.6.). It is clear that RNA molecules are never left unattended and they are always associated with RNA-binding proteins (RBPs) forming functional complexes termed messenger ribonucleoprotein particles or complexes (mRNPs) (S. F. Mitchell and Parker, 2014). mRNPs ensure correct processing and regulation of RNA to its full maturation and beyond. Currently it is estimated that there are approximately 1,500 RBPs involved in different stages of RNA regulation (Gerstberger et al., 2014). Mature processed RNA molecules are then exported from the nucleus through the nuclear pores to the cytoplasm where there are loaded onto ribosomes ready to be translated into proteins. For this to precisely occur without the

deleterious export of pre-mRNA, an elaborate mechanism of mRNA export has evolved to ensure correct gene expression.

TAP/NXF1 (nuclear export factor 1) forms the nuclear receptor protein responsible for the nuclear export of bulk mRNAs (Grüter et al., 1998). TAP/NXF1 has a highly conserved modular structure. It is composed of an amino-terminal RNA-binding domain (RBD), a leucine rich repeats region (LRR), a nuclear transport factor 2-like (NTF2-like) domain and a carboxyl-terminal ubiquitin-associated domain (UBA) (Herold et al., 2000). TAP/NXF1 functions as heterodimer with NXT1 (p15) that binds to the NTF2-like region. However, *in vitro* studies have shown that TAP/NXF1 has low intrinsic mRNA-binding activity (Liker et al., 2000). Interestingly, a subset of RBPs termed adaptor proteins including ALYREF, SF2 (SRSF1), Srp20 (SRSF3), 9G8 (SRSF7), UIF and Luzp4 bind TAP/NXF1 and increase its affinity for RNA by 4-fold (Hautbergue et al., 2008; Viphakone et al., 2012) (Table 1.2.). This interaction is mediated by another evolutionarily conserved complex, the **tr**anscription and **ex**port complex (TREX). TREX links co-transcriptional events such as splicing, capping and poly-adenylation with mRNA export (Fig.1.6.). It is a multimeric complex composed of different subunits – THO, DEAD-box helicase 39B (DDX39B; UAP56), ALYREF (THOC4) and other export proteins (Heath et al., 2016; Masuda et al., 2005). THO serves as the core scaffolding subunit and structurally represents a hexamer built of THOC1, 2, 3, 5, 6, and 7 (Dufu et al., 2010). TREX provides interdependent regulation of RNA processing by interacting with the carboxyl-terminal domain (CTD) of RNA polymerase II, the CAP-binding, exon-junction (spliceosome), and 3'-end processing complexes with export factors. The RNA helicase UAP56 associates with RNA followed by recruitment of nuclear export adaptors including ALYREF, UIF and Luzp4 resulting in transfer of mRNA from the helicase to the export adaptor (Chang et al., 2013; Dufu et al., 2010).

Table 1.2 Summary of mammalian nuclear export adaptors and co-adaptors.

ID	Adaptor/Co-adaptor	Reference
ALYREF (THOC4)	adaptor	(Strässer and Hurt, 2000; Stutz et al., 2000)
SRp20 (SRSF3)	adaptor	(Huang et al., 2003)
9G8 (SRSF7)	adaptor	(Huang et al., 2003)
ASF/SF2 (SRSF1)	adaptor	(Huang et al., 2003)
UIF	adaptor	(Hautbergue et al., 2009)
Luzp4	adaptor	(Viphakone et al., 2015)
THOC5	co-adaptor	(Katahira et al., 2009)
Chtop	co-adaptor	(Chang et al., 2013)

Next, UAP56 dissociates from adaptors upon their binding to TAP/NXF1:p15. Despite the initial notion that export adaptors bridge the interaction between TAP/NXF1 and mRNA, it was later demonstrated that a handover of RNA takes place indicating a mutually-exclusive binding of RNA and TAP/NXF1 by adaptor proteins (Hautbergue et al., 2008). Interestingly, there is no evidence for binding of SRSF1, 3 and 7 to UAP56 and presence of these RS-rich factors in TREX. However, a common characteristic of all export adaptors is their binding to the RBD of TAP/NXF1 (Hautbergue et al., 2009; 2008). In addition, a new subclass of export factors was identified and termed export co-adaptors due to their binding to the NTF2-like domain of TAP/NXF1 simultaneously while adaptors are bound to the RBD (Chang et al., 2013; Katahira et al., 2009). Such proteins are THOC5 and Chtop (Table 1.2.).
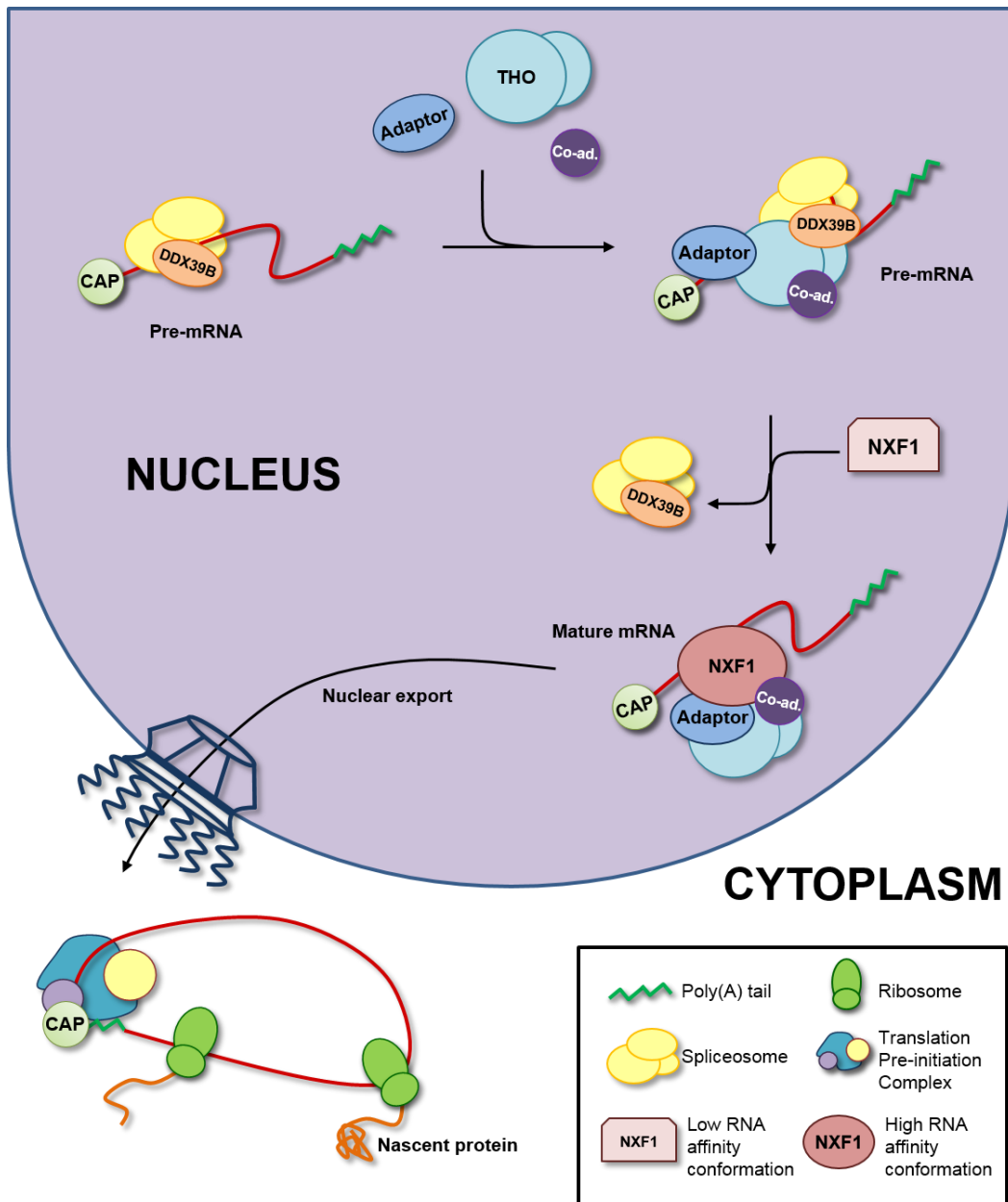
Figure 1.6 Eukaryotic RNA processing.

Once RNA has been transcribed from DNA, the pre-mRNA is capped at the 5'-end and poly-adenylated at the 3'-end. This RNA processing is also concomitant with recruitment of the spliceosome and DDX39B (UAP56) followed by the recruitment of export adaptors, co-adaptors and the THO complex to the RNA molecule. Once this has been recruited, the export adaptor and co-adaptors bind to NXF1 leading to its remodeling to a high RNA affinity binding state that promotes the handover of RNA. This results in the dissociation of the spliceosome and DDX39B. Mature mRNA is then exported to the cytoplasm through the nuclear pore complex (NPC) embedded in the nuclear membrane. mRNA is then translated into proteins by the ribosomes in the cytoplasm.

Adapted from Hautbergue, GM. (2017) Adv. Exp. Med. Biol.

Following the efficient mRNA handover, TAP/NXF1 exports the molecules into the cytoplasm. This event is mediated by interactions of its NTF2-like and UBA domains with phenylalanine-glycine (FG) repeats present in proteins part of the nuclear pore complex (NPC) (Hough et al., 2015; Milles et al., 2015). In the cytoplasm, export adaptors dissociate from the export complex leading to TAP/NXF1 assuming its innate structural conformation with low RNA-affinity. This ultimately results in the release of mRNA in cytoplasm allowing for its subsequent translation.

All reported nuclear export adaptors bind TAP/NXF1 directly. Structurally, export adaptors have one or two RRMs with a typical βαββαβ-fold linked to an RG- or RS-rich region via a unstructured sequence rich in arginines (Walsh et al., 2010). The RRMs of SRSF1, 3 and 7 are important for their RNA-binding ability. Conversely, interactions of ALYREF with RNA mainly involve the unstructured N-terminal Arginine-rich regions adjacent to the RRM region. Interestingly, this region overlaps with the TAP/NXF1-binding site of ALYREF. Furthermore, it has been demonstrated that TAP/NXF1 binds preferentially to arginine residues in the unstructured regions of export adaptors.

1.5. PGC-1[alpha] as a potential new mRNA nuclear export adaptor – hypothesis and aims

As shown before (Fig. 1.4.), PGC-1[alpha] C-terminal domain consists of an RRM and an upstream RS-rich region. These structural characteristics resemble RS class of splicing factors and suggest a role of PGC-1[alpha] in RNA processing (Tacke and Manley, 1999). One of the first studies on the transcriptional co-activator further strengthens this idea. Similar to splicing factors, PGC-1[alpha] was found to associate

with the C-terminal domain (CTD) of RNA polymerase II (Monsalve et al., 2000). Furthermore, PGC-1[alpha] colocalised and/or co-immunoprecipitated with splicing factors such as SC-35 (SRSF2), SRp75 (SRSF4), SRp40 (SRSF5) and SRp55 (SRSF6). While this does not characterise PGC-1[alpha] as a splicing factor, it strongly suggests a role in RNA processing.

Interestingly, association with SC-35 has also been observed with mRNA nuclear export factors such as ALYREF, TAP/NXF1 and UIF (Hautbergue et al., 2009; Williams et al., 2005; Zhou et al., 2000). In addition, structural homology analysis reveals close similarities of PGC-1[alpha] with export adaptors (Fig. 1.7.). The presence of a typical $\beta\alpha\beta\beta\alpha\beta$ RRM fold linked to an RS-rich region offers the attractive possibility that PGC-1[alpha] might be involved in mRNA nucleocytoplasmic transport.
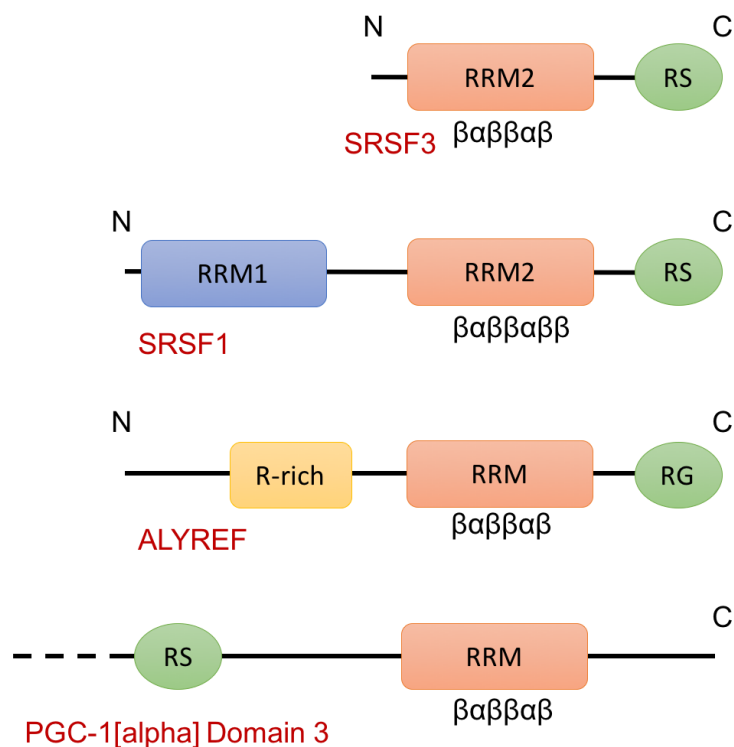
Figure 1.7 Schematic representation of structural homology between export adaptors and PGC-1[alpha].

Nuclear export adaptor proteins share a structural homology consisting of the presence of an RRM and downstream RS/RG-rich region. Similarly, PGC-1[alpha] has an RRM and a RS-rich region. However, unlike typical export adaptors, the RS-region of PGC-1[alpha] is upstream of the RRM. *Adapted from Walsh et.al. (2010) Biochem. Soc. Trans.*

Hypothesis

These structural similarities coupled with the extensive expertise of Dr Guillaume Hautbergue in the field led to the hypothesis of this doctorate work: **PGC-1[alpha] is a novel nuclear export adaptor and its function is biologically important.**

As discussed in section 1.3., PGC-1[alpha] is a master regulator of mitochondrial biogenesis and maintenance. Therefore, we hypothesise that its putative role as an export adaptor is directly related to mitochondrial homeostasis. This might be achieved through the nucleocytoplasmic transport of specific targets of PGC-1[alpha] such as NRF1 and TFAM. Conversely, any dysregulations of PGC-1[alpha]'s ability to export these target RNAs would result in their nuclear accumulation. This would lead to mitochondrial dysfunction and have a detrimental global impact contributing or even causing disease pathologies.

Aims

In order to characterise PGC-1[alpha] as a novel mRNA nuclear export adaptor and elucidate its biological importance for mitochondrial homeostasis, a set of aims was established creating the basis of this PhD work:

- Does PGC-1[alpha] bind RNA?
- Investigate the biological function of the putative RNA-binding function: Does PGC-1[alpha] interact with TREX and TAP/NXF1?
- Engineer cell models of PGC-1[alpha] to investigate the putative cellular RNA-binding activity of PGC-1[alpha]
- Evaluate the putative RNA-binding activity at the functional level on mitochondrial metabolism and ATP production

2. Materials and Methods

2.1. Materials

2.1.1. Bacterial strains

- ***Escherichia coli (E. coli)* DH5alpha (DH5α)** (Genotype: *fhuA2 lac(del)U169 phoA glnV44 Φ80' lacZ(del)M15 gyrA96 recA1 relA1 endA1 thi-1 hsdR17*)
    - Used as a host for molecular cloning of plasmid DNA.

- ***Escherichia coli (E. coli)* BL21 (DE3) pLysS** (Genotype: F$^-$ *ompT gal dcm lon hsdS$_B$($r_B^- m_B^-$)* λ(DE3 [*lacI lacUV5-T7p07 ind1 sam7 nin5*]) [*malB$^+$*]$_{K-12}$(λ^S) pLysS[*T7p20 ori*$_{p15A}$]); Cam^R
    - Used as a host for recombinant protein expression.

2.1.2. Mammalian cell lines

- **HEK293T – Human Embryonic Kidney cells**
    - High transfection efficiency; they carry SV40 T-antigen
    - Used in transient transfection studies

- **HEK293 Flp-In T-REx** (ThermoFisher)
    - Single flippase recognition target (FRT) site for stable integration of gene of interest (GOI)
    - Constitutively-expressed tetracyclin repressor
    - Used for the generation of stable inducible cell lines with GOI

- **LUHMES – Lund Human Mesencephalic cell line** (Provided in differentiated state by Miss Irina Vasquez, Prof Stephen Wharton group, SITraN)
    - Embryonic conditionally-immortalised neuronal cell line

- o Post-mitotic differentiation to dopamine-like neurones driven by tetracyclin induction
- o Used for immunocytochemistry of endogenous proteins

2.1.3. Growth/culture media

Bacterial cells

- **LB Broth, Miller** (Fisher Scientific)
  - o Granular dissolved in distilled water and autoclaved
  - o Used for growing bacteria in liquid media
- **LB Agar, Miller** (Fisher Scientific)
  - o Powder dissolved in distilled water and autoclaved
  - o Used for growing transformed bacteria on solid media
- **TB (Terrific Broth)**
  - o 1.2% w/v Tryptone, 2.4% w/v Yeast extract, 0.231% w/v KH_2PO_4, 1.254% w/v K_2HPO_4, 0.4% v/v Glycerol
  - o Used for recombinant protein expression in rich culture medium

Mammalian cells

- **Dulbecco's Modified Eagle's Medium (DMEM) – high glucose** (Sigma) (will be referred to as **glucose medium**)
  - o Supplemented with 10% v/v (Tetracycline-Free) Fetal Bovine Serum (FBS, Sigma) and 1% v/v Penicillin/Streptomycin (Penstrep, Lonza)
  - o Used for culturing HEK293T and HEK Flp-In cell lines
- **DMEM (1X, Gibco) – without glucose** (will be referred to as **galactose medium**)

- Supplemented with 10% Tet-Free FBS, 1% Penstrep, 5 mM D-(+)-galactose (Sigma)
- Used for culturing HEK Flp-In cells 24 hours prior to metabolic assays

- **DMEM/F-12 (1:1) (1X) + GlutaMAX-I** (Gibco)
  - Supplemented with 1% v/v N-2 (Gibco) and 1% v/v B-27 (Gibco)
  - Used for culturing induced neural progenitor cells (iNPCs)

- **Phosphate Buffered Saline (PBS)** (Oxoid)
  - Tablets
  - Used for washing cells
  - Treated with DEPC (where mentioned)

2.1.4. Antibiotics

Table 2.1 Antibiotics used for bacterial and mammalian cell culture.

Antibiotic	Working concentration (µg/ml)	Dissolved in	Used in
Ampicillin	100	H_2O	Bacterial culture
Kanamycin	50	H_2O	Bacterial culture
Chloramphenicol	34	100% Ethanol	Bacterial culture
Spectinomycin	50	H_2O	Bacterial culture
Blasticidin	15	H_2O	Mammalian culture
Zeocin	100	H_2O	Mammalian culture

Hygromycin	100	H_2O	Mammalian culture
Tetracycline	1	70% Ethanol	Mammalian culture

2.1.5. Vectors/plasmids

- **pET-9a-p15** (4.3 kbp)
    - Kanamycin^R
    - Contains p15 used for co-expression with TAP/NXF1 in *E. coli* for pull-down assays
    - No tag

- **pGEX-6p-1** (4.9 kbp)
    - Ampicillin^R
    - Contains TAP/NXF1 used for co-expression with p15, or deletion fragments of TAP/NXF1 in *E. coli* for pull-down assays
    - GST (Glutathione S-Transferase) tag

- **pcDNA5/FRT/TO HIS** (5.1 kbp) (Addgene 19446)
    - Ampicillin^R
    - Used for the insertion of 3XFLAG or chained miRNAs for PGC-1[alpha]
    - Plasmid with 3XFLAG used for the insertion of PGC-1[alpha] full length used for transfection in HEK293T
    - No or 3XFLAG tag

- **pcDNA6.2-GW/EmGFP-miR** (5.7 kbp) (LifeTechnologies)
    - Spectinomycin^R
    - Used for insertion of miRNAs for PGC-1[alpha] knockdown and for chaining miRNAs

- o +/- EmGFP

- **peT24b-GB1-6His** (5.5 kbp)

  - o Kanamycin[R]

  - o Used for insertion of PGC-1[alpha] full length or deletion fragments for recombinant protein expression in *E. coli* or in reticulocyte lysate assay

  - o GB1-6His tag

- **pIRES-NXF1-13myc** (8.4 kbp)

  - o Ampicillin[R]

  - o Used for mammalian expression of C-terminally 13myc-tagged NXF1 in CoIP studies

2.1.6. Primers

All primers were ordered from Sigma-Aldrich®

The name of each primer is constructed as follows: DNA name, start amino acid, restriction site, 5 – forward / 3 – reverse; stp – STOP codon.

For pcDNA5/FRT/TO 3xFLAG-PGC-1[alpha]:

PGC1a-1-BamHI5:

GGC GGG GGA TCC ATG GCG TGG GAC ATG TGC AAC C

PGC1a-798stp-Not13:

CCC GCC GCG GCC GC TTA CCT GCG CAA GCT TCT CTG AGC

For pcDNA6.2-GW/EmGFP-miR PGC-1[alpha] Domain 1:

PGC1a miR D1(133) top:

TGCTGAAAGCTGTCTGTATCCAAGTCGTTTTGGCCACTGACTGACGACTTGGA

CAGACAGCTTT

PGC1a miR D1(133) bottom:

CCTGAAAGCTGTCTGTCCAAGTCGTCAGTCAGTGGCCAAAACGACTTGGATAC

AGACAGCTTTC

For pcDNA6.2-GW/EmGFP-miR PGC-1[alpha] Domain 2:

PGC1a miR D2(997) top:

TGCTGTGTACCAGAAGACTCACTGTAGTTTTGGCCACTGACTGACTACAGTGAC

TTCTGGTACA

PGC1a miR D2(997) bottom:

CCTGTGTACCAGAAGTCACTGTAGTCAGTCAGTGGCCAAAACTACAGTGAGTC

TTCTGGTACAC

For pcDNA6.2-GW/EmGFP-miR PGC-1[alpha] Domain 3:

PGC1a miR D3(2135) top:

TGCTGAACCATAGCTGTCTCCATCATGTTTTGGCCACTGACTGACATGATGGAC

AGCTATGGTT

PGC1a miR D3(2135) bottom:

CCTGAACCATAGCTGTCCATCATGTCAGTCAGTGGCCAAAACATGATGGAGAC

AGCTATGGTTC

For pcDNA5 FRT/TO miRNA PGC-1[alpha] (chained):

miRNA PCR HindIII5:

GGC GGG AAG CTT GCT AAG CAC TTC GTG GCC GTC

miRNA PCR NotI3:

CCC GCC GCG GCC GC TCA GTT AGC CTC CCC CAT CAG

For pET24b/GB1-6His/PGC-1[alpha] full length and truncation constructs:

PGC1a-1-NdeI5:

GGC GGG CAT ATG GCG TGG GAC ATG TGC AAC

*PGC1a-234**stp**-XhoI3:*

CCC GCC CTC GAG TTA GTC TCT GCT GCT GTT TCT GTT C

PGC1a-254-NdeI5:

GGC GGG CAT ATG AAA CCA ACA ACT TTA TCT CTT C

*PGC1a-564**stp**-XhoI3:*

CCC GCC CTC GAG TTA CCT TTG GGG TCT TTG AGA AAA TAA G

PGC1a-565-NdeI5:

GGC GGG CAT ATG CGC TCT CGT TCA AGG TCC

*PGC1a-633**stp**-XhoI3:*

CCC GCC CTC GAG TTA CCT GGG CCG ACG GCT GTA GGG

PGC1a-634-NdeI5:

GGC GGG CAT ATG TAT GAC AGC TAC GAG GAA TAT C

*PGC1a-798**stp**-XhoI3:*

CCC GCC CTC GAG TTA CCT GCG CAA GCT TCT CTG AGC

QuickChange Site-Directed Mutagenesis:

PGC 4R_568/570/574/576_4E_fwd:

CAT CAT CAT ATG CGC TCT GAA TCA GAG TCC TTT TCT GAA CAC GAG TCG

TGT TCC GAA TCA CCA

PGC 4R_568/570/574/576_4E_rev

TGG TGA TTC GGA ACA CGA CTC GTG TTC AGA AAA GGA CTC TGA TTC

AGA GCG CAT ATG ATG ATG

PGC RR580/585EE fwd:

CGA CAC AGG TCG TGT TCC GAA TCA CCA TAT TCC GAG TCA AGA TCA

AGG TCT CCA

PGC RR580/585EE rev:

TGG AGA CCT TGA TCT TGA CTC GGA ATA TGG TGA TTC GGA ACA CGA

CCT GTG TCG

PGC 5R_580/585/587/589/594_5E fwd:

TCT CGA CAC AGG TCG TGT TCC GAA TCA CCA TAT TCC GAG TCA GAA TCA

GAG TCT CCA GGC AGT GAA TCC TCT TCA AGA TCC TGC TAT

PGC 5R_580/585/587/589/594_5E rev:

ATA GCA GGA TCT TGA AGA GGA TTC ACT GCC TGG AGA CTC TGA TTC

TGA CTC GGA ATA TGG TGA TTC GGA ACA CGA CCT GTG TCG AGA

PGC RRR621/623/625EEE fwd:

CGA AAT TCT CCC TTG TAT GTG GAA TCA GAG TCA GAA TCG CCC TAC AGC

CGT CGG CC

PGC RRR621/623/625EEE rev:

GG CCG ACG GCT GTA GGG CGA TTC TGA CTC TGA TTC CAC ATA CAA GGG

AGA ATT TCG

PGC RRR630/631/633EEE fwd:

CGT TCA AGA TCG CCC TAC AGC GAA GAG CCC GAG TAT GAC AGC TAC

GAG GAA TA

PGC RRR63/631/6330EEE rev:

TA TTC CTC GTA GCT GTC ATA CTC GGG CTC TTC GCT GTA GGG CGA TCT

TGA ACG

For miRNA resistance:

PGC miR1 res_fwd:

A CTA GAT GTG AAC GAC TTG GAC ACC GAT TCT TTC CTG GGT GGA CTC

AAG TGG TGC

PGC miR1 res_rev:

GCA CCA CTT GAG TCC ACC CAG GAA AGA ATC GGT GTC CAA GTC GTT

CAC ATC TAG T

PGC miR2 res_fwd:

A AAG AAG CCC AGG TAC AGT GAA AGC AGC GGC ACC CAA GGC AAT AAC

TCC ACC AAG

PGC miR2 res_rev:

CTT GGT GGA GTT ATT GCC TTG GGT GCC GCT GCT TTC ACT GTA CCT

GGG CTT CTT T

MUTATION(S) IN BLUE.

PGC1a ΔRS Divergent PCR:

PGC1a div_634_XmaI5:

GGC GGG CCC GGG TAT GAC AGC TAC GAG GAA TAT C

PGC1a div_564_XmaI3:

CCC GCC CCC GGG CCT TTG GGG TCT TTG AGA AAA TAA G

Quantitate Reverse Transcriptase Polymerase Chain Reaction (qRT-PCR)

Primers:

U1 snRNA (reference gene)

Fwd: CCATGATCACGAAGGTGGTT

Rev: ATGCAGTCGAGTTTCCCACA

PGC-1[alpha] 3'UTR

Fwd: GTGTGGAGTCCCTGGAATGG

Rev: GTGTTGGGCGAGAGAAAGGA

NRF-1

Fwd: TTCTCCCGAGGACACCTCTT

Rev: GGCCGTTTCCGTTTCTTTCC

mtTFAM

Fwd: AAGATTCCAAGAAGCTAAGGGTGA

Rev: AGAAGATCCTTTCGTCCAACTTCA

COX2

Fwd: CCCATCCCTACGCATCCTTT

Rev: AGGAGTTGAAGATTAGTCCGCC

More details about the qRT-PCR primers used including standard curve results and melting temperatures can be found in Appendix 1.

2.1.7. Restriction enzymes

Restriction enzymes that were used are: *Bam*HI, *Not*I, *Nde*I, *Xho*I, *Hind*III, *Dra*I

All enzymes were ordered from ThermoScientific and used following manufacturer's instructions.

2.1.8. Antibodies

Primary antibodies:

Table 2.2 Primary antibodies used in Western Blotting and Immunofluorescence

Antibody	Clonality	Origin (species)	Working concentration	Source
6xHIS (Biotin) (33D10.D2)	monoclonal	mouse	WB: 1/2000	Abcam, ab106261
Alpha-Tubulin (DM1A)	monoclonal	mouse	WB: 1/5000	Sigma, T9026
ALYREF (11G5)	monoclonal	mouse	WB: 1/1000	Sigma, A9979

Beta III Tubulin (Tuj-1)	polyclonal	chicken	IF: 1/1000	Abcam, ab41489
c-Myc (9E10)	monoclonal	mouse	WB: 1/1000	ThermoFisher, MA1-980
FLAG (M2)	monoclonal	mouse	WB: 1/2000 IF: 1/1000	Sigma, F1804
MAP2 (HM-2)	monoclonal	mouse	IF: 1/500	Sigma, M4403
Nestin (2C1.3A11)	monoclonal	mouse	IF: 1/1000	Abcam, 18102
NeuN (A60)	monoclonal	mouse	IF: 1/500	Millipore, MAB377
OXPHOS (antibody cocktail of 5)	Monoclonal (each antibody)	mouse	WB: 1/1000	Abcam, ab110411
Pax6	polyclonal	rabbit	IF: 1/1000	Abcam, ab5790
PGC-1[alpha]	polyclonal	rabbit	IF: 1/200	Abcam, ab54481
SSRP1 (10D1)	monoclonal	mouse	WB: 1/500	Biolegend
TAP/NXF1 (53H8)	monoclonal	mouse	IF: 1/500	Abcam, ab50609
TDP43 (C-terminal, Ag4003)	monoclonal	rabbit	WB, ICC: 1/1000	Proteintech, 12892-1-AP
THOC1, p84 (EPR5662(2))	monoclonal	rabbit	WB: 1/1000	Abcam, ab131268

Tom20 (FL-145)	polyclonal	rabbit	IF: 1/1000	SantaCruz, sc-11415
UAP56	monoclonal	rabbit	WB: 1/1000	Custom-made, courtesy of Prof Stuart Wilson

Secondary antibodies:

Table 2.3 Secondary antibodies used for Western Blotting and Immunofluorescence

Antibody	Working concentration	Source
Mouse HRP-conjugated	WB: 1/5000	Promega, W4021
Rabbit HRP-conjugated	WB: 1/5000	Promega, W4011
Alexa mouse/rabbit 488	IF: 1/1000	Abcam, ab150113/ab150077
Alexa mouse/rabbit 594	IF: 1/1000	Abcam, ab150116/ab150080
Alexa chicken 647	IF: 1/1000	Abcam, ab150171

2.2. Methods

2.2.1. Plasmid preparation

Plasmids were ordered as IMAGE cDNA clones where available or generated by RT-PCR using total RNA from HEK293T cells.

2.2.1.1. RNA extraction and preparation

One fully confluent T75 flask of HEK293T cells was harvested. Cell pellet was lysed in 250 µl of IP Lysis Buffer (150 mM NaCl, 1 mM EDTA, 1 mM DTT, 0.5% v/v Triton X-100, 50 mM HEPES, 10% v/v Glycerol, pH 7.5) and 10 u RNAse inhibitors (Ribosafe, Bioline) for 10 min on ice. To the lysate was added 750 µl PureZOL RNA isolation reagent (BioRad) and left for further 10 min at room temperature. 200 µl chloroform was added followed by vigorous agitation for 20 s. and incubation for 5 min at room temperature. Sample was then centrifuged for 10 min at 4°C, 11,600 xg. Supernatant (clear top layer) was then mixed with 1 µl Glycogen and 1 volume Isopropanol and left precipitating for 30 min at room temperature. After a centrifugation for 10 min at 4°C, 17,000 xg, the pellet was air-dried.

Air-dried pellet was DNase (Roche) treated for 30 min at 37°C. One volume Phenol saturated solution, pH 4.5 (Fisher) was added and vortexed for 2 min followed by centrifugation for 3 min at room temperature, 17,000 xg. Supernatant was transferred to a fresh microcentrifuge tube, mixed with 1 µl GlycoBlue (ThermoFisher) and 3 volumes 100% ethanol, and left precipitating for 30 min at -20°C. Sample was then centrifuged for 20 min at room temperature, 17,000 xg and pellet air-dried. The pellet was reconstituted in deionised H_2O (Milli-Q) to a final concentration of 1-2 µg/µl.

2.2.1.2. cDNA synthesis

cDNA was synthesised following the protocol by Bioline using BioscriptTM Reverse Transcriptase. Priming premix was prepared on ice (2 µg total RNA, 1 µM Oligo (dT)18, 4 µM Random Hexamer, 2 µM dNTP mix, DEPC-treated water up to 10 µl) and incubated for 5 min at 70°C followed by immediate incubation on ice for 1 min. 10 µl reaction premix (5x RT buffer, Ribosafe Bioline RNase Inhibitor, 200 U Bioscript Reverse Transcriptase, DEPC-treated H_2O) was added to the priming premix and incubated for 60 min at 42°C followed by incubation for 5 min at 85°C. cDNA was then stored at -20°C.

2.2.1.3. Polymerase Chain Reaction (PCR)

Gene of interest was amplified using total cDNA or IMAGE clone.

The amplification was achieved using Herculase II Fusion DNA Polymerase (HERII) (Agilent). The enzyme has proof-reading capability and is suitable for PCR products >2kbp. The protocol can be found in Table 2.4.

Table 2.4 PCR protocol for Herculase II fusion DNA polymerase

HERII PCR Protcol	
1 µl	cDNA
250 ng	DNA template
0.5 µM	Forward Primer
0.5 µM	Reverse Primer
1.6 mM	dNTP Mix (400 µM each dNTP)
5 µl	5x Herculase II Reaction Buffer
5%	DMSO

0.5 µl	Herculase II Fusion DNA Polymerase
Up to 25 µl	ddH$_2$O

The program used for HERII PCR on the thermal cycler was a Touchdown PCR. It can be found in Table 2.5.

Table 2.5 Touchdown PCR program for Herculase II DNA fusion polymerase

PCR Program for HERII		
Heated Lid	110ºC	
Temperature Step	95ºC	2 min
Touchdown		
Denaturing temperature	95ºC	20 s.
Max. Annealing temperature	65ºC	20 s.
Min. Annealing temperature	50ºC	
Elongation temperature	68ºC	2 min
Cycles	15	
Start Cycle	35x	
Temperature Step	95ºC	20 s.
Temperature Step	55ºC	20 s.
Temperature Step	68ºC	2 min
End Cycle		
Temperature Step	68ºC	4 min
Hold	10ºC	Infinite

2.2.1.4. Agarose Gel Electrophoresis

PCR products or DNA fragments were analysed and separated on an agarose gel. Briefly, agarose gels were prepared by dissolving agarose powder (Sigma) in 1x TAE (40 mM Tris, 20 mM acetic acid, 1 mM EDTA) buffer and adding 20 µg ethidium bromide per 100 ml of agarose gel. The gel percentage used was chosen depending on the size of the DNA fragments i.e. for products shorter than 1 kbp – 1-

2% w/v; longer than 1kbp – 0.8% w/v. A DNA ladder (GenerulerTM DNA Ladder Mix, ThermoScientific) was used and DNA was separated for 40-60 min at 80 V.

2.2.1.5. DNA gel extraction

DNA fragments of the correct for the gene/construct size were extracted using QIAquick® Gel Extraction Kit (QIAGEN) following manufacturer's instructions. To excised DNA fragment were added 3 volumes of QG buffer and the gel was dissolved at 50°C. After the addition of 1 volume isopropanol the sample was passed through a column. The column was then washed with 500 µl QG buffer followed by an additional wash with 750 µl Buffer PE. The DNA was eluted with 50 µl Buffer EB.

2.2.1.6. PCR product/vector digest

Both PCR product and vector were digested with the same restriction enzymes creating overlapping 'sticky' ends to facilitate subsequent ligation. Digest protocol can be found in Table 2.6.

Table 2.6 Restriction digest protocol for PCR product/vector DNA.

DNA Fragment	Vector
50 µl Eluted PCR DNA	5 µg Vector DNA
30 µl ddH2O	up to 50 µl ddH2O
10 µl 10x Fast Digest Buffer	5 µl 10x Fast Digest Buffer
5 µl Restriction Enzyme 1	2 µl Restriction Enzyme 1
5 µl Restriction Enzyme 2	2 µl Restriction Enzyme 2
Leave overnight at 37°C	Leave for 2 hrs at 37°C

2.2.1.7. DNA precipitation and ligation

Vector digest was dephosphorylated by treating it with 10 U Alkaline Phosphatase Calf Intestinal (CIP; Biolabs) for 15 min at 37°C.

For DNA precipitation 1 volume of phenol/chloroform/isoamyl alcohol was added and sample was vortexed for 1 min followed by centrifugation for 3 min at room temperature, 17,000 xg. Supernatant was mixed with 3 M sodium acetate and 3 volumes 100% ethanol and left to precipitate for 20 min at -20°C. Precipitated DNA was then centrifuged for 20 min at room temperature, 17,000 xg and pellet air-dried. Pellets from DNA fragments were reconstituted in 16 µl ddH$_2$O, and pellets from vector in 25 µl ddH$_2$O.

For the ligation 16 µl DNA fragment was mixed with 1 µl vector, 2 µl 10x Ligation Buffer and 1 µl (5U) T4 DNA Ligase, and left overnight at 16°C.

2.2.2. Molecular cloning of genes/gene constructs

2.2.2.1. Competent cells preparation – chemical method

DAY 1

50 ml Luria-Bertani (LB) Broth was inoculated with bacterial culture and left on an orbital shaker overnight at 37°C.

DAY 2

400 ml LB Broth was inoculated with overnight culture to $OD_{600} = 0.05$ (optical density) and left shaking at 37°C until reaching $OD_{600} = 0.48$. After reaching optimal OD, cells were centrifuged for 10 min at 4°C, 17,000 xg. Pellet was then resuspended in ice-cold 50 ml TfbI buffer (15% v/v Glycerol, 30 mM KAc, 100 mM $RbCl_2$, 10 mM $CaCl_2$, 50 mM $MnCl_2$; pH 5.8) and left on ice for 10 min. Cells were centrifuged again for 10 min at 4°C, 17,000 xg. Pellet was resuspended in 20 ml ice-cold TfbII buffer (10 mM MOPS, 75 mM $CaCl_2$, 100 mM $RbCl_2$, 15% v/v Glycerol; pH 6.5) and left on ice for 15 min. Cells were then transferred into pre-chilled microcentrifuge tubes and flash-frozen in LN_2 (liquid nitrogen).

The competency of the cells to uptake plasmids was subsequently checked.

2.2.2.2. Bacterial transformation

The transformation efficiency of freshly prepared competent cells was tested by transforming them with a known amount of an empty vector.

5 µl of ligated DNA was added to 50 µl competent cells and left on ice for 10 min. Cells were heat-shocked by incubation for 5 min at 37°C, then transferred back to ice for 2 min. 900 µl LB broth was added and cells were left recovering for 1 hour at 37°C. They were subsequently centrifuged for 1 min at room temperature, 7,000 rpm (benchtop centrifuge) and most of supernatant removed. The pellet was resuspended in leftover supernatant and cells were plated on LB agar plates supplied with the appropriate antibiotic(s). Plates were left upside-down overnight at 37°C.

2.2.2.3. Miniprep

For screening analysis, plasmids were isolated from transformed bacterial colonies and tested via restriction digest for the successful integration of DNA fragment/insert.

Bacterial colonies from agar plates were inoculated individually in LB Broth and grown overnight at 37°C. Bacterial cultures were then centrifuged for 1 min at 17,000 xg. Pellets were resuspended in 200 µl solution A (50 mM glucose, 25 mM Tris at pH 8.0, 10 mM EDTA, 0.1 mg/ml RNase A). To the samples was added 200 µl solution B (0.2 M NaOH, 1% w/v SDS) and inverted until fully mixed. After incubation for 5 min at room temperature, 300 µl solution C (3 M potassium acetate, 11.5 % v/v glacial acetic acid) was added and tubes were inverted 10 times. Lysates were centrifuged for 10 min at 17,000 xg and supernatant transferred to fresh microcentrifuge tubes. After the addition of 700 µl isopropanol, tubes were inverted and left for 10 min at room temperature followed by centrifugation for 10 min at 17,000 xg. Pellet was air-dried and resuspended in 50 µl ddH$_2$O.

To check for the insertion of the DNA fragments, 5 µl of each sample was digested by restriction enzymes and analysed on agarose gel.

2.2.2.4. Spinprep

For higher purity, plasmids were purified from the corresponding bacterial cultures using the commercially available QIAprep® Spin Miniprep Kit following manufacturer's guidelines.

Bacterial pellet was resuspended in 250 µl Buffer P1. 250 µl Buffer P2 was added and tube was inverted. Solution was neutralised by adding 350 µl Buffer N3. Sample was centrifuged for 10 min at 17,000 xg and supernatant was passed through a column. The column was then washed with 500 µl Buffer PB followed by a final wash with 750 µl Buffer PE. DNA was eluted upon addition of 50 µl Buffer EB.

Eluted DNA was sequenced.

2.2.2.5. DNA sequencing

Sanger sequencing was carried out by performing a sequencing PCR, precipitating the PCR product and sending it to Source Biosciences for analysis. The DNA sequence (chromatogram) received in *abi* format was then analysed using FinchTV software.

PCR was carried out as detailed in Tables 2.7 and 2.8.

Table 2.7 Sanger sequencing PCR protocol

Sequencing PCR (Applied Biosystems)	
1 µg	Spinprep DNA
2 µl	5X BigDye Terminator v3.1 Sequencing Buffer
1 µl	BigDye Terminator v3.1 Ready Reaction Mix
1 µl (1 pmol/µl)	Primer
Up to 10 µl	ddH2O

Table 2.8 PCR program used for DNA sequencing.

PCR Program for Sanger Sequencing		
Heated Lid	110ºC	
Start Cycle	45x	
Temperature Step	95ºC	30 s.
Temperature Ramp	1ºC per s.	
Temperature Step	50ºC	15 s.
Temperature Ramp	1ºC per s.	
Temperature Step	60ºC	4 min
End Cycle		
Hold	10ºC	Infinite

PCR product was mixed with 3 µl 3 M sodium acetate, 24.5 µl ddH$_2$O and 62.5 µl 100% ethanol. Samples were vortexed briefly and left for 20 min at room temperature followed by centrifugation for 20 min at 17,000 xg, room temperature. DNA pellet was washed with 150 µl 70% v/v ethanol and centrifuged for 10 min at 17,000 xg. Finally, pellet was air-dried and sent to Source Biosciences.

2.2.2.6. Midiprep

For a larger amount of higher-purity DNA, sequenced plasmids were amplified and purified using QIAGEN Plasmid *Plus* Kit.

100 ml of bacterial culture containing the plasmid of interest was centrifuged for 10 min at 17,000 xg and pellet was resuspended in 4 ml Buffer P1. To the sample was added 4 ml Buffer P2 and the tube was inverted and left for 2 min at room temperature. The solution was neutralised with 4 ml Buffer S3 and centrifuged for 5 min at 4,500 xg. The supernatant was filtered and mixed with 2 ml Buffer BB. Samples were incubated for 1 hour at -20°C. The solution was then passed through a column. The column was washed with 700 µl Buffer ETR followed by another wash with 700 µl Buffer PE. Plasmid DNA was eluted in 200 µl Buffer EB. DNA concentration was determined using NanoDrop 1000 (Thermo Scientific) and sample was diluted to a final concentration of 500 ng/µl.

1 µg purified plasmid was then digested and analysed on agarose gel to confirm its correctness.

2.2.2.7. miRNA design and chaining

Chaining of miRNAs was required for increased knockdown efficiency by simultaneously targeting two regions in the ORF of the gene. Specific primers for pre-miRNA were designed using Life Technologies' online tool (www.lifetechnologies.com/rnai).

Single miRNAs were generated following the same protocol for general palsmids and following manufacturer's instructions (Block-iT; LifeTechnologies). 50 μM of each top and bottom miRNA oligos were annealed together. 10 nM annealed oligos were used for molecular cloning. For the chaining miRNA was removed from one of the plasmids by double restriction digest. The digest was electrophoresed on agarose gel and the band for the miRNA was excised and purified as described above. The other plasmid was linearised by digestion and excised miRNA ligated in. The ligation was then transformed into *E. coli.* Colonies were inoculated and plasmid purified as described before. The functionality of the chained miRNA plasmid was checked via cell transfection and western blotting.

miRNAs were initially chained in pcDNA6.2 and later the cassette was transferred to pcDNA5/FRT via subcloning.

2.2.3. QuickChange® site-directed mutagenesis

QuickChange site-directed mutagenesis approach was used to introduce mutations (base substitutions). A high-fidelity DNA polymerase such as PfuTurbo® (Stratagene) was used to amplify vector DNA. The primers used for this amplification contain the desired mutation so that it is incorporated into the PCR product. Vector DNA was then

digested using DpnI to degrade methylated template DNA. DNA containing the base substitutions was then transformed into *E. coli* DH5α cells followed by inoculation, miniprep, spinprep and sequencing as explained in Section 2.2.2. The following tables (Tables 2.9 and 2.10) show the concentrations used for the PCR and the appropriate thermal cycler program.

Table 2.9 PCR protocol for use of PfuTurbo DNA polymerase in QuickChange procedures.

PfuTurbo DNA Polymerase PCR	
50 ng	Plasmid DNA
125 ng	Forward primer
125 ng	Reverse primer
5 µl	10X dNTPs (2 mM each)
5 µl	10X PfuTurbo Buffer
4 µl	DMSO
1 µl	PfuTurbo DNA polymerase (3U)
Up to 50 µl	ddH2O

Table 2.10 PCR program for PfuTurbo DNA polymerase PCR.

PCR Program for PfuTurbo		
Heated Lid	110°C	
Temperature Step	95°C	30 s.
Start Cycle	26x	
Temperature Step	95°C	30 s.
Temperature Step	55°C	1 min
Temperature Step	68°C	15 min
End Cycle		
Temperature Step	68°C	10 min
Hold	10°C	Infinite

PCR product was digested with 1 µl DpnI (10 U Roche) for 1 hour at 37°C. 10 µl were then transformed into *E. coli* DH5α. Colonies were inoculated into growth media and analysed via Miniprep and positive clones subjected to higher-purity Spinprep (QIAGEN) followed by sequencing.

2.2.4. Protein expression and purification

2.2.4.1. In bacteria

2.2.4.1.1. Protein expression

DNA plasmid containing desired insert was transformed in *E.coli* BL21 RP cells. Colonies were then inoculated in 50 ml terrific broth media (TB) supplied with appropriate antibiotic and grown overnight shaking at 37°C. 750 ml TB (with antibiotic)

was inoculated with overnight culture to an optical density OD_{600} = 0.05. Cells were grown at 37°C shaking until reaching OD_{600} = 0.7 followed by induction of protein expression via the addition of 400 µM Isopropyl β-D-1-thiogalactopyranoside (IPTG). Cells were then incubated shaking at room temperature overnight.

2.2.4.1.2. Protein purification

Induced overnight bacterial culture was centrifuged at 17,000 xg for 15 min at 4°C. 0.3 g cell pellet was then resuspended in 1 ml IP Lysis Buffer for GST-tagged proteins (50 mM HEPES at pH 7.4, 150 mM NaCl, 1x DTT, 0.5% v/v Triton-X100, 1 mM EDTA) or Cobalt Loading Buffer for GB1-tagged proteins (50 mM Tris, 1 M NaCl, 0.5% v/v Triton X-100) supplied with 20 µl PMSF (1 M; phenylmethylsulfonyl fluoride) and 20 µl 50X Sigmafast™ Protease Inhibitors Cocktail. Bacterial pellet was sonicated 3 times (30 s. breaks inbetween) for 5 s. at 100% Amplitude. Lysate was centrifuged for 5 min at 17,000 xg, 4°C. Supernatant was then incubated with appropriate 40 µl (slurry) pre-washed beads for 1 hour. Column was washed 5 times with IP Lysis Buffer (GST) or Cobalt Wash Buffer (GB1; 50 mM Tris, 1 M NaCl, 5 mM Imidazole) and eluted in 50 µl elution buffer (GSH Elution Buffer for GST-tag – 50 mM Tris at pH 7.5, 50 mM NaCl, 40 mM reduced Glutathione; Cobalt Elution Buffer for GB1-tag – 20 mM Tris, 500 mM NaCl, 200 mM Imidazole).

For Urea purification, bacterial pellet with GB1-tagged proteins were first resuspended and sonicated in Cobalt Loading Buffer as normal. Pellet after sonication was then resuspended in Urea Loading Buffer (0.5% v/v Triton X-100, 50 mM Tris at pH 8, 500 mM NaCl) and left shaking for 1 hour at room temperature. Samples were centrifuged for 15 min at 17,000 xg, room temperature. Supernatant was then loaded on pre-washed with Urea Loading Buffer cobalt beads and left shaking for 1 hour.

Supernatant was eluted and column was washed 4 times with Urea Wash Buffer (0.5% v/v Triton X-100, 50 mM Tris at pH 8, 500 mM NaCl, 5 mM Imidazole). Protein was eluted via washing the column three times with Urea Elution Buffer (0.5% v/v Triton X-100, 50 mM Tris at pH 8, 500 mM NaCl, 200 mM Imidazole).

2.2.4.1.3. Protein dialysis

5 ml of Urea-purified recombinant protein at a concentration 0.5 µg/µl was dialysed in 2 L 1X RNA Binding Buffer (15 mM HEPES at pH 7.5, 5 mM $MgCl_2$, 0.05% v/v Tween 20, 10% v/v glycerol) supplied with 100 mM NaCl and solubilising agents such as charged amino acids 5 mM Arg/Glu and 1 mM EDTA. After dialysis the protein was centrifuged for 1 min at 17,000 xg and supernatant was then dialysed again in the same buffer (fresh). Finally, dialysed protein was centrifuged for 1 min at 17,000 xg and protein concentration was quantified via Bradford assay.

2.2.4.2. In human cells

Human embryonic kidney cells (HEK293T) were cultured in Dulbecco's Modified Eagle Medium (DMEM; Sigma-Aldrich) supplied with 10% Foetal Calf Serum (FCS; Sigma-Aldrich) and 1% Penicillin Streptomycin (Penstrep; Lonza).

Cells were seeded on different plates depending on the nature of the assays. For general culturing and maintenance – T75 Nunc flask (ThermoFisher); pull-down assay – Nunc 10 cm plates (ThermoFisher); functional assessment of knockdown plasmid – 24-well plate; fluorescence work – 24-well plate with glass coverslips or black-walled 96-well plate (Greiner); ATP assay – white-walled 96-well plate (Greiner).

HEK293T cells were seeded as follows:

10 cm plate – 2,000,000 cells in 15 ml media

24-well plate – 50,000 cells in 500 µl media per well

24-well plate with coverslips – 10-20,000 cells in 500 µl media per well

2.2.4.2.1. Protein expression/cell transfection

Cells were transfected with a mix of plasmid DNA, transfection reagent (PEI – polyethylenimine from Sigma) and reduced serum media 24 hours after seeding as follows:

Table 2.11 Protocol for human cell transfection with PEI.

10 cm	24-well	24-well with coverslips
18 µg DNA	700 ng DNA	500 ng DNA
60 µg PEI	1.75 µg PEI	1 µg PEI
500 µl Opti-MEM®	50 µl Opti-MEM®	50 µl Opti-MEM®

2.2.4.2.2. Cell lysis

Cells were lysed 48 hours post-transfection. Media was removed followed by PBS wash. Cells were scraped and lysed for 12 min in 100 µl (24-well) or 500 µl (10 cm) IP Lysis Buffer (150 mM NaCl, 1 mM EDTA, 1 mM DTT, 0.5% v/v Triton X-100, 50 mM HEPES, 10% v/v Glycerol, pH 7.5). Samples were centrifuged for 5 min at 17,000 xg at 4°C. Supernatant was stored at -20°C.

2.2.4.3. Protein analysis

Protein concentration in human cell lysate was quantified via Bradford assay. Briefly, 3-5 µl lysate was added to 1 ml Bradford mix (Bradford reagent : water = 1:4; BioRad).

The concentration was measured at OD_{595}. 20-30 µg protein was used for protein gels.

2.2.4.3.1. Sodium Dodecyl Sulphate Polyacrylamide Gel Electrophoresis (SDS-PAGE)

Proteins were resolved on SDS-PAGE gel based on their apparent molecular mass.

Proteins were mixed with 4X Loading Buffer (200mM Tris.Cl at pH 6.8, 400mM DTT, 8% w/v SDS, 0.4% w/v bromophenol blue, 40% v/v glycerol) and heated for 5 min at 95°C. 20 µl was then loaded on an appropriate percentage gel and electrophoresed for 30 min at 50 V followed by ~1.5 hours at 100 V. Protein marker (BLUeye Prestained Protein Ladder; Geneflow) was also loaded for size reference. Gel was then either stained in Coomassie brilliant blue solution (50% v/v methanol, 40% v/v H_2O, 10% v/v glacial acetic acid, 0.1% w/v Brilliant Blue R-250) (for proteins expressed in bacteria and pull-down assays) or used for western blotting.

2.2.4.3.2. Western blotting

Proteins were transferred from gel to a nitrocellulose membrane using Bio-Rad Dry Western Blotting System via application of electric field (0.15 A for 1 hour). Membrane was blocked in milk solution (5% w/v Marvel powdered skimmed milk in 1X TBST) to reduce background unspecific binding of antibodies to proteins. Blocked membrane was then probed with a primary antibody for 1 hour followed by five washes with 1X TBST. It was next probed with appropriate secondary HRP-conjugated antibody for 30 min and washed five times with 1X TBST. Membrane was incubated with ECL solution for 1 min and imaged using Genius:BOX (G:BOX).

2.2.5. Pull-down assays

Pull-down assay is a method used in the assessment of protein:protein interactions. Briefly, a tagged protein (bait) expressed in bacteria or human cells is immobilised onto beads that bind the tag. Reticulocyte lysates with expressed protein of interest or recombinant purified protein are added to the column. Interacting proteins (prey) bind to the immobilised protein and elute together in the final step. Samples can be analysed on a gel or by western blotting and either identify binding partners or confirm/reject interaction between the immobilised protein and a protein of interest.

Bait protein was expressed and purified as described. Instead of eluting the protein immobilised on beads during purification, the column was washed with appropriate Lysis Buffer and incubated with whole-cell extract or purified recombinant protein for 1 hour. RNase was added to some samples to test for RNA-mediated interactions. Beads were then washed 5 times with Lysis Buffer. Elution buffer was added to the beads and left inverting for 12 min. Beads with bound proteins were centrifuged for 1 min at 500 xg. Supernatant containing interacting proteins was analysed via SDS-PAGE followed by staining or western blotting.

2.2.5.1. TnT® coupled reticulocyte lysate system

The TnT® Coupled Reticulocyte Lysate System (Promega) is a cell-free expression system that couples T7 RNA polymerase transcription of plasmid DNA and their translation. The reticulocyte system was used for the purposes of pull-down assay. The reaction mixture protocol can be found in Table 2.12.

Table 2.12 Protocol for expressing plasmid DNA in reticulocyte lysates.

TnT® Coupled Reticulocyte Lysate System	
12.5 µl	Reticulocyte lysate mix
1 µl	TnT Buffer
0.5 µl	T7 RNA polymerase
0.5 µl	Minus Methionine AA mix
1 µl	^{35}S-Methionine
0.5 µl	RNase Inhibitors
0.5 µg	DNA template
Up to 25 µl	Nuclease-free H_2O

Samples were incubated for 1.5 hours at 30ºC. 20 µl reticulocyte reaction was added to immobilised bait protein for pull-down assay as described.

Resulting SDS-PAGE gels were stained with Coomassie brilliant blue followed by destaining and vacuum-drying. The dried gel was then exposed on a screen and picture was developed using Typhoon FLA 7000 (GE Healthcare).

2.2.6. RNA-binding assay (RNA UV-crosslinking)

RNA UV-crosslinking is an *in vitro* approach used to test direct binding of proteins and RNA. Briefly, custom RNA is radiolabelled and incubated with purified recombinant

protein. The reaction mixture is subjected or not to UV-crosslinking which results in covalent bonding between interacting at near distances protein and RNA. Samples are then analysed via SDS-PAGE and phosphoimaging to detect for radioactive signal indicating interaction with RNA. Due to the small size of custom RNA used the protein bands expected on the gel are not different from the actual protein size.

RNA was radiolabelled on ice following the protocol in Table 2.13. The reaction mixture was incubated for 1 hour at 37°C.

Table 2.13 RNA labelling protocol.

RNA Radiolabelling	
1.5 µg	Custom RNA (5xAAAAUU or 5xGGGGCC)
3 µl	10X T4 PNK Forward Buffer
1 µl	T4 PNK Enzyme
0.5 µl	RNase Inhibitors
2 µl (approx. 1 MBq)	γ[^{32}P]-ATP
Up to 30 µl	ddH2O

RNA was phenol-extracted, precipitated and washed as described in Section 2.2.1.1. RNA pellet was resuspended in 20 µl ddH$_2$O.

For the UV-crosslinking, 600 ng of protein was incubated with 1 µl radiolabelled RNA in 1X RNA Binding Buffer (15 mM HEPES pH 7.9, 100 mM NaCl, 5 mM MgCl$_2$, 0.05% v/v Tween 20, 10% v/v glycerol) (25 µl final volume) for 20 min at room temperature.

Reactions were further incubated on ice for 20 min followed by UV-irradiation for 10 min. 8 μl of 4X Loading Buffer was added to the reactions and boiled at 95°C. 20 μl were then loaded on a gel and electrophoresed. The gel was stained with Coomassie brilliant blue. It was then destained and vacuum-dried followed by exposure and developing of the image using Typhoon FLA 7000 (GE Healthcare).

2.2.7. ATP measurement assay

Day 1

Cells were seeded onto white-walled 96-well plates at density of 13-15,000 cells/well. At least 12 wells were seeded for each cell line. To half of the wells was added tetracyclin at final concentration 1 μg/ml. Cells were cultured in DMEM medium supplied with selective antibiotics (hygromycin/blasticidin) for 48 hours.

Day 3

Medium from each well was replaced with new media replenishing tetracyclin. Each cell line was cultured in glucose or galactose media for further 24 hours.

Day 4

ATPlite Luminescence ATP Assay Detection kit from Perkin Elmer was used following manufacturer's instructions. Wells were washed with sterile PBS once and left in 100 μl PBS afterwards. 50 μl ATP lysis buffer was added (ATPlite kit, Perkin Elmer) and plate was incubated for 5 min on an orbital shaker at room temperature. This was followed by the addition of 50 μl ATP Substrate and further 5 min on the shaker. Plate was then transferred into a dark box and incubated further for 10 min. Luminescence signal was detected using FLUOstar Omega microplate reader (BMG Labtech).

A cell proliferation assay was performed to account for cell number in each well.

2.2.8. CyQUANT NF cell proliferation assay

The kit was purchased from ThermoFisher Scientific. Dye reagent was diluted 1:1,000 in sterile PBS. 50 µl of diluted dye was added to each well. Plate was agitated briefly on an orbital shaker. It was then covered in aluminium foil and incubated for 1 hour at 37°C. Fluorescent signal was measured using FLUOstar Omega microplate reader (BMG Labtech).

ATP measurement values were divided by the values obtained from the CyQUANT assay to normalise results to cell number.

2.2.9. RNA Fluorescent *In Situ* Hybridisation (FISH)

48 hours post-transfection cells were washed three times with sterile PBS. Cells were then fixed with 300 µl fix solution (4% PFA, 0.2% Triton X-100) for 20 min at room temperature. This was followed by three PBS washes. Glass coverslips were removed from plate and placed on 3 mm Whatman paper in a petri dish. 80 µl hybridisation mix (20% v/v formamide, 2X SSC, 10% w/v dextran sulphate, 1% w/v BSA, 4 µl ssDNA (salmon sperm), 1 µg/ml Cy3 oligo(dT)) was added to each coverslip. Dish was wrapped in cling film and aluminium foil and incubated for 2.5 hours at 37°C. Next, coverslips were returned to plate and washed three times with PBS. They were then blocked for 20 min at room temperature with 300 µl PBS with 2% w/v BSA. This was followed by incubation in 100 µl primary antibody (at appropriate concentration diluted in PBS) for 1 hour in the dark. Coverslips were washed three times with PBS and secondary Alexa antibody was added. They were incubated for 30 min – 1 hour in the dark. Next, secondary antibody was removed and

they were incubated in Hoechst for 10 min. Coverslips were washed three times with PBS and mounted onto glass slides using 5-7 µl Dako mounting medium (Agilent).

2.2.10. MTT cell proliferation assay

30,000 HEK293T cells were seeded per well onto a 24-well plate (Greiner) in DMEM medium. 24 hours post-plating non-inducible cells were transiently transfected. Stable inducible cell lines were induced with tetracyclin. 48 hours post-transfection, MTT assay was carried out. At the same time media of induced cells was changed, replenishing Tet and introducing galactose for 24 hours prior to assay.

For the proliferation assay, MTT was added to each well to a concentration of 0.5 mg/ml. Cells were incubated for 1 hour at 37°C. Next, lysis buffer (20% w/v SDS, 50% v/v dimethylformamide) was added at 1:1 ratio. This was thoroughly mixed by pipetting. Plate was wrapped in aluminium foil and incubated for 1 hour on an orbital shaker. Colourimetric signal was measured using FLUOstar Omega microplate reader (BMG Labtech).

2.2.11. FLAG Co-Immunoprecipitation (CoIP)

HEK293T cells were seeded on 10 cm culture dishes (Nunc). Cells were co-transfected on the following day with gene of interest/control and 13myc-TAP/NXF1. 48 hours post-transfection cells were washed with ice-cold PBS and lysed in IP Lysis buffer supplied with PIC and PMSF for 10 min. They were passed through a 21G needle 10 times prior to centrifugation for 5 min at 17,000 xg, 4°C. Protein concentrantation was determined and diluted to 1.5 mg/ml. 50 µl Anti-FLAG M2 agarose beads (Sigma) were blocked in IP Lysis buffer with 2% BSA, washed and

incubated with cell lysates (20 µl lysate was kept for input gel) in the presence of 10 µg/ml RNase A (Sigma). Samples were incubated rotating for 1.5 hours at 4°C. Beads were washed with PBS three times and protein was eluted in 60 µl FLAG elution buffer (1:20 FLAG peptide in IP Lysis buffer, Sigma) rotating for 1 hour at room temperature. Samples were centrifuged for 1 min at 17,000 xg. Eluates were resolved on 12% SDS-PAGE gels. Two gels were used, one for input protein samples and one for CoIP eluted protein. Western blotting was carried out as explained in Section 2.2.4.3.2.

2.2.12. Messenger Ribonucleoprotein (mRNP) capture assay

Cells were seeded and transfected as explained in section 2.2.11. Two plates per condition were used. One of the dishes was UV-crosslinked on ice in 1 ml DEPC-PBS at 0.3 J/cm^2. Both plates were then lysed in 500 µl lysis buffer (50 mM Tris.HCl at pH 7.5, 100 mM NaCl, 2 mM MgCl$_2$, 1 mM EDTA, 0.5% v/v Igepal C9-630 (NP40), 0.5% w/v Na-deoxycholate) supplemented with PIC and RiboSafe RNase inhibitor. Cells were then centrifuged for 5 min, 17,000 xg, 4°C. Protein concentration was determined and diluted to 2 mg/ml. Cell lysate was mixed with 2X Binding buffer (20 mM Tris.HCl at pH 7.5, 1 M NaCl, 1% w/v SDS, 0.2 mM EDTA) in 1:1 ratio. Leftover lysate was kept for input gel. Samples were then incubated with 25 µg oligo(dT) beads rotating for 1 hour at room temperature. Beads were washed three times with 1X Binding buffer and protein was eluted in 50 µl Elution buffer (10 mM Tris.HCl at pH 7.5, 1 mM EDTA) supplemented with 1 µg/ml RNase A for 30 min at 37°C. Samples were centrifuged for 1 min at 17,000 xg and protein resolved on 12% SDS-PAGE gel. Two gels were electrophoresed – input and mRNP capture. Western blot was carried out as explained in Section 2.2.4.3.2.

2.2.13. RNA Immunoprecipitation (RIP) assay

HEK293T cells were seeded on 10-cm dishes and transfected 24 hours later. 48 hours post-transfection, formaldehyde (36% stock, Sigma) was added to cells to a final concentration of 1%. Formaldehyde crosslinks interacting proteins and nucleic acids. Plates were incubated on an orbital shaker for 10 min at room temperature. The reaction was quenched upon the addition of 250 mM glycine and incubated on the shaker for further 5 min. Cells were then washed with DEPC-PBS on ice and lysed in 500 µl IP lysis buffer supplemented with PIC and RiboSafe. Cells were scraped and passed through a 21G needle followed by incubation on ice for 5 min. Samples were centrifuged for 5 min at 17,000 xg, 4°C. Protein concentration in cell lysate was measured and samples were diluted to 1 mg/ml. 50 µl was kept for total RNA extraction. The rest was incubated overnight with 50 µl pre-blocked anti-FLAG M2 agarose beads (blocked with 2% w/v BSA and 5 µl/ml salmon sperm DNA) at 4°C. Following this, samples were washed three times with IP lysis buffer. Proteins were eluted and reverse-crosslinked using 120 µl denaturing buffer (EZ-RNA isolation kit, Biological Industries) for 1 hour at 70°C (gently agitating samples every 10 min). Input samples kept for total RNA were treated in the same way. After centrifugation of agarose beads for 1 min at 500 xg, 100 µl supernatant was mixed with 300 µl PureZOL and RNA extracted as outlined in 2.2.15. Quantitative PCR was performed with the synthesised cDNA (2.2.15 and 2.2.16).

2.2.14. Building stable inducible cell lines

HEK293T FRT T-Rex cells were seeded on 10 cm dish at 1×10^6 in 15 ml DMEM (10% v/v Tetracycline-Free FBS (Sigma), 1% v/v Penstrep) with the addition of blasticidin (antibiotic concentrations in Table). 24 hours post plating cells were co-transfected with 10.8 µg pGKFLPobpA, 7.2 µg pcDNA5/FRT/FLAG-GOI using 50 µg PEI and 1 ml Opti-MEM (Gibco). Cells were left at 37°C for further 48 hours before being split into three 10 cm plates. Each dish of cells was supplied with 10 ml of a mix (1:1) of Fresh and Conditioned DMEM without antibiotics. Hygromycin and blasticidin were added on following day and cells were cultured for another 7 days. During this week cells that have not incorporated the GOI at the FRT site did not acquire Hygromicin resistance therefore they started to die. After 7 days all media was changed with 50/50 mix DMEM with antibiotics and cells were left in culture incubator for further 7 days. A week later, individual surviving colonies comprised of >100 cells were transferred to a single well on a 24-well plate. They were initially cultured in 50/50 mix media with antibiotics. The medium was changed every 3-4 days with fresh DMEM medium with antibiotics until cell reached ~90% confluency. 4/5th of each confluent well was transferred to a 6-well plate in fresh DMEM with Hyg/Blast. 1/5th was left in the same well and cultured in fresh DMEM with Hyg/Blast while the remaining 1/5th was transferred to a new well on the same 24-well plate and supplied with fresh DMEM with zeocin and blasticidin. Culturing medium was changed every 3-4 days using appropriate antibiotics. Cells that did not start to die in the presence of zeocin were discarded and deemed as unsuccessful indicating no integration of GOI at the FRT site. Colonies that have reached confluency on the 6-well plate and have started to die in zeocin were further expanded onto 10 cm dishes. Once that dish reached confluency, 9/10th of cells were frozen down in Tet-free FBS with 10% v/v DMSO. The rest of cells were cultured further and used to functionally test the inetegration of

GOI after induction with tetracyclin for 72 hours. Successful colonies were selected for further experiments.

2.2.15. Total/cytoplasmic RNA extraction and cDNA synthesis

For the extraction of total and cytoplasmic RNA, $1x10^6$ cells were seeded on each of two 10-cm dishes per cell line. Cells were induced with tetracyclin 24 hours post-transfection and it was replenished 48 hours later. Media was changed to galactose when required and 24 hours before RNA extraction. At 72 hours of induction, cells were lysed and RNA isolated.

2.2.15.1. Total cell lysis

One 10-cm dish (per cell line) was washed with DEPC-treated PBS. 400 µl 1X Reporter lysis buffer (Promega) with PIC and RiboSafe was added and cells were scraped and transferred to a pre-chilled microcentrifuge tube on ice.

2.2.15.2. Cytoplasmic (cyto) cell fractionation

The rest of plates were washed with DEPC-treated PBS. 1 ml DEPC PBS was added to each plate and cells were detached gently using a cut tip (to avoid cell membrane disruption). Cells were transferred to pre-chilled microcentrifuge tubes and centrifuged for 4 min, 400 xg, 4°C. Supernatant was removed and cell pellet was washed quickly in hypotonic buffer (10 mM HEPES at pH 7.9, 1.5 mM $MgCl_2$, 10 mM KCl, 0.5 mM DTT). Cell pellet was then resuspended in 400 µl hypotonic buffer with PIC and Ribosafe. This was carried out by gently pipetting with cut pipette tip until cells were fully suspended followed by incubation for 8 min on ice. Samples were centrifuged for 3 min, 1,500 xg, 4°C. Supernatant was transferred to a new tube and

centrifuged for 8 min, 3,500 xg, 4°C. Supernatant was transferred again to a new tube and centrifuged for 1 min, 17,000 xg, 4°C.

2.2.15.3. Western blotting

15 µl of leftover samples (total cell lysates were centrifuged and supernatant used) was resolved on 12% SDS-PAGE gels followed by western blotting. Membranes were probed for the presence of nuclear marker and respectively its absence in the cytoplasmic fraction.

2.2.15.4. RNA extraction and isolation

250 µl of total and cyto samples were taken and mixed with 750 µl PureZOL (Biorad). The mix was incubated for 10 min at room temperature. Samples were centrifuged for 10 min, 17,000 xg, 4°C. To supernatants was added 200 µl chloroform and tubes were agitated vigorously for 20 s. Samples were incubated for 10 min at room temperature and then centrifuged for 10 min, 12,000 xg, 4°C. 500 µl top clear layer was transferred to a new tube and mixed with 55 µl 3M NaCl and 555 µl 100% isopropanol. 1 µl Glycogen was added to each sample, they were inverted ten times and left precipitating overnight at -20°C. On following day, tubes were centrifuged for 20 min, 17,000 xg, 4°C. Nucleic acid pellet was washed with 75% v/v ethanol and centrifuged for further 5 min, 17,000 xg, 4°C. Pellet was air-dried and resuspended in 12.5 µl DEPC-treated H_2O. Sample was DNase-treated by adding 2.5 µl 10X DNase I incubation buffer (Roche) and 0.5 µl DNase I enzyme (5 U) and incubation for 30 min at 37°C. This was followed by enzyme inactivation at 75°C for 10 min.

2.2.15.5. cDNA synthesis

Concentration of extracted RNA was determined using NanoDrop 1000 (ThermoFisher). 1-2 µg RNA was used for cDNA synthesis. Priming premix (RNA, 1 µl 40 µM random hexamers (dN_6), 1 µl 10 mM dNTPs, DEPC H_2O up to 13.5 µl) was incubated at 70^oC for 5 min followed by immediate incubation on ice for 1 min. To premix was added 4 µl 5X First Strand buffer, 2 µl 0.1 M DTT and 1 µl M-MLV reverse transcriptase (RT; 200 U) (all reagents from Invitrogen). Samples were incubated for 10 min at 25^oC, followed by 60 min at 42^oC and 5 min at 85^oC. cDNA reactions were diluted by adding 40 µl DEPC H_2O and stored at -20^oC until required.

2.2.16. Quantitative PCR (qRT-PCR)

Forward and reverse qPCR primers were mixed and diluted to 5 µM each. Each qPCR reaction consisted of 1 µl cDNA, 1 µl primer pair mix, 3 µl DEPC H_2O, 5 µl Brilliant III Ultra-Fast SYBR® Green QPCR Master Mix (Agilent). Samples were used in duplicates. 2-step qPCR was carried out with 60^oC annealing temperature and 45 cycles. QPCR machine used was CFX96 Touch^{TM} Real-Time PCR Detection System (BioRad). Ct values for each target gene were normalised to the corresponding U1 Ct producing dCt. Relative concentrations were calculated using the equation 1/(2^dCt).

2.2.17. Immunocytochemistry

Medium was removed from wells. Cells were washed with sterile PBS three times. Cells were then fixed in 4% PFA for 10 min. They were then permeabilised and blocked with 0.05% v/v Triton X-100 and 5% v/v horse serum in PBS for 45 min at room temperature. Wells were washed three times with PBS and incubated with primary antibody in PBS with 5% horse serum overnight at 4^oC. Cells were washed

with PBS three times followed by incubation in secondary Alexa antibody in PBS with 5% horse serum for 1 hour at room temperature. PBS with antibodies was removed and Hoechst was added to each well for 1 min. Cells were washed three times with PBS and left in 100 µl PBS and wrapped in aluminium foil before proceeding with imaging.

Non-confocal images and confocal Z-stacks were taken using PerkinElmer Opera Phenix™ High Content Screening System.

2.2.18. Assessing protein colocalisation

Colocalising proteins were assessed using Harmony High-Content Imaging and Analysis software by PerkinElmer. Parameters used in the analysis included cell number based on nuclei detected; number of nuclear spots and results were reported as the incidence of one spot to colocalise with another spot and *vice versa*.

2.2.19. HEK293T Flp-In T-REx reprogramming to induced neural progenitor cells (iNPCs)

150,000-200,000 cells per well were seeded onto 6-well plate (Greiner) in DMEM (Tet-free FBS). 24 hours after seeding, they were transduced with three lentiviral vectors carrying genes for Oct3/4, Sox2 and Klf-4 at MOI (multiplicity of infection) 4-7. Vectors were then withdrawn 12 hours after transduction. Cells were washed with PBS 48 hours post induction and media changed to NPC medium (DMEM/F-12 Glutamax, 1% N2, 1% B27) supplemented with 20 ng/ml FGF-b and 20 ng/ml EGF and 5 µg/ml Heparin. Cells were cultured in these conditions for further two weeks replenishing media every 4-5 days. Cells were then assessed for the expression of

neural progenitor markers such as Nestin and Pax6. Upon confirmation of marker expression EGF and Heparin were withdrawn and FGF-b concentration was increased to 40 ng/ml. Cells were cultured on 10 cm dishes (Nunc) pre-coated for 5 min with 5 µg/ml human plasma fibronectin purified protein. Cells were maintained in culture for ~30 passages.

2.2.20. Statistical analysis

Statistical analyses were carried out using GraphPad Prism 7 using non-parametric *t*-Test, One-way or Multiple ANOVA. Error bars in each graph represent SEM.

3. Activity and role(s) of the putative RNA-binding domain of PGC-1[alpha]

3.1. Introduction

Computational analysis of the primary protein structure of PGC-1[alpha] revealed the presence of an RNA recognition motif (RRM) in the C-terminal region (aa 677-709) (Puigserver et al., 1998). The putative RNA-binding domain is linked to a predicted unstructured region rich in arginines and serines (RS-rich region). This is a typical structural conformation for RS-rich splicing factors (SRSF family of proteins). Splicing factors have been shown to interact with the hyperphosphorylated C-terminal domain of RNA polymerase II. Similarly, it has been shown that PGC-1[alpha] co-immunoprecipitates with RNA pol II and some splicing factors such as SC-35 (SRSF2), SRp40 (SRSF5), SRp55 (SRSF6) and SRp75 (SRSF4) (Monsalve et al., 2000). *In vitro* assays indicated a role of PGC-1[alpha] in the splicing of reporter constructs that are under the control of a PGC-1[alpha]-activated promoter, indicating that PGC-1[alpha] may be implicated in the splicing of transcripts it co-transcriptionally activates. This suggests a role of PGC-1[alpha] in mRNA processing, albeit it remains uncharacterised at the cellular level. Nevertheless, mutation studies demonstrated that deletion of the RRM or RS regions affects interactions with splicing factors and RNA polymerase II confirming the physiological importance of these domains (Monsalve et al., 2000).

Despite the work by Monsalve et al., little is known about the role and cellular importance of the carboxyl-terminal domain of PGC-1[alpha]. Answering this question should be a priority in future research as interestingly some isoforms lack this domain

(Martínez-Redondo et al., 2015). There is also no evidence to date whether PGC-1[alpha] is capable of directly binding RNA or whether it only serves a function to recruit the RNA polymerase II complex during mRNA processing.

This chapter aims to answer these fundamental questions and 1) investigate whether PGC-1[alpha] binds RNA directly, 2) potentially determine the minimal RNA-binding site and 3) test whether the loss of its RNA-binding activity affects the overall function of the protein.

3.2. Generating plasmids of PGC-1[alpha] for use in coupled transcription/translation or mammalian expression systems

In order to assess the putative RNA-binding capacity of PGC-1[alpha], a series of plasmids allowing for expression of various protein regions were built using a previously engineered pET24b-GB1-6xHis expression vector. The vector is suitable for protein expression in *E. coli* RP cells and contains an N-terminal GB1 solubility tag and a 6xHis tag to assist with purification of the recombinant proteins. In addition to full-length (FL), five different deletion fragments of PGC-1[alpha] were produced in order to also determine the potential minimal RNA-binding site. N-terminal domain (aa 1-234), middle domain (aa 254-564), C-terminal domain (aa 565-798), RS-rich domain (aa 565-633), and RRM-containing domain (aa 634-798) (Fig.3.1.). They will be referred to as D1, D2, D3, RS and RRM respectively in the following text and chapters.
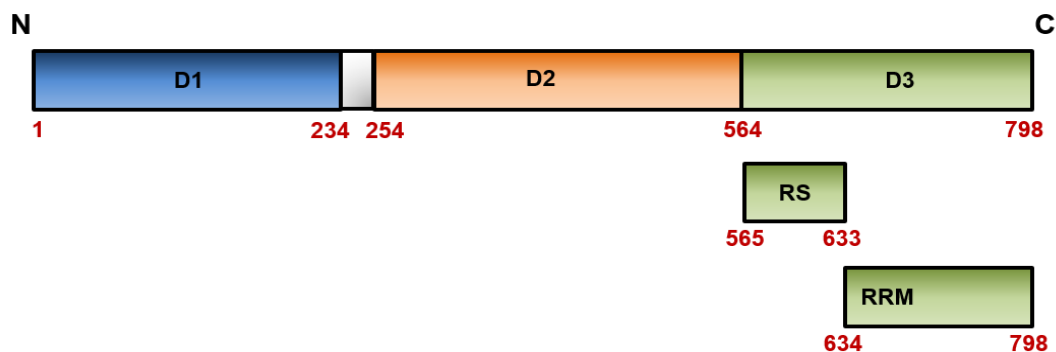
Figure 3.1 Schematic representation of PGC-1[alpha] deletion constructs.
Five deletion constructs were built to characterise the putative RNA-binding activity of PGC-1[alpha]. They encode: Domain 1 (D1; aa 1-234) the co-transcritional activation domain; Domain 2 (D2; aa 254-564), the phopho-regulatory domain; Domain 3 (D3; aa 565-798), the predicted RNA-binding domain; the Argenine/Serine-rich domain (RS; aa 565-633) and the RRM-containing domain (RRM; aa 634-798).

Each DNA insert was amplified by PCR and cloned from either total human cDNA for cloning the full length PGC-1[alpha] that was not commercially available, or a template plasmid following successful cloning of PGC-1[alpha] cDNA (example of PCR amplification in Fig.3.2.). Restricted PCR-amplified DNA fragments were ligated into the restricted bacterial expression vector using enzymes generating cohesive and compatible ends prior to transformation of the ligation reactions into *E.coli* DH5alpha cells. Grown bacterial colonies were then screened for plasmids containing DNA inserts of the right size (Fig.3.3.). This was followed by a large-scale preparation of the plasmids and Sanger sequencing to confirm the sequences of the engineered plasmids. Table 3.1. summarises the collection of newly-generated DNA plasmids used for the work described in this chapter.
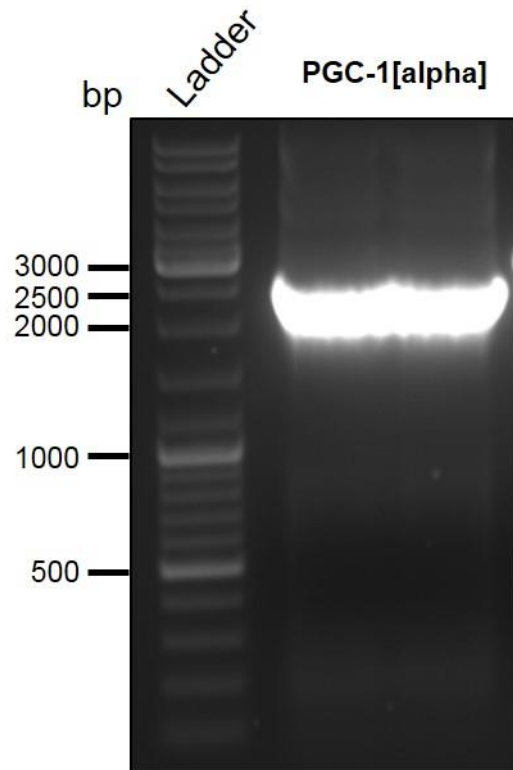
Figure 3.2 PCR amplification of full-length PGC-1[alpha] cDNA.

PGC-1[alpha] was amplified using cDNA synthesised from total human HEK293T RNA. The PCR product was resolved on a 2% agarose gel. The band is of the expected size (2400bp).
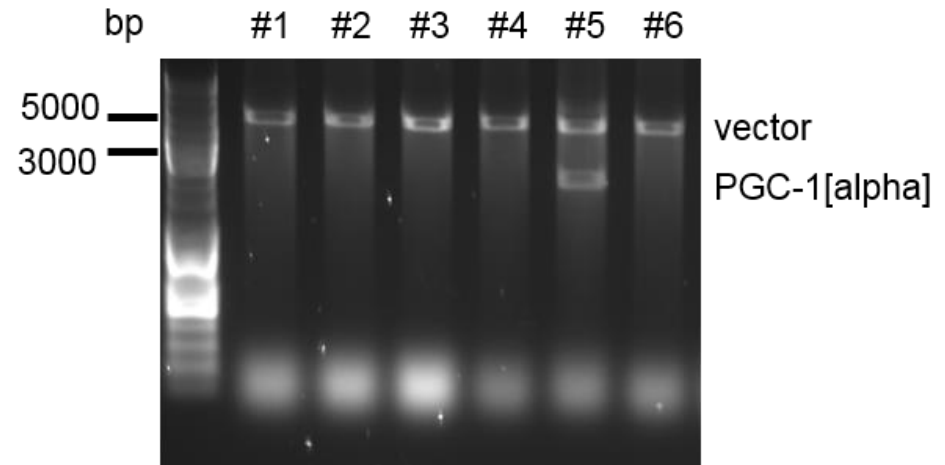
Figure 3.3 Bacterial colony screening for PGC-1[alpha] plasmid.

Ligation reactions (vector + DNA insert) were transformed into *E.coli* cells. Bacterial colonies were picked and plasmids purified. Only colony #5 shows two bands that representative for the vector backbone (higher) and PGC-1[alpha] (lower). Plasmidic DNA purified from this colony was taken further for Sanger sequencing.

Table 3.1 DNA plasmids generated for the experimental work in assessing the RNA-binding capacity of PGC-1[alpha].

Plasmid Construct	Vector Backbone	Tag	Cloning Strategy	Host Expression
PGC-1[alpha] 1-798 (FL)	pET24b	N-terminal – GB1 and 6xHis	PCR + NdeI/XhoI	bacterial
PGC-1[alpha] 1-234 (D1)	pET24b	N-terminal – GB1 and 6xHis	PCR + NdeI/XhoI	bacterial
PGC-1[alpha] 254-564 (D2)	pET24b	N-terminal – GB1 and 6xHis	PCR + NdeI/XhoI	bacterial
PGC-1[alpha] 565-798 (D3)	pET24b	N-terminal – GB1 and 6xHis	PCR + NdeI/XhoI	bacterial
PGC-1[alpha] 565-633 (RS)	pET24b	N-terminal – GB1 and 6xHis	PCR + NdeI/XhoI	bacterial
PGC-1[alpha] 634-798 (RRM)	pET24b	N-terminal – GB1 and 6xHis	PCR + NdeI/XhoI	bacterial
PGC-1[alpha] 1-798 (FL)	pcDNA5 FRT/TO	N-terminal 3xFLAG	PCR + BamHI/NotI	mammalian
PGC-1[alpha] miRNA1 (targeting D1)	pcDNA6.2	EmGFP	BLOCK-iT Kit	mammalian
PGC-1[alpha] miRNA2 (targeting D2)	pcDNA6.2	EmGFP	BLOCK-iT Kit	mammalian
PGC-1[alpha] miRNA3 (targeting D3)	pcDNA6.2	EmGFP	BLOCK-iT Kit	mammalian
PGC-1[alpha] miRNA1+2	pcDNA6.2	EmGFP	BLOCK-iT Kit	mammalian
PGC-1[alpha] WT complementation	pcDNA5/FRT/TO	N-terminal 3xFLAG	Section 3.3.	mammalian
PGC-1[alpha] ΔRS complementation	pcDNA5/FRT/TO	N-terminal 3xFLAG	Divergent PCR of WT	mammalian

3.3. Protein purification

pET24b-GB1-6xHis plasmids were transformed into *E. coli* RP cells and expression of recombinant PGC-1[alpha] proteins was induced by IPTG. Protein extracts were subjected to metal ion affinity chromatography (IMAC) onto cobalt-coated beads. D1 was readily soluble in comparison to the rest of the constructs which were present in inclusion bodies in the insoluble bacterial pellets being unable to be purified under native conditions (Fig.3.4.). These proteins were therefore solubilised and purified in denaturing conditions using buffers containing 8 M urea. Several attempts at gradual dialysis to remove urea proved unsuccessful leading to precipitation and almost complete loss of proteins in the form of insoluble aggregates. Moreover, full length PGC-1[alpha] protein was unable to express in bacterial cells (data not shown). Purity of each protein fragment was assessed on a 15% SDS-PAGE gel (Fig.3.5.). GB1-tagged recombinant proteins showed a high degree of purity and electrophoresed at the expected electrophoretic mobility size. The tag itself (GB1 6xHis) adds approximately 14.5 kDa to the protein weight.
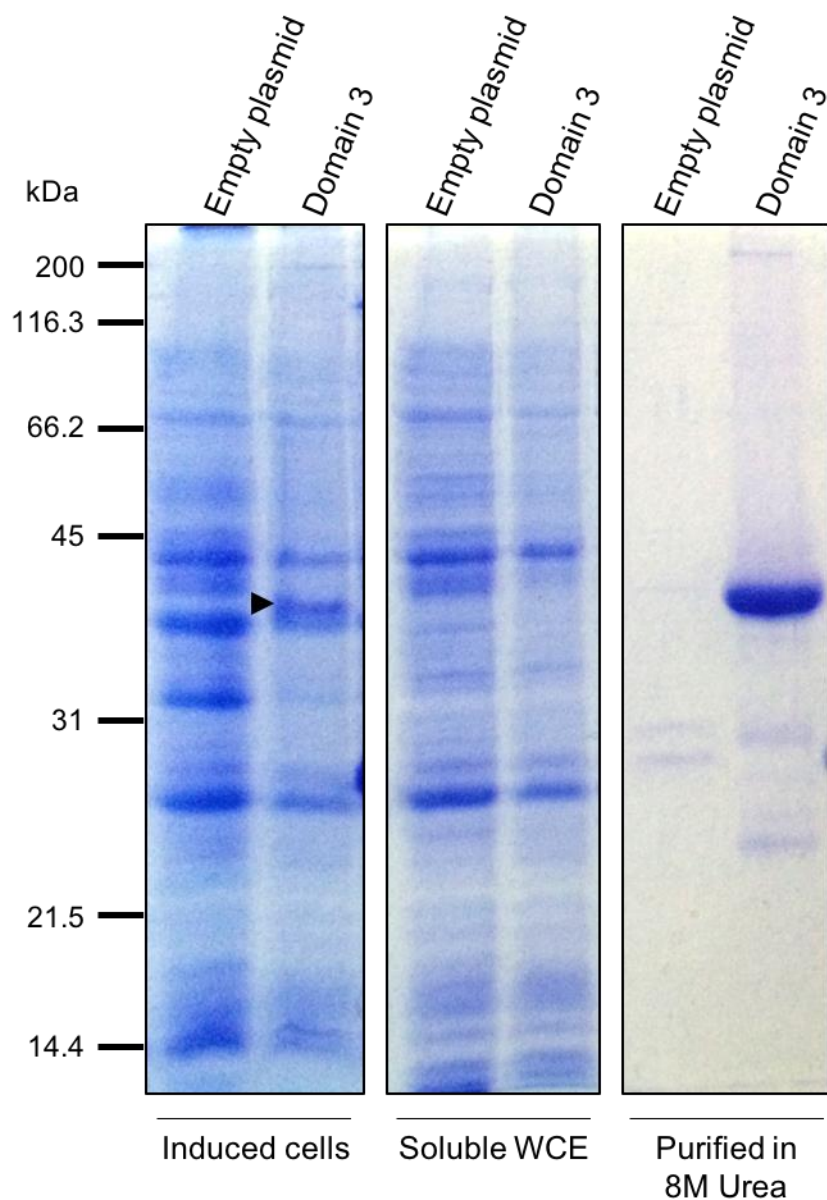
Figure 3.4 Coomassie-stained SDS-PAGE gel for analysis of protein purification.

Recombinant protein PGC-1[alpha] D3 aa565-798 was expressed in *E. coli* RP cells and purified. (Left) Induced total cell lysate shows expression of the protein (arrow). (Middle) In the soluble whole-cell lysate (WCE) the band disappears suggesting presence in the insoluble fraction in inclusion bodies. (Right) 8 M urea recovered the protein from the insoluble fraction. The resulting purified protein shows a high degree of purity sufficient for downstream analysis of the RNA-binding activity.
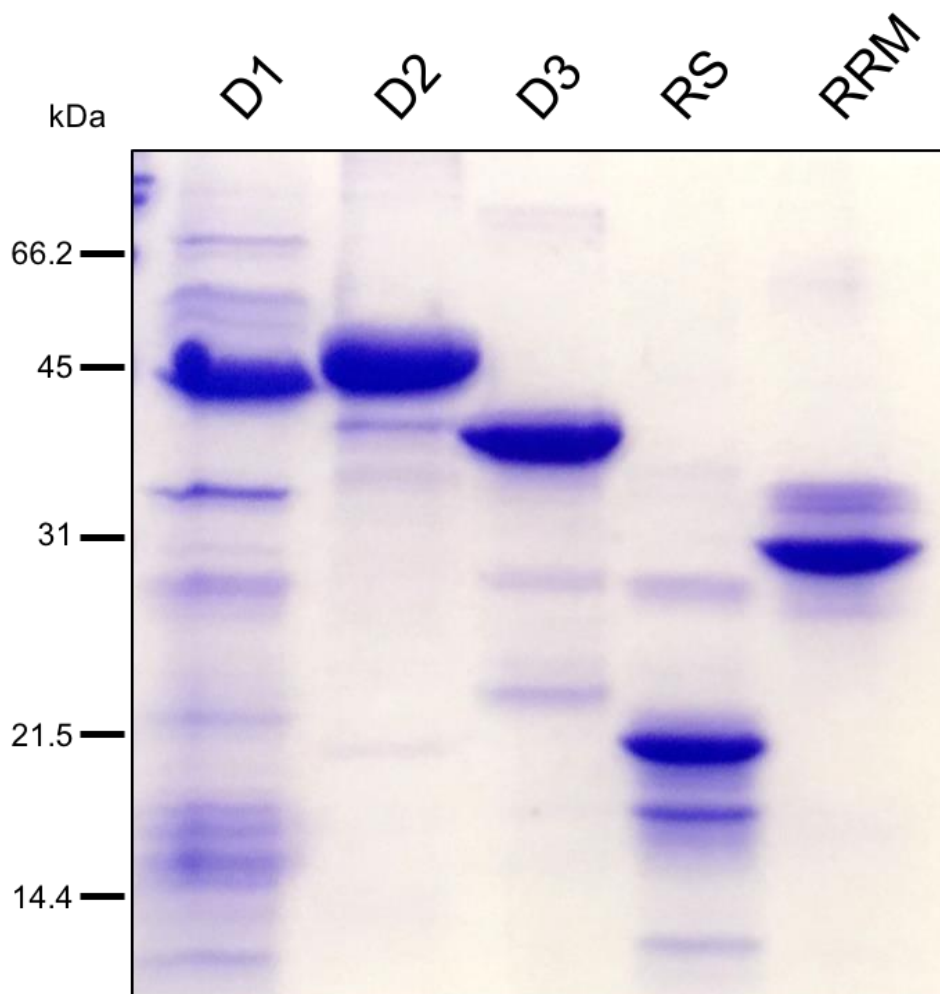
Figure 3.5 Coomassie-stained SDS-PAGE of purified recombinant proteins.
Resolving purified proteins on 15% SDS-PAGE shows high degree of purity and bands at the expected size. D1 (aa1-234) – 40.1 kDa; D2 (aa254-564) - 48.6 kDa; D3 (aa565-798) – 40.1; RS (aa565-633) – 22 kDa; RRM (aa634-798) – 32.5 kDa. All proteins were tagged with GB1 (13.5 kDa) and 6xHis (1 kDa). D1 was purified from the soluble bacterial extract while the remaining insoluble proteins were purified in denaturing conditions in presence of 8 M urea.

3.4. PGC-1[alpha] is capable of binding RNA directly

Since the potential RNA-binding activity of PGC-1[alpha] has not yet been investigated, the first aim was to design the RNA sequences that would be tested. Many RRM-containing proteins involved in the binding of multiple mRNA sequences have been shown to display poor or no RNA-binding specificity *in vitro* like ALYREF for example (Hautbergue et al., 2008) or semi-specific sequence binding like SRSF3 or SRSF7 (Hargous et al., 2006) and SRSF1 (Tintaru et al., 2007). Therefore, GC-rich and AU-rich RNA oligonucleotides were used to start testing the potential interaction of PGC-1[alpha] with RNA. RRM motifs typically bind 4-6 nucleotides and the RNA probes used in this assay were 20-30 nucleotides in length based on the fact that often there are additional interactions from the arginine-rich region. This has also been observed with nuclear export adaptors (Walsh et al., 2010).

In addition to the five PGC-1[alpha] deletion constructs, two control proteins were included. Magoh, a known component of the exon junction complex (EJC) which does not bind RNA (Bono et al., 2006) as a negative control; and ALYREF, the canonical mRNA nuclear export adaptor as a positive control (Hautbergue et al., 2008). For the binding reaction, each insoluble protein was diluted into the reaction buffer to decrease the final urea concentration to 200 mM. The same final concentration of urea was also added to the soluble D1 domain that was purified without urea. Rapid dilution of denatured protein in a final buffer that still contains some of the denaturant (<1 M urea or guanidine hydrochloride) allows bypass of the intermediate concentrations of denaturant (typically 2-4 M) that lead to high formation of intermolecular aggregation and misfolded proteins (Tsumoto et al., 2003; Yamaguchi and Miyazaki, 2014).

To carry out the protein:RNA UV-cross-linking assays, synthetic 30-mer $(GGGGCC)_5$ and $(AAAAUU)_5$ RNA oligonucleotides were 5'-end radiolabelled using $\gamma^{32}P$-ATP and polynucleotide kinase. The ^{32}P-labelled phosphate in position γ was incorporated into the phosphate group of the ribose. Purified protein domains were then incubated with the ^{32}P-radiolabelled RNA probes and subjected to UV exposure (or no exposure to serve as a negative control). UV cross-linking preferentially creates covalent bonds between the two closely juxtaposed aromatic rings of interacting aromatic amino acid moiety and RNA base. Upon loading of the reaction mixtures on SDS-PAGE, only the covalently UV cross-linked radiolabeled RNA:protein complexes remain associated. Interaction is detected when the Coomassie-stained protein bands covalently linked to the radiolabeled RNA and the radiolabelled signal show similar electrophoretic mobility.

First, D3, the putative RNA-binding domain, was incubated with both the $(GGGGCC)_5$ or $(AAAAUU)_5$ RNA probes to assess putative binding. Then, all deletion fragments were incubated with one of the probes to further define the minimal binding domain that interacts with RNA. Proteins were resolved on 15% SDS-PAGE gels and phosphoimage acquired. Coomassie gels show single bands for each construct indicating high purity and stability of the proteins. Due to the small size of the RNA probes no shift in bands is observed on either Coomassie gels or phosphoimages. ^{32}P signal is observed only in lanes where proteins interact with RNA and have been UV cross-linked. The signal can be observed at the size of the interacting protein construct.

No signal was observed for Magoh and the opposite for ALYREF as expected (Fig. 3.6.). This shows that the assay is functional and the presence of 200 mM urea does not affect the binding of the ALYREF control protein to RNA.

Top panel confirms direct binding of D3 to both AU-rich and GC-rich RNA probes as observed by the strong signal on the phosphoimage (Fig.3.6.). This indicates that D3 is capable of directly interacting with both GC- and AU-rich RNAs suggesting that PGC-1[alpha] is able to bind RNA without sequence specificity as reported for ALYREF and also shown here. Bottom panels show Coomassie-stained gels with input recombinant proteins and their purity and intactness. Subsequently, Fig.3.7. demonstrates that D1 and D2 do not bind RNA, serving as internal negative controls as both regions do not possess RNA-binding motifs. Again, signal was observed with D3 on the phosphoimage showing direct binding to RNA. Dissection of D3 showed no binding for the RRM-containing domain. Conversely, the RS region appears to bind RNA stronger in comparison to D3. The phosphoimages show that the RS-rich domain of D3 is the minimal region of PGC-1[alpha] that mediates direct interactions with RNA *in vitro*.
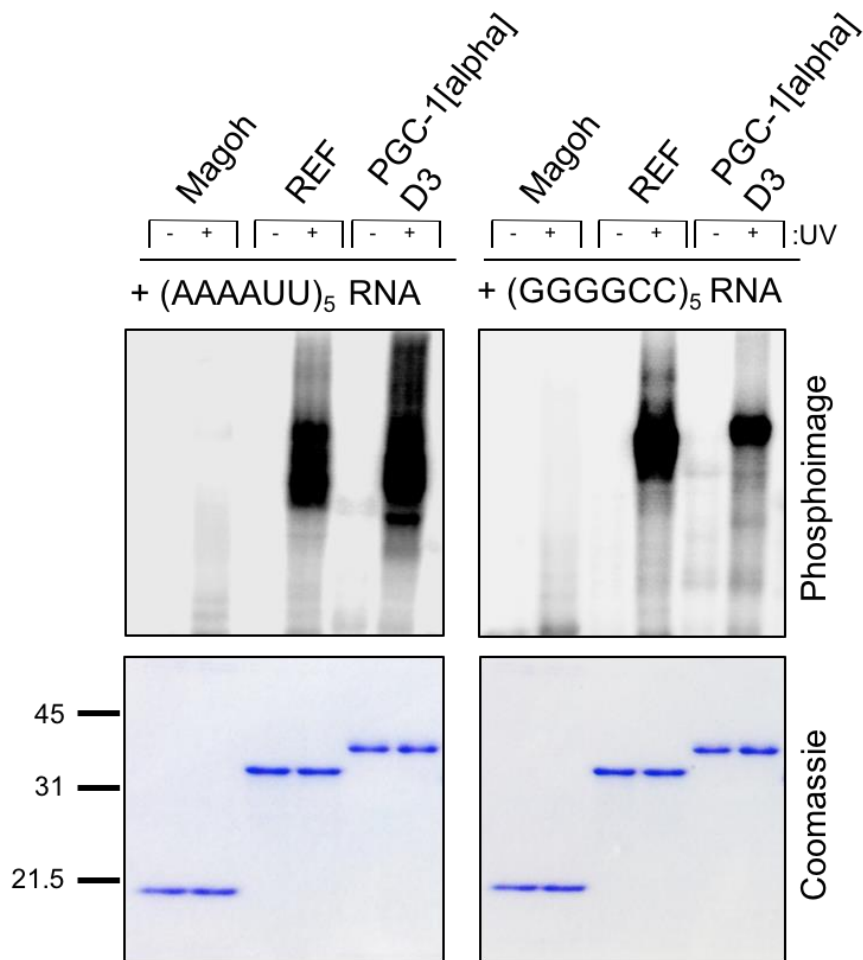
Figure 3.6 Direct RNA-binding of PGC-1[alpha] aa565-798 to AU- and GC-rich probes.

AU and GC RNA probes were radiolabeled with ^{32}P, incubated with recombinant proteins and crosslinked (UV-exposed). Top panels are phosphoimages showing radioactive signal, and bottom panels are Coomassie-stained polyacrylamide gels of recombinant proteins. D3 was capable of binding both AU- and GC-rich RNA probes. Magoh did not show any signal as expected in comparison to the positive control REF. RNA binding was carried out in the presence of 200 mM urea.
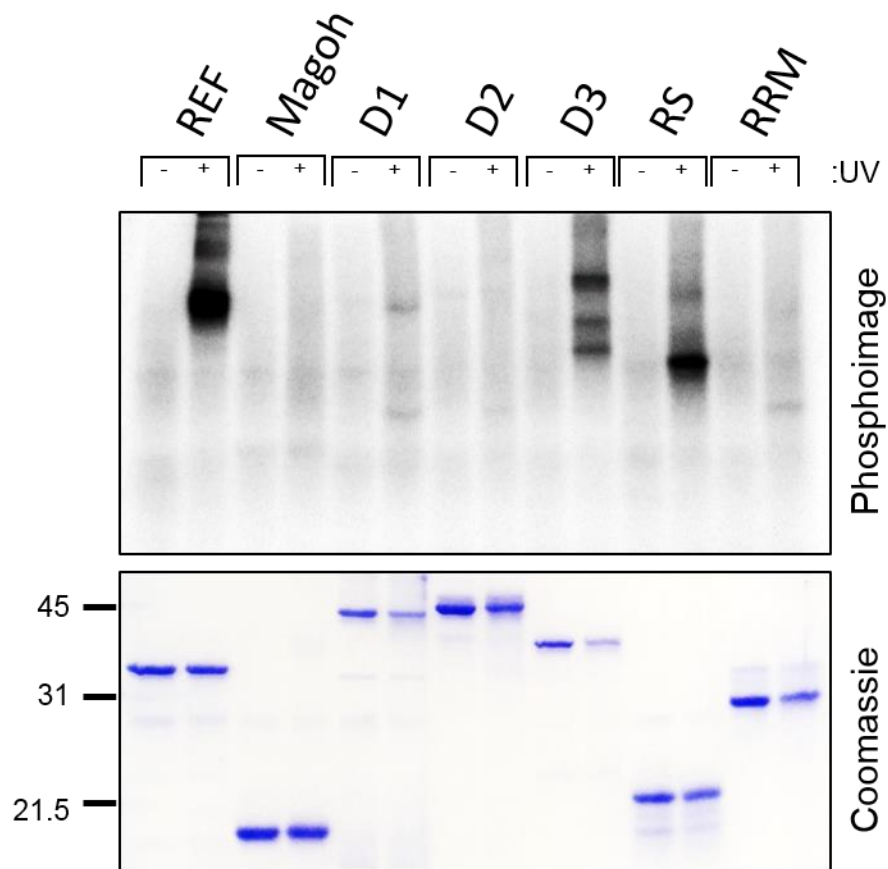
Figure 3.7 RNA binding of PGC-1[alpha] domains.

Recombinant proteins were incubated with GC-rich ^{32}P-labelled RNA probe and exposed to UV. D1, D2 and RRM do not show any detectable signal confirming no binding to RNA. In comparison, D3 and RS were capable of direct binding to RNA. RS signal appears stronger indicating stronger binding. REF and Magoh as positive and negative controls behaved as expected. All binding reactions were carried out in the presence of 200 mM urea.

3.5. Testing the biological importance of the RNA-binding activity of PGC-1[alpha]

Following the identification of PGC-1[alpha]'s capability of binding RNA directly, the next questions were (1) whether this finding could be replicated in mammalian cells, (2) whether loss of the RS-rich region would result in loss of RNA binding, and (3) whether the RNA-binding property of PGC-1[alpha] is playing a physiological role in cells.

To answer these questions, a complementation system in which simultaneous knockdown of the endogenously expressed PGC-1[alpha] and replacement (complementation) with either wild type (WT) or a deletion mutant lacking the RS-rich domain (Δ565-633) was built.

Since the system was to be used in mammalian cells (HEK293), a suitable vector was required. The choice was pcDNA5/FRT, a commercial vector which harbors a CMV promoter allowing for mammalian expression. The vector also contains a recombination FRT site utilised later for the engineering of isogenic stable inducible HEK cell lines (described in Chapter 5). Due to the poor quality of commercially available anti-PGC-1[alpha] antibodies, an N-terminal 3xFLAG tag was introduced into the vector similar to methodology reported by other groups (Adamovich et al., 2013; Sakai et al., 2012). The available anti-FLAG antibodies are highly specific allowing for unambiguous detection of the tagged protein. Following this, PGC-1[alpha] PCR-amplified cDNA was cloned into the pcDNA5-FRT/3xFLAG vector. The generated wild-type PGC-1[alpha] (WT) plasmid was then used as a template to produce a mutant PGC-1[alpha] that lacks the RS-region aa565-633 (ΔRS). This was

achieved by divergent PCR where DNA was amplified in opposite directions away from aa565 and aa633, followed by ligation of the newly created linear product.

The complementation system also required the use of RNA interference to efficiently knockdown PGC-1[alpha]. For this, three micro RNAs (miRNAs) expressed in cells as a pre-miRNA cassette that is physiologically processed by Drosha and Dicer were designed. Each of them was targeting one of the three functional domains of PGC-1[alpha]. To assess their capacity at knocking-down PGC-1[alpha] they were transiently transfected in HEK293T cells, individually or in combination (Fig.3.8.). All miRNAs were co-transfected with the FLAG-tagged PGC-1[alpha] plasmid and a western blot using anti-FLAG antibody was carried out. Two of the miRNAs targeting D1 and D2 appeared to be more potent in comparison to miRNA for D3. Moreover, a combination of any two miRNAs resulted in higher knockdown efficiency, therefore miRNAs for D1 and D2 were chained together, where miRNA2 was introduced downstream in the miRNA1 plasmid.

The control and PGC-1[alpha] pre-miRNA (chained) cassettes were then cloned into the plasmids downstream of 3xFLAG WT or ΔRS PGC-1[alpha] cDNAs within the 3'UTR region of the pcDNA5 FRT vectors. This allows for the simultaneous expression of PGC-1[alpha] and the chained pre-miRNA that is subsequently processed into mature miRNAs.
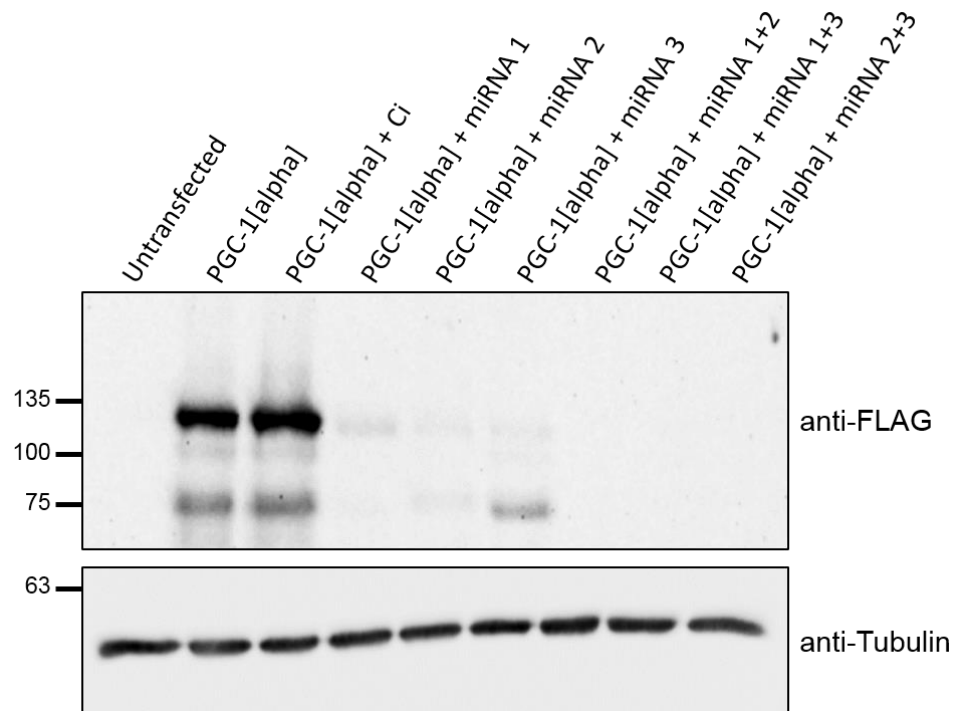
Figure 3.8 Screening of miRNAs targeting PGC-1[alpha].

HEK293T cells were co-transfected with full-length PGC-1[alpha] plasmid and control miRNA (Ci) or three different miRNAs targeting D1, D2 or D3, respectively. All three miRNAs were capable of knocking-down PGC-1[alpha]. Combination of any two miRNAs resulted in further knockdown of the protein. Bottom panel shows western blotting of tubulin as a loading control.

The final, third, step for building of the complementation system was to allow expression of the replacement transgenes (WT and ΔRS) by silently mutating the plasmidic sequence targeted by the PGC-1[alpha] miRNAs. This was achieved by introducing point mutations in WT and ΔRS that do not affect the protein sequence of PGC-1[alpha] but make it unrecognisable by the miRNAs. Figure 3.9. illustrates the plasmid configuration that constitutes the complementation system.

Finally, the functionality of the complementation system plasmids was assessed by transiently transfecting HEK293T cells (Fig.3.10). The western blot image shows that the chained miRNA plasmid efficiently knocks down PGC-1[alpha] and that both complementation system plasmids are functional demonstrating the resistance of WT and ΔRS to the miRNAs.
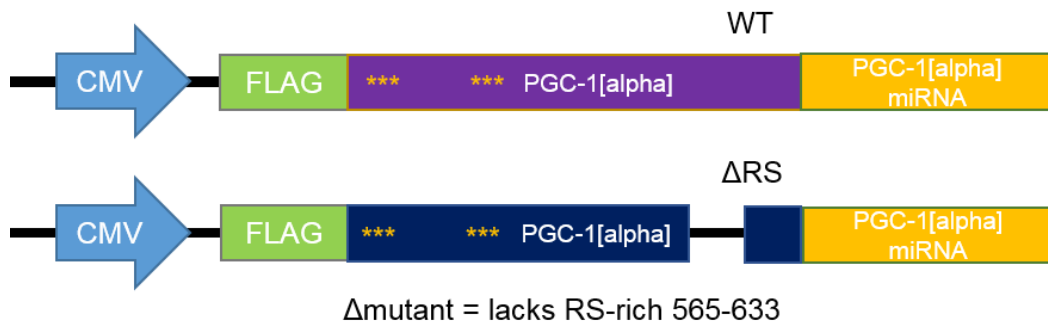
Figure 3.9 Schematic representation of complementation system plasmids.

Two plasmids were built for the complementation system. Each of them has CMV mammalian expression promoter; N-terminal 3xFLAG tag; PGC-1[alpha] WT or ΔRS; and PGC-1[alpha] miRNA. Yellow asterisks indicate point mutations that make PGC-1[alpha] resistant (unrecognisable) to the miRNA. These plasmids allow for the simultaneous knockdown of endogenous PGC-1[alpha] and its replacement with WT or delta mutant.
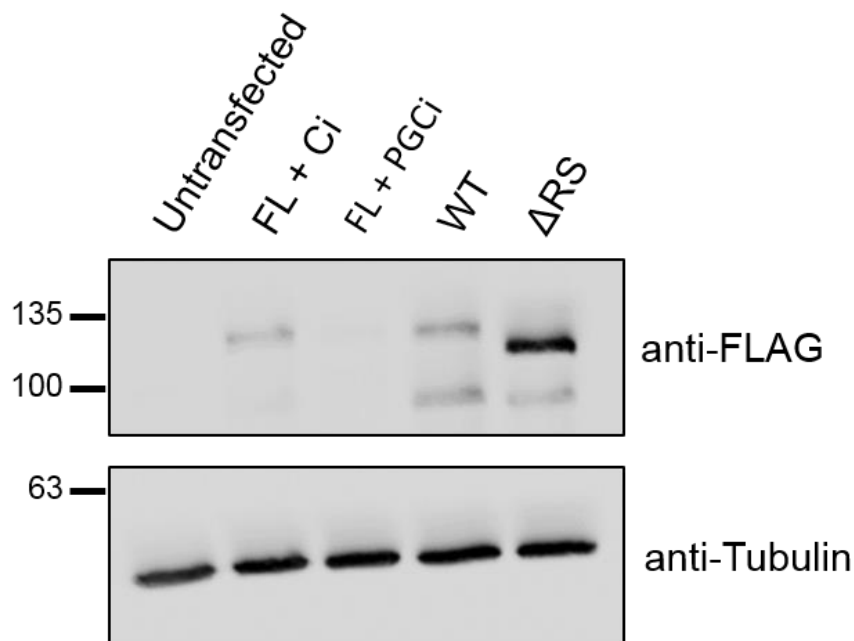
Figure 3.10 Western blotting of proteins using the complementation system plasmids.

HEK293T cells were transfected as follows (from left to right): untransfected; PGC-1[alpha] full length + Control miRNA; PGC-1[alpha] full length + PGC-1[alpha] miRNA; Complementation system WT plasmid; Complementation system delta plasmid. Both complementation system plasmids express PGC-1[alpha] indicating their resistance to the miRNA. Bottom panel shows anti-Tubulin blotting used as a loading control.

3.6. Evaluating the poly-A+ RNA-binding activity of PGC-1[alpha] *in vivo* in cells

Since PGC-1[alpha] was suggested to play a role in the splicing of a pre-mRNA reporter, it was further investigated whether PGC-1[alpha] could interact with messenger ribonucleoprotein complexes (mRNPs) using an oligo-dT mRNP capture assay performed on human HEK293T cell extracts in denaturing conditions. HEK293T cells were transfected with both complementation system plasmids or an empty plasmid that carries only the 3XFLAG tag. 48 hours post transfection, cells were subjected to UV exposure (or no exposure as a negative control) prior to lysis and incubation with oligo(dT)-cellulose beads. Oligo(dT) beads bind to the poly(A)-tail of mRNA. Eluted proteins were resolved on a 12% SDS-PAGE gel and a western blot was carried out. The membrane was then incubated with anti-FLAG antibody to assess the binding of PGC-1[alpha] to mRNA.

An input (total cell lysate) western blot was performed alongside the mRNP capture western blot to evaluate the transfection of the plasmid constructs and their expression in HEK293T cells (Fig.3.11.). The input WB (left panel) represents 3% of all HEK293T cell lysate incubated with the cellulose beads. From left to right, a faint band is observed for FLAG followed by strong bands for PGC-1[alpha] WT and a marginally lower molecular weight band for ΔRS. This shows successful transfection of cells and detectable protein expression from the plasmids. Right panel represents the mRNP capture assay showing no binding for FLAG as expected. Signal is only observed with the WT construct when subjected to UV cross-linking demonstrating specific binding of PGC-1[alpha] to poly-A+ mRNA. This interaction is notably lost with the delta mutant. This confirms that PGC-1[alpha] binds RNA directly in cells (use of

a denaturing buffer, only covalently cross-linked RNA:protein complexes can be purified) and that the RS-rich region is the minimal site responsible for RNA binding in agreement with the *in vitro* experiments using purified recombinant proteins.
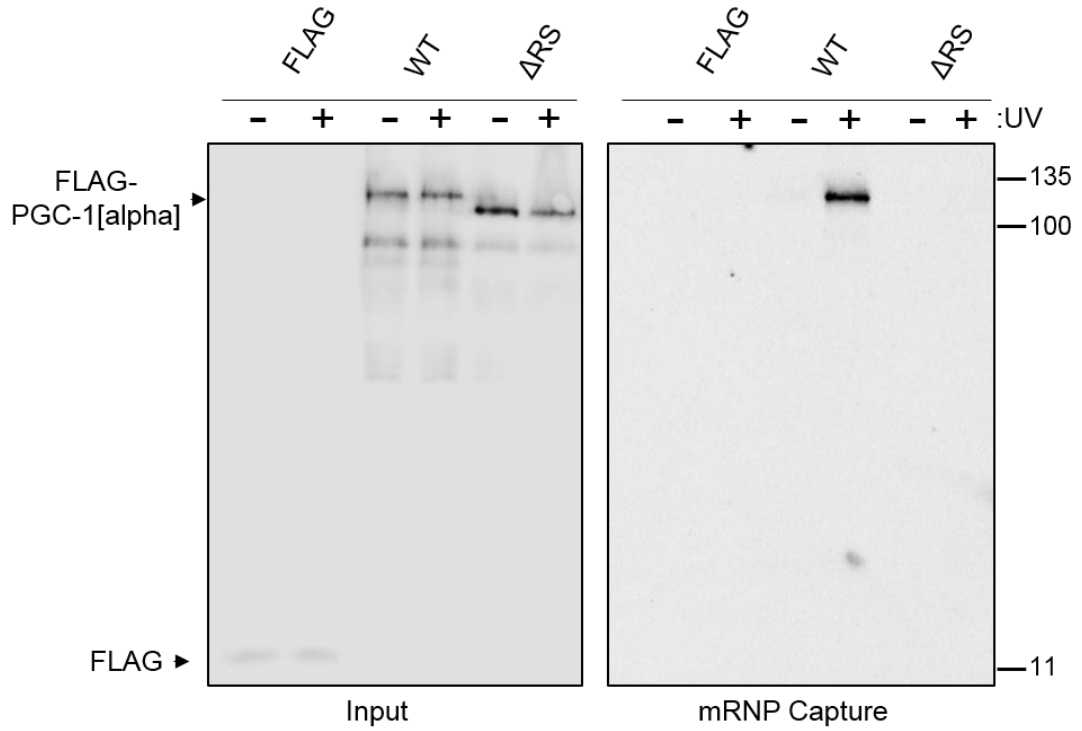
Figure 3.11 mRNP capture with PGC-1[alpha] WT and ΔRS.

Three plasmids were transfected in HEK293T cells: FLAG (negative control), WT and ΔRS. Left panel shows total cell lysate (input) demonstrating the expression of the plasmids. The right panel shows the mRNP capture. Only WT was capable of binding mRNA when exposed to UV. ΔRS lost its RNA-binding capacity.

In addition, preliminary data (n=1) show that PGC-1[alpha] binds the mRNA of some of its target proteins. Briefly, RNA immunoprecipitation (RIP) was performed using transfected HEK293T cells with FLAG (empty plasmid as a negative control), WT, and ΔRS. Cells were cross-linked with formaldehyde and lysed. FLAG-tagged proteins were then immobilised onto anti-FLAG beads and interacting RNA eluted. qRT-PCR with input and eluted RNA was carried out to assess for binding to NRF-1, mtTFAM, and COX2 mRNAs. Figure 3.12. shows that PGC-1[alpha] WT is capable of binding all three targets. In comparison, binding of ΔRS to NRF-1, mtTFAM and COX2 was dramatically reduced. This further confirms that the RS-region of PGC-1[alpha] is involved in RNA-binding. FLAG alone, shows no binding or background non-specific signal.
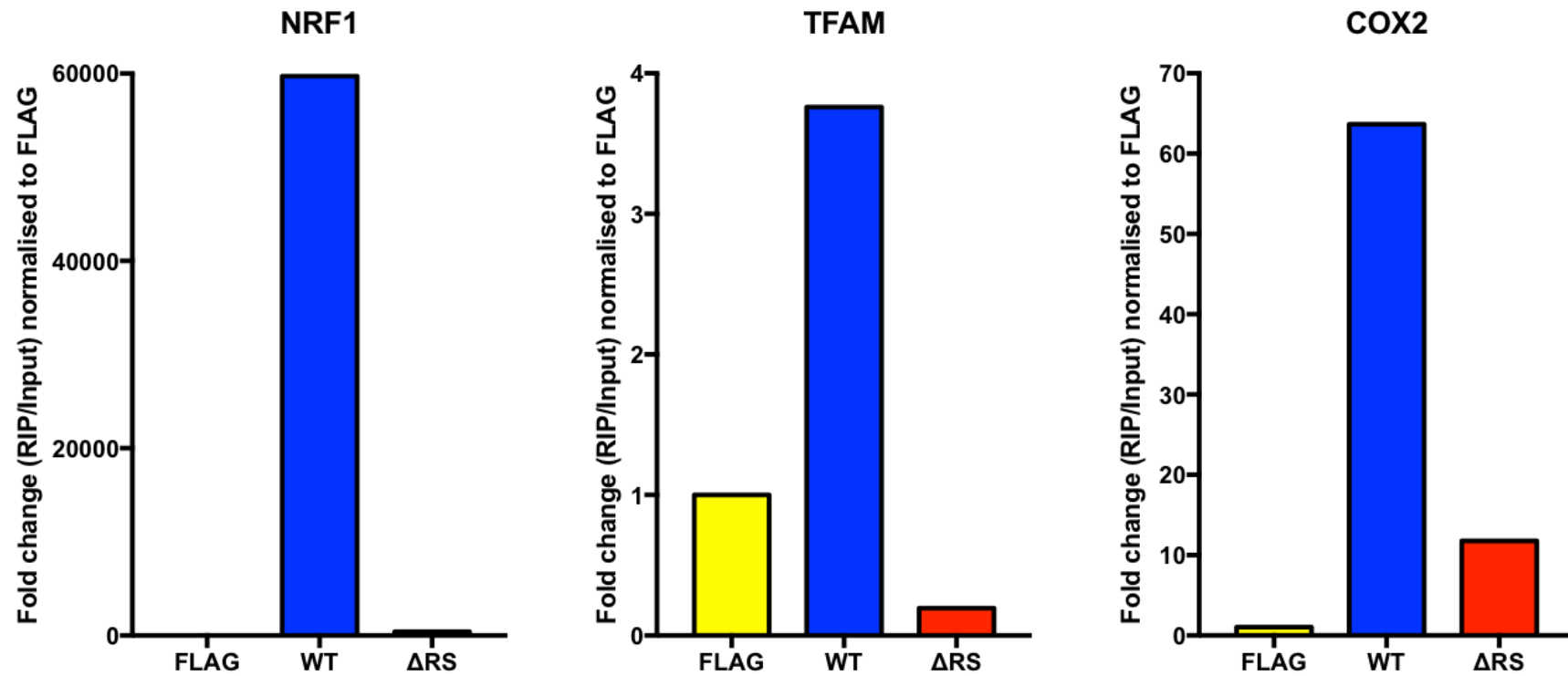
Figure 3.12 RNA-immunoprecipitation assay shows diminished binding of target mRNAs with ΔRS.

Transiently expressed FLAG, WT and ΔRS in HEK293T cells were crosslinked and immobilised on anti-FLAG beads. Eluted RNA was used in qRT-PCR and mRNA levels of NRF-1, TFAM and COX2 assessed. WT is capable of binding all three target mRNAs as compared to FLAG negative control. ΔRS mutant shows reduced or no binding to any of targets. Represented as the ratio of RIP/Input and normalised to FLAG (set at 1). n=1.

3.7. Evaluating the biological importance of the RNA-binding function of PGC-1[alpha]

To test the overall importance of PGC-1[alpha] and its RNA-binding function importance, HEK293T cells were transfected with the appropriate constructs (Control miRNA - Ci, PGC-1[alpha] miRNA - PGCi, WT, and ΔRS) and an MTT cell proliferation assay was carried out (Fig. 3.13.). MTT is a rapid colourimetric assay that measures cell proliferation related to mitochondrial metabolism. It is based on cell number, therefore it was conducted by seeding the same number of cells at the beginning of the assay. Any decrease in end readings would indicate impaired metabolism and/or toxicity of the expressed protein.

Ci plasmid construct was used as a negative control for PGCi, and WT as a negative control for ΔRS.
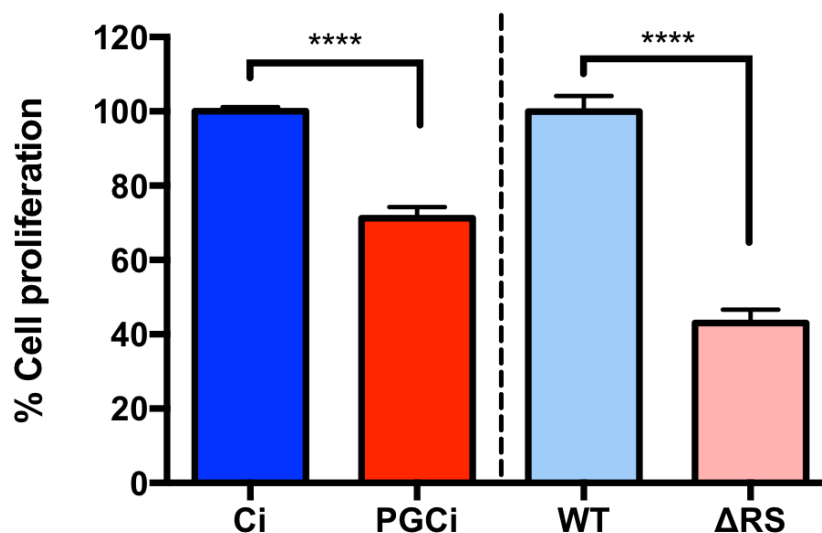
Figure 3.13 MTT cell proliferation assay in transiently transfected HEK293T cells.
HEK293T cells were transiently transfected for 72hrs with Control miRNA (Ci), PGC-1[alpha] miRNA (PGCi), and complementation system plasmids wild-type (WT), Δ565-633 (ΔRS). PGCi is normalised to Ci, ΔRS is normalised to WT. Decreased in MTT cell viability is prominent and significant in both PGC-1[alpha] knockdown and ΔRS complementation. Ci and WT set at 100% (Mann-Whitney *U* test, **** $p < 0.0001$).

Knocking-down PGC-1[alpha] in mammalian cells for 72 hours resulted in significant reduction of cell proliferation by 28.76% (Ci 100±3.65, PGCi 71.21±9.47; p<0.0001). Similarly, replacing the endogenously expressed PGC-1[alpha] with the delta mutant showed significantly decreased cell proliferation by 56.92% (WT 100±17.32, ΔRS 43.08±15.04; p<0.0001). This reduction was greater compared to the knockdown.

3.8. Discussion

As aforementioned, it has been reported as early as 2000 that PGC-1[alpha] might be involved in RNA processing through interaction with RNA polymerase II and splicing factors (Monsalve et al., 2000). Nevertheless it is surprising that there are no reports thus far indicating that PGC-1[alpha] binds RNA. The experimental work presented in this chapter demonstrates that PGC-1[alpha] does not only associate with the RNA pol II complex but is also able to directly bind RNA and poly-A+ mRNA in cultured mammalian cells.

Using recombinant proteins from deletion constructs of PGC-1[alpha] and ^{32}P-labelled RNA probes, it was shown that the co-transcriptional activator physically associates with RNA. As predicted, domains 1 and 2 are not capable of binding RNA. This is not surprising as both domains do not possess RNA-recognition motifs. In comparison, the carboxyl-terminal domain 3 is able to bind RNA. Further dissection of D3 demonstrates that, contrary to expectations, the RNA-recognition motif does not interact with RNA. This role is reserved for the juxtaposed RS-rich region identifying it as the minimal RNA-binding domain. While this presents novel information and understanding about the RNA-binding capacity of PGC-1[alpha], such RS-mediated interactions have been observed with other RNA-binding proteins (RBPs) (Järvelin et al., 2016; Varadi et al., 2015). Positively charged arginine residues play an important

role in binding RNA via electrostatic interactions with the negatively charged nucleic acid backbone. Moreover, RS-rich RNA-binding regions often lack defined secondary and tertiary structure. Indeed, computational prediction analysis assessing the probability for the presence of intrinsically disordered regions in proteins, noticeably indicates that the RS-rich (aa 565-633) region of PGC-1[alpha] possesses such features (Fig.3.14.). This structural flexibility might contribute to the binding of different RNA molecules.

These results were further validated via mRNP capture assay in cultured human cells and show that PGC-1[alpha] is not only capable of binding RNA *in vitro*. Moreover, deleting the RS region resulted in complete abolition of mRNA-binding. This confirms that the RS region is solely responsible for the interaction with RNA.

Instinctively, this raised the fundamental question about the exact mRNA targets of PGC-1[alpha]. The most logical avenue was to test whether PGC-1[alpha] regulates its target proteins at the mRNA level as well. Preliminary data suggested that this might be the case. PGC-1[alpha] was found to be bound to NRF-1 mRNA. It was also able to bind the mRNA of mtTFAM, a non-direct target of PGC-1[alpha]. This indicates an extra level of regulation of its targets that might allow for more precise response to stimuli. However, what was more surprising is that PGC-1[alpha] was able to bind the mRNA of a gene that is encoded by the mitochondrial genome i.e. COX2. This might suggest a possible role of PGC-1[alpha] in mitochondria and there have already been accounts of an isoform of the protein that has been found to reside in the mitochondria (J. Choi et al., 2013). All of these interactions were lost when the RS region was deleted from the protein. However, it is worth noting that RNA RIP was performed only once and further replicates are required to fully confirm these results.
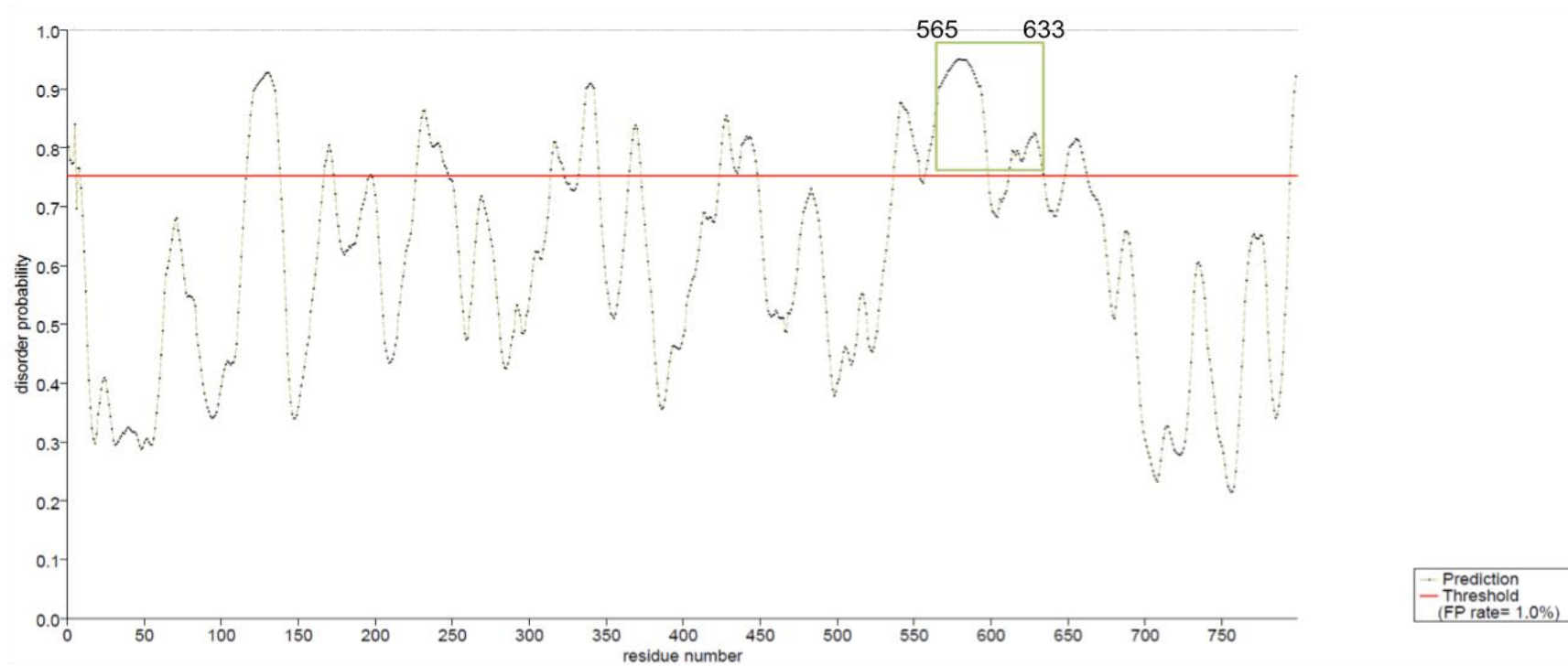
Figure 3.14 Prediction disorder analysis of PGC-1[alpha] protein.

Computational prediction analysis shows high (>0.75) disorder probability of the RS-rich (green box) region of PGC-1[alpha] carboxyl-terminal.

Source: *www.prdos.hgc.jp*

It is interesting that PGC-1[alpha] is able to bind mRNA, however it is more intriguing whether this function is physiologically important in cells. First, knockdown studies in transfected cells showed reduced cell viability as measured by MTT assay but no cell death. This suggests that PGC-1[alpha] is not essential and there might be an alternative mechanism that compensates for its loss. Moreover, protein homology analysis using Basic Local Alignment Search Tool (BLAST) yields a hit with a single protein – CUGBP Elav-like family member 4 (CELF4). CELF4 is an RNA-binding protein that is involved in RNA splicing, localisation and translation and is highly abundant in brain tissue (Karunakaran et al., 2013; Singh et al., 2004; Yang et al., 2007). Similar to PGC-1[alpha], CELF4 has been associated with behavioural disorder and obesity (Halgren et al., 2012). This makes CELF4 an attractive candidate that might show functional redundancy with PGC-1[alpha]. Next, transfecting cells with ΔRS showed greater reduction of cell viability indicating the importance of the RNA-binding function of PGC-1[alpha]. MTT assays measure cell proliferation as a direct function of metabolism directly relating to mitochondria. Thus, taken together with the mRNA-binding studies of its targets, it can be suggested that the RNA-binding role of PGC-1[alpha] has great impact on mitochondrial maintenance and is required for the overall functioning of the PGC-1[alpha] protein.

All these data show that the master regulator of mitochondria is capable of binding RNA and this function is important for cellular homeostasis.

Finally, it is worth mentioning that on a practical level, most constructs of PGC-1[alpha] are insoluble and dialysis after 8 M urea purification results in loss of protein. However, conducting the RNA-binding studies in the presence of 200 mM urea does not appear to interfere with intermolecular interactions as seen from the negative and positive controls, Magoh and ALYREF, respectively.

4. PGC-1[alpha] exhibits the hallmark of a novel mRNA nuclear export adaptor

4.1. Introduction

As previously mentioned, computational analysis of primary protein sequence of PGC-1[alpha] reveals structural similarities to splicing factors where a putative RRM is linked to an RS-rich region. This hypothesis is further strengthened by the observation that PGC-1[alpha] co-immunoprecipitates with another splicing factor SC-35 (Monsalve et al., 2000). However, the identification of PGC-1[alpha]'s ability to directly interact with RNA via its RS region as opposed to its RRM in Chapter 3 is reminiscent of a class of proteins called nuclear export adaptors associated with the nucleocytoplasmic transport of mRNAs.

Nuclear export adaptors such as ALYREF, UIF, shuttling proteins SRSF3, SRSF7 and SRSF1 have typical conformational architecture (Hautbergue et al., 2009; Walsh et al., 2010 also described in more detail in Chapter 1). They are composed of one or two RRMs linked to a carboxyl-terminal RS/RG-rich region via an unstructured linker sequence. This spatial protein organisation has been shown to be important for binding to RNA and the bulk mRNA export factor TAP/NXF1. The interaction with RNA involves RRM and the adjacent region. Moreover, this overlaps with the region responsible for TAP/NXF1 binding.

As demonstrated before, PGC-1[alpha] is a challenging protein that is not readily soluble making it difficult to solve its three-dimensional structure. However, prediction analyses of its secondary structure indicate that the protein lacks defined structure (Adamovich et al., 2013). This demonstrates structural similarities between PGC-

1[alpha] and nuclear export adaptors. Unlike adaptors, PGC-1[alpha] is linked to an N-terminal RS-region. This homology prompted the need to investigate the putative role of PGC-1[alpha] as a novel nuclear export adaptor.

This chapter investigates the potential role of PGC-1[alpha] as a nuclear export adaptor *in vitro*. The main aim is to answer fundamental questions such as 1) is PGC-1[alpha] able to bind TAP/NXF1, 2) which is the minimal binding domain required for the interaction, and 3) does PGC-1[alpha] act as an adaptor or co-adaptor?

Information about the DNA plasmids generated for the work in this chapter can be found in Table 4.1. They were constructed following the methodology outlined in Chapter 3 Section 3.2. in addition to Chapter 2 Materials and Methods.

Table 4.1 Plasmid constructs generated to facilitate the experimental work in characterising the TAP/NXF1-binding ability of PGC-1[alpha].

Plasmid Construct	Vector Backbone	Tag	Cloning Strategy	Host Expression
PGC-1[alpha] 1-565 (D1+D2)	pET24b	N-terminal – GB1 and 6xHis	PCR + NdeI/XhoI	bacterial
PGC-1[alpha] 254-798 (D2+D3)	pET24b	N-terminal – GB1 and 6xHis	PCR + NdeI/XhoI	bacterial
PGC-1[alpha] 565-798 RR580/585EE	pET24b	N-terminal – GB1 and 6xHis	Site-directed mutagenesis	bacterial
PGC-1[alpha] 565-798 RRRR568/570/574/576EEEE	pET24b	N-terminal – GB1 and 6xHis	Site-directed mutagenesis	bacterial
PGC-1[alpha] 565-798 RRRRR580/585/587/589/594EEEEE	pET24b	N-terminal – GB1 and 6xHis	Site-directed mutagenesis	bacterial
PGC-1[alpha] 565-798 R621E	pET24b	N-terminal – GB1 and 6xHis	Site-directed mutagenesis	bacterial
PGC-1[alpha] 565-798 R630E	pET24b	N-terminal – GB1 and 6xHis	Site-directed mutagenesis	bacterial
TAP/NXF1 1-198 (RBD)	pGEX-6P-1	N-terminal GST	PCR + BamHI/XhoI	bacterial
TAP/NXF1 204-356 (LRR)	pGEX-6P-1	N-terminal GST	PCR + BamHI/XhoI	bacterial
TAP/NXF1 372-550 (NTF2L)	pGEX-6P-1	N-terminal GST	PCR + BamHI/XhoI	bacterial
TAP/NXF1 551-619 (UBA)	pGEX-6P-1	N-terminal GST	PCR + BamHI/SalI	bacterial

4.2. Investigating the potential *in vitro* interaction of PGC-1[alpha] with TAP/NXF1

In order to assess the putative interaction of PGC-1[alpha] with TAP/NXF1:p15 *in vitro*, an array of pull-down assays was performed.

The first experiment used a coupled transcription/translation reticulocyte lysate system. The pET24b-GB1-6xHis plasmids (described in Chapter 3) have the T7 promoter sequence upstream of the cloned gene of interest. They were incubated with rabbit reticulocyte lysates containing T7 RNA polymerase allowing for the transcription of the plasmids. The lysates also have all necessary amino acids needed for translation except L-Methionine. The mixture reaction was then supplied with ^{35}S-L-Methionine which is incorporated into the newly synthesised proteins and allows for quantifiable and sensitive detection. Meanwhile, induced bacterial pellets expressing GST-tagged TAP/NXF1:p15 were incubated with preblocked GSH sepharose beads for immobilisation of TAP/NXF1-p15 onto beads. Pull-down was carried out using the *in vitro* synthesised and the immobilised proteins. Eluted proteins were then subjected to SDS-PAGE stained with Coomassie blue and analysed by phosphoimage.

In the first of the series of pull-downs, full-length wild-type PGC-1[alpha] and ALYREF as a positive control were used. The Coomassie-stained gel of the pull-down shows either GST (as a negative control) or GST-TAP/NXF1:p15 immobilised onto the beads (Fig.4.1.). The phosphoimage of the input shows that both plasmids for ALYREF and PGC-1[alpha] were expressed in the system. The pull-down, as expected, shows that ALYREF interacts with GST-TAP/NXF1:p15 but not with GST on its own. Similarly, binding to GST-TAP/NXF1 is observed with PGC-1[alpha] full length but not to GST.

The samples were also treated in parallel with RNase to assess the protein:protein interaction as opposed to an interaction via RNA intermediate. This was required as ALYREF, PGC-1[alpha] and TAP/NXF1 are able to bind to RNA. The binding does not appear to be affected by the RNase treatment indicating protein:protein interaction.

To further evaluate the specificity of this interaction of PGC-1[alpha] with TAP/NXF1, the same pull-down was repeated with increasing volumes (5, 10, 20, 40 and 80 µl) of lysate expressing PGC-1[alpha] (Fig.4.2.). Again, as aforementioned, the Coomassie stain shows successful binding of GST or GST-TAP/NXF1:p15 onto the glutathione-coated beads. The phosphoimage shows the expression of PGC-1[alpha] in the reticulocyte lysate and its binding to TAP/NXF1:p15 with increasing volumes. The signal appears to be increasing proportionally to the increase of volume. Statistical analysis for one-site protein binding (hyperbola) revealed specific binding of PGC-1[alpha] to TAP/NXF1 as indicated by the R^2 value of 0.954 (Fig.4.2. right). The densitometry analysis of the phosphoimage was carried out using Quantity One (BioRad) software and GraphPad Prism to perform the statistical analysis and accompanying graph.
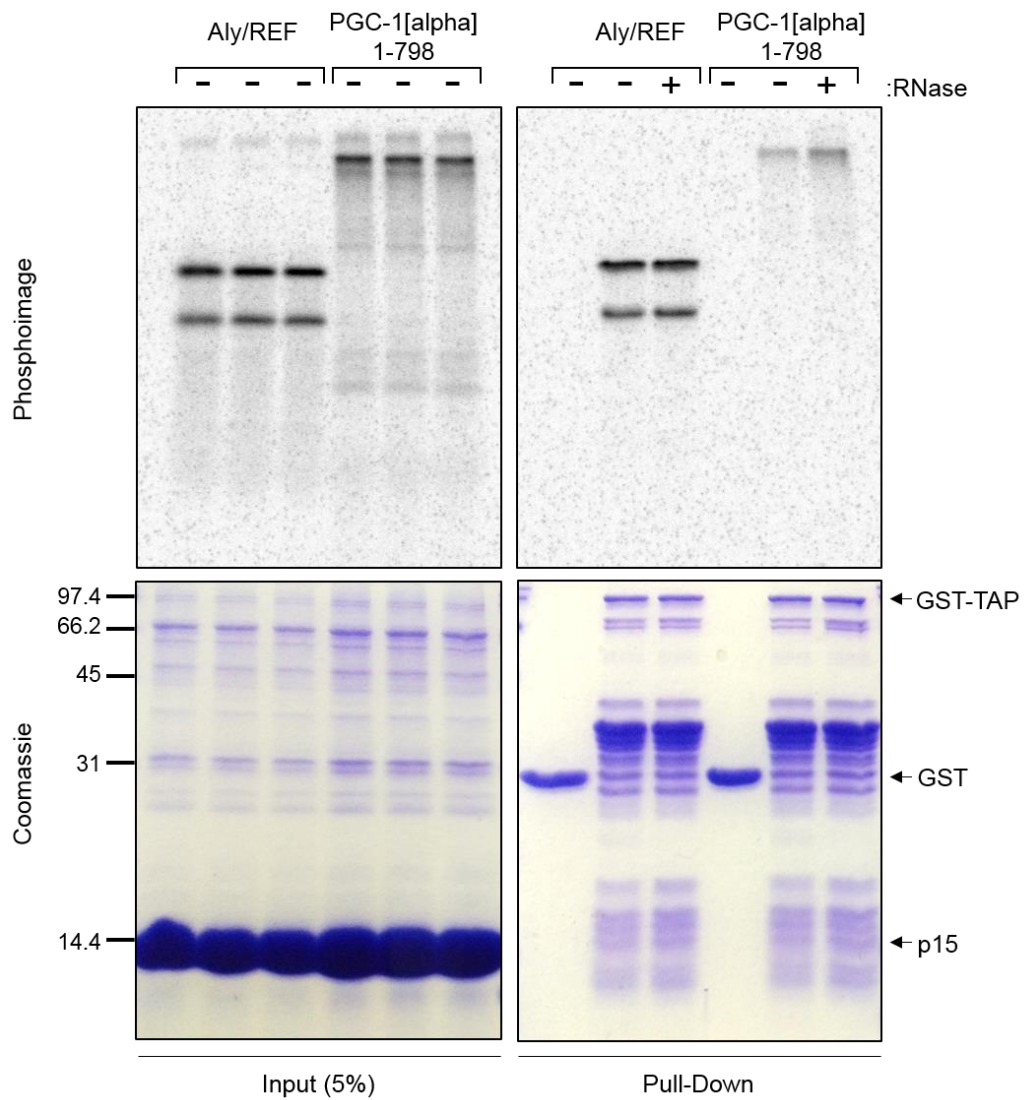
Figure 4.1 PGC-1[alpha] binding to GST-TAP/NXF1:p15.

PGC-1[alpha] was expressed and ^{35}S-labelled in rabbit reticulocyte lysate followed by incubation with GST or GST-TAP/NXF1:p15. ALYREF was used as a positive control. Commassie images (bottom) show input and pull-down with immobilised GST and GST-TAP/NXF1:p15. Phoshoimages (top) show the expression of the plasmids used (left). Pull-down image shows the binding of PGC-1[alpha] to TAP/NXF1 but not to GST (right). The interaction is not ablated by RNase treatment.
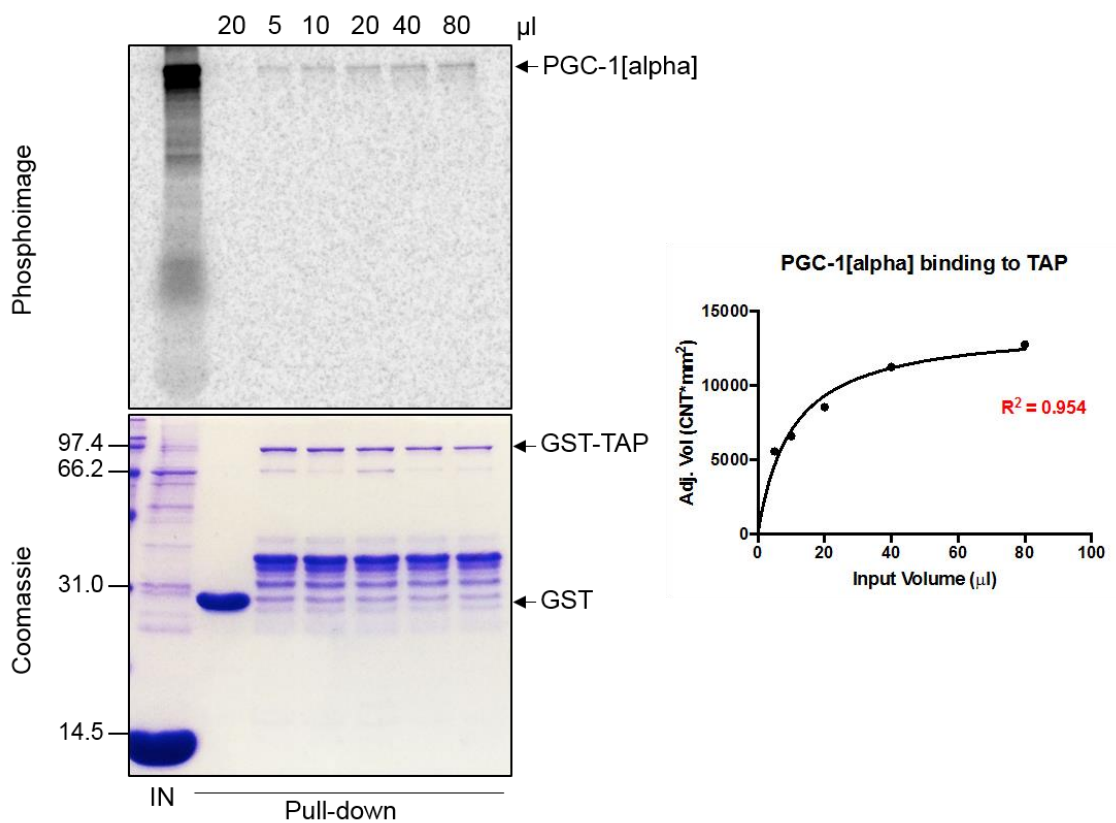
Figure 4.2 Specific binding of PGC-1[alpha] to TAP/NXF1.

Increasing volumes of ^{35}S-labelled PGC-1[alpha] FL were incubated with the same amount of TAP/NXF1:p15. Commassie gel (bottom panel) shows input lane and immobilised GST/GST-TAP/NXF1:p15. Phosphoimage (top panel) shows the expression of the PGC-1[alpha] plasmid in reticulocyte lysate and its binding to TAP/NXF1. One-site binding hyperbola was produced using Quantity One software for densitometry analysis and GraphPad Prism to plot graph. Increasing volumes of PGC-1[alpha] correspond to increasing binding to TAP/NXF1 with R^2=0.954 demonstrating specific protein binding.

Following this, in order to assign the TAP/NXF1-binding capacity of PGC-1[alpha] to a particular functional domain, the same reticulocyte pull-down was carried out with various deletion fragments of PGC-1[alpha]. All constructs were cloned into pET24b-GB1-6xHis plasmid. The constructs used were PGC-1[alpha] FL, D1, D2, D3, D1+2, D2+3 and ALYREF as a positive control. All reactions were subjected to RNase treatment during incubation with immobilised GST or GST-TAP/NXF1:p15. Phosphoimage of the input (left) shows equal expression of PGC-1[alpha] FL compared to D1+2 and D2+3, and similar expression levels of ALYREF compared to D1, D2 and D3 (Fig.4.3.). The right top panel shows the interaction of REF and PGC-1[alpha] with TAP/NXF1. The binding of FL to TAP/NXF1 was confirmed again. Furthermore, this interaction appears to be stronger in comparison to D1 and D2 but equal to D3. This suggests that D3 is responsible for the interaction with TAP/NXF1 as initially hypothesised. Moreover, the signal for D2+3 seems to be greater as compared to D1+2 further indicating the involvement of D3 in the binding of the nuclear export factor. Again, as seen before, RNase treatment does not seem to abolish this protein:protein interaction.

4.3. Mapping the carboxyl-terminal TAP/NXF1-binding domain of PGC-1[alpha]

In a quest to further identify the minimal binding domain of PGC-1[alpha] for TAP/NXF1, the C-terminal domain 3 was dissected, as before, to RS and RRM and another reticulocyte pull-down assay was carried out. Similarly, the input phosphoimage shows the expression of D3, RS and RRM in the *in vitro* system (Fig.4.4.). The pull-down phosphoimage confirms the binding of D3 to TAP/NXF1. In addition, it appears that RS binds TAP/NXF1 stronger than RRM and RNase

treatment does not prevent this interaction. This is in conjunction with the expectations for this particular region as it has been shown previously for all other nuclear export adaptors that the interaction with TAP/NXF1 is facilitated by arginine residues.
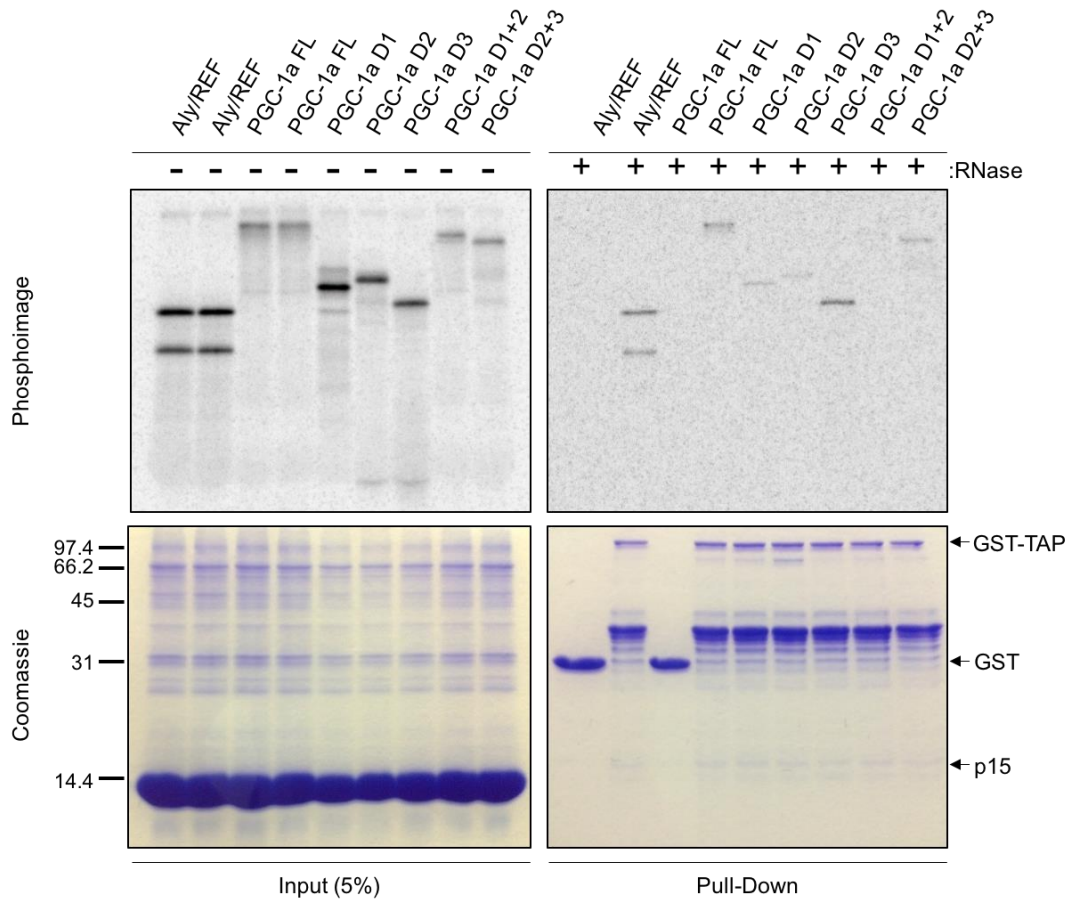
Figure 4.3 Mapping the interaction of PGC-1[alpha] with TAP/NXF1.

Domains were expressed and ^{35}S-labelled in rabbit reticulocyte lysate followed by incubation with GST or GST-TAP/NXF1:p15. ALYREF was used as a positive control. Coomassie images (bottom) show input and pull-down with immobilised GST and GST-TAP/NXF1:p15. Phoshoimages (top) show the expression of the plasmids used (left). Pull-down image shows strong binding of FL and D3 to TAP/NXF1 in comparison to D1 and D2 (right). Signal from D2+3 is stronger than D1+2. All samples were treated with RNase.

All *in vitro* pull-down assays thus far demonstrate a protein:protein interaction of PGC-1[alpha] with TAP/NXF1:p15. This, however, does not exclude the possibility of a protein intermediate(s). Therefore, to assess whether the binding is direct, PGC-1[alpha] D1, D2, D3, RS and RRM were expressed and purified from bacterial cells (as described in Chapters 2 and 3).
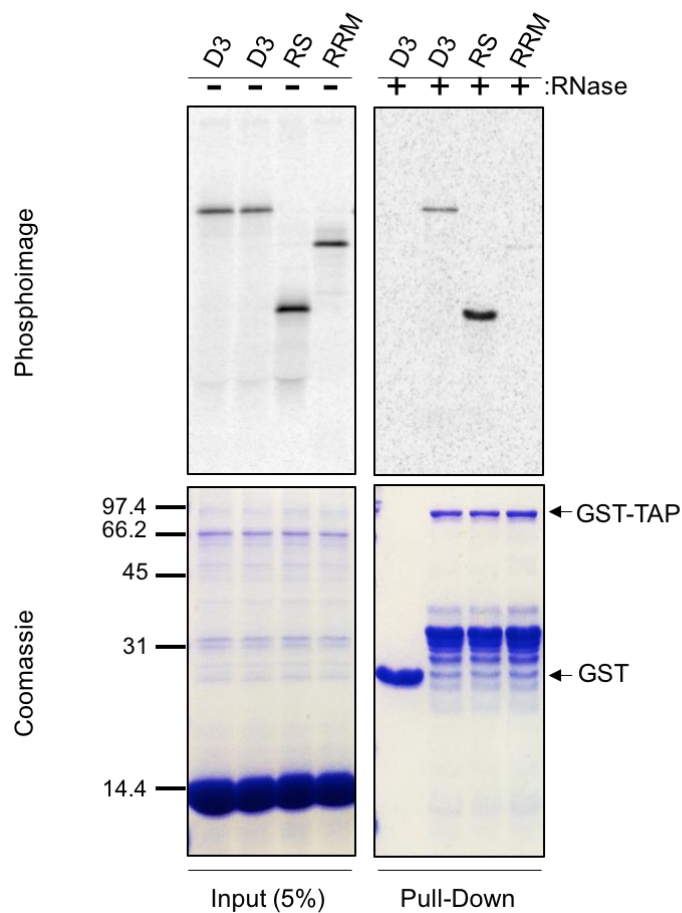
Figure 4.4 RS is the minimal TAP/NXF1-binding domain of PGC-1[alpha].
The C-terminal domain of PGC-1[alpha] was dissected into two subdomains i.e. RS and RRM. The pull-down phosphoimage (right) indicates stronger binding of RS to TAP/NXF1 in comparison to RRM.

Recombinant constructs were incubated with GST or GST-TAP/NXF1:p15 immobilised on GSH beads. Coomassie-stained SDS-PAGE gel reveals the presence of a band of the size of RS (~18 kDa; Fig.4.5. top panel). This indicates that RS is interacting with TAP/NXF1 physically in a direct manner making it the minimal binding domain for the nuclear export factor. Unfortunately, D3 cannot be seen on the Coomassie image in comparison to the reticulocyte assays. PGC-1[alpha] constructs carry a 6xHis-tag downstream of GB1. Therefore, a western blot was performed with pull-down samples and probed with anti-6xHis antibody. Western blotting is a more sensitive detection approach compared to Coomassie-blue staining. However, bands were detected for all constructs used in this pull-down assay suggesting unspecific binding due to 'sticky' proteins (Fig.4.5. bottom panel). Nevertheless, the RS signal appeared the strongest and its presence on the Coomassie image demonstrates strong and specific interaction.

Next, the immediate question was whether deleting the RS region of PGC-1[alpha] would affect its binding to TAP/NXF1. To answer this, another reticulocyte assay was carried out using the WT and ΔRS pET24b plasmids. This pull-down assay revealed that ΔRS is still able to bind TAP/NXF1, however this interaction appears to be weaker in comparison to WT as indicated by the weaker band on the phosphoimage (Fig.4.6.). This further confirms that the RS region is involved in the binding of TAP/NXF1.
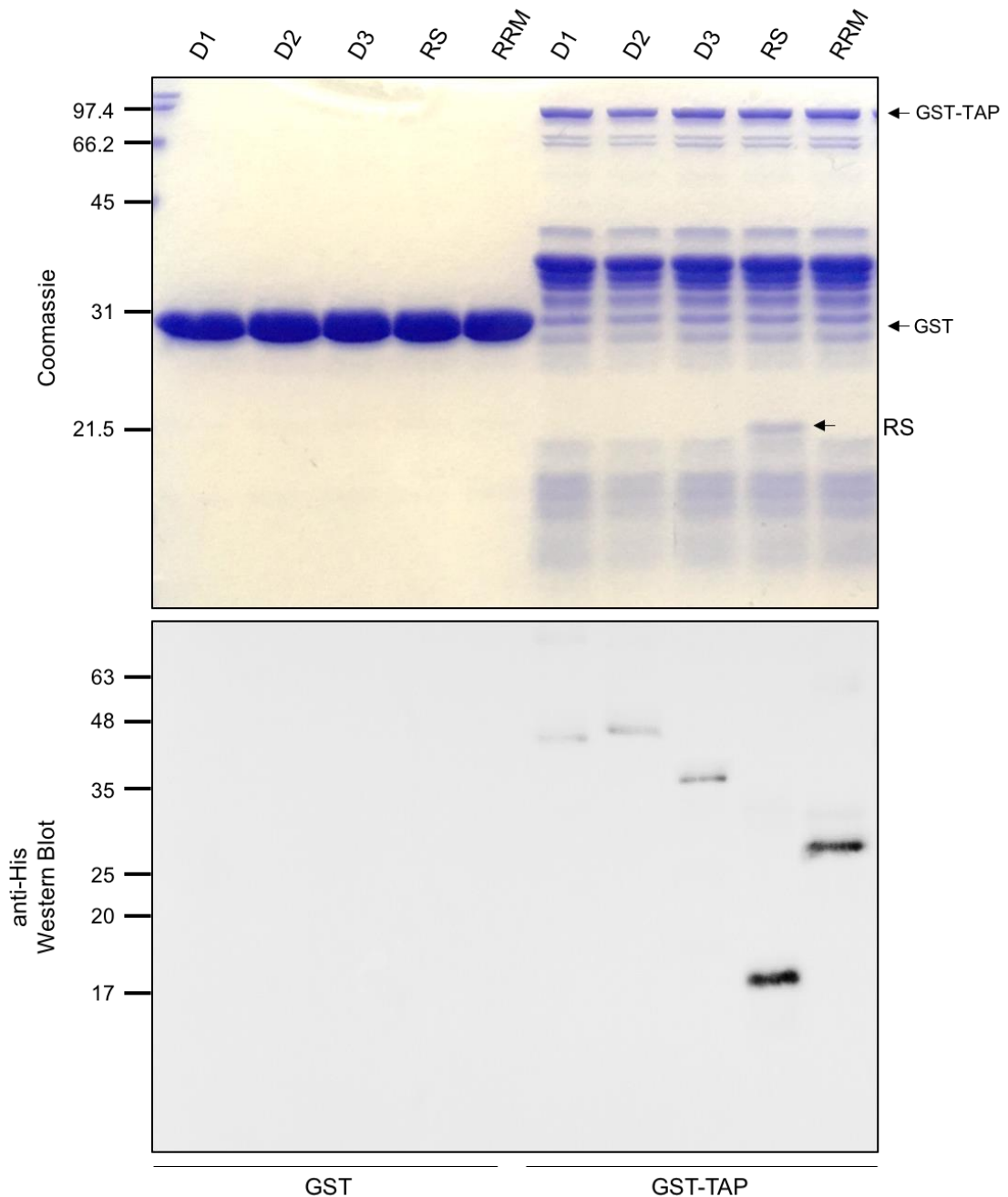
Figure 4.5 Direct binding of PGC-1[alpha] to TAP/NXF1.
Recombinant deletion constructs of PGC-1[alpha] – D1 (1-234), D2 (254-564), D3 (565-798), RS (565-633) and RRM (634-798), were incubated with purified GST/GST-TAP/NXF1:p15. Top panel shows a coomassie SDS-PAGE gel showing the pull-down of RS region with TAP/NXF1:p15 demonstrating direct protein binding. Bottom panel represents a western blot analysis showing the presence of all five constructs which might suggest unspecific protein binding. Nevertheless, the band for RS appears to be the strongest complementing the coomassie result.
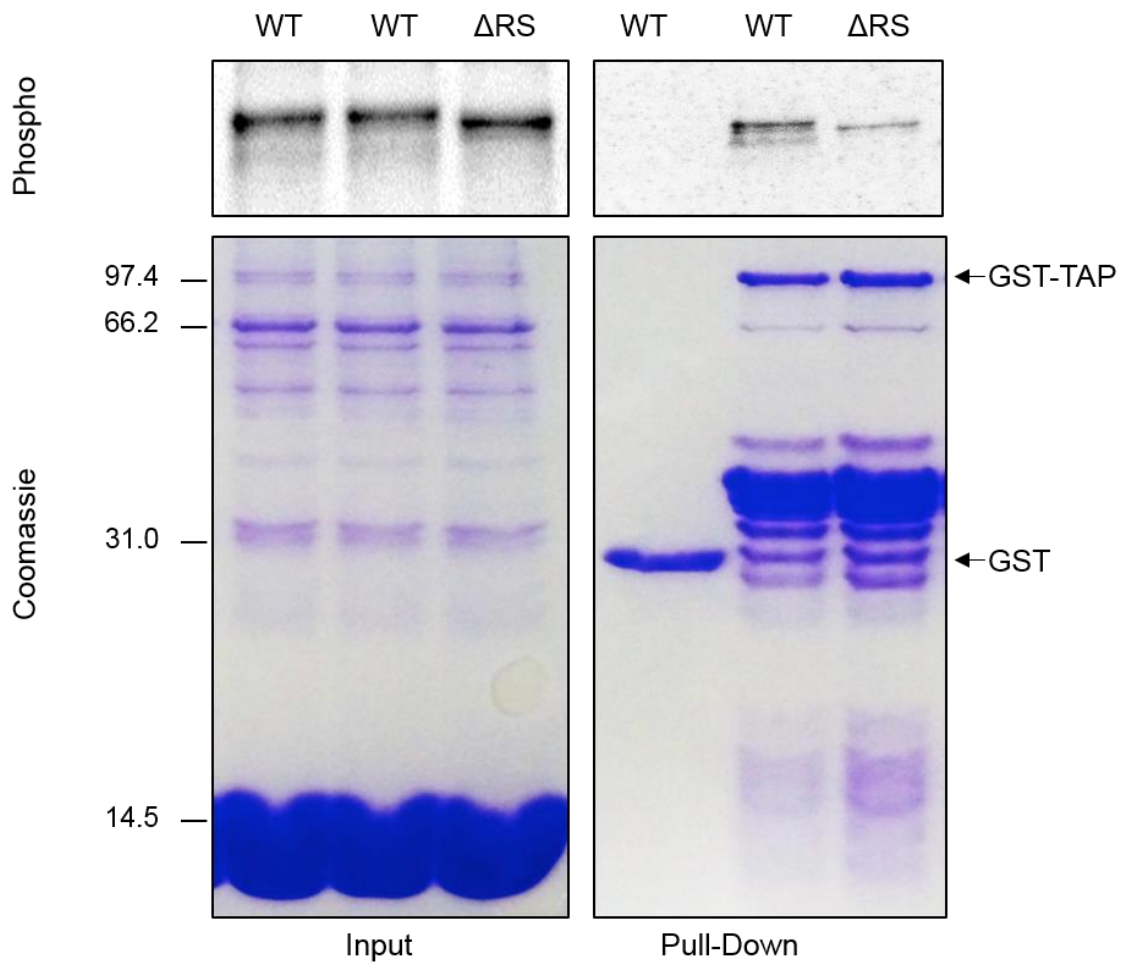
Figure 4.6 Wild-type and mutant PGC-1[alpha] binding to TAP/NXF1:p15.

Pull-down assay with ^{35}S-labelled PGC-1[alpha] WT and ΔRS and TAP/NXF1:p15 showed decrease binding of the mutant to TAP/NXF1 compared to wild-type. This shows the involvement of the RS domain in mediating interactions with TAP/NXF1. Coomassie gels (bottom) show the reticulocyte lysate input (left) and the immobilised GST/GST-TAP/NXF1:p15 (right). Phosphoimages show the expression of PGC-1[alpha] (left) and its binding to TAP/NXF1 (right).

4.4. Potential involvement of PGC-1[alpha] arginines in the binding to TAP/NXF1

It has been long established that typical nuclear export adaptors use arginines to bind to TAP/NXF1. To check whether this was the case for PGC-1[alpha], site-directed mutagenesis was carried out. Positively charged arginines in the RS-rich region (aa565-633) were mutated to negatively charged glutamic acid residues. The study involved mutations of a single or multiple amino acids (1, 4 and 5 amino acids) in the RS-rich region of D3. Similar to previous assays, pET24b plasmids carrying mutated PGC-1[alpha] were expressed in reticulocyte lysates and used in a pull-down assay with GST-TAP/NXF1:p15. Unfortunately, no changes in ^{35}S signal were observed with any of the mutations (Fig. 4.7.). This might suggest that arginines are not essential for facilitating the interaction of PGC-1[alpha] with TAP/NXF1 or that other non-mutated arginines can interact with TAP/NXF1.
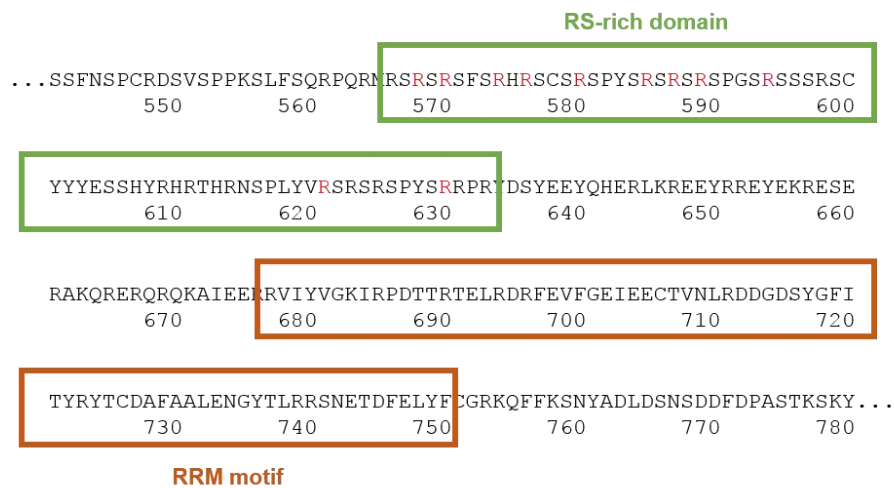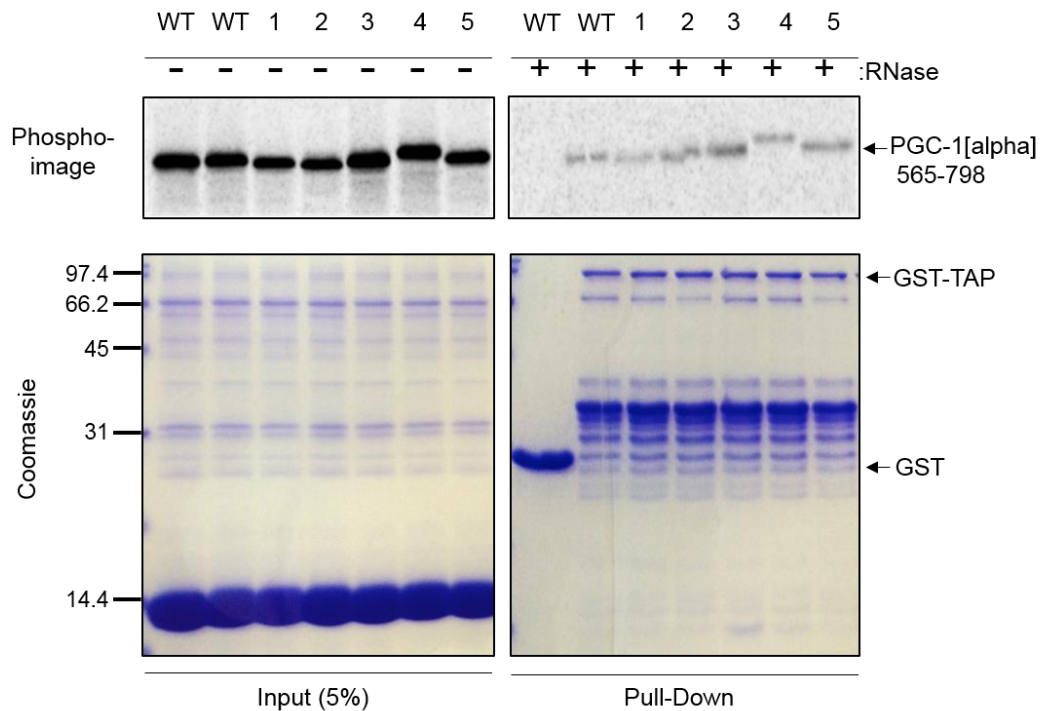
Figure 4.7 Pull-down assay with different Arginine mutants of PGC-1[alpha].

Arginine residues in the RS region of PGC-1[alpha] D3 were substituted for Glutamic acid residues. Constructs were expressed and ^{35}S-labelled in reticulocyte lysates and incubated with GST/GST-TAP/NXF1:p15. Commassie SDS-PAGE gels shows the lysate input (left) and immobilised GST/GST-TAP/NXF1:p15 (right). Phosphoimage shows equal expression of all constructs (left). Pull-down (right) shows no apparent difference in binding of the mutant constructs to TAP/NXF1 compared to the wild-type form of PGC-1[alpha]. Bottom panel shows the primary protein sequence of a part of D3. RS and RRM regions are indicated with green and orange circles, respectively. Arginine residues (R) that have been mutated are shown in red. Mutations are as follows: **1** – R580E+R585E; **2** – R568E+R570E+R574E+R576E; **3** – R580E+R585E+R587E+R589E+R594E; **4** – R621E; **5** – R630E.

4.5. Investigating the binding of TAP/NXF1 with PGC-1[alpha]

Another important question to be answered was whether PGC-1[alpha] exhibits properties of a nuclear export adaptor or co-adaptor in its binding of TAP/NXF1. TAP/NXF1 is a modular protein that is structurally subdivided into four distinct functional domains – N-terminal RNA-binding domain (RBD), leucine-rich repeat (LRR), middle nuclear transport factor 2-like domain (NTF2L), a C-terminal ubiquitin-associated domain (UBA) (Fig. 4.8.) (Herold et al., 2000). Typically, nuclear export adaptors bind to the RBD, while co-adaptors bind to the NTF2L domain. This has been observed with the canonical export adaptor ALYREF and the co-adaptor THOC5, which allows for simultaneous binding to TAP/NXF1 resulting in the export of specific mRNA targets such as Hsp70 (Katahira et al., 2009).
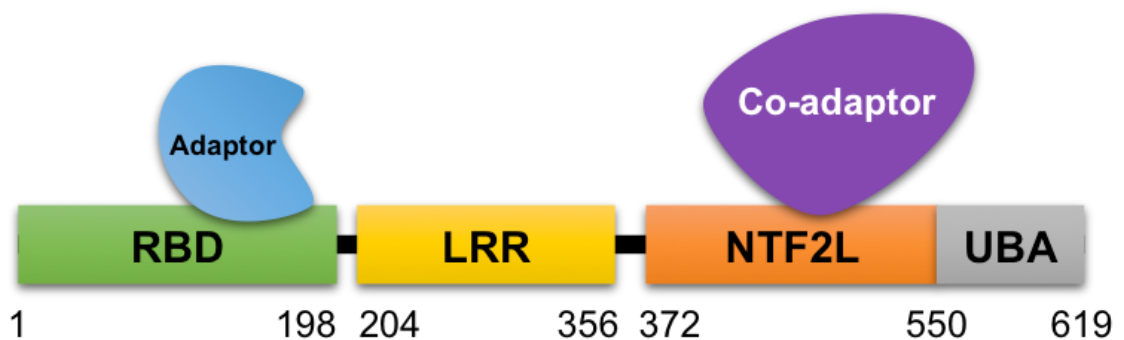
Figure 4.8 Schematic representation of TAP/NXF1 domains.

Adaptors such as ALYREF, SRSF1, SRSF3, SRSF7 and UIF bind to the RBD domain of TAP/NXF1, whereas co-adaptors such as THOC5 and CHTOP bind to the NTF2L region.
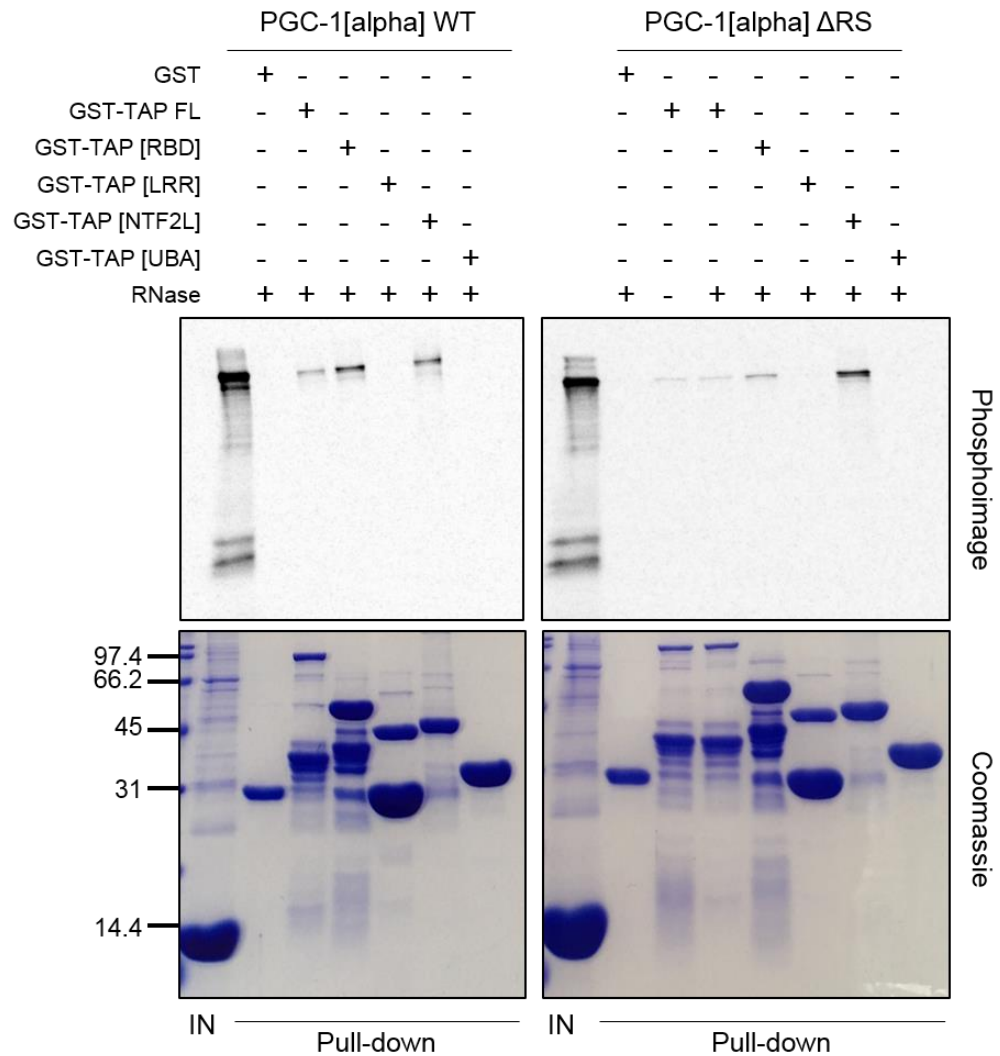
Figure 4.9 Pull-down assays with PGC-1[alpha] WT/ΔRS and TAP/NXF1 domains.

Full-length PGC-1[alpha] WT and ΔRS was expressed in reticulocyte lysates and ^{35}S-labelled and incubated with full-length TAP/NXF1 or its composing domains – RBD, LRR, NTF2L and UBA. Coomassie SDS-PAGE gels show lysate input and immobilised GST and and GST-tagged TAP/NXF1 domains. Phosphoimage shows the binding of PGC-1[alpha] WT to TAP/NXF1 FL, RBD and NTF2L with a strong signal for RBD. Conversely, ΔRS appears to bind to FL, RBD and NTF2L with a strong binding to the NTF2L domain. IN - input

In order to assess the exact binding site of PGC-1[alpha] on TAP/NXF1, all four TAP/NXF1 domains were expressed in bacterial cells and purified. This was accomplished using plasmids expressing N-terminal GST fusions of TAP/NXF1. Individual domain proteins were immobilised on GSH sepharose alongside GST-TAP/NXF1:p15 and GST. They were then incubated with ^{35}S-labeled full-length wild-type PGC-1[alpha] or ΔRS mutant expressed in reticulocyte lysates. Surprisingly, phosphoimages reveal binding of PGC-1[alpha] WT to both RBD and NTF2L but no binding to LRR or UBA. Binding to RBD appears to be marginally stronger in comparison to NTF2L. Furthermore, ΔRS shows decreased binding to RBD and significantly increased binding to NTF2L. This suggests that the RS domain of PGC-1[alpha] binds to the adaptor-binding site of TAP/NXF1 and ultimately may contribute to a new role of PGC-1[alpha] as a nuclear export adaptor.

4.6. PGC-1[alpha] is present in the TREX complex

As mentioned before, it has previously been shown that other nuclear export adaptors are present in a larger complex called TREX (transcription-export) involved in the processing of RNA (described in Chapter 1). Therefore, it was sought to find out whether PGC-1[alpha] is part of this complex. To answer this, HEK293T cells were co-transfected with FLAG-PGC-1[alpha] (WT or ΔRS) and c-Myc-tagged TAP/NXF1 prior to co-immunoprecipitation assay using anti-FLAG coated beads. An empty control plasmid carrying only the 3xFLAG tag was also co-transfected with c-Myc-TAP/NXF1 serving as a negative control. Input and eluted samples were used for western blotting. Membranes were probed with antibodies for FLAG – to detect PGC-1[alpha]; c-Myc – to detect TAP/NXF1; and antibodies against some of the TREX subunits such as ALYREF, UAP56 and THOC1. The input western blot image (left)

shows the expression of the co-transfected plasmids along with the endogenously expressed ALYREF, UAP56 and THOC1 (Fig. 4.10.). The FLAG-IP (right) shows that the WT and ΔRS were successfully immobilised onto the agarose beads as indicated by the enriched signal in comparison to the input image. Moreover, this shows that PGC-1[alpha] co-immunoprecipitates with TAP/NXF1, REF, UAP56 and THOC1. Interestingly, this is not ablated in the lack of the RS region. On the contrary, the signals for ALYREF, UAP56 and THOC1 that co-immunoprecipitate with ΔRS appear to be stronger as compared to WT. This study demonstrates that PGC-1[alpha] interacts with the TREX complex in an RNA independent manner. This is consistent with the fact that the deletion of the TAP/NXF1-binding region (RS) also implicated in RNA-binding does not affect the recruitment of PGC-1[alpha] to TREX. It was also noted that TREX subunits are more efficiently co-immunoprecipitated with ΔRS mutant of PGC-1[alpha].
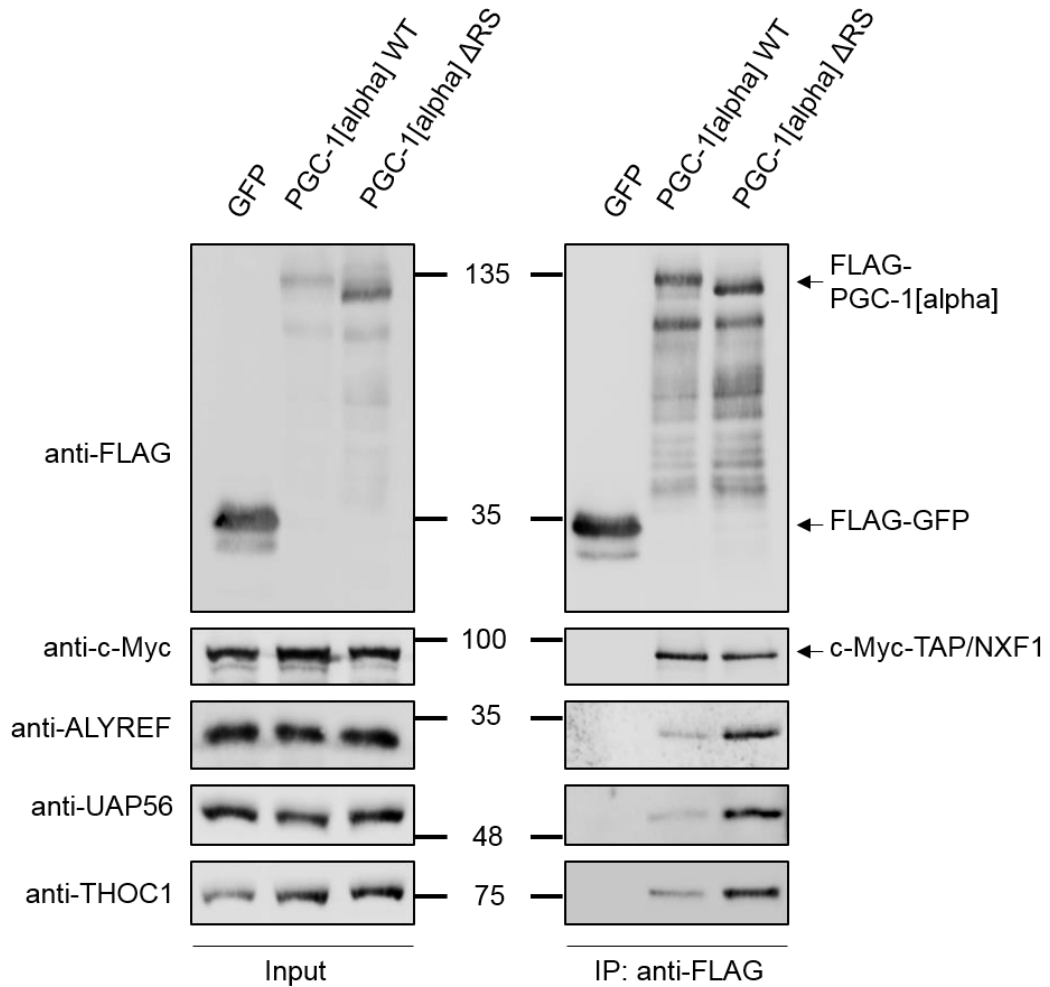
Figure 4.10 Involvement of PGC-1[alpha] in the TREX complex.

HEK293T cells were transiently co-transfected with plasmids expressing FLAG-tagged PGC-1[alpha] WT, ΔRS or GFP as a control and c-Myc-tagged TAP/NXF1. Whole-cell lysates were incubated with anti-FLAG beads and proteins (complexes) immunoprecipitated. Western blot was carried out with antibodies for FLAG, c-Myc, ALYREF, UAP56 and THOC1. Left panel shows input image with the expression of each of the plasmid constructs and the immunoprecipitated proteins. Right panel represents FLAG IP. None of the TREX complex proteins tested were found to interact with the negative control GFP. Conversely, all of them were found to interact with PGC-1[alpha] WT and ΔRS. The signal for ALYREF, UAP56 and THOC1 appears to be stronger in the IP with ΔRS. These data indicate the presence of PGC-1[alpha] in the TREX complex.

4.7. Cellular distribution of PGC-1[alpha] and TAP/NXF1 in differentiated neuronal cells

As aforementioned, PGC-1[alpha] has been implicated in the molecular pathology of several neurodegenerative diseases such as PD, AD, HD and ALS. This raises the question of whether TAP/NXF1 and PGC-1[alpha] are simultaneously expressed in the nuclei of cells of neuronal lineage. To assess this, Lund human mesencephalic (LUHMES) cells were co-stained with antibodies for endogenous PGC-1[alpha] and TAP/NXF1. Luhmes cells are a conditionally immortalised cell line. They have been generated by retroviral infection with an oncogene-containing (v-myc) vector which results in cell immortalisation. The expression of v-myc is under the control of a tetracycline activator in the same vector. The activator is inhibited upon addition of tetracycline which results in silencing of the v-myc gene and post-mitotic induction. Luhmes were differentiated to dopaminergic-like TH[+]-neurones (primary cell type affected in the pathology of PD) using tetracycline. The differentiated cells were kindly provided by Miss Irina Vazquez Villasenor in Prof Stephen Wharton's group, SITraN. After an hour incubation with primary antibodies followed by an hour in Alexa secondary antibodies, cells were imaged using confocal microscopy. Immunocytochemistry revealed nuclear regions with accumulation and some co-localisation of PGC-1[alpha] and TAP/NXF1 (Fig. 4.11.). in speckle-like formations. This indicates that both TAP/NXF1 and PGC-1[alpha] are expressed in the nuclei of neurones and suggests they interact as part of a similar complex. However, while the antibody recognising endogenous PGC-1[alpha] appears to be specific, it failed to produce a band of the right size when used in western blotting (data not shown). This can be addressed and validated by knocking-down PGC-1[alpha] in cells followed by immunofluorescence.
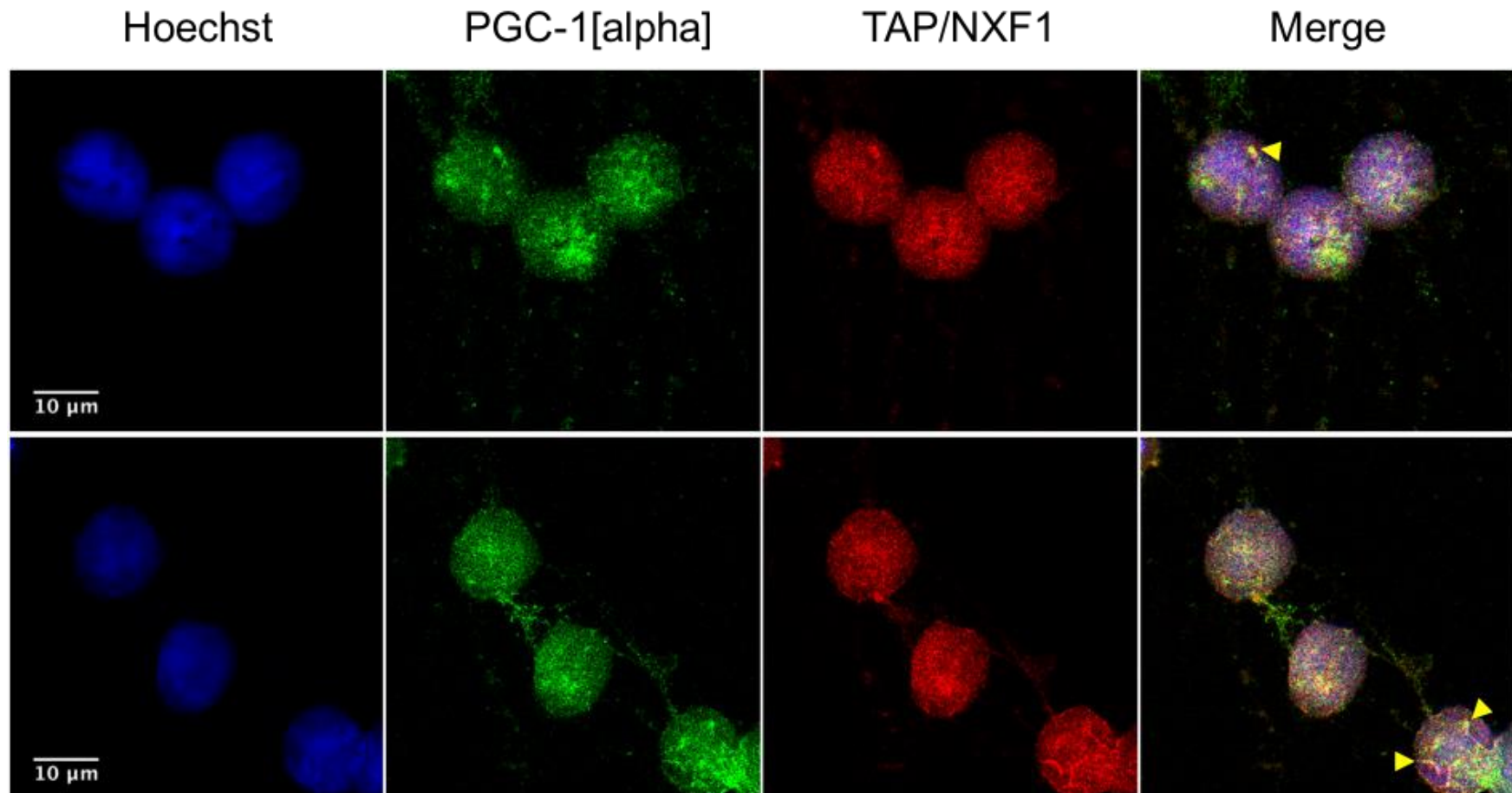
Figure 4.11 Colocalisation of endogenous PGC-1[alpha] and TAP/NXF1 in differentiated Luhmes cells.

Luhmes cells were differentiate to DA-like neurones using Tetracycline. Immunocytochemistry was performed for PGC-1[alpha] and TAP/NXF1 and confocal microscopy images taken for Z-stack. Nuclear PGC-1[alpha] (green) puncti appear to colocalise with TAP/NXF1 (red) puncti (yellow arrows).

145

4.8. Distribution of Poly-A+ RNA in cells overexpressing PGC-1[alpha]

Finally, another typical assay used for the characterisation of nuclear mRNA export adaptors, is the investigation of the cellular distribution of poly-A+ RNA by FISH (fluorescent *in situ* hybridisation) in cells overexpressing the protein of interest (Hautbergue et al., 2009; 2008). HEK293T cells were transiently transfected with FLAG-tagged plasmids for 48 hours followed by their fixation, immunostaining and oligo-(dT) FISH. Two negative controls were used for this assay i.e. untransfected cells and cells transfected with e1BAP5. e1BAP5 is an RNA- and TAP/NXF1-binding protein involved in the nucleocytoplasmic transport of mRNA. However, the protein does not possess biological abilities of nuclear export adaptor. In addition, cells were transfected with ALYREF, the canonical export adaptor, and full-length PGC-1[alpha]. All cells were also co-stained with Cy3-oligo(dT) that binds to the poly(A) tail of mRNA.

Untransfected cells show normal distribution of mRNA across the nucleus and the cytoplasm (Fig. 4.12.). Similarly, cells overexpressing e1BAP5 do not show abnormalities in their mRNA distribution. Conversely, cells highly overexpressing ALYREF show increased poly-A+ mRNA staining in the nucleus and decreased staining in the cytoplasm. The nuclear accumulation of mRNA indicates that the bulk mRNA nuclear export is inhibited or blocked. This is likely due to the disrupted balance between the overexpressed adaptor protein and the processing of mRNAs. It is likely that the excess of free overexpressed adaptors triggers abnormal interaction with free TAP/NXF1 locking TAP/NXF1 into an inactive state as RNA handover from the adaptor to TAP/NXF1 cannot occur. Cells overexpressing PGC-1[alpha] also showed nuclear accumulation of poly-A+ mRNAs and concomitant decrease in the cytoplasm

indicating that PGC-1[alpha] exhibits the hallmark of mRNA nuclear export adaptors when highly overexpressed in mammalian cells.
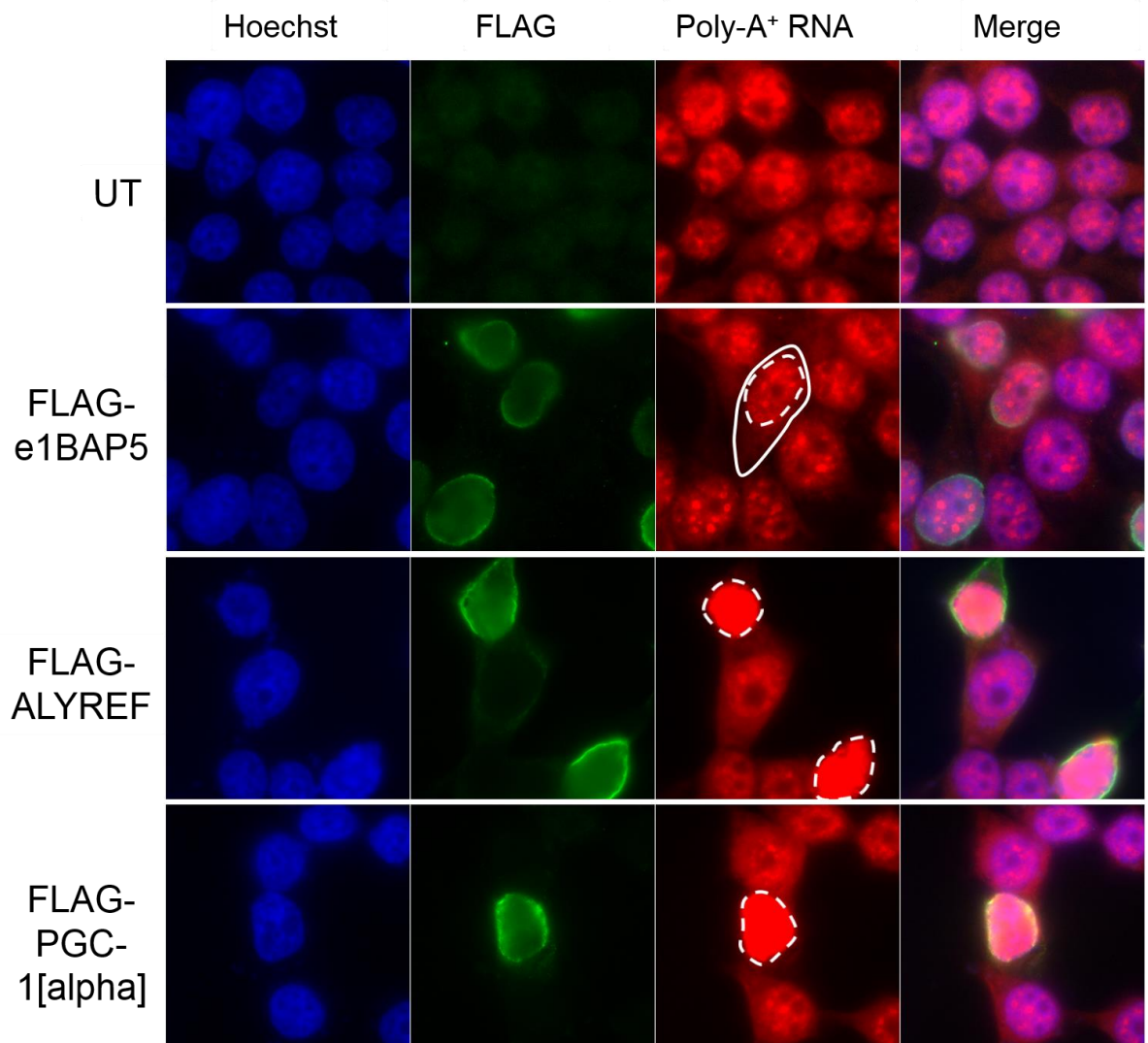
Figure 4.12 Bulk mRNA cellular distribution upon overexpression of PGC-1[alpha].

HEK293T cells were transiently transfected with e1BAP5 (negative control), ALYREF (positive control) and PGC-1[alpha] FL. Cells were stained with anti-FLAG antibody (green) to visualise transfected cells and Cy3-oligo(dT) (red) that binds to the poly(A) tail of mRNA molecules. Bulk mRNA appears equally distributed between nucleus (dashed line) and cytoplasm (continuous line) in untransfected cells (UT) and cells overexpressing e1BAP5. Conversely, cells highly overexpressing ALYREF and PGC-1[alpha] show accumulation of bulk mRNA in the nucleus. This is indicative of block of mRNA nuclear export.

4.9. Conclusions and discussions

This chapter summarised the work undertaken to characterise PGC-1[alpha]'s ability to bind TAP/NXF1:p15 and interact with the TREX complex in human cells.

Pull-down studies with recombinant TAP/NXF1:p15 and radiolabelled PGC-1[alpha] expressed in reticulocyte lysates showed the interaction between the proteins. Both PGC-1[alpha] and TAP/NXF1 have the ability to bind to RNA. This raises the logical question whether RNA molecules serve as a bridge between both proteins, a scenario in which PGC-1[alpha] and TAP/NXF1 are bound simultaneously on different regions of the same nucleic acid. However, it was shown that RNase treatment of the samples did not affect the binding demonstrating protein:protein interaction. Moreover, increasing amounts of PGC-1[alpha] protein directly correlate to proportional increase in pull-down signal indicating specific binding of PGC-1[alpha] to TAP/NXF1:p15.

Deletion studies of PGC-1[alpha] showed that the carboxyl-terminal binds TAP/NXF1 with a higher affinity compared to D1 and D2. This is according to expectations as D3 structurally resembles the typical conformation of nuclear export adaptors i.e. an RRM linked to an RS-region via an unstructured linker sequence. D1 and D2 do not share any homology to export adaptors, therefore the significantly decreased signal observed is not surprising. The presence of minimal signal is likely due to background unspecific binding that might be caused by altered 3D structure of the domains when expressed alone. However, this does not exclude the possibility of somewhat weak interaction between D1, D2 and TAP/NXF1. Nevertheless, the combination of D1 + D2 does not seem to be able to bind to TAP/NXF1, whereas D2 + D3 is able to interact with the nuclear export factor. This further confirms that the molecular crosstalk of PGC-1[alpha] and TAP/NXF1 is mediated by the C-terminal domain.

Subsequently, examining the carboxyl-terminal domain revealed that the RS region is responsible for the TAP/NXF1 binding but not the RRM. This was further confirmed using recombinant protein constructs of PGC-1[alpha] showing direct interaction of the RS. Moreover, deleting this region resulted in weakened binding to TAP/NXF1. Thus far, it appears that the RNA- and TAP/NXF1-binding domains of PGC-1[alpha] overlap, a common feature of mRNA nuclear export adaptors (Walsh et al., 2010).

Biochemical studies of this class of proteins have demonstrated that the binding to TAP/NXF1 is governed by the positively charged arginine amino acid. However, site-directed mutagenesis experiments in D3 of PGC-1[alpha], where arginines were substituted for negatively-charged glutamic amino acids, did not show any alterations in the ability of PGC-1[alpha] to bind TAP/NXF1. This suggests redundancy of arginines allowing for the use of multiple arginines, possibly in different combinations when some of them are unavailable (mutated). Another explanation includes the possibility of PGC-1[alpha] binding to TAP/NXF1 in a non-canonical manner. This has not yet been observed with other export adaptors, however, the co-transcriptional activator might use amino acids different to arginines in order to bind to the export factor. To elucidate this biochemical mechanism of protein interaction, structural studies involving NMR or crystallography need to be undertaken due to the lack of such in relation to the C-terminal domain. Unfortunately, as shown in Chapter 3, the purification of D3 proved to be challenging resulting in the need of denaturing conditions in order to obtain the recombinant protein. Not only that, but further attempts at dialysis led to the loss of PGC-1[alpha] due to precipitation.

The putative non-canonical binding of PGC-1[alpha] to TAP/NXF1 raised the question of whether it can play a role of an emerging new class of proteins denoted as co-adaptors. As aforementioned, such example is THOC5 which acts as a co-adaptor, and together with ALYREF, binds to TAP/NXF1 concomitantly. This possibility was

149

examined with binding studies of PGC-1[alpha] to the different domains of TAP/NXF1. It was shown that wild-type PGC-1[alpha] is able to bind to the adaptor-binding RBD and the co-adaptor-binding NTF2L domains. Moreover, deleting the RS resulted in increased binding to the NTF2L region. This suggests a putative dual role of PGC-1[alpha] acting simultaneously as a nuclear export adaptor and a co-adaptor. Indeed, PGC-1[alpha] is three times (on average) the size of most export adaptors and co-adaptors (except for THOC5) (Table 4.2.). The size of PGC-1[alpha] might have an impact on the spatial organisation of its domains assuming a particular 3D conformation that would facilitate both adaptor and co-adaptor functions.

Table 4.2 Summary table of known nuclear export adaptors and co-adaptors and their amino acid lengths and protein weight.

ID	Adaptor/Co-adaptor	Amino acids	Weight
PGC-1[alpha]	?	798	92 kDa
ALYREF (THOC4)	adaptor	257	27 kDa
SRp20 (SRSF3)	adaptor	164	19 kDa
9G8 (SRSF7)	adaptor	238	27 kDa
ASF/SF2 (SRSF1)	adaptor	248	28 kDa
UIF	adaptor	318	36 kDa
THOC5	co-adaptor	683	79 kDa
Chtop	co-adaptor	248	26 kDa

A key identifiable characteristic of export (co-)adaptors is their involvement in the TREX complex. FLAG co-immunoprecipitation confirmed the association of PGC-1[alpha] with the TREX complex. In particular, the coactivator immunoprecipitated

with key subunits of the complex such as TAP/NXF1, ALYREF, UAP56 and THOC1. Interestingly, deleting the RS region of PGC-1[alpha] resulted in increased association with ALYREF, UAP56 and THOC1 but not TAP/NXF1. The assembly and dissociation of these subunits is a transient event allowing for tightly controlled RNA processing. The increased binding is likely due to freezing of the dynamic process that allows for mRNA nuclear export and which requires handover of the RNA from the export adaptor to NXF1. The ΔRS mutant is unable to bind RNA resulting in the lack of handover to TAP/NXF1. Moreover, this in conjunction with what has been published before (Monsalve et al., 2000). Deletion of the RS region resulted in larger nuclear speckle formations colocalising with splicing factors such as SC-35. It was then hypothesised that PGC-1[alpha] gets stalled in the spliceosome, a phenomenon observed with another splicing factor/nuclear export adaptor SRSF1 in mutational studies where the RS region was deleted (Misteli et al., 1998). Interestingly, such increase in signal was not observed with TAP/NXF1. This is suggestive of diminished recruitment of TAP/NXF1 to the TREX complex, possibly via a different subunit but not PGC-1[alpha] as already the lack of RS results in decreased binding to the export factor.

The TAP/NXF1-binding ability of PGC-1[alpha] was further evaluated in neuronal differentiated cells. Immunocytochemistry of endogenous PGC-1[alpha] and TAP/NXF1 showed co-localisation of both proteins in nuclear speckle-like formations. Moreover, the images were captured using confocal microscopy and producing a Z-stack as opposed to 2D image further strengthening the observation. In addition, this interaction was observed in differentiated Luhmes that exhibits some features of dopaminergic neurones. The implication of this result allows for further studies in a neuronal context and ultimately in diseases such as neurodegenerative disorders. Indeed, Luhmes cells have been serving as a cell model in Alzheimer's and

Parkinson's research (Zhang et al., 2014). This also suggests that the nuclear export adaptor role of PGC-1[alpha] is not cell-type specific.

Finally, it was shown that overexpression of PGC-1[alpha] in HEK293T cells results in block of mRNA nuclear export characterised with nuclear accumulation of bulk mRNA. This has been observed with all identified export adaptors and as already mentioned it could be explained with overloading of TAP/NXF1 with RNA-free adaptors resulting in export impairment.

In conclusion, the set of studies in this chapter clearly demonstrates that PGC-1[alpha] acts as a nuclear export adaptor and possibly a co-adaptor *in vitro*.

5. Investigating the potential role of the RNA-binding activity of PGC-1[alpha] in energy homeostasis and mRNA nuclear export

5.1. Introduction

Following the characterisation of the RNA and NXF1-binding activities of PGC-1[alpha], it was sought to investigate whether the RNA-binding activity of PGC-1[alpha] is implicated in the maintenance of energy metabolism homeostasis and whether PGC-1[alpha] plays a role in the NXF1-dependent nuclear export of mRNA in stable isogenic human cell models. Transient transfection of cells, as used in experimental procedures in previous chapters, results in the overexpression of proteins and can reach non-physiological expression levels up to 50-100 fold. Therefore, it was set on establishing stable isogenic cell lines that would (i) allow for induction of PGC-1[alpha] knockdown and/or expression of a mutant form of PGC-1[alpha] that does not bind mRNA without the use of transfection and (ii) lead to a moderate overexpression of the integrated genes of interest. In addition, the expression is constitutively repressed and can be induced when necessary allowing for the precise characterisation of a biological role of a specific protein such as PGC-1[alpha] and moreover, the effect of the ΔRS mutant. Similarly, the mRNA nucleocytoplasmic transport function of other export adaptors such as UIF has been validated in stable inducible cell models (Hautbergue et al., 2009).

Following the successful generation of isogenic stable inducible cell lines of PGC-1[alpha] knockdown and wild-type substitution for ΔRS mutant, they had to be

functionally characterised. The reason for this was to determine whether these cell lines would exhibit any molecular pathology in relation to PGC-1[alpha] and significant deviation from controls. This would deem them as suitable cell models to study specific pathways and in particular mRNA nuclear export in the context of the current research work.

PGC-1[alpha] is a key player in mitochondrial homeostasis and changes in the levels of the protein would result in changes in mitochondrial biogenesis and maintenance. Therefore, it was hypothesised that the newly built cell lines would demonstrate mitochondrial impairment. Suitable assays to study energy dysfunction are MTT, ATP and western blotting to assess the protein levels of the complexes of the mitochondrial ETC. Therefore, these methods were employed in characterising the cell lines. However, several studies have reported that cells grown in high-glucose culturing medium rely predominantly on glycolysis for their energy production (Aguer et al., 2011; Rossignol et al., 2004). Glycolysis takes place outside the mitochondria resulting in the rapid production of ATP making the role of mitochondria in producing energy less essential. This often masks mitochondrial dysfunction (Aguer et al., 2011). Therefore, studies assessing mitochondrial homeostasis often use glucose-free medium supplemented with galactose. Galactose is metabolised at slower rates by cells and while it feeds directly into glycolysis it does not result in the net production of ATP. Cells are then forced to rely predominantly on mitochondria, hence why any dysregulation of metabolism might have detrimental or negative impact on cellular homeostasis (B. H. Robinson et al., 1992). This clearly demonstrates the importance of methodology design and the use of galactose as a mitochondrial challenger was utilised in the functional characterisation studies of PGC-1[alpha] cell lines.

Lastly, mitochondrial defects were assessed further at the mRNA level and in particular their nucleocytoplasmic transport.

In addition, the fast developing field of stem cells and cell reprogramming provides an exciting opportunity for a novel approach of generating neural progenitor cells from HEK293 cell models of PGC-1[alpha]. This would allow for research in the context of brain cells and ultimately brain-related ageing and diseases.

This chapter describes the experimental work carried out for the building of HEK293 stable inducible cell models of PGC-1[alpha] deficiency or a cell line expressing the ΔRS mutant and their functional characterisation. It also explains the novel reprogramming of these cell lines to induced neural progenitor cells. The fundamental questions sought to be answered were: (1) does knockdown of PGC-1[alpha] result in mitochondrial impairment such as ATP production; (2) does this dysregulation relate to any changes of mitochondrial protein levels; (3) are these changes due to impaired mRNA nuclear export; (4) does the lack of RNA- and decreased TAP/NXF1-binding function in the ΔRS mutant recapitulate the molecular phenotypes observed in PGCi and (5) can immortalised HEK293 Flp-In T-REx cells be reprogrammed to induced neural progenitors.

5.2. Generating HEK293 stable inducible cell models of PGC-1[alpha] deficiency and mutant complementation

To build stable inducible cell lines of PGC-1[alpha], HEK293 Flp-In™ T-REx™ host cell line was purchased from Invitrogen (Life Technologies). The host line has been generated by the sequential transfection of HEK293 cells with a vector carrying a Flp Recombination Target (FRT) site downstream of a SV40 early promoter and an ATG site alongside a vector carrying tetracycline repressor (TetR) downstream of a CMV promoter. This has resulted in the sequential, random and independent genomic integration of both vectors. Successfully transformed cells have been selected based on their ability to survive in the presence of zeocin and blasticidin. This acquired antibiotic resistance is coming from FRT and TetR vectors, respectively. All of these steps in generating a host cell line have been accomplished by Invitrogen prior to commercial distribution.

Following this, cells were seeded on a 10-cm dish and cultured to confluency of >80%. They were then co-transfected with the pcDNA5/FRT plasmid carrying PGC-1[alpha] miRNAs or pcDNA5/FRT/3XFLAG with the complementation system (described in Chapter 3) and a plasmid expressing Flp recombinase. Control miRNA cell line has been generated previously in the laboratory of Prof Stuart Wilson (Hautbergue et al., 2009) and was kindly provided for this work. Flp recombinase catalyses the homologous DNA recombination at FRT sites facilitating the stable genomic integration of the gene of interest (GOI) from the pcDNA5/FRT plasmids (Fig. 5.1.). Successful homologous recombination results in loss of zeocin resistance and gain of hygromycin resistance. pcDNA5 vector also carries two tetracycline operators (TetO$_2$) directly upstream of the GOI and downstream of the CMV promoter. TetO$_2$

region is occupied by the constitutively expressed TetR blocking access of RNA Polymerase II to GOI resulting in transcription inhibition. However, upon addition of tetracyclin to culturing medium, tetracyclin binds to TetR resulting in its dissociation from $TetO_2$ and ultimately leading to GOI expression. Subsequently, cells were grown in culture media containing hygromycin and blasticidin. This allowed for the efficient screening of surviving cell colonies carrying GOI. Individual colonies were then transferred to 24-well plates and grown to ~80-90% confluency. Each confluent colony was split into two wells and each well was grown in hygromycin or zeocin. Cell survival was monitored where cell death in zeocin and further survival in hygromycin demonstrated integration of GOI at FRT site. Successful colonies were then expanded and frozen down in liquid nitrogen.
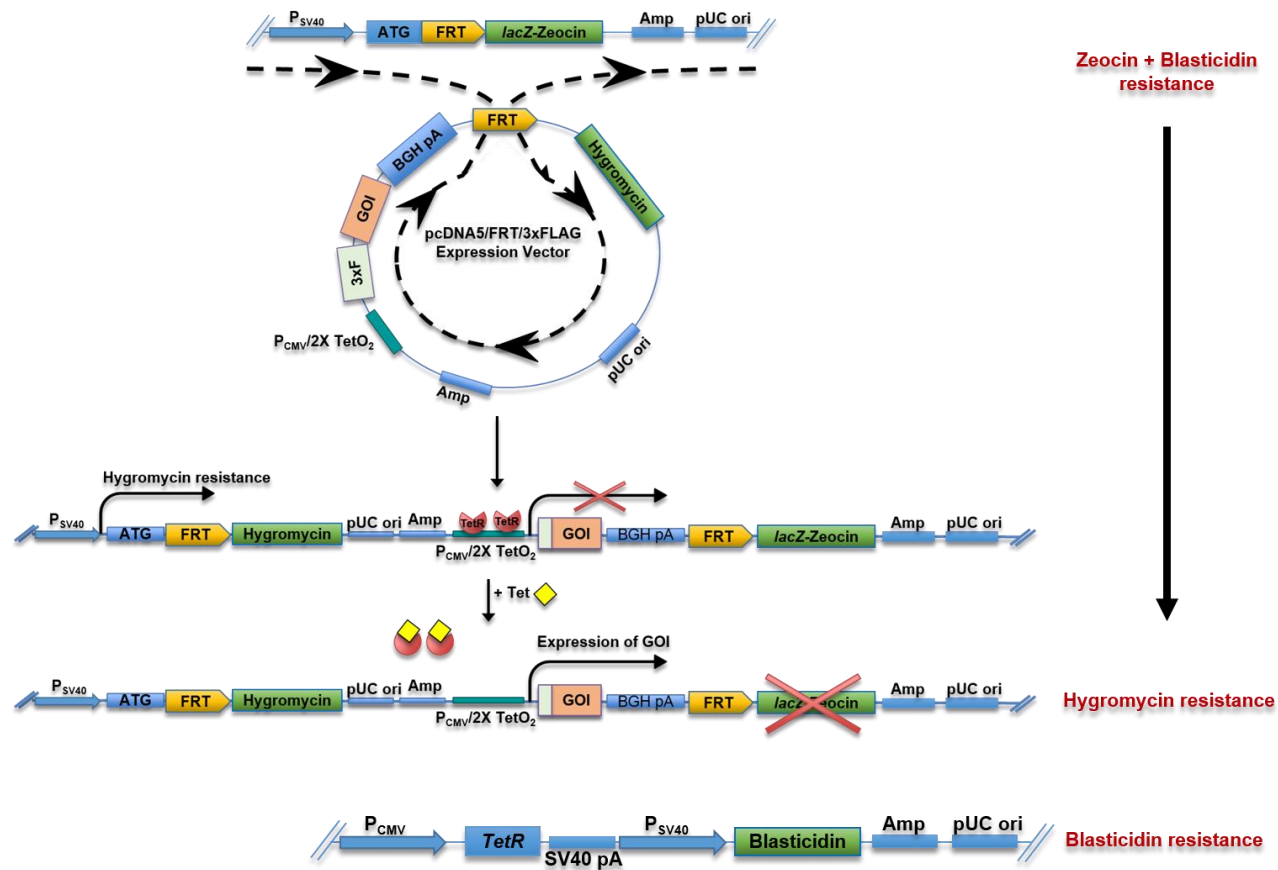
Figure 5.1 Schematic representation of HEK293 Flp-InTM T-RExTM stable inducible cell line generation.

Host cell line is co-transfected with a vector carrying GOI and another one carrying Flp recombinase enzyme. Recombinase drives DNA homologous recombination between FRT sites of host cell line and GOI plasmid. Successful integration of GOI results in switch of antibiotic resistance from zeocin and blasticidin to hygromycin and blasticidin. Addition of Tetracycline (Tet) to culturing media results in disinhibition of CMV promoter/Tet operator and subsequent gene expression.

As aforementioned, two sets of two cell lines were generated. The first set included cells expressing control miRNA and cells expressing PGC-1[alpha] miRNA resulting in gene silencing. The second set included the two complementation plasmids WT and ΔRS where endogenous PGC-1[alpha] was silenced and replaced with a miRNA-resistant WT or ΔRS.

37 colonies of PGCi survived hygromycin switch after transfection. This resulted in 20 PGCi colonies dying in zeocin. Six of them were then selected and tested for the expression of GOI upon addition of tetracyclin. Cells were induced for 72 hours with tetracyclin and compared to Ci line via qRT-PCR assessing PGC-1[alpha] mRNA levels (Fig. 5.2. A). Five of the colonies showed ~70% reduction in mRNA levels and two of them, 1/18 and 3/10 were selected for further analysis. The decision was called based upon the rate of cell growth where both colonies had cell-doubling rate typical of other HEK293 stable inducible cell lines available in the lab. These were then induced as mentioned above and compared to non-induced cells for PGC-1[alpha] mRNA levels (Fig. 5.2. B). Analysis of qRT-PCR data revealed that the mRNA levels of PGC-1[alpha] in 3/10 were affected (~40% decrease) even in the absence of tetracyclin deeming it unsuitable for further studies. Fortunately, colony 1/18 showed no changes in PGC-1[alpha] without induction compared to Ci and observable ~70% reduction post induction. 1/18 was taken forward for subsequent characterisation of PGC-1[alpha] knockdown.
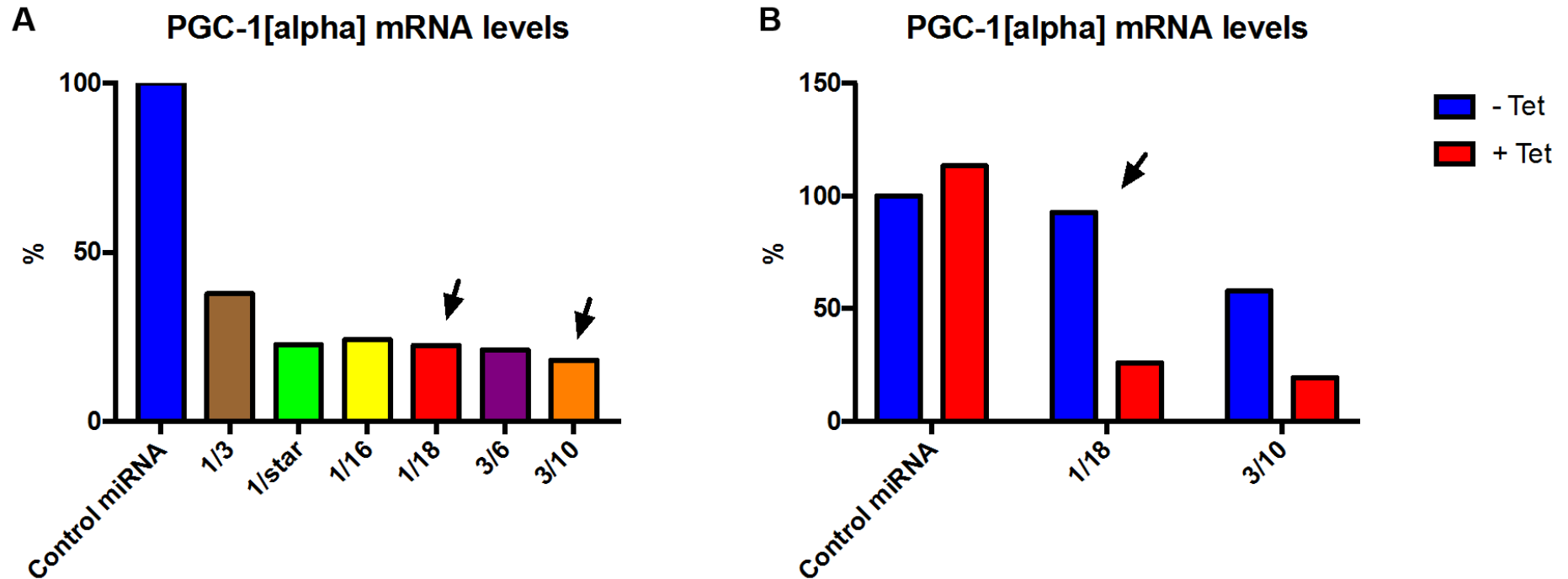
Figure 5.2 Selection of PGC-1[alpha] knockdown clones.

A) Clones surviving in hygromycin and dying in zeocin were selected and induced with Tetracycline for 72 hours. The mRNA levels of PGC-1[alpha] levels were assessed via QPCR and clones 1/18 and 3/10 chosen for further studies. **B)** 1/18 and 3/10 cells were cultured with or without the presence of Tetracycline. PGC-1[alpha] mRNA levels were determined across the different conditions and compared to control line. 1/18 showed no reduction in the absence of Tet and 70% reduction when induced. 3/10 showed reduction of ~30% in the absence of Tet showing abnormal inducible system, therefore it was discarded. 1/18 was chosen for further studies.

Following this, the WT and ΔRS cell lines were generated. 23 colonies of WT and 27 colonies of ΔRS were grown in zeocin after hygromycin switch. Three and six colonies for WT and ΔRS, respectively, were taken forward for further screening. Colonies were grown in the absence and presence of tetracyclin for 72 hours, as aforementioned, and their ability to induce protein expression was assessed via western blotting (Fig. 5.3. A). miRNA-resistant PGC-1[alpha] in both cell lines carries 3xFLAG-tag, therefore an anti-FLAG antibody was used. All colonies were successful in expressing WT or ΔRS only in the presence of tetracyclin. WT colony 8 was selected based on the higher expression compared to the two other colonies. ΔRS expression appeared similar in all six colonies, therefore a decision was made again based on growth rate, and colony 2 was taken forward. The mRNA levels of endogenous PGC-1[alpha] were also assessed and its knockdown confirmed as compared to Ci and PGCi in the two colonies selected (Fig. 5.3. B). WT and ΔRS showed similar to PGCi knockdown of endogenous PGC-1[alpha]. The qRT-PCR primer pair used was specifically designed so it recognises the 3'-untranslated region (3'UTR) of PGC-1[alpha]. This allows for detection of the endogenous PGC-1[alpha] transcripts as the integrated open reading frames are under the control of a bGH cleavage/poly-adenylation sequence.
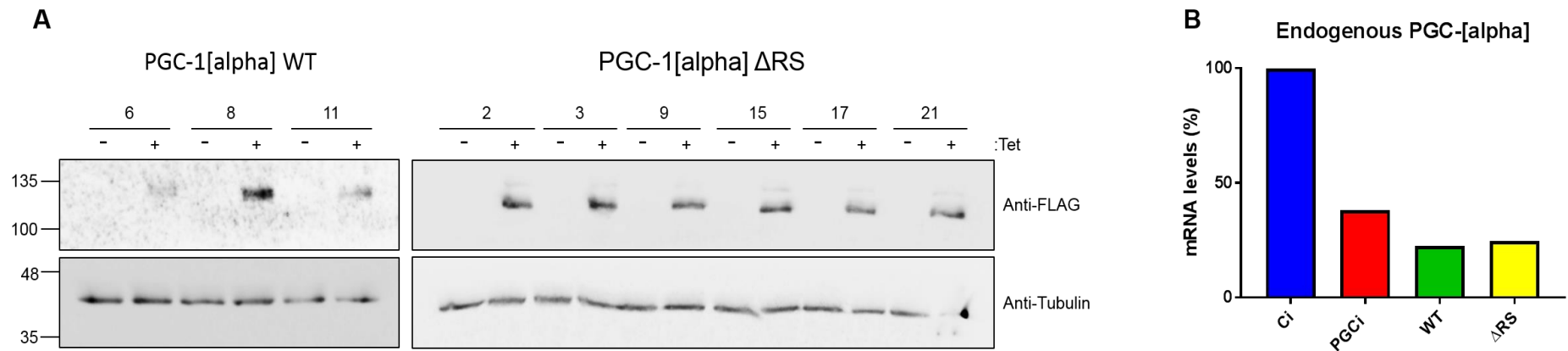
Figure 5.3 Selection of WT and ΔRS clones.

A) Western blotting analysis of WT and ΔRS grown in the absence or presence of Tetracycline shows successful repression/induction of PGC-1[alpha] (top panel). Tubulin levels appear similar between samples indicating equal loading (bottom panel). Clones 8 and 2 were selected for further analysis.
B) QPCR analysis of endogenous mRNA levels in WT and ΔRS upon induction of PGC-1[alpha] show similar to PGCi decrease as compared to Ci.

5.3. Functional characterisation of stable inducible cell lines

5.3.1. Control versus PGC-1[alpha]-deficient cells

5.3.1.1. PGC-1[alpha] knockdown is robust and reproducible

The robustness of the system in achieving reproducible knockdown of PGC-1[alpha] was first examined. Total RNA was extracted from biological replicates of both Ci and PGCi. Each replicate was represented by a subsequent cell passage. The same reduction of ~63% of PGC-1[alpha] mRNA levels was observed for each replicate achieving high reproducibility indicated by small error bars and low p-value (Difference 62.84±10.29; p<0.001; n=5) (Fig. 5.4.).
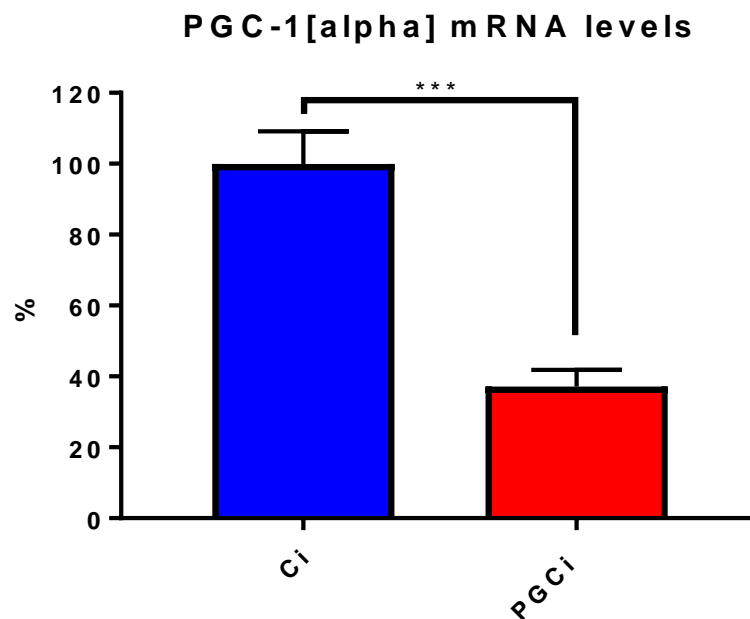
Figure 5.4 qRT-PCR of PGC-1[alpha] knockdown in stable inducible cell lines.
Ci and PGCi cells were induced with Tetracycline for 72 hours and their total RNA extracted. From that, cDNA was synthesised and levels of PGC-1[alpha] quantified using qRT-PCR. PGC-1[alpha] show robust decrease of 62.84±10.29 indicating reproducible knockdown upon induction. Unpaired *t*-test; *** p<0.001. Error bars represent SEM. n=5.

5.3.1.2. PGC-1[alpha]-deficient cells show decreased cell proliferation

Following the confirmation of the efficiency of the cell lines, the effect of PGC-1[alpha] knockdown on cell proliferation was examined. For this an MTT cell proliferation assay was undertaken. MTT is a metabolic colourimetric-based assay that measures the reduction of yellow tetrazole salt to purple formazan achieved by cell enzymatic activity of the mitochondria directly related to proliferation (Sylvester, 2011).

MTT assay was carried out with cells that had been cultured in glucose or galactose media with or without tetracyclin for 72 hours. As expected, the MTT results from the non-induced cells grown in high-glucose media showed no differences in cell metabolism (proliferation) (Fig. 5.5. A). Interestingly, the knockdown of PGC-1[alpha] also had no observable effect on proliferation as compared to the control. However, a switch to glucose-free media with added galactose resulted in significant differences (Fig. 5.5. B). Regardless of tetracyclin induction, cells showed significant reduction in cell proliferation by ~35% upon PGC-1[alpha] knockdown. A possible reason for this
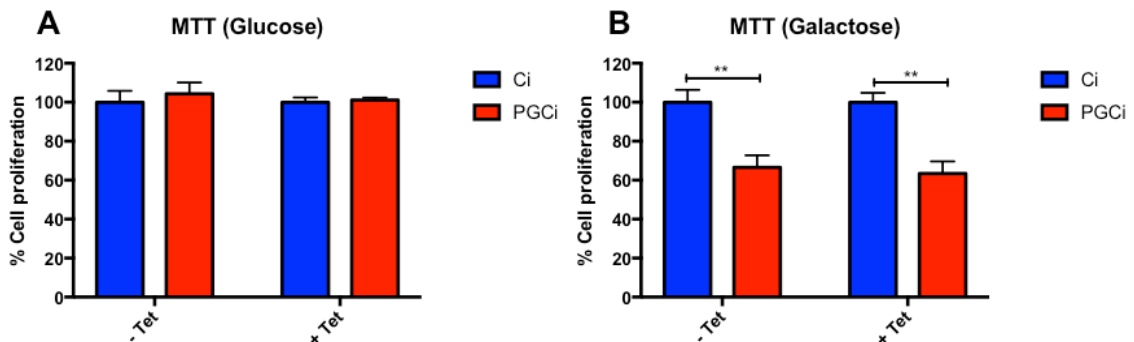
Figure 5.5 MTT cell proliferation assay shows decrease in PGCi cell lines cultured in galactose.

A) MTT cell proliferation assay was carried out with Ci and PGCi cell lines cultured in glucose in the presence or absence of Tetracycline. No differences in cell metabolism were observed between the conditions. **B)** Same MTT was carried out with cells grown in galactose. This revealed significant reduction in cell proliferation in PGCi compared to control. This was independent of Tetracycline induction as seen for both conditions (-Tet difference 33.5±8.4; + Tet difference 36.53±8.4). Two-way ANOVA. ** $p < 0.01$. Error bars represent SEM. n=3.

might be the fact that the inducible system does not provide 100% repression resulting in leakiness of gene transcription and expression.

5.3.1.3. Knockdown of PGC-1[alpha] results in decreased ATP production in mitochondria

Results from MTT cell proliferation assay indicated reduced metabolism when cells were challenged with glucose-free galactose culturing media upon knockdown of PGC-1[alpha]. Along with this, it is a well-known fact that PGC-1[alpha] is the master mitochondrial regulator. Therefore, the ATP levels of cells were measured both in glucose and galactose, without or with tetracyclin induction. Cells were induced for 72 hours as aforementioned with media change 24 hours prior to assay. Cells were first lysed in wells to release ATP and then incubated with substrate that binds to ATP and along with luciferase enzyme produces luminescent signal that is directly relevant to the amount of ATP present in cells. The signal was measured and this was followed by CyQUANT NF Cell Proliferation assay. Plate was incubated with CyQUANT dye reagent that binds to cellular DNA molecules of lysed cells and produces fluorescent signal. The DNA content is proportional to cell number, therefore CyQUANT values were used to normalise ATP readings in order to avoid plating errors and different growth rates between the cell lines. The effect of PGC-1[alpha] knockdown was determined by dividing normalised results from PGCi cell line by normalised results from Ci cell line in the appropriate conditions. PGC-1[alpha]-deficient cells that were cultured in glucose-rich media did not show any differences to non-induced cells (Fig. 5.6.). However, when glucose was changed for galactose as a metabolite, clear differences were observed. Similar to MTT, non-induced cells showed decrease in ATP levels by ~20% possibly due to leakiness. However, the ATP levels of induced cells were reduced further by a total of ~35% indicating the effect of PGC-1[alpha]

knockdown on ATP production. This further confirms the functionality of the stable inducible cell lines and the impact of PGC-1[alpha] on mitochondrial production of ATP.
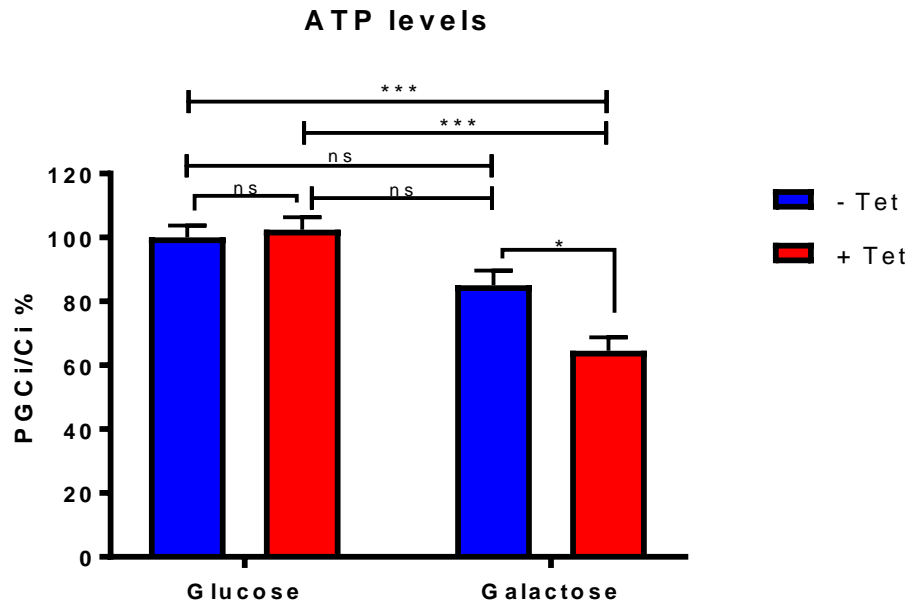
ATP levels

Figure 5.6 Measuring ATP levels upon knockdown of PGC-1[alpha].

Cells grown in glucose did not show any significant differences in their ATP production even upon induction with Tetracycline. In contrasts, cells cultured in galactose showed insignificant decrease in ATP levels without Tetracycline, however induced cells demonstrated significant reduction in ATP levels as compared to glucose -/+ Tet (35.5 ± 5.879/37.95 ± 5.879) and galactose –Tet (20.55 ± 5.879) conditions. Two-way ANOVA. * p<0.05, *** p<0.001. Error bars represent SEM. n=3.

5.3.1.4. Knockdown of PGC-1[alpha] affects COX2 protein levels in response to mitochondrial stimulus

Thus far, MTT cell proliferation assay identified metabolic dysregulation upon knockdown of PGC-1[alpha]. Furthermore, it was detected that this metabolic dysfunction is related to decreased production of ATP from mitochondria. As

166

explained in Chapter 1, mitochondrial ATP is produced via the ETC on the inner membrane of mitochondria. Therefore, it was sought to answer the fundamental question whether the decrease in ATP is due to dysregulation of any of the complexes of the ETC. This was assessed using a cocktail OXPHOS antibody – a mixture of five primary antibodies, each of which recognises a single subunit of each of the five respiratory complexes.

Cells were cultured in glucose or galactose media in the presence of tetracyclin for 72 hours. Non-induced cells were not used for this assay based on the result obtained from MTT and ATP assays that show further dysregulation in induced cells. This was followed by lysis and western blotting. The arbitrary protein levels were determined from triplicate data obtained from consecutive cell passages. Each subunit quantity was calculated as a proportion of the named subunit from the accumulative amount of all five subunits for each condition.

No significant difference was observed in protein levels for complexes I, II, III and V. Galactose had no significant effect on these complexes (where their protein levels were slightly increased compared to glucose). Surprisingly, PGC-1[alpha] deficiency had prominent and significant impact on COX2 in complex IV. In glucose, COX2 protein levels were comparable between Ci and PGCi. In contrast, when glucose was substituted for galactose, COX2 levels were significantly decreased by ~200% in PGCi as compared to Ci. Protein levels in Ci had significant increase by ~3–fold in galactose in comparison to glucose, while they remained unchanged in PGCi. This indicated that in physiologically 'normal' HEK293 cells COX2 protein expression increases when cells are challenged with galactose. However, this upregulation is absent in cells deficient for PGC-1[alpha] which could be a direct cause for the decreased production of ATP.
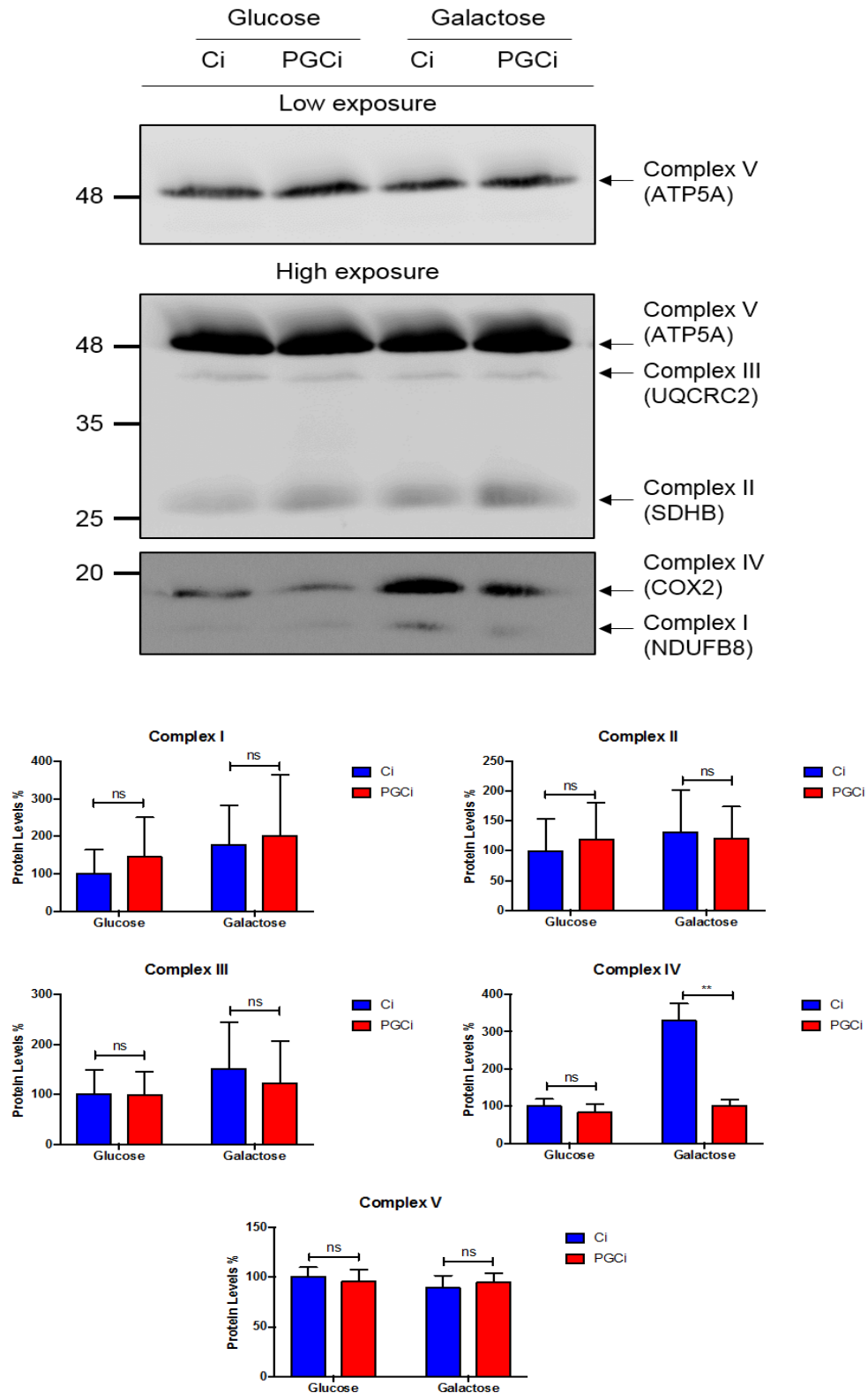
Figure 5.7 OXPHOS western blotting shows decrease in complex IV (COX2) protein levels.
Ci and PGCi stable cell lines were induced and cultured in glucose or galactose followed by cocktail anti-OXPHOS western blotting. No differences were observed for complexes I, II, III and V. Complex IV subunit COX2 showed no differences between cells cultured in glucose. This was followed by significant increase of protein expression in control lines and failure at upregulation in PGCi resulting in significant difference between Ci and PGCi (227 ± 23.55). Bar charts represent proportion of each complex from the total mitochondrial protein amount (the sum of all five complexes). Two-way ANOVA. ** p<0.01. Error bars represent SEM. n=3.

5.3.1.5. Block of nuclear export of mitochondrial regulatory genes is observed in PGC-1[alpha]-deficient cells

Downregulation of protein expression often correlates with decrease of its mRNA levels. Therefore, it was sought to investigate whether mRNA levels of COX2 were changed upon knockdown of PGC-1[alpha] or whether this might be a result of an alternative process such block of mRNA nuclear export of mitochondrial regulators. For this, the mRNA levels of key mitochondrial transcription factors NRF-1 and TFAM were assessed in total RNA or RNA isolated from cytoplasmic fractions.

Induced cells were cultured in glucose media followed by RNA extraction. Cytoplasmic cellular fractionation was performed using hypotonic buffer that breaks open the cell membrane leaving intact the nuclear envelope. These fractions were then validated by western blotting and probed for an exclusively nuclear marker such as the chromatin remodeling factor SSRP1, a subunit of the FACT complex (Fig. 5.8. A). FACT (<u>fa</u>cilitates <u>c</u>hromatin <u>t</u>ranscription) is a heterodimeric histone chaperone complex located in the nucleus. After confirmation of absence of nuclear contamination, RNA was extracted and used in qRT-PCR. Preliminary data (n=2) showed expected decrease of PGC-1[alpha] mRNA levels in PGCi cells (Fig. 5.8. B). Surprisingly, decrease in total levels of NRF-1, TFAM and COX2 was not observed. However, the cytoplasmic levels of NRF-1 and TFAM were significantly decreased as compared to control and presented as a ratio Cyto/Total (Fig. 5.8. B and C). This indicated block or inhibition of mRNA nuclear export in PGC-1[alpha]-deficient cells and further suggested a role of PGC-1[alpha] as an export adaptor. COX2 cytoplasmic levels remained the same as expected due to the fact that COX2 is mitochondrially encoded and potentially relying on mitochondrial ribosomes for its translation.
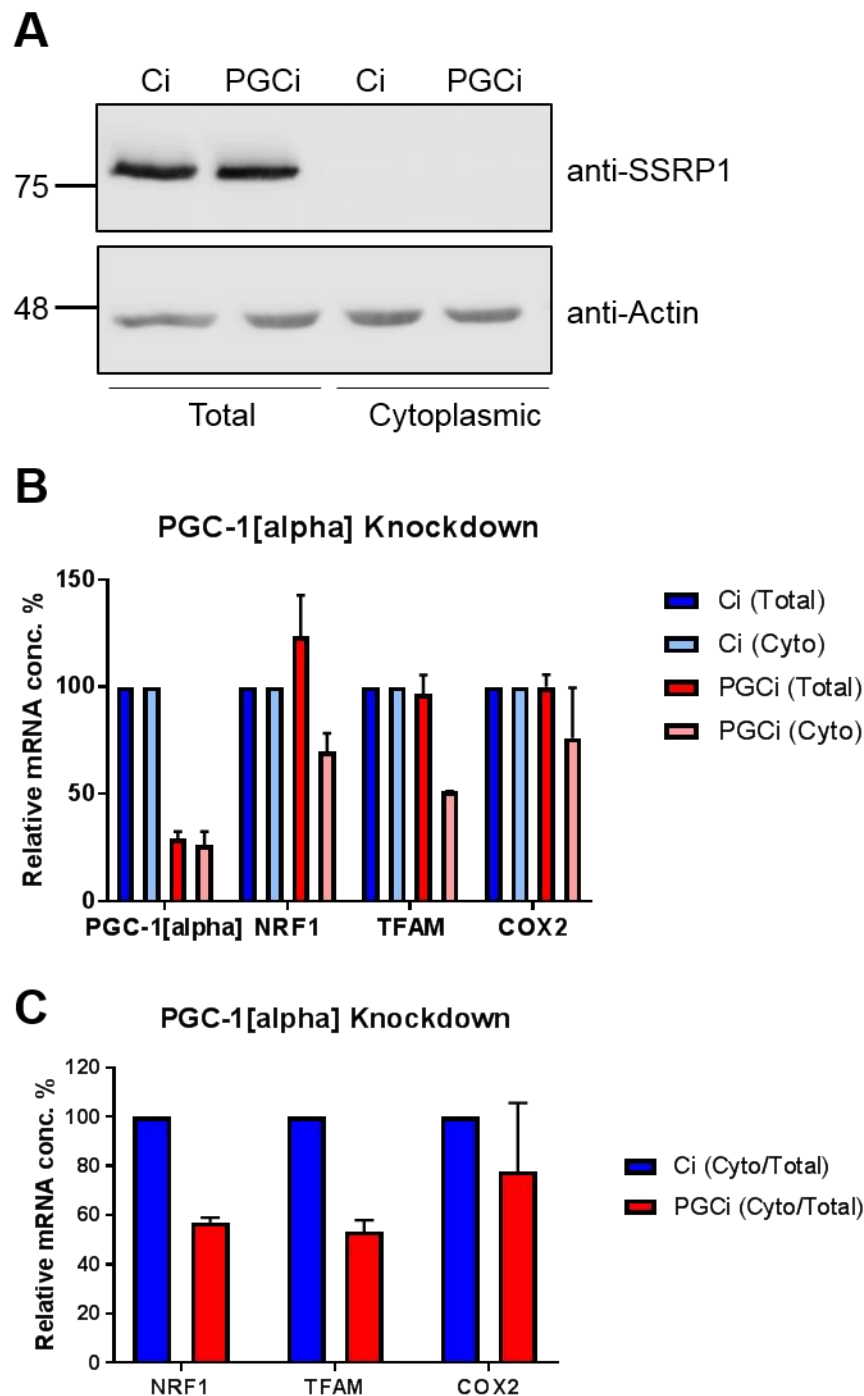
Figure 5.8 Reduction in mRNA nuclear export of key transcription factors involved in mitochondrial homeostasis after knockdown of PGC-1[alpha].

Ci and PGCi cells were grown in glucose in the presence of Tetracycline. Total RNA and cytoplasmic RNA was isolated and used for qRT-PCR assessment. **A)** shows anti-SSRP1 western blotting for nuclear marker assessing the purity of the cytoplasmic fraction. It appears that there is no nuclear contamination in the cytoplasmic fraction. **B)** shows total and cytoplasmic mRNA levels of PGC-1[alpha], NRF1, TFAM and mitochondrially encoded COX2. PGC-1[alpha] shows successful knockdown. No changes are detected at total levels for each of the other genes. NRF1 and TFAM show reduction of cytoplasmic mRNA. **C)** NRF1 and TFAM show decrease of ~50% in nucleocytolasmic transport upon PGC-1[alpha] knockdown. COX2 mRNA levels appear to be unchanged. n=2. Ci set at 100%. Error bars represent SEM.

5.3.2. Wild-type versus ΔRS mutant of PGC-1[alpha] cell models

It is clear that PGC-1[alpha] deficiency has a significant negative effect on mitochondrial homeostasis. Following this, the remaining question was whether the lack of the RS-region in the ΔRS mutant of PGC-1[alpha] would recapitulate any of these molecular phenotypes and ultimately whether it would result in dysregulation of nucleocytoplasmic transport of NRF-1 and TFAM mRNA.

5.3.2.1. ATP reduction is observed in PGC-1[alpha] mutant cells

Firstly, ATP levels were measured in WT and ΔRS cells cultured in glucose or galactose media in the presence or absence of tetracyclin.

Similarly to Ci and PGCi, no significant differences were observed between ΔRS and WT in glucose-rich media regardless of induction conditions (Fig. 5.9.). Conversely, switch from glucose to galactose revealed significant differences between ΔRS and WT. ATP levels were equally decreased in ΔRS in the absence or presence of tetracycline possibly due to the leakiness of the inducible system. Therefore, induced cells were used in further studies.
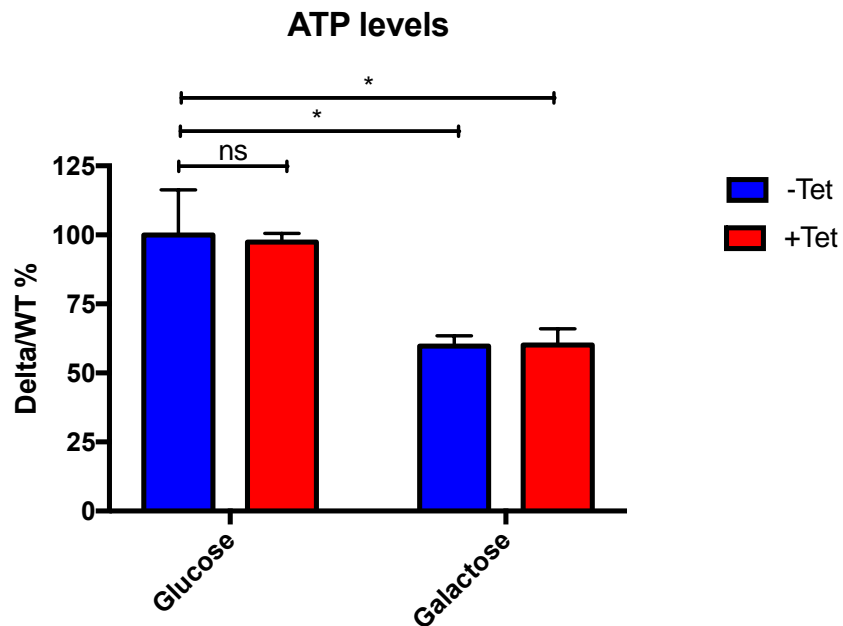
Figure 5.9 ATP reduction is observed when ΔRS PGC-1[alpha] mutant cells are cultured in galactose.

No differences in ATP production were observed in cells grown in glucose. Switch to galactose media revealed significant downregulation of ATP generation in ΔRS mutants regardless of induction (-Tet 59.73 ± 12.72; +Tet 60.14 ± 12.72). Bars are presented as ΔRS/WT ratio. Two-way ANOVA. * $p < 0.05$. Error bars represent SEM. n=3.

5.3.2.2. Expression of ΔRS affects COX2 protein levels upon mitochondrial challenge

The reduction of ATP production in ΔRS cells replicated the results observed upon knockdown of PGC-1[alpha]. This raised again the question whether the mitochondrial generation of ATP is due to dysregulation of protein expression of any of the five complexes of the ETC.

OXPHOS western blot was performed as mentioned above in induced WT and ΔRS cells and protein levels quantified (Fig. 5.10.). No significant differences were detected between both cells lines under conditions of high glucose recapitulating PGC-1[alpha] knockdown. Interestingly, COX2 (Complex IV) protein expression was similar in glucose followed by significant increase in WT when switched to galactose. Surprisingly, the protein levels of Complex IV subunit failed again to increase in ΔRS cells when cultured in galactose. This clearly indicates that the lack of the RS-rich region in the carboxyl-terminal of PGC-1[alpha] has an overall negative effect on its biological function resulting in specific dysregulation of COX2 under mitochondrially-challenging conditions. This mimicks the molecular phenotype produced by PGC-1[alpha] deficiency.
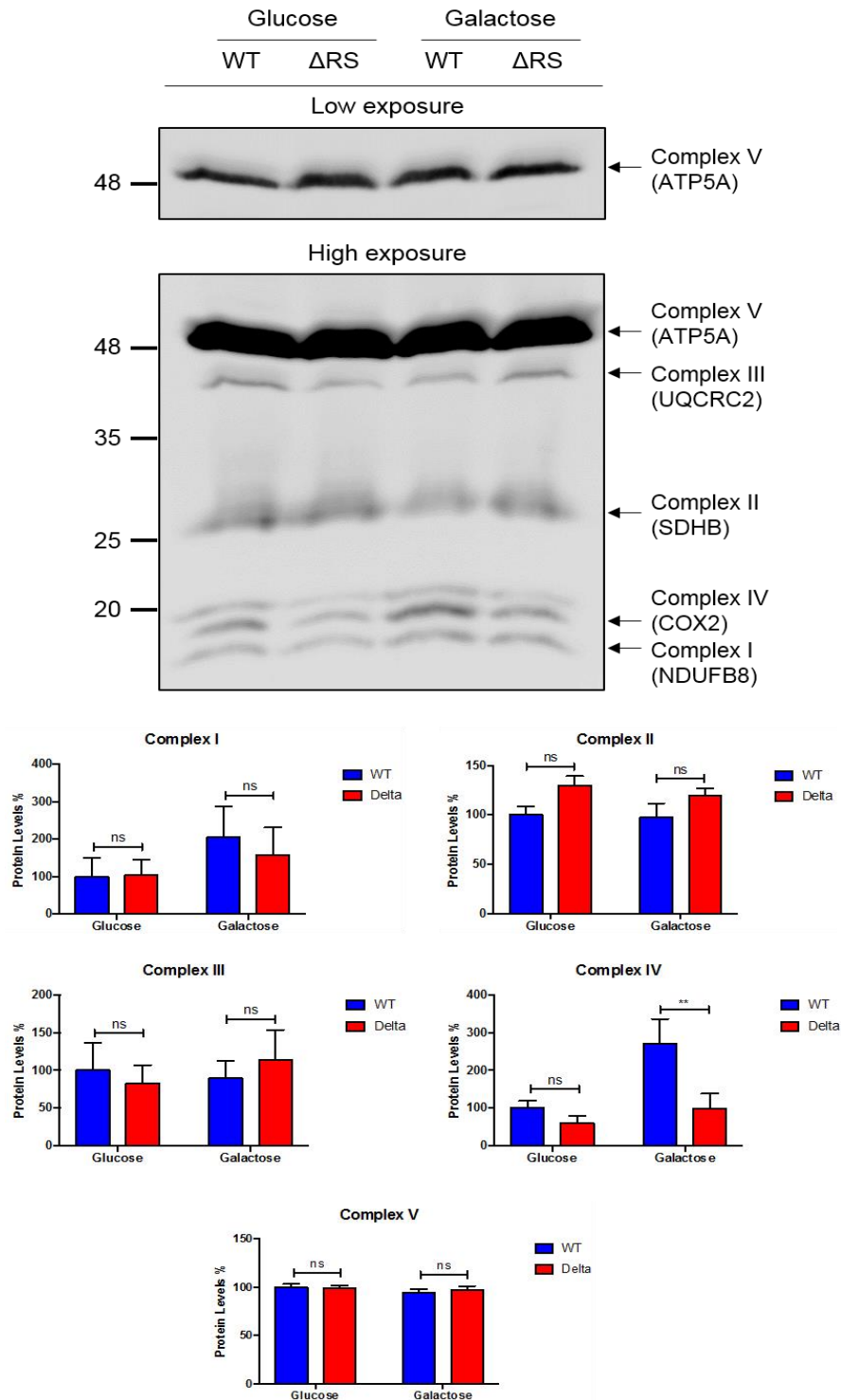
Figure 5.10 PGC-1[alpha] ΔRS mutant shows similar molecular phenotype to PGC-1[alpha]-deficient cells.

Induced WT and ΔRS cells were grown in glucose or galactose media and protein levels of ETC complexes assessed via OXPHOS western blotting. There were no differences in protein levels of complexes I, II, III and V. Complex IV, subunit COX2 showed no differences in glucose, however switch to galactose resulted in significant upregulation of WT and failure to do so in ΔRS. This demonstrated significant differences between WT and ΔRS (171 ± 20.94) replicating results observed with PGC-1[alpha] knockdown. Bar charts represent proportion of each complex from the total mitochondrial protein amount (the sum of all five complexes). Two-way ANOVA. ** $p < 0.01$. n=3.

5.3.2.3. ΔRS mutant expression suggests block of nuclear export of TFAM.

Similar molecular phenotype of COX2 decrease in protein levels in ΔRS indicated that this might also be due to impairment of mRNA nuclear export of NRF-1 and TFAM rather than downregulation of COX2 transcription. Therefore, qRT-PCR was carried out assessing the total and cytoplasmic levels of NRF-1, TFAM and COX2 in cells grown in glucose. Along with anti-SSRP1 western blotting to confirm pure cytoplasmic fractions, anti-FLAG western blotting was performed to validate the expression of WT and ΔRS (Fig. 5.11 A). Preliminary data (n=1) showed that the total levels of all three targets remained unchanged whereas the cytoplasmic levels of TFAM were greatly decreased suggesting again block or inhibition of mRNA export (Fig. 5.11. B and C). Surprisingly, NRF-1 did not show any block of export. In addition, COX2 mRNA levels showed some reduction in the cytoplasm. These data again indicated the novel biological function of PGC-1[alpha] as an export adaptor. Moreover, the RS-rich region appeared to be central for this molecular role.
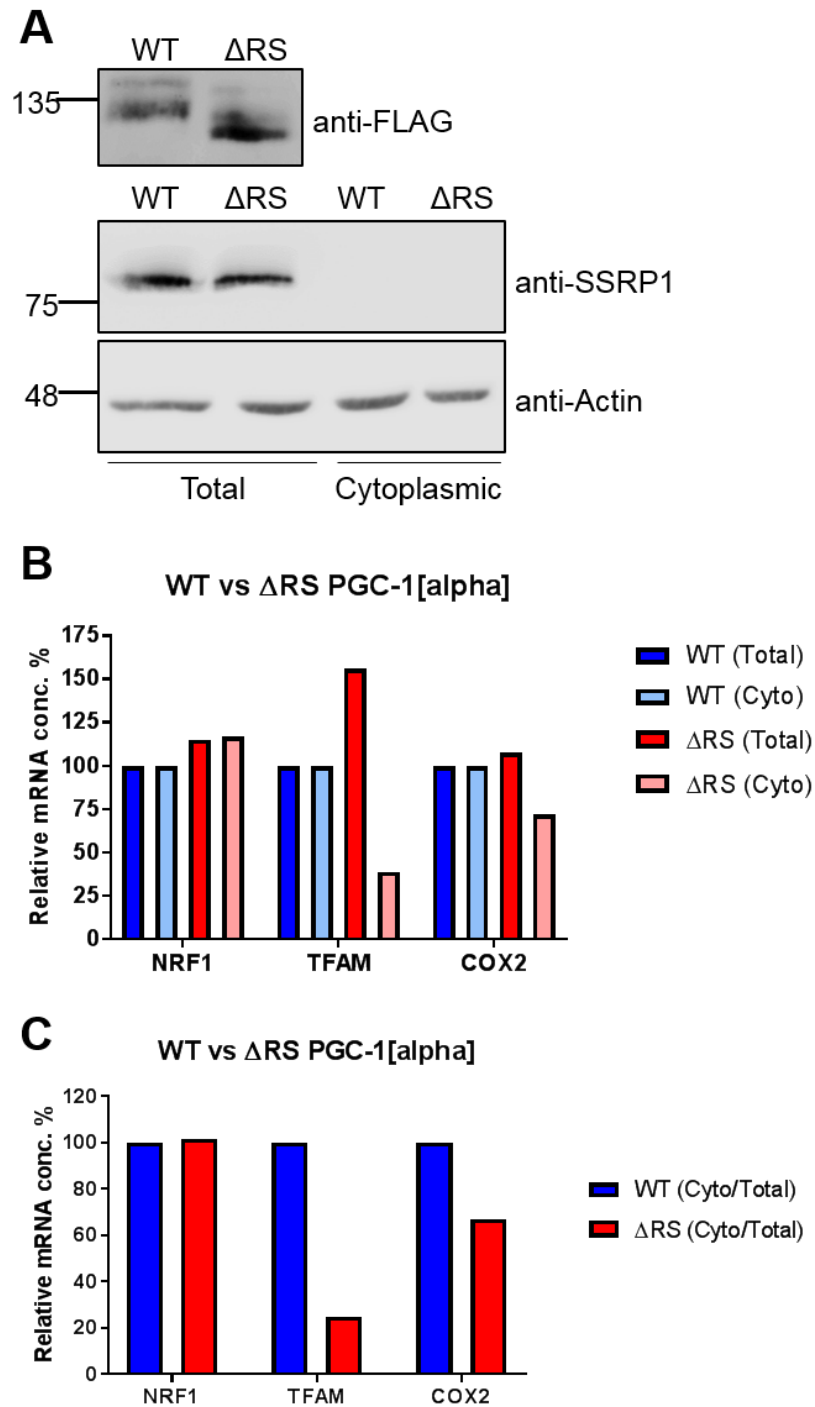
Figure 5.11 qRT-PCR analysis reveals reduction in nuclear export of TFAM mRNA.
WT and ΔRS cells were induced and cultured in glucose. Total and Cytoplasmic cell fractions were obtained and RNA extracted from them. **A)** shows the induction of WT and ΔRS and the cellular fractionation with pure cytoplasmic fraction free of nuclear marker using anti-FLAG and anti-SSRP1 western blotting, respectively. **B)** Preliminary data from qRT-PCR analysis reveal no differences in NRF-1, TFAM and COX2 total levels. This was also true for cytoplasmic NRF-1 mRNA. In contrast, TFAM shows dramatic decrease in cytoplasmic RNA whereas COX2 shows some decrease. **C)** Cyto/Total ratio for TFAM shows decrease indicating inhibition of nuclear export. n=1. WT set at 100%.

5.3.2.4. Decreased nuclear colocalisation between PGC-1[alpha] mutant and TAP/NXF1

To further investigate the block of mRNA export, colocalisation studies for PGC-1[alpha] and TAP/NXF1 were carried out in the HEK293 stable inducible cell lines, similarly to Chapter 4 Section 4.7. Cells were stained for PGC-1[alpha] and TAP/NXF1 in WT and ΔRS cultured in glucose with or without tetracyclin. Two-way automated counting was carried out where first, PGC-1[alpha] nuclear spots were identified and TAP/NXF1 puncti colocalising with them counted. Second, this was repeated in the reverse order where TAP/NXF1 spots were identified and PGC-1[alpha] puncti colocalising with them counted. Preliminary results (n=1) demonstrated increased colocalisation of PGC-1[alpha] and TAP/NXF1 in puncta in WT in response to tetracyclin induction. Interestingly, this was not observed with ΔRS where the number of colocalising spots remained the same. This might suggest the inability of ΔRS to functionally participate in the TREX complex.
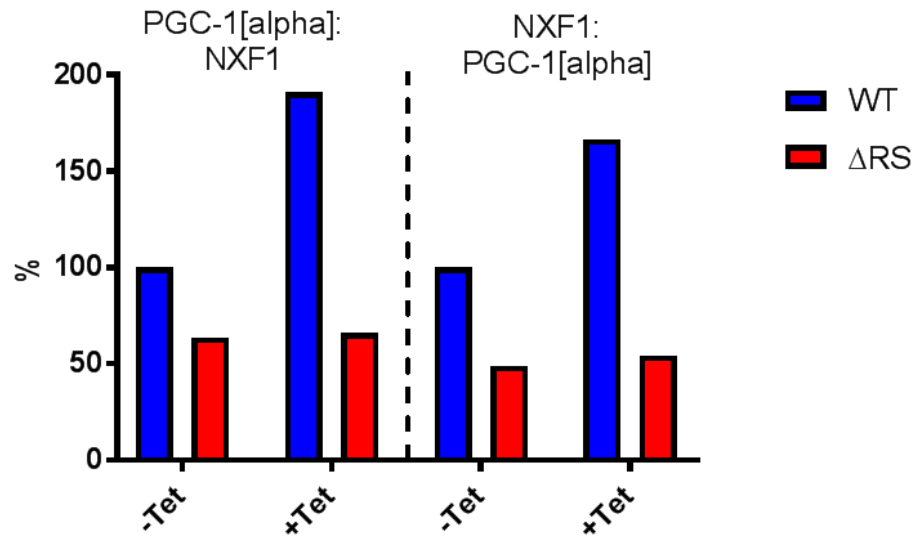
Figure 5.12 Confocal microscopy analysis shows decreased colocalisation of PGC-1[alpha] and TAP/NXF1 when ΔRS is expressed.

Cells were induced and cultured in galactose. They were then fixed and stained for PGC-1[alpha] and NXF1. Automated counting was used to determine the number of nuclear spots for both protein and their colocalisation. The analysis was carried out in a two-way approach. First (left), PGC-1[alpha] puncti were identified and NXF1 colocalising spots counted. Second (right), NXF1 spots were identified and colocalisation of PGC-1[alpha] counted. WT cells consistently showed increased colocalisation with NXF1 that was further increased in response to tetracycline. Colocalisation counts remained lower and the same with or without Tetracycline in the ΔRS mutant. n=1.

5.4. Reprogramming of HEK293 stable inducible cell lines to induced neural progenitor cells (iNPCs)

Following the generation and functional characterisation of isogenic HEK293 stable models of PGC-1[alpha], the ultimate goal of this work was to assess the function of PGC-1[alpha] in a neuronal context. HEK293 cells are believed to be of kidney origin therefore attempts were made to generate stable inducible cell lines in SH-SY5Y neuroblastoma cells with the same plasmids mentioned above. SH-SY5Y Flp-In T-REx is not available commercially and required the construction of host cell line with stably integrated FRT site and constitutively expressed TetR. Unfortunately, attempts at generating this host line for the last few years were unsuccessful (Adrian Higginbottom and Guillaume Hautbergue), likely due to high rate of genomic rearrangements in SH-SY5Y cells. This led us to try a novel approach involving the reprogramming of the HEK Flp-In line, an immortalised cell line, to induced neural progenitor cells (iNPCs). Reprogramming to iNPCs has been successfully undertaken with primary cells such as skin fibroblasts (Meyer et al., 2014), however reprogramming of immortalised cells has never been reported.

Cell reprogramming was attempted with previously generated and readily available in the lab HEK293 stable inducible cell models of ALS to then use with PGC-1[alpha] stable lines once the protocol had been established. Two cell lines were generated by Dr Adrian Higginbottom (SITraN) and characterised by Dr Jennifer Dodd (SITraN). A Sham line that has undergone the same process of GOI integration but carrying an empty plasmid without GOI was built alongside a cell line that carries TDP-43 with the most common pathogenic mutation Q331K.

HEK293 control and TDP-43 stable inducible cell lines were reprogrammed using the protocol described in (Meyer et al., 2014) under the supervision of Dr Laura Ferraiuolo. Cells were transduced with three lentiviral vectors – octamer-binding transcription factor 3/4 (Oct3/4), SRY-box 2 transcription factor (Sox2) and Kruppel-like factor 4 (Klf4) (Fig. 5.13.). All three transcription factors are implicated in cell self-renewal and pluripotency and have been successfully used in the production of induced pluripotent stem cells (iPSCs) and in the direct conversion of human and mouse fibroblasts to iNPCs (Janghwan Kim et al., 2011; Meyer et al., 2014; Okita et al., 2007; Wernig et al., 2007). Contrary to the original protocol, c-Myc was not transduced in cells due to the already immortalised state of HEK293. Moreover, it has been shown previously that c-Myc is dispensable in reprogramming mouse fibroblasts (Wernig et al., 2008). Twelve hours post-transduction, lentiviral vectors were withdrawn and cells were cultured in HEK medium for a further 48 hours. Following this, medium was changed to iNPC medium supplemented with N-2, B-27, FGF-b, EGF and Heparin. These growth factors induce the conversion of HEK293 cells to iNPCs. Cells were cultured and media replenished approx. every 3 days until morphology was fully changed which took ~2 weeks (Fig. 5.13.). Following this, EGF and Heparin were withdrawn and concentration of FGF-b was doubled to maintain self-proliferation state of newly generated iNPCs. Neural progenitor identity was confirmed by immunocytochemistry with the NPC markers Pax6 and Nestin (Fig. 5.14.). The expression of both markers was compared to HEK293 cells. iNPCs had well defined cytoplasmic expression of Nestin (green) and nuclear staining for Pax6 (red) as opposed to diffused background staining of HEK293 cells. Some TDP-43 Q331K HEK293 cells showed nuclear expression of Pax6, however the cytoplasmic localisation of Nestin was more pronounced in their iNPC conversion. After confirmation of their NPC nature, cells were cultured on human fibronectin-coated dishes and were introduced to hygromycin and blasticidin at the same concentration used for HEK293 stable inducible cell lines. Even though this concentration did not

appear to be lethal, cells looked rounder than usual and tended to grow together as opposed to dispersed growth. This suggested that the drug concentration might be too high and cause cellular stress therefore it was reduced to 50% of the original amount. Cells appeared 'healthier' with normal morphology and more dispersed distribution on the culturing dish.
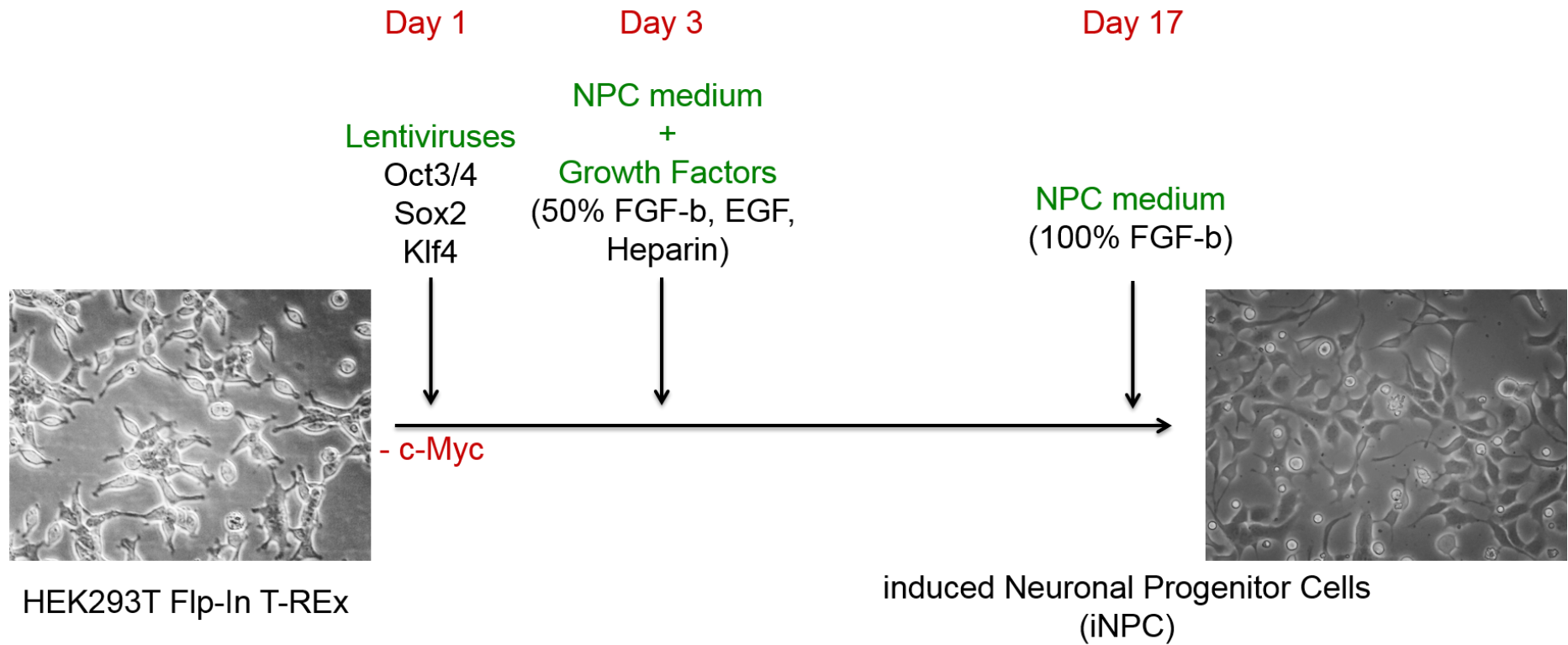
Figure 5.13 Timeline of HEK293 cell reprogramming to induced neural progenitor cells (iNPCs).

HEK cells were transduced with lentiviral vectors carrying the transcription factors Oct3/4, Sox and Klf4. c-Myc was not used as HEK cells are already immortalised. Cells are cultured in iNPC medium post transduction, supplemented with growth factors facilitating the reprogramming to neural progenitors. At the end of the protocol, cells have different morphology including elongated cell processes and irregular cell body shape as opposed to spindle-like morphology of HEK293 stable inducible cells.
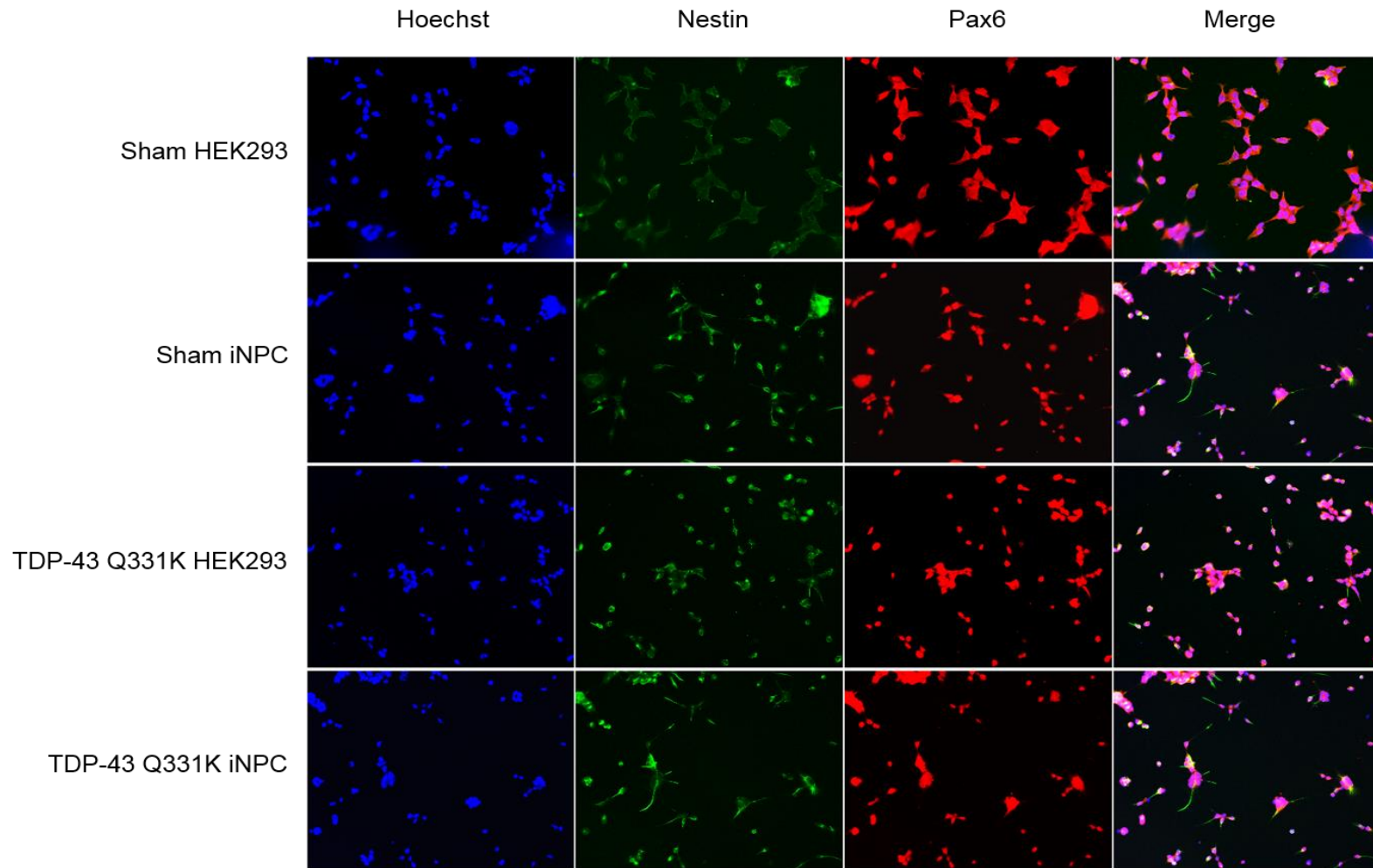
Figure 5.14 NPC marker expression in HEK-derived iNPCs.

Nestin (green) and Pax6 (red) expression was compared between iNPCs and their HEK293 parental lines. Sham HEK cells show background signal for both markers as opposed to the specific cytoplasmic Nestin and nuclear Pax6 expression in Sham iNPCs. TDP-43 Q331K HEK cells appear to have some nuclear Pax6 expression, however, Nestin expression appears to be more localised and stronger in cell processes of iNPCs in comparison to HEKs.

Following this, it was sought to determine whether iNPCs retained the Flp-In T-REx system and whether GOI expression was repressed and able to be induced. This was necessary due to the fact that in rare cases stable inducible cell lines can reject the system when exposed to high levels of stress such as that reprogramming might cause. Cells were induced for 48 hours with the already established in HEK293 concentration of tetracyclin followed by lysis and western blotting (Fig. 5.15.). Protein expression was confirmed using anti-TDP-43 antibody. This demonstrated that the inducible system was intact and still under the regulation of tetracyclin. Sham cells showed weak bands only for endogenous TDP-43, whereas the TDP-43 cell line showed the induction of TDP-43 Q331K as shown by the increase of signal in Tet as opposed to non-induced cells.

Pax6/Nestin expression and retention of the Flp-In T-Rex system deemed the reprogramming experimental work as successful paving the way for the stable inducible cell lines of PGC-1[alpha]. The work is currently ongoing and preliminary results appear to be positive.

In addition, iNPCs are tripotent and capable of being differentiated to neurones, astrocytes or oligodendrocytes. The differentiation protocol to iNeurones is currently being developed, optimised and validated in TDP-43 iNPCs. Preliminary data suggest differences in post-mitotic neuronal markers MAP2 and NeuN expression in differentiated iNeurones and HEK293 cells (data not shown).
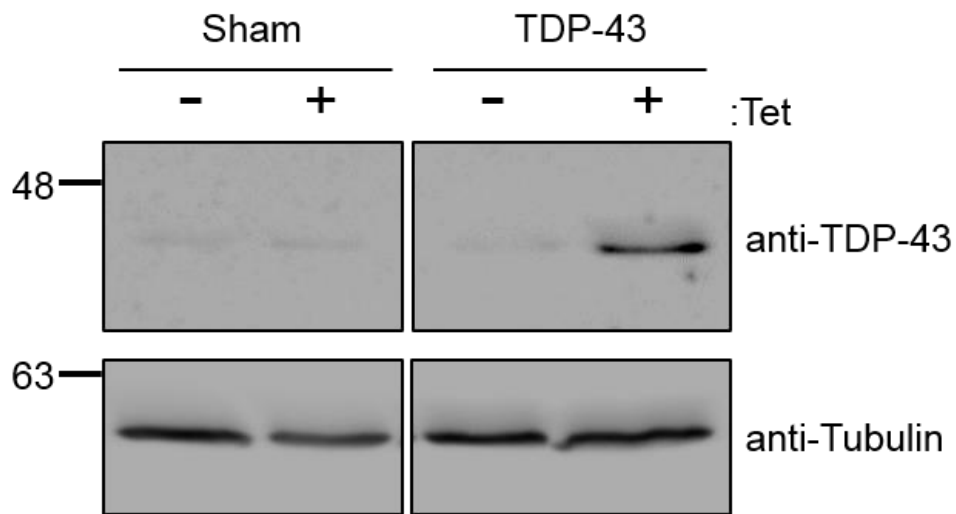
Figure 5.15 Western Blot analysis for the retention of the Flp-In T-Rex system in HEK293-derived iNPCs.

iNPCs were cultured in the presence and absence of Tetracycline for 48 hours and their ability to repress/induce the expression of TD-43 Q331K was assessed. Sham cells show band only for the endogenously-expressed TDP-43. TDP-43 Q331K cell line shows the successful induction of TDP-43 expression upon addition of Tetracycline.

5.5. Conclusions and discussions

Stable inducible cell lines of PGC-1[alpha] deficiency and wild-type or ΔRS mutant complementation system were built utilising DNA homologous recombination. These cell models were built in HEK293T cells. PGC-1[alpha] knockdown was confirmed upon induction and in comparison to Ci resulting in ~70% decrease of mRNA levels. The non-induced cells did not show any significant deviation from the control line. Similarly, the WT and ΔRS stable lines showed the expression of FLAG-tagged PGC-1[alpha] resistant to miRNA only when induced with tetracyclin. In addition, the endogenous mRNA levels were decreased to an equal or greater level as compared to the PGCi line.

HEK293 Flp-In T-REx host cells are commercially available allowing for the efficient and rapid generation of stable inducible cell lines. In addition, HEK293 cells are easy to culture and manipulate offering fast and reproducible methods for studying gene/protein function(s). Their doubling time of ~24 hours makes them attractive in studies requiring a large number of cells in a short time span. HEK293 stable lines are isogenic eliminating genetic variability between the generated cell models. This ensures that GOIs are integrated at the same genomic location across different lines. Moreover, the inducibility of the system provides an elegant way of functional characterisation of the biological role of the gene of interest when expressed.

There has been a long tradition in the field of neuroscience to use HEK293 cells for the study of neurone-specific proteins in isolation in a non-neuronal context. This was based on the belief that HEK293 cells have been isolated from the kidney of aborted female embryo. However, many research groups have challenged this widespread belief in the quest of identifying their true cell lineage. Surprisingly, spontaneous electrical signals and the expression of different ion-gated channels in HEK293 cells have been observed as early as 1998 (Zhu et al., 1998). This was later expanded by the finding that HEK293 cells from different sources of distribution express neurofilamental subunits such as NF-M and NF-L characteristic of neuronal lineage (G. Shaw et al., 2002). In addition, the study also identified increased mRNA levels of various neurone-specific proteins such as ENO2 (enolase). In a more recent study, whole-genome sequencing of various different HEK293 cell lines such as HEK293T and HEK293S was carried out and their gene expression profiles were compared to the cell-type-specific transcriptomic signatures of adrenal, kidney and central nervous system tissues (Y.-C. Lin et al., 2014). It was concluded that HEK293 cells are closer to adrenal gland cells and least related to kidney cells. The adrenal gland in developing embryos is partly of neural crest origin again suggesting the neuronal-like

faith of HEK293 cells. These are the reasons why HEK293 were selected for this doctoral work. It would not only give insights on the biological role of PGC-1[alpha] but also relate them to a semi-neuronal nature where the effects of the protein and its deficiency might be more pronounced.

After establishing consistent knockdown of PGC-1[alpha] upon tetracyclin induction, cell lines were functionally characterised. Exploratory MTT cell proliferation assay showed no significant differences between control cell line and PGC-1[alpha]-deficient cells when cultured in glucose. However, evidence from experimental work on other cells lines shows that some cells are highly glycolytic vastly relying on glucose metabolism to generate cellular energy as opposed to ATP produced from OXPHOS in the mitochondria. This possibility was addressed and indeed, when glucose was substituted for galactose that does not result in the net production of ATP, differences between cell lines became apparent. Knockdown of PGC-1[alpha] resulted in reduced cell proliferation regardless of induction state. This could be potentially due to leakage of the system where miRNA is produced at lower levels in the absence of tetracyclin. However, MTT assay is based on colourimetric readings that tend to be less sensitive compared to other assays. This might lead to difficulties in assessing differences between non-induced and induced cells. To overcome this problem, a highly sensitive luminescence-based ATP assay was carried out. As expected, cells grown in glucose did not show any differences in their ATP production. Switch to galactose, however, showed decrease in ATP levels upon PGC-1[alpha] knockdown that were further diminished when cells were induced. This clearly showed PGC-1[alpha]-related mitochondrial impairment. Similarly, PGC-1[alpha]-deficient mice show decrease in ATP concentration in heart samples (Arany et al., 2005).

As mentioned in Chapter 1, mitochondrial ATP is produced via the five complexes of the ETC embedded in the inner mitochondrial membrane. Therefore, it was hypothesised that reduction in ATP might be due to changes in protein levels of some or all of the complexes. OXPHOS cocktail antibody western blotting showed no differences in protein expression of subunits of each of the complexes when cells were cultured in glucose. Interestingly, when mitochondria were challenged with galactose, marked upregulation of complex IV, COX2 subunit, was observed in control miRNA cells. PGC-1[alpha]-deficient cells failed to induce the expression of COX2 indicating the importance of PGC-1[alpha] in Complex IV biogenesis. As shown in Chapter 2, PGC-1[alpha] is able to bind to the mRNA of NRF-1, TFAM and COX2. Therefore, it could be hypothesised that reduction of the co-transcriptional activator might result in RNA processing dysregulation of NRF-1 and TFAM, which in turn would negatively impact mtDNA transcription. This will ultimately lead to a decrease of COX2 mRNA levels resulting in the reduction of its protein levels. Alternatively, PGC-1[alpha] deficiency could affect the RNA metabolism of COX2 either impacting its stability or even potential export to the cytoplasm. Surprisingly, total mRNA levels of all three targets remained unchanged upon knockdown of PGC-1[alpha] as compared to the control cell line. Nevertheless, the cytoplasmic levels of NRF-1 and TFAM were significantly reduced suggesting block or inhibition of nuclear export again confirming the role of PGC-1[alpha] as a novel export adaptor. This nuclear RNA accumulation could lead to the reduced protein expression of both transcription factors. This, in turn, could potentially impact mitochondrial homeostasis and while it does not appear to affect COX2 mRNA levels, it might dysregulate other mitochondrial genes. Western blotting analysis for NRF-1 and TFAM would be able to determine their protein levels. In addition, the OXPHOS cocktail antibody recognises only one subunit in each ETC complex, therefore assessing the mitochondrial transcriptome and proteome might identify additional key players involved in PGC-1[alpha]-responsive energy production. It is worth noting that qRT-PCR data was obtained

from cells cultured in glucose and subsequent substitution for galactose might result in further block of mRNA nuclear export and potential reduction in COX2 levels. Nevertheless, recent evidence shows that COX2 levels are not necessarily regulated at the RNA level. It has been observed that mutations or deletions of the nuclear-encoded Complex IV assembly factor COA6 negatively influences COX2 protein stability (Ghosh et al., 2016; 2014; Pacheu-Grau et al., 2015; Stroud et al., 2015). COA6 is involved in the biogenesis and maturation of COX2 and its inactivity or deficiency leads to impaired assembly of Complex IV. This results in the degradation of COX2 and diminished activity of Complex IV and has been associated with cardiomyopathies. This suggests an attractive novel possibility where PGC-1[alpha] might be involved in the nuclear export of COA6 RNA and deficiency of the mitochondrial master regulator might lead to the block of export of COA6 which in turn would result in impaired assembly of Complex IV, reduction in COX2 levels and ultimately reduction in ATP production. Interestingly, these data were reproduced with the WT and ΔRS stable cell lines. Diminished ATP levels, failure in COX2 upregulation upon glucose substitution for galactose and reduction of nuclear export of TFAM were observed with the PGC-1[alpha] mutant. This again indicates the importance of the RNA-binding function of PGC-1[alpha] in its overall biological role and the detrimental impact on mitochondrial homeostasis upon its loss. Moreover, colocalisation analysis showed decreased nuclear colocalisation between ΔRS and TAP/NXF1 as compared to WT cells. This further demonstrates that the RS-rich region is not only involved in RNA-binding but TAP/NXF1-binding as well.

While this is novel and groundbreaking data, these results have been obtained in HEK293T stable cell lines and the ultimate goal would be to assess the function of PGC-1[alpha] in brain cells. The limitation of HEK293 cells is that there is no established protocol for their differentiation into brain-specific cells such as neurones,

astrocytes or oligodendrocytes, if at all possible. Therefore, a novel approach was undertaken where the stable inducible cell lines were directly reprogrammed to iNPCs using an established protocol that has been shown to result in the successful generation of iNPCs from adult human-derived skin fibroblasts from controls and ALS patients. The HEK293 stable inducible cells available at the time were Sham and TDP-43 Q331K. They were successfully reprogrammed to iNPCs as indicated by the specific expression of the neural progenitor markers Pax6 and Nestin in virtually all cells. In addition, the newly generated iNPCs retained both cassettes of the Flp-In T-REx system, where they showed constitutive repression of TDP-43 Q331K that was induced upon the addition of tetracyclin. This provides an exciting new possibility to study the effect of the pathogenic mutation in a brain-specific context. Moreover, previous characterisation by Dr Jennifer Dodd demonstrated that the HEK293 TDP-43 Q331K cells do not show the typical pathology of TDP-43 proteinopathy where the protein gets mislocalised to the cytoplasm. This indeed would be the main priority of the new iNPCs to determine whether they can recapitulate disease pathology when differentiated to neurones which, in turn, might indicate cell-specific pathogenesis. This work is currently ongoing and preliminary results appear to be promising.

The reprogramming of these cells was based on the use of four transcription factors termed 'the Yamanaka factors' in the field of stem cell biology – Oct3/4, Sox2, Klf4 and c-Myc. They have been demonstrated to drive the **de**differentiation of cells. Yamanaka and his group were the first to report successful reprogramming of somatic (post-mitotic) cells to induced pluripotent stem cells (iPSCs) that closely resemble embryonic stem cells (Takahashi and Yamanaka, 2006). However, there are major limitations associated with the generation of iPSCs and concerns about their use. Firstly, the conversion to iPSCs is characterised by the selection of clones which results in clonal variability and different efficiencies and capabilities of downstream

differentiation between the different clones (Takahashi and Yamanaka, 2006). It has also been reported that some iPSCs retain epigenetic imprints of their somatic ancestors or acquire aberrant epigenetic modifications unlike embryonic stem cells (Lister et al., 2011; Marchetto et al., 2009; T. Wang et al., 2013). In addition, studies raise a concern that iPSC cells possess high genomic instability potentially capable of leading to tumorogenecity that could make these cells not only dangerous in clinics but also not suitable for basic research (detailed review in Yoshihara et al., 2017). Ultimately, the process of reprogramming cells to iPSCs is time-consuming (over 30 days) and associated with high costs. On the contrary, iNPCs can be generated in under 4 weeks (fibroblasts) (Meyer et al., 2014) or in the case of HEK293 cells – 2 weeks and they are not expanded from single clones avoiding clonal variability that occurs through potential selection of clones with mutations or chromosomal rearrangements. Moreover, this approach is highly reproducible and cheaper in comparison to iPSCs. Differentiated iNPCs are tripotent and can be generated to i-astrocystes, i-neurones and i-oligodendrocytes. I-astrocytes and i-oligodendrocytes derived from sporadic and familial cases of ALS show toxicity to motor neurones and i-neurones from ALS/FTD patients show reduced autophagy recapitulating different aspects of the pathology seen in primary patient cells (Ferraiuolo et al., 2016; Meyer et al., 2014; Webster et al., 2016). Thus, the newly generated HEK293-derived iNPCs could help understand disease mechanisms better in a precise manner. Moreover, the role of PGC-1[alpha] has been implicated in brain as discussed in Chapter 1, however, little is known whether its biological role is restricted or modulated in a brain-cell specific manner. Therefore, such iNPCs could shed further light and give clues about the function of PGC-1[alpha] and ultimately its export adaptor capabilities in neurones and glia. Moreover, PGC-1[alpha] i-neurones would constitute an elegant human neuronal model of induced ageing in a dish.

6. Conclusions and Discussion

Considerable effort has been invested to elucidate pathways and specific biological roles of PGC-1[alpha]. As aforementioned, it has a tissue-specific function, however it is ultimately linked to energy production through mitochondrial master regulation. PGC-1[alpha] is a co-transcriptional activator that binds to transcription factors including NRF-1 and activates them which in turn initiate the transcription of their target genes such as *TFAM*. It has also been found in association with the splicing factor SC-35 and RNA polymerase II (Monsalve et al., 2000). Moreover, computational analysis revealed the presence of an RRM and RS-rich region in its carboxyl-terminal. These are typical characteristics of splicing factors. This firmly defines PGC-1[alpha] as a participant and/or regulator of RNA processing. It is surprising, however, that despite the rich body of knowledge, elucidating the role of PGC-1[alpha] in RNA metabolism has been overlooked.

While PGC-1[alpha] exhibits features of splicing factors, it also resembles structurally a class of proteins termed mRNA nuclear export adaptors. Export adaptors have an essential function in coupling the processes of transcription, RNA maturation and its nucleocytoplasmic transport through the nuclear pore to allow for its subsequent translation by the ribosomes, located in the cytoplasm (Hautbergue, 2017). This doctoral thesis described the experimental work undertaken to characterise and classify PGC-1[alpha] as a novel nuclear export adaptor. In order to do so, as general criteria were accepted that a typical adaptor i) is able to bind RNA and TAP/NXF1 directly; ii) is present in the TREX complex and iii) that its overexpression results in nuclear accumulation of bulk mRNA.

6.1. PGC-1[alpha]'s nuclear role as a novel export adaptor

6.1.1. PGC-1[alpha] binds RNA directly and mRNA in human cells

This work provides the first evidence that PGC-1[alpha] binds RNA directly and the minimal binding domain of PGC-1[alpha] was identified as the RS-rich region (aa565-633). Similarly, comprehensive *in silico* analysis of three protein databases – Pfam, PBD and SwissProt, indicates high conservation of the positively charged amino acids Arginine and Lysine that facilitate interactions with RNA molecules (Varadi et al., 2015). This is likely due to favourable electrostatic interactions with negatively charged RNA molecules.

The RNA-binding activity of PGC-1[alpha] is specific but does not appear to be governed by sequence consensus as seen from binding with both AU- and GC-rich RNA probes. This suggests that the protein would be able to bind multiple RNA molecules, independently of their nucleotide sequences. Indeed, charged amino acids, in particular arginines, are often present in regions with intrinsic structural disorder of proteins (Bayer et al., 2005; C. A. Smith et al., 2000). Undefined protein structure provides conformational flexibility leading to efficient adaptation to various RNA molecules. Moreover, it has been shown that the intrinsically disordered region of RNA-binding proteins is highly conserved throughout evolution (Varadi et al., 2015). Similarly, prediction analysis of PGC-1[alpha] structure shows high degree of intrinsic disorder especially in the RS-region.

Following this, it was shown that PGC-1[alpha] also binds mRNA in human cells and deletion of the RS-region results in loss of binding. In addition, removal of the RS leads to metabolic impairment of cell proliferation that appears to have greater

negative effect as compared to PGC-1[alpha] deficiency. It was also shown that PGC-1[alpha] is able to bind to the mRNA of NRF-1, TFAM and COX2 and conversely, the inability of the ΔRS mutant. It is not surprising that PGC-1[alpha] binds NRF-1 and TFAM mRNAs because they are known direct targets of the protein and are encoded by the nuclear genome where PGC-1[alpha] is predominantly localised. However, binding to the mitochondrially-encoded COX2 mRNA could suggest the presence of PGC-1[alpha] in the mitochondria. Indeed, there is already evidence of a mitochondrially-localised isoform of PGC-1[alpha] in brain but it lacks the C-terminal domain that contains the RNA-binding region (J. Choi et al., 2013). This requires further analysis where mitochondrial cellular fractions need to be examined for the presence of C-terminal-containing PGC-1[alpha]. Moreover, due to the tissue specificity of the protein it would be necessary that different cell types be studied and compared. Another possibility might be associated with export of COX2 mRNA to the cytoplasm for translation. Even though there is a translational machinery (ribosomes) present in the mitochondrial matrix, this area of research is poorly understood. Indeed, various mitochondrial tRNAs and in particular tRNA[Met] have been found present in the cytosol of mammalian cells (Maniataki and Mourelatos, 2005). This clearly indicates that RNA export from the mitochondria to the cytoplasm does exist. This favours speculation that PGC-1[alpha] might bind COX2 and facilitate its export. However, such research has not been conducted and might be of vital importance in order to identify novel pathways of mitochondrial homeostasis. Furthermore, proteomic analyses of mitochondrial fractions can shed light on the potential presence of such export proteins.

It is worth noting that lack of RNA-binding research in the field of PGC-1[alpha] is a great disadvantage leading to the absence of important knowledge about the exact RNA targets of PGC-1[alpha]. This would inevitably be the future direction of the

research undertaken following this doctoral study. Target RNAs will be immunoprecipitated with WT and ΔRS PGC-1[alpha] followed by RNA deep sequencing. This holds great promise to answer key questions about the specific RNA targets of PGC-1[alpha]. Moreover, such data might uncover novel pathways that are under the control of the protein.

6.1.2. PGC-1[alpha] binds TAP/NXF1 through its RS-rich region

It was next determined that PGC-1[alpha] is able to directly bind the nuclear export factor TAP/NXF1 using recombinant proteins synthesised in *E. coli* but it was also shown that this interaction occurs in cells. This binding was accomplished by the carboxyl-terminal RNA-binding domain of PGC-1[alpha] as expected due to the structural similarities to other nuclear export adaptors. Subsequent analysis revealed that the RS-region interacts strongly with TAP/NXF1 compared to the RRM and binds directly to the export factor.

As aforementioned, typical characteristics of nuclear export adaptors include binding to TAP/NXF1 through arginine residues (Hautbergue et al., 2009; 2008; Walsh et al., 2015). Unfortunately, site-directed mutagenesis analyses could not identify single arginine amino acids that affect the binding to TAP/NXF1. This suggests that there might be a redundancy in the residues involved in this protein-protein interaction or non-canonical binding via different amino acids might take place. Similar properties have been observed with RNA-binding proteins. Intrinsically disordered regions can use different arginine residues to bind different RNA molecules by assuming different conformational structures (C. A. Smith et al., 2000). Similarly, as already discussed PGC-1[alpha] lacks defined structure in its RS-domain which might exert beneficial effects upon amino acid substitution. The protein might be able to use different

residues due to its structural flexibility. Despite the inability to identify a single amino acid, deleting the RS-region resulted in decreased binding to TAP/NXF1 confirming its importance for the interaction. Interestingly, it appears that the RNA- and TAP/NXF1-binding regions overlap which has already been seen with other nuclear export adaptors.

What was more striking was the fact that PGC-1[alpha] was able to bind to the RBD and NTF2L domains of TAP/NXF1 that are typically associated with export adaptors and co-adaptors, respectively (Chang et al., 2013; Katahira et al., 2009). This might indicate a dual role of PGC-1[alpha], able to act as an adaptor and a co-adaptor simultaneously binding to TAP/NXF1 and opening its closed conformation leading to its increased affinity for RNA. This would deem PGC-1[alpha] as unique as this feature has not been observed with any of the currently identified export adaptors and co-adaptors. Moreover, ΔRS mutant showed decreased binding to the RBD and increased binding to the NTF2L domain. This suggests that the lack of RS-region affects the ability of PGC-1[alpha] to act as an export adaptor.

The potential novel biological function of PGC-1[alpha] was further characterised by demonstrating that it associates with the TREX complex following co-immunoprecipitation of TAP/NXF1, ALYREF, THOC1 and UAP56. On the other hand, the ΔRS mutant showed increased co-immunoprecipitation of ALYREF, THOC1 and UAP56 but not of NXF1. This suggests that its inability to bind RNA and therefore remodel NXF1, an essential RNA-handover step for RNA nuclear export, would stall the TREX complex-dependent co-transcriptional processing of mRNA. This result reinforces the role of PGC-1[alpha] as a nuclear export adaptor.

These results were followed by the identification of nuclear colocalisation of endogenous PGC-1[alpha] and TAP/NXF1 in neuronal cells. This indicates that the role of PGC-1[alpha] as an export adaptor is not cell type specific making this novel biological function an attractive area of research in brain-related conditions such as neurodegenerative diseases or physiological ageing. Moreover, the cell type used in this experiment is differentiated Luhmes cells that have been used as a cell model for Parkinson's disease and Alzheimer's disease (Zhang et al., 2014). Additionally, overexpression of the transcriptional coactivator in HEK293T cells resulted in block of mRNA nuclear export typical of other export adaptors such as ALYREF.

Collectively, these results show the unequivocal resemblance of PGC-1[alpha] to nuclear export adaptors. However, the fundamental proof of this novel biological role would be block of mRNA nuclear export of specific targets of PGC-1[alpha] as a result of its deficiency or a substitution for the ΔRS mutant that is unable to bind RNA and has decreased binding to TAP/NXF1. To answer this, isogenic stable inducible cell lines were generated and mRNA distribution assessed.

6.2. PGC-1[alpha] deficiency or its RNA-binding inability result in block of mRNA nuclear export associated with mitochondrial impairments

Four stable inducible HEK293 Flp-In T-REx cell lines were successfully generated – control miRNA, PGC-1[alpha] miRNA, WT and ΔRS. Functional characterisation of the cell lines revealed that HEK293T cells are highly glycolytic and rely on energy produced via the breakdown of glucose as opposed to energy produced from OXPHOS in mitochondria. Consequently, this masks any potential mitochondrial

defects as cells do not profoundly depend on mitochondria when grown in glucose. This was observed with PGC-1[alpha]-deficient cells that did not show any differences in cell proliferation as measured by MTT metabolic assay. However, when the glucose energy source was substituted for galactose, making cell more reliant on mitochondria, there was a significant decrease in MTT cell proliferation upon knockdown of PGC-1[alpha]. This was the first evidence that the cell lines do exhibit mitochondrial defects as expected. This raises questions about the discrepancy in MTT assay results between the stable models and transiently transfected cells (Figures 3.13. and 5.5.). While cells transiently transfected with all four constructs used to generate the stable lines, show significant decrease of cell proliferation when cultured in glucose, this is not surprising. As aforementioned, transient transfection results in 50-100-fold overexpression of episomal DNA. This would lead to even greater knockdown of PGC-1[alpha] and might have dramatic effect on mitochondria making impairments prominent even in glucose media compared to the stable cell lines with moderate overexpression of PGC-1[alpha]. Nevertheless, MTT assay is a fast and reliable way of screening for metabolic defects or protein toxicity. It is based on colourimetric readings that are not always sensitive. More sensitive methods employ luminescent signal readouts such as ATP assays and are extensively used in the field of mitochondrial research (Mortiboys et al., 2015; Petty et al., 1995). Further analysis of the cell lines revealed diminished ATP levels in PGCi and ΔRS in galactose culturing media as compared to their respective controls. This shows that the loss of PGC-1[alpha] or its RNA/NXF1-binding region results in mitochondrial defects. While it is expected that knockdown of the mitochondrial master regulator would have negative effect on energy homeostasis, this is the first evidence demonstrating that the RS-region of PGC-1[alpha] is essential for the global biological role of the protein. ATP in the mitochondria is produced via the OXPHOS electron transport chain, therefore individual subunits of the five complexes were examined. None of the complexes showed any differences in protein levels in any of the four cell

lines cultured in glucose media. Conversely, switch to galactose resulted in significant upregulation of COX2 (Complex IV) expression in control lines, while PGCi and ΔRS failed to increase its protein expression. This suggests that inability to express COX2 under stress conditions results in net decrease of ATP production that is linked to PGC-1[alpha] function. Protein synthesis requires high supply of energy and it has been shown that glucose starvation of cells results in decrease in bulk mRNA nuclear export and reduced protein expression in HeLa cells associated with diminished cell growth and ATP production (Shan et al., 2017). Interestingly, this effect is mediated by SIRT1. Under stress conditions such as glucose starvation or fasting, SIRT1 deacetylates PABP1, a protein that binds the poly(A) tail of RNA. Deacetylated PABP1 then translocates from the cytoplasm to the nucleus and is no longer able to bind RNA which results in its nuclear accumulation. As aforementioned, SIRT1 also directly regulates the activity of PGC-1[alpha] by deacetylating it and leading to its activation. This could serve as a rescue mechanism where active PGC-1[alpha] stimulates OXPHOS upregulation in order to compensate for energy loss via glycolysis. Moreover, PGC-1[alpha] has long been implicated in fasting so this mechanism of action would not be surprising. Contrary to this, loss of PGC-1[alpha] or its function would result in failure to upregulate protein expression of mitochondrial genes such as COX2, the result observed with these stable inducible cell lines. Nevertheless, it is of note that the OXPHOS antibody cocktail recognises only a single subunit of each multimeric complex of the ETC. Transcriptomic or proteomic studies of these cell lines could shed more light and show whether there are further changes in expression levels of other proteins involved in OXPHOS. Indeed, there is already evidence of PGC-1[alpha]-responsive OXPHOS genes in the context of Parkinson's disease where differential expression of genes involved in all five ETC complexes that are under the control of PGC-1[alpha] was reported (Zheng et al., 2010a). In addition, a quick and reliable functional approach would be to measure the enzymatic activity of the mitochondrial complexes. It would be important to determine whether reduced

protein levels of COX2 correlate with reduced activity of Complex IV leading to diminished ATP production.

Interestingly, assessing the mRNA levels of key mitochondrial genes and direct targets of PGC-1[alpha] – NRF-1, TFAM and COX2 did not show any differences in total RNA levels that might be associated with decrease in mitochondrial homeostasis. However, preliminary qRT-PCR analysis of cytoplasmic/total cell fractions revealed reduced nuclear export of NRF-1 and TFAM mRNAs in PGC-1[alpha]-deficient cells and reduction in the export of TFAM in ΔRS. This again indicates the role of PGC-1[alpha] as an export adaptor and loss of the full-length protein or the RS-region results in block of mRNA nuclear export. It is worth noting that these experiments were carried out in glucose conditions. While ATP assays or western blotting did not show any differences in such conditions, as aforementioned there might be an underlying dysregulation such as block of mRNA export that does not affect overall energy homeostasis when cells rely almost exclusively on energy produced from glycolysis. Similar analysis is yet to be carried out on cells cultured in galactose where the nuclear export of NRF-1 and TFAM mRNA might be affected at a greater level. In addition, the total levels of COX2 remained unchanged. These data might also suggest dysfunctional assembly of Complex IV where inability to assemble the complex might result in proteasomal degradation of its subunits that cannot be detected at the RNA level.

Lastly, colocalisation studies of endogenous PGC-1[alpha] and TAP/NXF1 show decreased nuclear association between ΔRS mutant and the export factor as compared to WT PGC-1[alpha]. This further indicates the inability of ΔRS to interact with TAP/NXF1.

Taken together, these results show that these newly generated isogenic stable inducible cell lines of PGC-1[alpha] deficiency or mutational substitution are invaluable cell models that demonstrate expected mitochondrial dysfunction and will aid more detailed research in the field of PGC-1[alpha]. They are easy to maintain and manipulate in culture obtaining high-quality and reproducible data. Nevertheless, as discussed in the previous chapter, HEK293T cells have their limitations concerning their tissue origin and inability to differentiate to neurones in order to facilitate research on neurodegeneration and brain ageing. Therefore, a novel scientific avenue was explored involving the generation of induced neural progenitor cells.

6.3. Establishing novel neuronal cell models to study the biological role of PGC-1[alpha]

To overcome the limitations of HEK293T cells and to provide a more suitable brain-related cell model of PGC-1[alpha], they were reprogrammed to iNPCs using a modified protocol described in (Meyer et al., 2014) and based on Yamanaka's factors. The stable inducible cell lines available at the time were Sham and TDP-43 Q331K, therefore they were used for optimisation of the protocol and proof of principle. TDP-43 cell models are ideal tools for this novel approach of reprogramming immortalised cell lines based on the fact that the characteristic brain pathology of TDP-43 mislocalisation to the cytoplasm is not recapitulated in HEK293T cell lines suggesting cell specificity. HEK293T-derived iNPCs were generated for the first time and they expressed the typical neural progenitor markers Nestin and Pax6. Moreover, the stable inducible system was retained during the reprogramming. iNPCs are tripotent in their nature and can be differentiated to neurones, astrocytes and

oligodendrocytes. Their neuronal differentiation is currently being optimised and preliminary results suggest that the expected TDP-43 proteinopathy can be observed in these cells. Work on reprogramming PGC-1[alpha] HEK293T cell lines will commence soon. This is an exciting and invaluable new approach to studying the novel biological role of PGC-1[alpha] as a nuclear export adaptor in the context of brain cells. Interestingly, recent research implicates the role of nuclear export adaptors in pluripotency and neuronal differentiation. Thus far, only SRSF1, 3 and 7 from the RS-rich protein family of splicing factors have been characterised as nuclear export adaptors that are able to bind to TAP/NXF1 and are present in the TREX complex. None of the other members of this class of proteins was demonstrated to interact with TAP/NXF1. However, recent efforts indicated that both SRSF2 and SRSF5 are able to shuttle from the nucleus to the cytoplasm and back (Botti et al., 2017). This was observed only in P19 pluripotent cells but not in HeLa somatic cells. Surprisingly, SRSF5 co-immunoprecipitated with TAP/NXF1 in these cells and as would be expected, arginine substitutions decreased this interaction. It was also discovered that SRSF5 binds to the mRNA of key genes implicated in pluripotency such as Oct4 and Lin28a. Binding to these mRNAs and shuttling of SRSF5, however, decreased upon differentiation of P19 cells to neuronal cells indicating the importance of nuclear export regulation. Similarly, PGC-1[alpha] might bind different target RNAs depending on the state and type of cells. Therefore, iNPCs are an indispensable cell model because HEK293T were reprogrammed using Oct4 lentivirus amongst others. Moreover, RNA sequencing analysis of PGC-1[alpha] WT and ΔRS RNA targets can be undertaken in HEK293T, iNPC, i-neurone, i-astrocyte and i-oligodendrocyte in order to determine whether PGC-1[alpha] target mRNAs differ across different cell types. Lastly, progressive knockdown of PGC-1[alpha] would mimic molecular phenotypes typical of physiological ageing (as discussed in Chapter 1) which provides the unique opportunity to use the newly generated iNPCs as models of induced brain ageing.

6.4. Future work

This doctoral research highlights the urgent need for identifying the exact RNA targets of PGC-1[alpha] and analysing their nuclear export in the context of disease. This would be carried out using RNA deep sequencing of RNA targets immunoprecipitated with either WT or ΔRS. The cellular distribution of these specific targets will then be assessed in the stable inducible HEK293T and iNPC cell lines in order to validate whether PGC-1[alpha] plays a vital role in the nuclear export of its target genes.

In addition, another somewhat neglected aspect of PGC-1[alpha] is its putative role as a splicing factor. As aforementioned, PGC-1[alpha] has been found in association with the splicing factor SC-35 (SRSF2). Preliminary mass spectrometry data generated during the this PhD work (data not shown) showed the binding of PGC-1[alpha] carboxyl-terminal or its RS-domain to the splicing factors SRSF1, 2, 3, 5, 7. This suggests that PGC-1[alpha] might play an essential role in RNA splicing and further analysis is required to determine whether the protein is truly multifunctional acting at different steps of RNA processing such as transcriptional co-activation, splicing and mRNA nuclear export of its targets.

While this research provides invaluable cell models to more precisely uncover a novel biological function of PGC-1[alpha], *in vivo* models would also be an important complementation to this work. The Jackson Laboratory has readily available important mouse models of PGC-1[alpha] including a null mutant that shows impaired mitochondrial function and spongiform brain lesions and gliosis. However, no research has been conducted on these mouse models to evaluate mRNA cell

distribution. In addition, the role of PGC-1[alpha] has also been implicated in αSyn zebrafish models where expression of PGC-1[alpha] exerts a neuroprotective function (O'Donnell et al., 2014). There is currently only one zebrafish PGC-1[alpha] knockdown model available showing skeletal muscle abnormalities (Hanai et al., 2007). However, the model has been generated using antisense morpholino oligonucleotides. This approach has recently been associated with increasing concerns of off-target effects and poor association of morpholino effect and disease phenotype (Kok et al., 2015). Therefore, the preferential and more reliable use of CRISPR/Cas9 system can be utilised in the generation of novel knockout/knockdown models of PGC-1[alpha] (J. Liu et al., 2017). Moreover, assessment of mRNA distribution in zebrafish brain has already been reported providing an operational protocol for future work with PGC-1[alpha] (Seytanoglu et al., 2016).

In conclusion, figures 6.1. and 6.2. provide illustrative summary of the findings from this doctoral work.
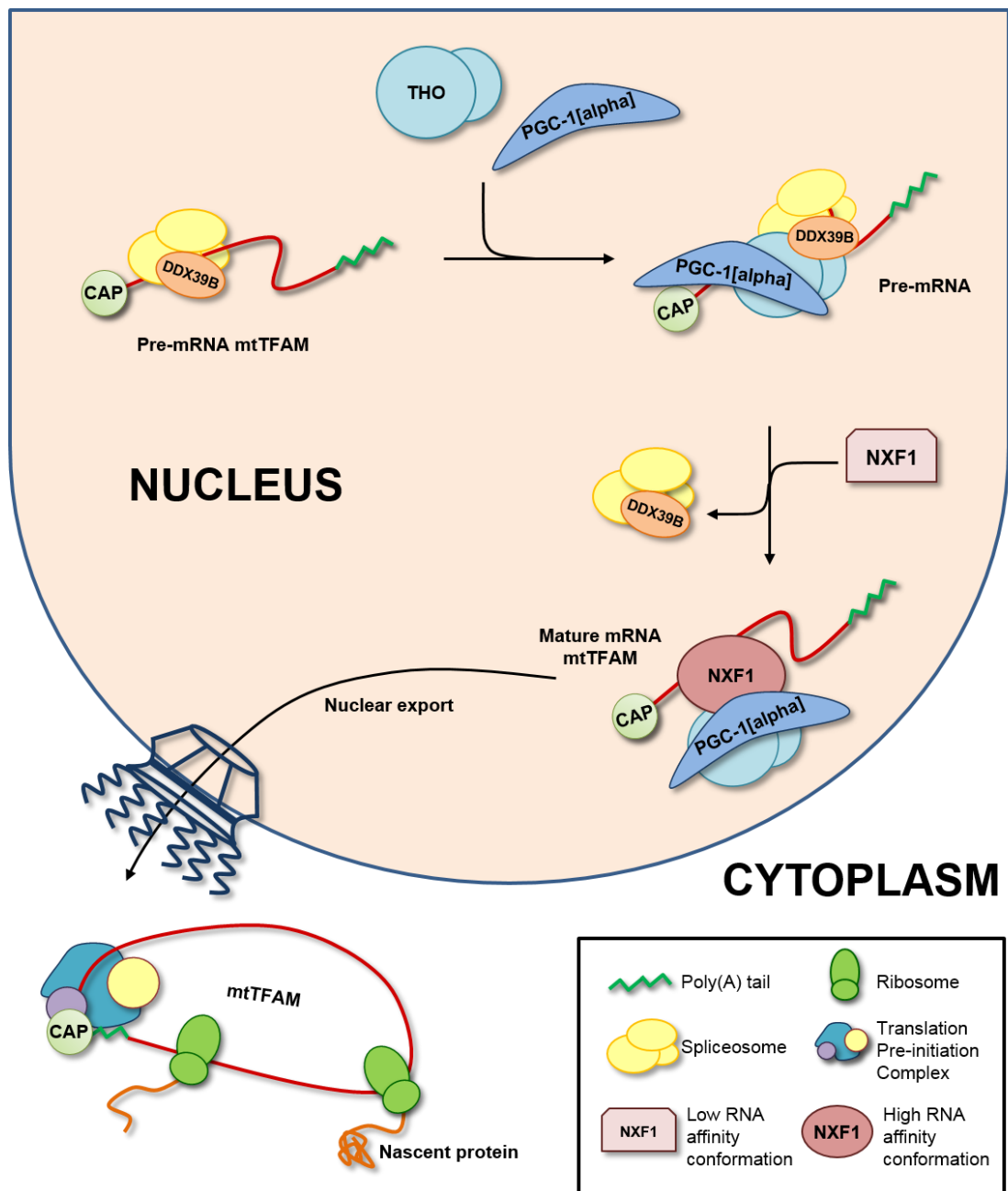
Figure 6.1 Involvement of wild-type PGC-1[alpha] in RNA processing and nuclear export.

PGC-1[alpha] and THO complex assemble the TREX complex by binding to the mtTFAM pre-mRNA. This is followed by the binding of PGC-1[alpha] to NXF1 leading to a conformational change in NXF1 and increased affinity for RNA. This is how efficient handover of the RNA molecule is accomplished. Mature mtTFAM mRNA is then exported into the cytoplasm through the nuclear pore complex. In the cytoplasm, mtTFAM is translated into protein via the ribosomes. This leads to the successful stimulation of mitochondrial biogenesis.
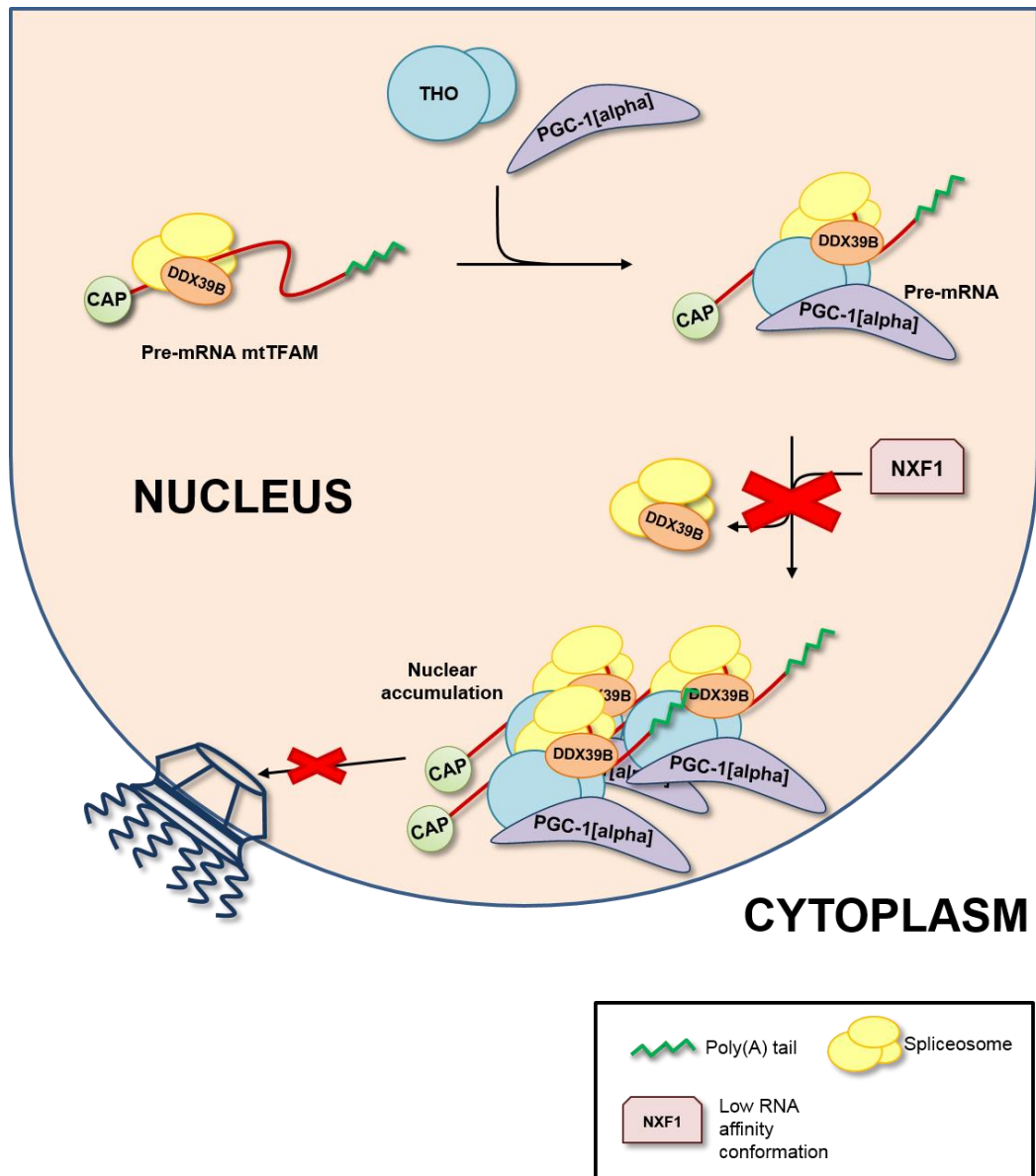
Figure 6.2 ΔRS mutant of PGC-1[alpha] causes block of mRNA nuclear export.

PGC-1[alpha] lacking the RS-rich region is no longer able to bind RNA. However, PGC-1[alpha] is still able to associate with RNA via its binding to subunits of the THO complex. This results in the inability of NXF1 binding to RNA which leads to nuclear accumulation of mtTFAM. Block of nuclear export of important mitochondrial regulator affects mitochondrial homeostasis and results in diminished energy (ATP) production.

7. Bibliography

Adamovich, Y., Shlomai, A., Tsvetkov, P., Umansky, K.B., Reuven, N., Estall, J.L., Spiegelman, B.M., Shaul, Y., 2013. The Protein Level of PGC-1 alpha, a Key Metabolic Regulator, Is Controlled by NADH-NQO1. Molecular and cellular biology 33, 2603–2613. doi:10.1128/mcb.01672-12

Aguer, C., Gambarotta, D., Mailloux, R.J., Moffat, C., Dent, R., McPherson, R., Harper, M.-E., 2011. Galactose enhances oxidative metabolism and reveals mitochondrial dysfunction in human primary muscle cells. PloS one 6, e28536. doi:10.1371/journal.pone.0028536

Ahmetov, I.I., Williams, A.G., Popov, D.V., Lyubaeva, E.V., Hakimullina, A.M., Fedotovskaya, O.N., Mozhayskaya, I.A., Vinogradova, O.L., Astratenkova, I.V., Montgomery, H.E., Rogozkin, V.A., 2009. The combined impact of metabolic gene polymorphisms on elite endurance athlete status and related phenotypes. Hum. Genet. 126, 751–761. doi:10.1007/s00439-009-0728-4

Aksenov, M.Y., Tucker, H.M., Nair, P., Aksenova, M.V., Butterfield, D.A., Estus, S., Markesbery, W.R., 1999. The expression of several mitochondrial and nuclear genes encoding the subunits of electron transport chain enzyme complexes, cytochrome c oxidase, and NADH dehydrogenase, in different brain regions in Alzheimer's disease. Neurochem. Res. 24, 767–774.

Alexeyev, M., Shokolenko, I., Wilson, G., LeDoux, S., 2013. The maintenance of mitochondrial DNA integrity--critical analysis and update. Cold Spring Harb Perspect Biol 5, a012641–a012641. doi:10.1101/cshperspect.a012641

Alvarez-Erviti, L., Rodriguez-Oroz, M.C., Cooper, J.M., Caballero, C., Ferrer, I., Obeso, J.A., Schapira, A.H.V., 2010. Chaperone-mediated autophagy markers in Parkinson disease brains. Arch. Neurol. 67, 1464–1472. doi:10.1001/archneurol.2010.198

Andrews-Hanna, J.R., Snyder, A.Z., Vincent, J.L., Lustig, C., Head, D., Raichle, M.E., Buckner, R.L., 2007. Disruption of large-scale brain systems in advanced aging. Neuron 56, 924–935. doi:10.1016/j.neuron.2007.10.038

Anglade, P., Vyas, S., Javoy-Agid, F., Herrero, M.T., Michel, P.P., Marquez, J., Mouatt-Prigent, A., Ruberg, M., Hirsch, E.C., Agid, Y., 1997. Apoptosis and autophagy in nigral neurons of patients with Parkinson's disease. Histol. Histopathol. 12, 25–31.

Arany, Z., Foo, S.Y., Ma, Y., Ruas, J.L., Bommi-Reddy, A., Girnun, G., Cooper, M., Laznik, D., Chinsomboon, J., Rangwala, S.M., Baek, K.H., Rosenzweig, A., Spiegelman, B.M., 2008. HIF-independent regulation of VEGF and angiogenesis by the transcriptional coactivator PGC-1alpha. Nature 451, 1008–1012. doi:10.1038/nature06613

Arany, Z., He, H., Lin, J., Hoyer, K., Handschin, C., Toka, O., Ahmad, F., Matsui, T., Chin, S., Wu, P.-H., Rybkin, I.I., Shelton, J.M., Manieri, M., Cinti, S., Schoen, F.J., Bassel-Duby, R., Rosenzweig, A., Ingwall, J.S., Spiegelman, B.M., 2005. Transcriptional coactivator PGC-1 alpha controls the energy state and contractile function of cardiac muscle. Cell metabolism 1, 259–271. doi:10.1016/j.cmet.2005.03.002

Arrasate, M., Mitra, S., Schweitzer, E.S., Segal, M.R., Finkbeiner, S., 2004. Inclusion body formation reduces levels of mutant huntingtin and the risk of neuronal death. Nature 431, 805–810. doi:10.1038/nature02998

Attardi, G., Schatz, G., 1988. BIOGENESIS OF MITOCHONDRIA. Annu. Rev. Cell Biol. 4, 289–333. doi:10.1146/annurev.cb.04.110188.001445

Baker, B.M., Haynes, C.M., 2011. Mitochondrial protein quality control during biogenesis and aging. Trends Biochem. Sci. 36, 254–261. doi:10.1016/j.tibs.2011.01.004

Ballard, J.W.O., Whitlock, M.C., 2004. The incomplete natural history of mitochondria. Mol. Ecol. 13, 729–744. doi:10.1046/j.1365-294X.2003.02063.x

Bargut, T.C.L., Aguila, M.B., Mandarim-de-Lacerda, C.A., 2016. Brown adipose tissue: Updates in cellular and molecular biology. Tissue Cell 48, 452–460. doi:10.1016/j.tice.2016.08.001

Barrès, R., Osler, M.E., Yan, J., Rune, A., Fritz, T., Caidahl, K., Krook, A., Zierath, J.R., 2009. Non-CpG methylation of the PGC-1alpha promoter through DNMT3B controls mitochondrial density. Cell metabolism 10, 189–198. doi:10.1016/j.cmet.2009.07.011

Barroso, I., Luan, J., Sandhu, M.S., Franks, P.W., Crowley, V., Schafer, A.J., O'Rahilly, S., Wareham, N.J., 2006. Meta-analysis of the Gly482Ser variant in PPARGC1A in type 2 diabetes and related phenotypes. Diabetologia 49, 501–505. doi:10.1007/s00125-005-0130-2

Bayer, T.S., Booth, L.N., Knudsen, S.M., Ellington, A.D., 2005. Arginine-rich motifs present multiple interfaces for specific binding by RNA. RNA 11, 1848–1857. doi:10.1261/rna.2167605

Bender, A., Krishnan, K.J., Morris, C.M., Taylor, G.A., Reeve, A.K., Perry, R.H., Jaros, E., Hersheson, J.S., Betts, J., Klopstock, T., Taylor, R.W., Turnbull, D.M., 2006. High levels of mitochondrial DNA deletions in substantia nigra neurons in aging and Parkinson disease. Nature Genet. 38, 515–517. doi:10.1038/ng1769

Benecke, R., Strümper, P., Weiss, H., 1993. Electron transfer complexes I and IV of platelets are abnormal in Parkinson's disease but normal in Parkinson-plus syndromes. Brain 116 (Pt 6), 1451–1463.

Bertram, L., Lill, C.M., Tanzi, R.E., 2010. The Genetics of Alzheimer Disease: Back to the Future. Neuron 68, 270–281. doi:10.1016/j.neuron.2010.10.013

Bertram, L., Tanzi, R.E., 2012. The genetics of Alzheimer's disease. Prog Mol Biol Transl Sci 107, 79–100. doi:10.1016/B978-0-12-385883-2.00008-4

Bhalla, K., Liu, W.-J., Thompson, K., Anders, L., Devarakonda, S., Dewi, R., Buckley, S., Hwang, B.-J., Polster, B., Dorsey, S.G., Sun, Y., Sicinski, P., Girnun, G.D., 2014. Cyclin D1 represses gluconeogenesis via inhibition of the

transcriptional coactivator PGC1α. Diabetes 63, 3266–3278. doi:10.2337/db13-1283

Bishop, N.A., Lu, T., Yankner, B.A., 2010. Neural mechanisms of ageing and cognitive decline. Nature 464, 529–535. doi:10.1038/nature08983

Bono, F., Ebert, J., Lorentzen, E., Conti, E., 2006. The crystal structure of the exon junction complex reveals how it maintains a stable grip on mRNA. Cell 126, 713–725. doi:10.1016/j.cell.2006.08.006

Bostrom, P., Wu, J., Jedrychowski, M.P., Korde, A., Ye, L., Lo, J.C., Rasbach, K.A., Bostrom, E.A., Choi, J.H., Long, J.Z., Kajimura, S., Zingaretti, M.C., Vind, B.F., Tu, H., Cinti, S., Hojlund, K., Gygi, S.P., Spiegelman, B.M., 2012. A PGC1-alpha-dependent myokine that drives brown-fat-like development of white fat and thermogenesis. Nature 481, 463–468. doi:10.1038/nature10777

Botta-Orfila, T., Sànchez-Pla, A., Fernández, M., Carmona, F., Ezquerra, M., Tolosa, E., 2012. Brain transcriptomic profiling in idiopathic and LRRK2-associated Parkinson's disease. Brain Res. 1466, 152–157. doi:10.1016/j.brainres.2012.05.036

Botti, V., McNicoll, F., Steiner, M.C., Richter, F.M., Solovyeva, A., Wegener, M., Schwich, O.D., Poser, I., Zarnack, K., Wittig, I., Neugebauer, K.M., Müller-McNicoll, M., 2017. Cellular differentiation state modulates the mRNA export activity of SR proteins. J. Cell Biol. 216, 1993–2009. doi:10.1083/jcb.201610051

Boutant, M., Joffraud, M., Kulkarni, S.S., García-Casarrubios, E., García-Roves, P.M., Ratajczak, J., Fernández-Marcos, P.J., Valverde, A.M., Serrano, M., Cantó, C., 2015. SIRT1 enhances glucose tolerance by potentiating brown adipose tissue function. Mol Metab 4, 118–131. doi:10.1016/j.molmet.2014.12.008

Brockmann, K., Apel, A., Schulte, C., Schneiderhan-Marra, N., Pont-Sunyer, C., Vilas, D., Ruiz-Martinez, J., Langkamp, M., Corvol, J.-C., Cormier, F., Knorpp, T., Joos, T.O., Gasser, T., Schüle, B., Aasly, J.O., Foroud, T., Marti-Masso, J.F.,

Brice, A., Tolosa, E., Marras, C., Berg, D., Maetzler, W., 2016. Inflammatory profile in LRRK2-associated prodromal and clinical PD. J Neuroinflammation 13, 122. doi:10.1186/s12974-016-0588-5

Cai, R., Yu, T., Huang, C., Xia, X., Liu, X., Gu, J., Xue, S., Yeh, E.T.H., Cheng, J., 2012. SUMO-specific protease 1 regulates mitochondrial biogenesis through PGC-1α. J. Biol. Chem. 287, 44464–44470. doi:10.1074/jbc.M112.422626

Calkins, M.J., Manczak, M., Mao, P., Shirendeb, U., Reddy, P.H., 2011. Impaired mitochondrial biogenesis, defective axonal transport of mitochondria, abnormal mitochondrial dynamics and synaptic degeneration in a mouse model of Alzheimer's disease. Human molecular genetics 20, 4515–4529. doi:10.1093/hmg/ddr381

Camandola, S., Mattson, M.P., 2017. Brain metabolism in health, aging, and neurodegeneration. Embo J. 36, 1474–1492. doi:10.15252/embj.201695810

Chang, C.-T., Hautbergue, G.M., Walsh, M.J., Viphakone, N., van Dijk, T.B., Philipsen, S., Wilson, S.A., 2013. Chtop is a component of the dynamic TREX mRNA export complex. Embo J. 32, 473–486. doi:10.1038/emboj.2012.342

Charos, A.E., Reed, B.D., Raha, D., Szekely, A.M., Weissman, S.M., Snyder, M., 2012. A highly integrated and complex PPARGC1A transcription factor binding network in HepG2 cells. Genome research 22, 1668–1679. doi:10.1101/gr.127761.111

Chaturvedi, R.K., Adhihetty, P., Shukla, S., Hennessy, T., Calingasan, N., Yang, L., Starkov, A., Kiaei, M., Cannella, M., Sassone, J., Ciammola, A., Squitieri, F., Beal, M.F., 2009. Impaired PGC-1alpha function in muscle in Huntington's disease. Human molecular genetics 18, 3048–3065. doi:10.1093/hmg/ddp243

Cheng, A.W., Wan, R.Q., Yang, J.L., Kamimura, N., Son, T.G., Ouyang, X., Luo, Y.Q., Okun, E., Mattson, M.P., 2012. Involvement of PGC-1 alpha in the formation and maintenance of neuronal dendritic spines. Nature

communications 3. doi:10.1038/ncomms2238

Cherubini, M., Ginés, S., 2017. Mitochondrial fragmentation in neuronal degeneration: Toward an understanding of HD striatal susceptibility. Biochem. Biophys. Res. Commun. 483, 1063–1068. doi:10.1016/j.bbrc.2016.08.042

Choi, B.-K., Choi, M.-G., Kim, J.-Y., Yang, Y., Lai, Y., Kweon, D.-H., Lee, N.K., Shin, Y.-K., 2013. Large α-synuclein oligomers inhibit neuronal SNARE-mediated vesicle docking. Proc. Natl. Acad. Sci. U.S.A. 110, 4087–4092. doi:10.1073/pnas.1218424110

Choi, J., Batchu, V.V.K., Schubert, M., Castellani, R.J., Russell, J.W., 2013. A novel PGC-1α isoform in brain localizes to mitochondria and associates with PINK1 and VDAC. Biochem. Biophys. Res. Commun. 435, 671–677. doi:10.1016/j.bbrc.2013.05.041

Choi, J., Ravipati, A., Nimmagadda, V., Schubert, M., Castellani, R.J., Russell, J.W., 2014. Potential roles of PINK1 for increased PGC-1α-mediated mitochondrial fatty acid oxidation and their associations with Alzheimer disease and diabetes. Mitochondrion 18, 41–48. doi:10.1016/j.mito.2014.09.005

Chu, Y., Dodiya, H., Aebischer, P., Olanow, C.W., Kordower, J.H., 2009. Alterations in lysosomal and proteasomal markers in Parkinson's disease: relationship to alpha-synuclein inclusions. Neurobiol. Dis. 35, 385–398. doi:10.1016/j.nbd.2009.05.023

Clark, J., Silvaggi, J.M., Kiselak, T., Zheng, K., Clore, E.L., Dai, Y., Bass, C.E., Simon, D.K., 2012. Pgc-1alpha overexpression downregulates Pitx3 and increases susceptibility to MPTP toxicity associated with decreased Bdnf. PloS one 7, e48925. doi:10.1371/journal.pone.0048925

Coon, K.D., Myers, A.J., Craig, D.W., Webster, J.A., Pearson, J.V., Lince, D.H., Zismann, V.L., Beach, T.G., Leung, D., Bryden, L., Halperin, R.F., Marlowe, L., Kaleem, M., Walker, D.G., Ravid, R., Heward, C.B., Rogers, J., Papassotiropoulos, A., Reiman, E.M., Hardy, J., Stephan, D.A., 2007. A high-

density whole-genome association study reveals that APOE is the major
susceptibility gene for sporadic late-onset Alzheimer's disease. J Clin Psychiatry
68, 613–618.

Cooper-Knock, J., Bury, J.J., Heath, P.R., Wyles, M., Higginbottom, A., Gelsthorpe,
C., Highley, J.R., Hautbergue, G., Rattray, M., Kirby, J., Shaw, P.J., 2015.
C9ORF72 GGGGCC Expanded Repeats Produce Splicing Dysregulation which
Correlates with Disease Severity in Amyotrophic Lateral Sclerosis. PloS one 10,
e0127376. doi:10.1371/journal.pone.0127376

Cruts, M., Gijselinck, I., Van Langenhove, T., van der Zee, J., Van Broeckhoven, C.,
2013. Current insights into the C9orf72 repeat expansion diseases of the
FTLD/ALS spectrum. Trends Neurosci. 36, 450–459.
doi:10.1016/j.tins.2013.04.010

Cui, L., Jeong, H., Borovecki, F., Parkhurst, C.N., Tanese, N., Krainc, D., 2006.
Transcriptional repression of PGC-1alpha by mutant huntingtin leads to
mitochondrial dysfunction and neurodegeneration. Cell 127, 59–69.
doi:10.1016/j.cell.2006.09.015

Da Cruz, S., Parone, P.A., Lopes, V.S., Lillo, C., McAlonis-Downes, M., Lee, S.K.,
Vetto, A.P., Petrosyan, S., Marsala, M., Murphy, A.N., Williams, D.S.,
Spiegelman, B.M., Cleveland, D.W., 2012. Elevated PGC-1α activity sustains
mitochondrial biogenesis and muscle function without extending survival in a
mouse model of inherited ALS. Cell metabolism 15, 778–786.
doi:10.1016/j.cmet.2012.03.019

Devi, L., Raghavendran, V., Prabhu, B.M., Avadhani, N.G., Anandatheerthavarada,
H.K., 2008. Mitochondrial import and accumulation of alpha-synuclein impair
complex I in human dopaminergic neuronal cultures and Parkinson disease
brain. J. Biol. Chem. 283, 9089–9100. doi:10.1074/jbc.M710012200

Di Nottia, M., Masciullo, M., Verrigni, D., Petrillo, S., Modoni, A., Rizzo, V., Di Giuda,
D., Rizza, T., Niceta, M., Torraco, A., Bianchi, M., Santoro, M., Bentivoglio, A.R.,

Bertini, E., Piemonte, F., Carrozzo, R., Silvestri, G., 2017. DJ-1 modulates mitochondrial response to oxidative stress: clues from a novel diagnosis of PARK7. Clin. Genet. 92, 18–25. doi:10.1111/cge.12841

DiFiglia, M., 1997. Aggregation of Huntingtin in Neuronal Intranuclear Inclusions and Dystrophic Neurites in Brain. Science 277, 1990–1993. doi:10.1126/science.277.5334.1990

Diot, A., Hinks-Roberts, A., Lodge, T., Liao, C., Dombi, E., Morten, K., Brady, S., Fratter, C., Carver, J., Muir, R., Davis, R., Green, C.J., Johnston, I., Hilton-Jones, D., Sue, C., Mortiboys, H., Poulton, J., 2015. A novel quantitative assay of mitophagy: Combining high content fluorescence microscopy and mitochondrial DNA load to quantify mitophagy and identify novel pharmacological tools against pathogenic heteroplasmic mtDNA. Pharmacol. Res. 100, 24–35. doi:10.1016/j.phrs.2015.07.014

Dominy, J.E., Puigserver, P., 2013. Mitochondrial biogenesis through activation of nuclear signaling proteins. Cold Spring Harb Perspect Biol 5, a015008. doi:10.1101/cshperspect.a015008

Dölle, C., Flønes, I., Nido, G.S., Miletic, H., Osuagwu, N., Kristoffersen, S., Lilleng, P.K., Larsen, J.P., Tysnes, O.-B., Haugarvoll, K., Bindoff, L.A., Tzoulis, C., 2016. Defective mitochondrial DNA homeostasis in the substantia nigra in Parkinson disease. Nature communications 7, 13548. doi:10.1038/ncomms13548

Dufu, K., Livingstone, M.J., Seebacher, J., Gygi, S.P., Wilson, S.A., Reed, R., 2010. ATP is required for interactions between UAP56 and two conserved mRNA export proteins, Aly and CIP29, to assemble the TREX complex. Genes Dev. 24, 2043–2053. doi:10.1101/gad.1898610

Duncan, J.G., 2011. Peroxisome proliferator activated receptor-alpha (PPARalpha) and PPAR gamma coactivator-1alpha (PGC-1alpha) regulation of cardiac metabolism in diabetes. Pediatric cardiology 32, 323–328. doi:10.1007/s00246-

011-9889-8

Eguchi, K., Taoufiq, Z., Thorn-Seshold, O., Trauner, D., Hasegawa, M., Takahashi, T., 2017. Wild-Type Monomeric α-Synuclein Can Impair Vesicle Endocytosis and Synaptic Fidelity via Tubulin Polymerization at the Calyx of Held. J. Neurosci. 37, 6043–6052. doi:10.1523/JNEUROSCI.0179-17.2017

Ekstrand, M.I., Terzioglu, M., Galter, D., Zhu, S.W., Hofstetter, C., Lindqvist, E., Thams, S., Bergstrand, A., Hansson, F.S., Trifunovic, A., Hoffer, B., Cullheim, S., Mohammed, A.H., Olson, L., Larsson, N.G., 2007. Progressive parkinsonism in mice with respiratory-chain-deficient dopamine neurons. Proc. Natl. Acad. Sci. U.S.A. 104, 1325–1330. doi:10.1073/pnas.0605208103

Engl, E., Attwell, D., 2015. Non-signalling energy use in the brain. J. Physiol. (Lond.) 593, 3417–3429. doi:10.1113/jphysiol.2014.282517

Eschbach, J., Einem, von, B., Müller, K., Bayer, H., Scheffold, A., Morrison, B.E., Rudolph, K.L., Thal, D.R., Witting, A., Weydt, P., Otto, M., Fauler, M., Liss, B., McLean, P.J., Spada, A.R.L., Ludolph, A.C., Weishaupt, J.H., Danzer, K.M., 2015. Mutual exacerbation of peroxisome proliferator-activated receptor γ coactivator 1α deregulation and α-synuclein oligomerization. Ann. Neurol. 77, 15–32. doi:10.1002/ana.24294

Eschbach, J., Schwalenstocker, B., Soyal, S.M., Bayer, H., Wiesner, D., Akimoto, C., Nilsson, A.C., Birve, A., Meyer, T., Dupuis, L., Danzer, K.M., Andersen, P.M., Witting, A., Ludolph, A.C., Patsch, W., Weydt, P., 2013. PGC-1alpha is a male-specific disease modifier of human and experimental amyotrophic lateral sclerosis. Human molecular genetics. doi:10.1093/hmg/ddt202

Fanelli, M., Filippi, E., Sentinelli, F., Romeo, S., Fallarino, M., Buzzetti, R., Leonetti, F., Baroni, M.G., 2005. The Gly482Ser missense mutation of the peroxisome proliferator-activated receptor gamma coactivator-1 alpha (PGC-1 alpha) gene associates with reduced insulin sensitivity in normal and glucose-intolerant obese subjects. Dis. Markers 21, 175–180. doi:10.1155/2005/576748

Ferraiuolo, L., Meyer, K., Sherwood, T.W., Vick, J., Likhite, S., Frakes, A., Miranda, C.J., Braun, L., Heath, P.R., Pineda, R., Beattie, C.E., Shaw, P.J., Askwith, C.C., McTigue, D., Kaspar, B.K., 2016. Oligodendrocytes contribute to motor neuron death in ALS via SOD1-dependent mechanism. Proc. Natl. Acad. Sci. U.S.A. 113, E6496–E6505. doi:10.1073/pnas.1607496113

Ferreira, M., Massano, J., 2017. An updated review of Parkinson's disease genetics and clinicopathological correlations. Acta Neurol. Scand. 135, 273–284. doi:10.1111/ane.12616

Flinn, L., Mortiboys, H., Volkmann, K., Koster, R.W., Ingham, P.W., Bandmann, O., 2009. Complex I deficiency and dopaminergic neuronal cell loss in parkin-deficient zebrafish (Danio rerio). Brain 132, 1613–1623. doi:10.1093/brain/awp108

Fusco, F.R., Zuccato, C., Tartari, M., Martorana, A., De March, Z., Giampa, C., Cattaneo, E., Bernardi, G., 2003. Co-localization of brain-derived neurotrophic factor (BDNF) and wild-type huntingtin in normal and quinolinic acid-lesioned rat brain. Eur. J. Neurosci. 18, 1093–1102. doi:10.1046/j.1460-9568.2003.02844.x

Ganguly, G., Chakrabarti, S., Chatterjee, U., Saso, L., 2017. Proteinopathy, oxidative stress and mitochondrial dysfunction: cross talk in Alzheimer"s disease and Parkinson"s disease. Drug Des Devel Ther 11, 797–810. doi:10.2147/DDDT.S130514

Gao, Jie, Yan, J., Xu, M., Ren, S., Xie, W., 2015. CAR Suppresses Hepatic Gluconeogenesis by Facilitating the Ubiquitination and Degradation of PGC1α. Mol. Endocrinol. 29, 1558–1570. doi:10.1210/me.2015-1145

Gao, Ju, Wang, L., Liu, J., Xie, F., Su, B., Wang, X., 2017. Abnormalities of Mitochondrial Dynamics in Neurodegenerative Diseases. Antioxidants (Basel) 6, 25. doi:10.3390/antiox6020025

Gaugler, M.N., Genc, O., Bobela, W., Mohanna, S., Ardah, M.T., El-Agnaf, O.M., Cantoni, M., Bensadoun, J.-C., Schneggenburger, R., Knott, G.W., Aebischer,

P., Schneider, B.L., 2012. Nigrostriatal overabundance of α-synuclein leads to decreased vesicle density and deficits in dopamine release that correlate with reduced motor activity. Acta Neuropathol. 123, 653–669. doi:10.1007/s00401-012-0963-y

Gerstberger, S., Hafner, M., Tuschl, T., 2014. A census of human RNA-binding proteins. Nat. Rev. Genet. 15, 829–845. doi:10.1038/nrg3813

Ghosh, A., Pratt, A.T., Soma, S., Theriault, S.G., Griffin, A.T., Trivedi, P.P., Gohil, V.M., 2016. Mitochondrial disease genes COA6, COX6Band SCO2have overlapping roles in COX2 biogenesis. Human molecular genetics 25, 660–671. doi:10.1093/hmg/ddv503

Ghosh, A., Trivedi, P.P., Timbalia, S.A., Griffin, A.T., Rahn, J.J., Chan, S.S.L., Gohil, V.M., 2014. Copper supplementation restores cytochrome c oxidase assembly defect in a mitochondrial disease model of COA6 deficiency. Human molecular genetics 23, 3596–3606. doi:10.1093/hmg/ddu069

Giannoccaro, M.P., La Morgia, C., Rizzo, G., Carelli, V., 2017. Mitochondrial DNA and primary mitochondrial dysfunction in Parkinson's disease. Mov. Disord. 32, 346–363. doi:10.1002/mds.26966

Gil, J.M., Rego, A.C., 2008. Mechanisms of neurodegeneration in Huntington's disease. Eur. J. Neurosci. 27, 2803–2820.

Gineviciene, V., Jakaitiene, A., Aksenov, M.O., Aksenova, A.V., Druzhevskaya, A.M., Astratenkova, I.V., Egorova, E.S., Gabdrakhmanova, L.J., Tubelis, L., Kucinskas, V., Utkus, A., 2016. Association analysis of ACE, ACTN3 and PPARGC1A gene polymorphisms in two cohorts of European strength and power athletes. Biol Sport 33, 199–206. doi:10.5604/20831862.1201051

Godin, K.S., Varani, G., 2007. How arginine-rich domains coordinate mRNA maturation events. RNA biology 4, 69–75.

Grimm, A., Eckert, A., 2017. Brain aging and neurodegeneration: from a mitochondrial point of view. J. Neurochem. 45, 580. doi:10.1111/jnc.14037

Grüter, P., Tabernero, C., Kobbe, von, C., Schmitt, C., Saavedra, C., Bachi, A., Wilm, M., Felber, B.K., Izaurralde, E., 1998. TAP, the human homolog of Mex67p, mediates CTE-dependent RNA export from the nucleus. Mol. Cell 1, 649–659.

Guedes-Dias, P., Pinho, B.R., Soares, T.R., de Proença, J., Duchen, M.R., Oliveira, J.M.A., 2016. Mitochondrial dynamics and quality control in Huntington's disease. Neurobiol. Dis. 90, 51–57. doi:10.1016/j.nbd.2015.09.008

Guzman, J.N., Sanchez-Padilla, J., Wokosin, D., Kondapalli, J., Ilijic, E., Schumacker, P.T., Surmeier, D.J., 2010. Oxidant stress evoked by pacemaking in dopaminergic neurons is attenuated by DJ-1. Nature 468, 696–700. doi:10.1038/nature09536

Haase, T.N., Ringholm, S., Leick, L., Bienso, R.S., Kiilerich, K., Johansen, S., Nielsen, M.M., Wojtaszewski, J.F.P., Hidalgo, J., Pedersen, P.A., Pilegaard, H., 2011. Role of PGC-1 alpha in exercise and fasting-induced adaptations in mouse liver. Am. J. Physiol.-Regul. Integr. Comp. Physiol. 301, R1501–R1509. doi:10.1152/ajpregu.00775.2010

Halgren, C., Bache, I., Bak, M., Myatt, M.W., Anderson, C.M., Brøndum-Nielsen, K., Tommerup, N., 2012. Haploinsufficiency of CELF4 at 18q12.2 is associated with developmental and behavioral disorders, seizures, eye manifestations, and obesity. Eur. J. Hum. Genet. 20, 1315–1319. doi:10.1038/ejhg.2012.92

Hanai, J.-I., Cao, P., Tanksale, P., Imamura, S., Koshimizu, E., Zhao, J., Kishi, S., Yamashita, M., Phillips, P.S., Sukhatme, V.P., Lecker, S.H., 2007. The muscle-specific ubiquitin ligase atrogin-1/MAFbx mediates statin-induced muscle toxicity. The Journal of clinical investigation 117, 3940–3951. doi:10.1172/JCI32741

Hara, K., Tobe, K., Okada, T., Kadowaki, H., Akanuma, Y., Ito, C., Kimura, S., Kadowaki, T., 2002. A genetic variation in the PGC-1 gene could confer insulin resistance and susceptibility to Type II diabetes. Diabetologia 45, 740–743.

doi:10.1007/s00125-002-0803-z

Hardy, J., 2009. The amyloid hypothesis for Alzheimer's disease: a critical

reappraisal. J. Neurochem. 110, 1129–1134. doi:10.1111/j.1471-

4159.2009.06181.x

Hargous, Y., Hautbergue, G.M., Tintaru, A.M., Skrisovska, L., Golovanov, A.P.,

Stévenin, J., Lian, L.-Y., Wilson, S.A., Allain, F.H.-T., 2006. Molecular basis of

RNA recognition and TAP binding by the SR proteins SRp20 and 9G8. Embo J.

25, 5126–5137. doi:10.1038/sj.emboj.7601385

Hautbergue, G.M., 2017. RNA Nuclear Export: From Neurological Disorders to

Cancer. Adv. Exp. Med. Biol. 1007, 89–109. doi:10.1007/978-3-319-60733-7_6

Hautbergue, G.M., Hung, M.-L., Golovanov, A.P., Lian, L.-Y., Wilson, S.A., 2008.

Mutually exclusive interactions drive handover of mRNA from export adaptors to

TAP. Proc. Natl. Acad. Sci. U.S.A. 105, 5154–5159.

doi:10.1073/pnas.0709167105

Hautbergue, G.M., Hung, M.-L., Walsh, M.J., Snijders, A.P.L., Chang, C.-T., Jones,

R., Ponting, C.P., Dickman, M.J., Wilson, S.A., 2009. UIF, a New mRNA export

adaptor that works together with REF/ALY, requires FACT for recruitment to

mRNA. Curr. Biol. 19, 1918–1924. doi:10.1016/j.cub.2009.09.041

Haynes, C.M., Petrova, K., Benedetti, C., Yang, Y., Ron, D., 2007. ClpP mediates

activation of a mitochondrial unfolded protein response in C. elegans. Dev. Cell

13, 467–480. doi:10.1016/j.devcel.2007.07.016

Haynes, C.M., Yang, Y., Blais, S.P., Neubert, T.A., Ron, D., 2010. The matrix

peptide exporter HAF-1 signals a mitochondrial UPR by activating the

transcription factor ZC376.7 in C. elegans. Mol. Cell 37, 529–540.

doi:10.1016/j.molcel.2010.01.015

Heath, C.G., Viphakone, N., Wilson, S.A., 2016. The role of TREX in gene

expression and disease. Biochem. J. 473, 2911–2935.

doi:10.1042/BCJ20160010

Heery, D.M., Kalkhoven, E., Hoare, S., Parker, M.G., 1997. A signature motif in transcriptional co-activators mediates binding to nuclear receptor. Nature 387, 733–736.

Helisalmi, S., Vepsalainen, S., Hiltunen, M., Koivisto, A.M., Salminen, A., Laakso, M., Soininen, H., 2008. Genetic study between SIRT1, PPARD, PGC-1alpha genes and Alzheimer's disease. Journal of neurology 255, 668–673. doi:10.1007/s00415-008-0774-1

Heo, J.Y., Park, J.H., Kim, S.J., Seo, K.S., Han, J.S., Lee, S.H., Kim, J.M., Park, J.I., Park, S.K., Lim, K., Hwang, B.D., Shong, M., Kweon, G.R., 2012. DJ-1 null dopaminergic neuronal cells exhibit defects in mitochondrial function and structure: involvement of mitochondrial complex I assembly. PloS one 7, e32629. doi:10.1371/journal.pone.0032629

Hernandez-Alvarez, M.I., Thabit, H., Burns, N., Shah, S., Brema, I., Hatunic, M., Finucane, F., Liesa, M., Chiellini, C., Naon, D., Zorzano, A., Nolan, J.J., 2010. Subjects with early-onset type 2 diabetes show defective activation of the skeletal muscle PGC-1{alpha}/Mitofusin-2 regulatory pathway in response to physical activity. Diabetes care 33, 645–651. doi:10.2337/dc09-1305

Herold, A., Suyama, M., Rodrigues, J.P., Braun, I.C., Kutay, U., Carmo-Fonseca, M., Bork, P., Izaurralde, E., 2000. TAP (NXF1) belongs to a multigene family of putative RNA export factors with a conserved modular architecture. Molecular and cellular biology 20, 8996–9008.

Hoffner, G., Kahlem, P., Djian, P., 2002. Perinuclear localization of huntingtin as a consequence of its binding to microtubules through an interaction with beta-tubulin: relevance to Huntington's disease. J. Cell. Sci. 115, 941–948.

Holtzman, D.M., Fagan, A.M., Mackey, B., Tenkova, T., Sartorius, L., Paul, S.M., Bales, K., Ashe, K.H., Irizarry, M.C., Hyman, B.T., 2000. Apolipoprotein E facilitates neuritic and cerebrovascular plaque formation in an Alzheimer's disease model. Ann. Neurol. 47, 739–747.

Hough, L.E., Dutta, K., Sparks, S., Temel, D.B., Kamal, A., Tetenbaum-Novatt, J., Rout, M.P., Cowburn, D., 2015. The molecular mechanism of nuclear transport revealed by atomic-scale measurements. Elife 4, 635. doi:10.7554/eLife.10027

Hroudová, J., Singh, N., Fišar, Z., 2014. Mitochondrial dysfunctions in neurodegenerative diseases: relevance to Alzheimer's disease. Biomed Res Int 2014, 175062–9. doi:10.1155/2014/175062

Huang, Y., Gattoni, R., Stévenin, J., Steitz, J.A., 2003. SR splicing factors serve as adapter proteins for TAP-dependent mRNA export. Mol. Cell 11, 837–843.

Ihara, R., Matsukawa, K., Nagata, Y., Kunugi, H., Tsuji, S., Chihara, T., Kuranaga, E., Miura, M., Wakabayashi, T., Hashimoto, T., Iwatsubo, T., 2013. RNA binding mediates neurotoxicity in the transgenic Drosophila model of TDP-43 proteinopathy. Human molecular genetics 22, 4474–4484. doi:10.1093/hmg/ddt296

Ingram, T., Chakrabarti, L., 2016. Proteomic profiling of mitochondria: what does it tell us about the ageing brain? Aging (Albany NY) 8, 3161–3179. doi:10.18632/aging.101131

Jager, S., Handschin, C., St-Pierre, J., Spiegelman, B.M., 2007. AMP-activated protein kinase (AMPK) action in skeletal muscle via direct phosphorylation of PGC-1alpha. Proc. Natl. Acad. Sci. U.S.A. 104, 12017–12022. doi:10.1073/pnas.0705070104

Jaunmuktane, Z., Mead, S., Ellis, M., Wadsworth, J.D.F., Nicoll, A.J., Kenny, J., Launchbury, F., Linehan, J., Richard-Loendt, A., Walker, A.S., Rudge, P., Collinge, J., Brandner, S., 2015. Evidence for human transmission of amyloid-β pathology and cerebral amyloid angiopathy. Nature 525, 247–250. doi:10.1038/nature15369

Järvelin, A.I., Noerenberg, M., Davis, I., Castello, A., 2016. The new (dis)order in RNA regulation. Cell Communication and Signaling 14, 547. doi:10.1186/s12964-016-0132-3

Jemaa, Z., Kallel, A., Sleimi, C., Mahjoubi, I., Feki, M., Ftouhi, B., Slimane, H., Jemaa, R., Kaabachi, N., 2015. The Gly482Ser polymorphism of the peroxisome proliferator-activated receptor-γ coactivator-1α (PGC-1α) is associated with type 2 diabetes in Tunisian population. Diabetes Metab Syndr 9, 316–319. doi:10.1016/j.dsx.2013.10.011

Jiang, T., Yin, F., Yao, J., Brinton, R.D., Cadenas, E., 2013. Lipoic acid restores age-associated impairment of brain energy metabolism through the modulation of Akt/JNK signaling and PGC1α transcriptional pathway. Aging Cell 12, 1021–1031. doi:10.1111/acel.12127

Jimenez-Sanchez, M., Licitra, F., Underwood, B.R., Rubinsztein, D.C., 2017. Huntington's Disease: Mechanisms of Pathogenesis and Therapeutic Strategies. Cold Spring Harb Perspect Med 7, a024240. doi:10.1101/cshperspect.a024240

Kahn, S.E., Cooper, M.E., Del Prato, S., 2014. Pathophysiology and treatment of type 2 diabetes: perspectives on the past, present, and future. Lancet 383, 1068–1083. doi:10.1016/S0140-6736(13)62154-6

Kalfalah, F., Sobek, S., Bornholz, B., Götz-Rösch, C., Tigges, J., Fritsche, E., Krutmann, J., Köhrer, K., Deenen, R., Ohse, S., Boerries, M., Busch, H., Boege, F., 2014. Inadequate mito-biogenesis in primary dermal fibroblasts from old humans is associated with impairment of PGC1A-independent stimulation. Experimental Gerontology 56, 59–68. doi:10.1016/j.exger.2014.03.017

Karunakaran, D.K.P., Congdon, S., Guerrette, T., Banday, A.R., Lemoine, C., Chhaya, N., Kanadia, R., 2013. The expression analysis of Sfrs10 and Celf4 during mouse retinal development. Gene Expr. Patterns 13, 425–436. doi:10.1016/j.gep.2013.07.009

Katahira, J., Inoue, H., Hurt, E., Yoneda, Y., 2009. Adaptor Aly and co-adaptor Thoc5 function in the Tap-p15-mediated nuclear export of HSP70 mRNA. Embo J. 28, 556–567. doi:10.1038/emboj.2009.5

Kennedy, S.R., Salk, J.J., Schmitt, M.W., Loeb, L.A., 2013. Ultra-sensitive
    sequencing reveals an age-related increase in somatic mitochondrial mutations
    that are inconsistent with oxidative damage. PLoS Genet. 9, e1003794.
    doi:10.1371/journal.pgen.1003794

Kim, Hong Joo, Kim, N.C., Wang, Y.-D., Scarborough, E.A., Moore, J., Diaz, Z.,
    MacLea, K.S., Freibaum, B., Li, S., Molliex, A., Kanagaraj, A.P., Carter, R.,
    Boylan, K.B., Wojtas, A.M., Rademakers, R., Pinkus, J.L., Greenberg, S.A.,
    Trojanowski, J.Q., Traynor, B.J., Smith, B.N., Topp, S., Gkazi, A.-S., Miller, J.,
    Shaw, C.E., Kottlors, M., Kirschner, J., Pestronk, A., Li, Y.R., Ford, A.F., Gitler,
    A.D., Benatar, M., King, O.D., Kimonis, V.E., Ross, E.D., Weihl, C.C., Shorter,
    J., Taylor, J.P., 2013. Mutations in prion-like domains in hnRNPA2B1 and
    hnRNPA1 cause multisystem proteinopathy and ALS. Nature 495, 467–473.
    doi:10.1038/nature11922

Kim, Hyung-Jun, Raphael, A.R., LaDow, E.S., McGurk, L., Weber, R.A.,
    Trojanowski, J.Q., Lee, V.M.-Y., Finkbeiner, S., Gitler, A.D., Bonini, N.M., 2014.
    Therapeutic modulation of eIF2α phosphorylation rescues TDP-43 toxicity in
    amyotrophic lateral sclerosis disease models. Nature Genet. 46, 152–160.
    doi:10.1038/ng.2853

Kim, Janghwan, Efe, J.A., Zhu, S., Talantova, M., Yuan, X., Wang, S., Lipton, S.A.,
    Zhang, K., Ding, S., 2011. Direct reprogramming of mouse fibroblasts to neural
    progenitors. Proc. Natl. Acad. Sci. U.S.A. 108, 7838–7843.
    doi:10.1073/pnas.1103113108

Kok, F.O., Shin, M., Ni, C.-W., Gupta, A., Grosse, A.S., van Impel, A., Kirchmaier,
    B.C., Peterson-Maduro, J., Kourkoulis, G., Male, I., DeSantis, D.F., Sheppard-
    Tindell, S., Ebarasi, L., Betsholtz, C., Schulte-Merker, S., Wolfe, S.A., Lawson,
    N.D., 2015. Reverse genetic screening reveals poor correlation between
    morpholino-induced and mutant phenotypes in zebrafish. Dev. Cell 32, 97–108.
    doi:10.1016/j.devcel.2014.11.018

Kraytsberg, Y., Kudryavtseva, E., McKee, A.C., Geula, C., Kowall, N.W., Khrapko, K., 2006. Mitochondrial DNA deletions are abundant and cause functional impairment in aged human substantia nigra neurons. Nature Genet. 38, 518–520. doi:10.1038/ng1778

Kubli, D.A., Gustafsson, A.B., 2012. Mitochondria and Mitophagy The Yin and Yang of Cell Death Control. Circ.Res. 111, 1208–1221. doi:10.1161/circresaha.112.265819

Kujoth, G.C., Hiona, A., Pugh, T.D., Someya, S., Panzer, K., Wohlgemuth, S.E., Hofer, T., Seo, A.Y., Sullivan, R., Jobling, W.A., Morrow, J.D., Van Remmen, H., Sedivy, J.M., Yamasoba, T., Tanokura, M., Weindruch, R., Leeuwenburgh, C., Prolla, T.A., 2005. Mitochondrial DNA mutations, oxidative stress, and apoptosis in mammalian aging. Science 309, 481–484. doi:10.1126/science.1112125

Kumar, A., Singh, A., Ekavali, 2015. A review on Alzheimer's disease pathophysiology and its management: an update. Pharmacol Rep 67, 195–203. doi:10.1016/j.pharep.2014.09.004

Kunej, T., Petrovic, M.G., Dovc, P., Peterlin, B., Petrovic, D., 2004. A Gly482Ser polymorphism of the peroxisome proliferator-activated receptor-gamma coactivator-1 (PGC-1) gene is associated with type 2 diabetes in Caucasians. Folia Biologica 50, 157–158.

Kwong, J.Q., Beal, M.F., Manfredi, G., 2006. The role of mitochondria in inherited neurodegenerative diseases. J. Neurochem. 97, 1659–1675. doi:10.1111/j.1471-4159.2006.03990.x

Lagier-Tourenne, C., Cleveland, D.W., 2009. Rethinking ALS: The FUS about TDP-43. Cell 136, 1001–1004. doi:10.1016/j.cell.2009.03.006

Langston, J.W., Ballard, P., Tetrud, J.W., Irwin, I., 1983. CHRONIC PARKINSONISM IN HUMANS DUE TO A PRODUCT OF MEPERIDINE-ANALOG SYNTHESIS. Science 219, 979–980. doi:10.1126/science.6823561

Lazarou, M., Jin, S.M., Kane, L.A., Youle, R.J., 2012. Role of PINK1 binding to the

TOM complex and alternate intracellular membranes in recruitment and activation of the E3 ligase Parkin. Dev. Cell 22, 320–333. doi:10.1016/j.devcel.2011.12.014

Lees, A.J., Hardy, J., Revesz, T., 2009. Parkinson's disease. Lancet 373, 2055–2066.

Lehman, J.J., Barger, P.M., Kovacs, A., Saffitz, J.E., Medeiros, D.M., Kelly, D.P., 2000. Peroxisome proliferator-activated receptor gamma coactivator-1 promotes cardiac mitochondrial biogenesis. The Journal of clinical investigation 106, 847–856. doi:10.1172/jci10268

Leone, T.C., Lehman, J.J., Finck, B.N., Schaeffer, P.J., Wende, A.R., Boudina, S., Courtois, M., Wozniak, D.F., Sambandam, N., Bernal-Mizrachi, C., Chen, Z., Holloszy, J.O., Medeiros, D.M., Schmidt, R.E., Saffitz, J.E., Abel, E.D., Semenkovich, C.F., Kelly, D.P., 2005. PGC-1alpha deficiency causes multi-system energy metabolic derangements: muscle dysfunction, abnormal weight control and hepatic steatosis. PLoS biology 3, e101. doi:10.1371/journal.pbio.0030101

Lerin, C., Rodgers, J.T., Kalume, D.E., Kim, S.H., Pandey, A., Puigserver, P., 2006. GCN5 acetyltransferase complex controls glucose metabolism through transcriptional repression of PGC-1alpha. Cell metabolism 3, 429–438. doi:10.1016/j.cmet.2006.04.013

Li, S., 1998. Aggregation of N-terminal huntingtin is dependent on the length of its glutamine repeats. Human molecular genetics 7, 777–782. doi:10.1093/hmg/7.5.777

Li, X., Monks, B., Ge, Q., Birnbaum, M.J., 2007. Akt/PKB regulates hepatic metabolism by directly inhibiting PGC-1alpha transcription coactivator. Nature 447, 1012–1016. doi:10.1038/nature05861

Liang, H., Ward, W.F., Jang, Y.C., Bhattacharya, A., Bokov, A.F., Li, Y., Jernigan, A., Richardson, A., Van Remmen, H., 2011. PGC-1α protects neurons and

alters disease progression in an amyotrophic lateral sclerosis mouse model. Muscle & nerve 44, 947–956. doi:10.1002/mus.22217

Liker, E., Fernandez, E., Izaurralde, E., Conti, E., 2000. The structure of the mRNA export factor TAP reveals a cis arrangement of a non-canonical RNP domain and an LRR domain. Embo J. 19, 5587–5598. doi:10.1093/emboj/19.21.5587

Lin, J., Handschin, C., Spiegelman, B.M., 2005. Metabolic control through the PGC-1 family of transcription coactivators. Cell metabolism 1, 361–370. doi:10.1016/j.cmet.2005.05.004

Lin, J., Wu, H., Tarr, P.T., Zhang, C.Y., Wu, Z.D., Boss, O., Michael, L.F., Puigserver, P., Isotani, E., Olson, E.N., Lowell, B.B., Bassel-Duby, R., Spiegelman, B.M., 2002. Transcriptional co-activator PGC-1 alpha drives the formation of slow-twitch muscle fibres. Nature 418, 797–801. doi:10.1038/nature00904

Lin, J., Wu, P.H., Tarr, P.T., Lindenberg, K.S., St-Pierre, J., Zhang, C.Y., Mootha, V.K., Jager, S., Vianna, C.R., Reznick, R.M., Cui, L., Manieri, M., Donovan, M.X., Wu, Z., Cooper, M.P., Fan, M.C., Rohas, L.M., Zavacki, A.M., Cinti, S., Shulman, G.I., Lowell, B.B., Krainc, D., Spiegelman, B.M., 2004. Defects in adaptive energy metabolism with CNS-linked hyperactivity in PGC-1alpha null mice. Cell 119, 121–135. doi:10.1016/j.cell.2004.09.013

Lin, Y.-C., Boone, M., Meuris, L., Lemmens, I., Van Roy, N., Soete, A., Reumers, J., Moisse, M., Plaisance, S., Drmanac, R., Chen, J., Speleman, F., Lambrechts, D., Van de Peer, Y., Tavernier, J., Callewaert, N., 2014. Genome dynamics of the human embryonic kidney 293 lineage in response to cell biology manipulations. Nature communications 5, 4767. doi:10.1038/ncomms5767

Ling, S.-C., Polymenidou, M., Cleveland, D.W., 2013. Converging mechanisms in ALS and FTD: disrupted RNA and protein homeostasis. Neuron 79, 416–438. doi:10.1016/j.neuron.2013.07.033

Liot, G., Valette, J., Pépin, J., Flament, J., Brouillet, E., 2017. Energy defects in

Huntington's disease: Why 'in vivo' evidence matters. Biochem. Biophys. Res. Commun. 483, 1084–1095. doi:10.1016/j.bbrc.2016.09.065

Lister, R., Pelizzola, M., Kida, Y.S., Hawkins, R.D., Nery, J.R., Hon, G., Antosiewicz-Bourget, J., O'Malley, R., Castanon, R., Klugman, S., Downes, M., Yu, R., Stewart, R., Ren, B., Thomson, J.A., Evans, R.M., Ecker, J.R., 2011. Hotspots of aberrant epigenomic reprogramming in human induced pluripotent stem cells. Nature 471, 68–73. doi:10.1038/nature09798

Liu, E.Y., Cali, C.P., Lee, E.B., 2017. RNA metabolism in neurodegenerative disease. Dis Model Mech 10, 509–518. doi:10.1242/dmm.028613

Liu, J., Zhou, Y., Qi, X., Chen, J., Chen, W., Qiu, G., Wu, Z., Wu, N., 2017. CRISPR/Cas9 in zebrafish: an efficient combination for human genetic diseases modeling. Hum. Genet. 136, 1–12. doi:10.1007/s00439-016-1739-6

Loerch, P.M., Lu, T., Dakin, K.A., Vann, J.M., Isaacs, A., Geula, C., Wang, J., Pan, Y., Gabuzda, D.H., Li, C., Prolla, T.A., Yankner, B.A., 2008. Evolution of the aging brain transcriptome and synaptic regulation. PloS one 3, e3329. doi:10.1371/journal.pone.0003329

Lou, X., Kim, J., Hawk, B.J., Shin, Y.-K., 2017. α-Synuclein may cross-bridge v-SNARE and acidic phospholipids to facilitate SNARE-dependent vesicle docking. Biochem. J. 474, 2039–2049. doi:10.1042/BCJ20170200

Love, J.E., Hayden, E.J., Rohn, T.T., 2015. Alternative Splicing in Alzheimer's Disease. J Parkinsons Dis Alzheimers Dis 2. doi:10.13188/2376-922X.1000010

López-Otín, C., Blasco, M.A., Partridge, L., Serrano, M., Kroemer, G., 2013. The hallmarks of aging. Cell 153, 1194–1217. doi:10.1016/j.cell.2013.05.039

Löw, P., 2011. The role of ubiquitin-proteasome system in ageing. Gen. Comp. Endocrinol. 172, 39–43. doi:10.1016/j.ygcen.2011.02.005

Lu, T., Pan, Y., Kao, S.-Y., Li, C., Kohane, I., Chan, J., Yankner, B.A., 2004. Gene regulation and DNA damage in the ageing human brain. Nature 429, 883–891. doi:10.1038/nature02661

Majounie, E., Renton, A.E., Mok, K., Dopper, E.G.P., Waite, A., Rollinson, S., Chiò, A., Restagno, G., Nicolaou, N., Simon-Sanchez, J., van Swieten, J.C., Abramzon, Y., Johnson, J.O., Sendtner, M., Pamphlett, R., Orrell, R.W., Mead, S., Sidle, K.C., Houlden, H., Rohrer, J.D., Morrison, K.E., Pall, H., Talbot, K., Ansorge, O., Chromosome 9-ALS/FTD Consortium, French research network on FTLD/FTLD/ALS, ITALSGEN Consortium, Hernandez, D.G., Arepalli, S., Sabatelli, M., Mora, G., Corbo, M., Giannini, F., Calvo, A., Englund, E., Borghero, G., Floris, G.L., Remes, A.M., Laaksovirta, H., McCluskey, L., Trojanowski, J.Q., Van Deerlin, V.M., Schellenberg, G.D., Nalls, M.A., Drory, V.E., Lu, C.-S., Yeh, T.-H., Ishiura, H., Takahashi, Y., Tsuji, S., Le Ber, I., Brice, A., Drepper, C., Williams, N., Kirby, J., Shaw, P., Hardy, J., Tienari, P.J., Heutink, P., Morris, H.R., Pickering-Brown, S., Traynor, B.J., 2012. Frequency of the C9orf72 hexanucleotide repeat expansion in patients with amyotrophic lateral sclerosis and frontotemporal dementia: a cross-sectional study. Lancet Neurol. 11, 323–330. doi:10.1016/S1474-4422(12)70043-1

Mancuso, M., Filosto, M., Bosetti, F., Ceravolo, R., Rocchi, A., Tognoni, G., Manca, M.L., Solaini, G., Siciliano, G., Murri, L., 2003. Decreased platelet cytochrome c oxidase activity is accompanied by increased blood lactate concentration during exercise in patients with Alzheimer disease. Exp. Neurol. 182, 421–426.

Mandal, P.K., Tripathi, M., Sugunan, S., 2012. Brain oxidative stress: detection and mapping of anti-oxidant marker "Glutathione" in different brain regions of healthy male/female, MCI and Alzheimer patients using non-invasive magnetic resonance spectroscopy. Biochem. Biophys. Res. Commun. 417, 43–48. doi:10.1016/j.bbrc.2011.11.047

Maniataki, E., Mourelatos, Z., 2005. Human mitochondrial tRNAMet is exported to the cytoplasm and associates with the Argonaute 2 protein. RNA 11, 849–852. doi:10.1261/rna.2210805

Marchetto, M.C.N., Yeo, G.W., Kainohana, O., Marsala, M., Gage, F.H., Muotri,

A.R., 2009. Transcriptional signature and memory retention of human-induced pluripotent stem cells. PloS one 4, e7076. doi:10.1371/journal.pone.0007076

Marin, C., Aguilar, E., 2011. In vivo 6-OHDA-induced neurodegeneration and nigral autophagic markers expression. Neurochem. Int. 58, 521–526. doi:10.1016/j.neuint.2011.01.010

Martin, R., Hackert, P., Ruprecht, M., Simm, S., Brüning, L., Mirus, O., Sloan, K.E., Kudla, G., Schleiff, E., Bohnsack, M.T., 2014. A pre-ribosomal RNA interaction network involving snoRNAs and the Rok1 helicase. RNA 20, 1173–1182. doi:10.1261/rna.044669.114

Martínez, G., Duran-Aniotz, C., Cabral-Miranda, F., Vivar, J.P., Hetz, C., 2017. Endoplasmic reticulum proteostasis impairment in aging. Aging Cell 16, 615–623. doi:10.1111/acel.12599

Martínez-Redondo, V., Pettersson, A.T., Ruas, J.L., 2015. The hitchhiker's guide to PGC-1α isoform structure and biological functions. Diabetologia 58, 1969–1977. doi:10.1007/s00125-015-3671-z

Masuda, S., Das, R., Cheng, H., Hurt, E., Dorman, N., Reed, R., 2005. Recruitment of the human TREX complex to mRNA during splicing. Genes Dev. 19, 1512–1517. doi:10.1101/gad.1302205

McGowan, D.P., van Roon-Mom, W., Holloway, H., Bates, G.P., Mangiarini, L., Cooper, G.J., Faull, R.L., Snell, R.G., 2000. Amyloid-like inclusions in Huntington's disease. Neuroscience 100, 677–680.

McKinstry, S.U., Karadeniz, Y.B., Worthington, A.K., Hayrapetyan, V.Y., Ozlu, M.I., Serafin-Molina, K., Risher, W.C., Ustunkaya, T., Dragatsis, I., Zeitlin, S., Yin, H.H., Eroglu, C., 2014. Huntingtin is required for normal excitatory synapse development in cortical and striatal circuits. J. Neurosci. 34, 9455–9472. doi:10.1523/JNEUROSCI.4699-13.2014

Medeiros, D.M., 2008. Assessing mitochondria biogenesis. Methods (San Diego, Calif.) 46, 288–294. doi:10.1016/j.ymeth.2008.09.026

Meyer, K., Ferraiuolo, L., Miranda, C.J., Likhite, S., McElroy, S., Renusch, S., Ditsworth, D., Lagier-Tourenne, C., Smith, R.A., Ravits, J., Burghes, A.H., Shaw, P.J., Cleveland, D.W., Kolb, S.J., Kaspar, B.K., 2014. Direct conversion of patient fibroblasts demonstrates non-cell autonomous toxicity of astrocytes to motor neurons in familial and sporadic ALS. Proceedings of the National Academy of Sciences 111, 829–832. doi:10.1073/pnas.1314085111

Milles, S., Mercadante, D., Aramburu, I.V., Jensen, M.R., Banterle, N., Koehler, C., Tyagi, S., Clarke, J., Shammas, S.L., Blackledge, M., Gräter, F., Lemke, E.A., 2015. Plasticity of an ultrafast interaction between nucleoporins and nuclear transport receptors. Cell 163, 734–745. doi:10.1016/j.cell.2015.09.047

Misteli, T., Cáceres, J.F., Clement, J.Q., Krainer, A.R., Wilkinson, M.F., Spector, D.L., 1998. Serine phosphorylation of SR proteins is required for their recruitment to sites of transcription in vivo. J. Cell Biol. 143, 297–307.

Mitchell, S.F., Parker, R., 2014. Principles and properties of eukaryotic mRNPs. Mol. Cell 54, 547–558. doi:10.1016/j.molcel.2014.04.033

Mitchell, S.J., Martin-Montalvo, A., Mercken, E.M., Palacios, H.H., Ward, T.M., Abulwerdi, G., Minor, R.K., Vlasuk, G.P., Ellis, J.L., Sinclair, D.A., Dawson, J., Allison, D.B., Zhang, Y., Becker, K.G., Bernier, M., de Cabo, R., 2014. The SIRT1 Activator SRT1720 Extends Lifespan and Improves Health of Mice Fed a Standard Diet. Cell Rep 6, 836–843. doi:10.1016/j.celrep.2014.01.031

Monsalve, M., Wu, Z., Adelmant, G., Puigserver, P., Fan, M., Spiegelman, B.M., 2000. Direct coupling of transcription and mRNA processing through the thermogenic coactivator PGC-1. Mol. Cell 6, 307–316.

Mootha, V.K., Lindgren, C.M., Eriksson, K.F., Subramanian, A., Sihag, S., Lehar, J., Puigserver, P., Carlsson, E., Ridderstrale, M., Laurila, E., Houstis, N., Daly, M.J., Patterson, N., Mesirov, J.P., Golub, T.R., Tamayo, P., Spiegelman, B., Lander, E.S., Hirschhorn, J.N., Altshuler, D., Groop, L.C., 2003. PGC-1 alpha-responsive genes involved in oxidative phosphorylation are coordinately

downregulated in human diabetes. Nature Genet. 34, 267–273.
doi:10.1038/ng1180

Morais, V.A., De Strooper, B., 2010. Mitochondria Dysfunction and
Neurodegenerative Disorders: Cause or Consequence. Journal of Alzheimers
Disease 20, S255–S263. doi:10.3233/jad-2010-100345

Moreira, P.I., Zhu, X.W., Wang, X.L., Lee, H.G., Nunomura, A., Petersen, R.B.,
Perry, G., Smith, M.A., 2010. Mitochondria: A therapeutic target in
neurodegeneration. Biochim. Biophys. Acta-Mol. Basis Dis. 1802, 212–220.
doi:10.1016/j.bbadis.2009.10.007

Mortiboys, H., Furmston, R., Bronstad, G., Aasly, J., Elliott, C., Bandmann, O.,
2015. UDCA exerts beneficial effect on mitochondrial dysfunction in
LRRK2G2019Scarriers and in vivo. Neurology 85, 846–852.
doi:10.1212/WNL.0000000000001905

Mortiboys, H., Johansen, K.K., Aasly, J.O., Bandmann, O., 2010. Mitochondrial
impairment in patients with Parkinson disease with the G2019S mutation in
LRRK2. Neurology 75, 2017–2020. doi:10.1212/WNL.0b013e3181ff9685

Mortiboys, H., Thomas, K.J., Koopman, W.J.H., Klaffke, S., Abou-Sleiman, P.,
Olpin, S., Wood, N.W., Willems, P., Smeitink, J.A.M., Cookson, M.R.,
Bandmann, O., 2008. Mitochondrial Function and Morphology Are Impaired in
parkin-Mutant Fibroblasts. Ann. Neurol. 64, 555–565. doi:10.1002/ana.21492

Mortiboys, H.J., Schaefer, J., Reichmann, H., Jackson, S., 2007. Mitochondrial
dysfunction in Parkinson's disease - revisited. Neurol. Neurochir. Pol. 41, 150–
159.

Mudo, G., Makela, J., Di Liberto, V., Tselykh, T.V., Olivieri, M., Piepponen, P.,
Eriksson, O., Malkia, A., Bonomo, A., Kairisalo, M., Aguirre, J.A., Korhonen, L.,
Belluardo, N., Lindholm, D., 2012. Transgenic expression and activation of
PGC-1alpha protect dopaminergic neurons in the MPTP mouse model of
Parkinson's disease. Cellular and molecular life sciences : CMLS 69, 1153–

1165. doi:10.1007/s00018-011-0850-z

Muller, Y.L., Bogardus, C., Pedersen, O., Baier, L., 2003. A Gly482Ser missense mutation in the peroxisome proliferator-activated receptor gamma coactivator-1 is associated with altered lipid oxidation and early insulin secretion in Pima Indians. Diabetes 52, 895–898.

Mutisya, E.M., Bowling, A.C., Beal, M.F., 1994. Cortical cytochrome oxidase activity is reduced in Alzheimer's disease. J. Neurochem. 63, 2179–2184.

Neumann, M., Sampathu, D.M., Kwong, L.K., Truax, A.C., Micsenyi, M.C., Chou, T.T., Bruce, J., Schuck, T., Grossman, M., Clark, C.M., McCluskey, L.F., Miller, B.L., Masliah, E., Mackenzie, I.R., Feldman, H., Feiden, W., Kretzschmar, H.A., Trojanowski, J.Q., Lee, V.M.-Y., 2006. Ubiquitinated TDP-43 in frontotemporal lobar degeneration and amyotrophic lateral sclerosis. Science 314, 130–133. doi:10.1126/science.1134108

Nicholls, D.G., Budd, S.L., 2000. Mitochondria and neuronal survival. Physiol. Rev. 80, 315–360.

Nunnari, J., Suomalainen, A., 2012. Mitochondria: in sickness and in health. Cell 148, 1145–1159. doi:10.1016/j.cell.2012.02.035

O'Donnell, K.C., Lulla, A., Stahl, M.C., Wheat, N.D., Bronstein, J.M., Sagasti, A., 2014. Axon degeneration and PGC-1α-mediated protection in a zebrafish model of α-synuclein toxicity. Dis Model Mech 7, 571–582. doi:10.1242/dmm.013185

Okita, K., Ichisaka, T., Yamanaka, S., 2007. Generation of germline-competent induced pluripotent stem cells. Nature 448, 313–317. doi:10.1038/nature05934

Pacelli, C., De Rasmo, D., Signorile, A., Grattagliano, I., di Tullio, G., D'Orazio, A., Nico, B., Comi, G.P., Ronchi, D., Ferranini, E., Pirolo, D., Seibel, P., Schubert, S., Gaballo, A., Villani, G., Cocco, T., 2011. Mitochondrial defect and PGC-1 alpha dysfunction in parkin-associated familial Parkinson's disease. Biochim. Biophys. Acta-Mol. Basis Dis. 1812, 1041–1053. doi:10.1016/j.bbadis.2010.12.022

Pacheu-Grau, D., Bareth, B., Dudek, J., Juris, L., Vögtle, F.N., Wissel, M., Leary, S.C., Dennerlein, S., Rehling, P., Deckers, M., 2015. Cooperation between COA6 and SCO2 in COX2 Maturation during Cytochrome c Oxidase Assembly Links Two Mitochondrial Cardiomyopathies. Cell metabolism 21, 823–833. doi:10.1016/j.cmet.2015.04.012

Palacino, J.J., Sagi, D., Goldberg, M.S., Krauss, S., Motz, C., Wacker, M., Klose, J., Shen, J., 2004. Mitochondrial dysfunction and oxidative damage in parkin-deficient mice. J. Biol. Chem. 279, 18614–18622. doi:10.1074/jbc.M401135200

Papkovskaia, T.D., Chau, K.-Y., Inesta-Vaquera, F., Papkovsky, D.B., Healy, D.G., Nishio, K., Staddon, J., Duchen, M.R., Hardy, J., Schapira, A.H.V., Cooper, J.M., 2012. G2019S leucine-rich repeat kinase 2 causes uncoupling protein-mediated mitochondrial depolarization. Human molecular genetics 21, 4201–4213. doi:10.1093/hmg/dds244

Patti, M.E., Butte, A.J., Crunkhorn, S., Cusi, K., Berria, R., Kashyap, S., Miyazaki, Y., Kohane, I., Costello, M., Saccone, R., Landaker, E.J., Goldfine, A.B., Mun, E., DeFronzo, R., Finlayson, J., Kahn, C.R., Mandarino, L.J., 2003. Coordinated reduction of genes of oxidative metabolism in humans with insulin resistance and diabetes: Potential role of PGC1 and NRF1. Proc. Natl. Acad. Sci. U.S.A. 100, 8466–8471. doi:10.1073/pnas.1032913100

Payne, B.A.I., Chinnery, P.F., 2015. Mitochondrial dysfunction in aging: Much progress but many unresolved questions. Biochim. Biophys. Acta 1847, 1347–1353. doi:10.1016/j.bbabio.2015.05.022

Peskind, E.R., Li, G., Shofer, J.B., Millard, S.P., Leverenz, J.B., Yu, C.-E., Raskind, M.A., Quinn, J.F., Galasko, D.R., Montine, T.J., 2014. Influence of lifestyle modifications on age-related free radical injury to brain. JAMA Neurol 71, 1150–1154. doi:10.1001/jamaneurol.2014.1428

Petty, R.D., Sutherland, L.A., Hunter, E.M., Cree, I.A., 1995. Comparison of MTT and ATP-based assays for the measurement of viable cell number. J. Biolumin.

Chemilumin. 10, 29–34. doi:10.1002/bio.1170100105

Pickrell, A.M., Youle, R.J., 2015. The roles of PINK1, parkin, and mitochondrial fidelity in Parkinson's disease. Neuron 85, 257–273. doi:10.1016/j.neuron.2014.12.007

Plá, V., Barranco, N., Pozas, E., Aguado, F., 2017. Amyloid-β Impairs Vesicular Secretion in Neuronal and Astrocyte Peptidergic Transmission. Front Mol Neurosci 10, 202. doi:10.3389/fnmol.2017.00202

Poewe, W., Seppi, K., Tanner, C.M., Halliday, G.M., Brundin, P., Volkmann, J., Schrag, A.-E., Lang, A.E., 2017. Parkinson disease. Nat Rev Dis Primers 3, 17013. doi:10.1038/nrdp.2017.13

Puigserver, P., 2003. Peroxisome Proliferator-Activated Receptor-gamma Coactivator 1alpha (PGC-1alpha): Transcriptional Coactivator and Metabolic Regulator. Endocrine reviews 24, 78–90. doi:10.1210/er.2002-0012

Puigserver, P., Adelmant, C., Wu, Z.D., Fan, M., Xu, J.M., O'Malley, B., Spiegelman, B.M., 1999. Activation of PPAR gamma coactivator-1 through transcription factor docking. Science 286, 1368–1371. doi:10.1126/science.286.5443.1368

Puigserver, P., Rhee, J., Donovan, J., Walkey, C.J., Yoon, J.C., Oriente, F., Kitamura, Y., Altomonte, J., Dong, H., Accili, D., Spiegelman, B.M., 2003. Insulin-regulated hepatic gluconeogenesis through FOXO1-PGC-1alpha interaction. Nature 423, 550–555. doi:10.1038/nature01667

Puigserver, P., Rhee, J., Lin, J., Wu, Z., Yoon, J.C., Zhang, C.Y., Krauss, S., Mootha, V.K., Lowell, B.B., Spiegelman, B.M., 2001. Cytokine stimulation of energy expenditure through p38 MAP kinase activation of PPARgamma coactivator-1. Mol. Cell 8, 971–982.

Puigserver, P., Wu, Z.D., Park, C.W., Graves, R., Wright, M., Spiegelman, B.M., 1998. A cold-inducible coactivator of nuclear receptors linked to adaptive thermogenesis. Cell 92, 829–839. doi:10.1016/s0092-8674(00)81410-5

Qin, W.P., Haroutunian, V., Katsel, P., Cardozo, C.P., Ho, L., Buxbaum, J.D.,

Pasinetti, G.M., 2009. PGC-1 alpha Expression Decreases in the Alzheimer Disease Brain as a Function of Dementia. Arch. Neurol. 66, 352–361.

Reeve, A.K., Ludtmann, M.H.R., Angelova, P.R., Simcox, E.M., Horrocks, M.H., Klenerman, D., Gandhi, S., Turnbull, D.M., Abramov, A.Y., 2015. Aggregated α-synuclein and complex I deficiency: exploration of their relationship in differentiated neurons. Cell Death Dis 6, e1820. doi:10.1038/cddis.2015.166

Reiner, A., Albin, R.L., Anderson, K.D., D'Amato, C.J., Penney, J.B., Young, A.B., 1988. Differential loss of striatal projection neurons in Huntington disease. Proc. Natl. Acad. Sci. U.S.A. 85, 5733–5737.

Renton, A.E., Majounie, E., Waite, A., Simon-Sanchez, J., Rollinson, S., Gibbs, J.R., Schymick, J.C., Laaksovirta, H., van Swieten, J.C., Myllykangas, L., Kalimo, H., Paetau, A., Abramzon, Y., Remes, A.M., Kaganovich, A., Scholz, S.W., Duckworth, J., Ding, J., Harmer, D.W., Hernandez, D.G., Johnson, J.O., Mok, K., Ryten, M., Trabzuni, D., Guerreiro, R.J., Orrell, R.W., Neal, J., Murray, A., Pearson, J., Jansen, I.E., Sondervan, D., Seelaar, H., Blake, D., Young, K., Halliwell, N., Callister, J.B., Toulson, G., Richardson, A., Gerhard, A., Snowden, J., Mann, D., Neary, D., Nalls, M.A., Peuralinna, T., Jansson, L., Isoviita, V.-M., Kaivorinne, A.-L., Hölttä-Vuori, M., Ikonen, E., Sulkava, R., Benatar, M., Wuu, J., Chiò, A., Restagno, G., Borghero, G., Sabatelli, M., ITALSGEN Consortium, Heckerman, D., Rogaeva, E., Zinman, L., Rothstein, J.D., Sendtner, M., Drepper, C., Eichler, E.E., Alkan, C., Abdullaev, Z., Pack, S.D., Dutra, A., Pak, E., Hardy, J., Singleton, A., Williams, N.M., Heutink, P., Pickering-Brown, S., Morris, H.R., Tienari, P.J., Traynor, B.J., 2011. A hexanucleotide repeat expansion in C9ORF72 is the cause of chromosome 9p21-linked ALS-FTD. Neuron 72, 257–268. doi:10.1016/j.neuron.2011.09.010

Rera, M., Bahadorani, S., Cho, J., Koehler, C.L., Ulgherait, M., Hur, J.H., Ansari, W.S., Lo, T., Jones, D.L., Walker, D.W., 2011. Modulation of longevity and tissue homeostasis by the Drosophila PGC-1 homolog. Cell metabolism 14,

623–634. doi:10.1016/j.cmet.2011.09.013

Rha, G.B., Wu, G., Shoelson, S.E., Chi, Y.-I., 2009. Multiple binding modes between HNF4alpha and the LXXLL motifs of PGC-1alpha lead to full activation. J. Biol. Chem. 284, 35165–35176. doi:10.1074/jbc.M109.052506

Robinson, A., Grosgen, S., Mett, J., Zimmer, V.C., Haupenthal, V.J., Hundsdorfer, B., C, P.S., Slobodskoy, Y., Muller, U.C., Hartmann, T., Stein, R., Grimm, M.O., 2013. Upregulation of PGC-1alpha expression by Alzheimer's disease-associated pathway: presenilin 1/amyloid precursor protein (APP)/intracellular domain of APP. Aging Cell. doi:10.1111/acel.12183

Robinson, B.H., Petrova-Benedict, R., Buncic, J.R., Wallace, D.C., 1992. Nonviability of cells with oxidative defects in galactose medium: a screening test for affected patient fibroblasts. Biochem. Med. Metab. Biol. 48, 122–126.

Rodgers, J.T., Lerin, C., Haas, W., Gygi, S.P., Spiegelman, B.M., Puigserver, P., 2005. Nutrient control of glucose homeostasis through a complex of PGC-1 alpha and SIRT1. Nature 434, 113–118. doi:10.1038/nature03354

Rogers, R.P., Rogina, B., 2014. Increased mitochondrial biogenesis preserves intestinal stem cell homeostasis and contributes to longevity in Indy mutant flies. Aging (Albany NY) 6, 335–350. doi:10.18632/aging.100658

Rojek, A., Cielecka-Prynda, M., Przewlocka-Kosmala, M., Laczmanski, L., Mysiak, A., Kosmala, W., 2014. Impact of the PPARGC1A Gly482Ser polymorphism on left ventricular structural and functional abnormalities in patients with hypertension. J Hum Hypertens 28, 557–563. doi:10.1038/jhh.2014.26

Ross, C.A., Tabrizi, S.J., 2011. Huntington's disease: from molecular pathogenesis to clinical treatment. Lancet Neurol. 10, 83–98. doi:10.1016/s1474-4422(10)70245-3

Rossignol, R., Gilkerson, R., Aggeler, R., Yamagata, K., Remington, S.J., Capaldi, R.A., 2004. Energy substrate modulates mitochondrial structure and oxidative capacity in cancer cells. Cancer Res. 64, 985–993.

Rothstein, J.D., 2009. Current Hypotheses for the Underlying Biology of
Amyotrophic Lateral Sclerosis. Ann. Neurol. 65, S3–S9. doi:10.1002/ana.21543

Rytinki, M.M., Palvimo, J.J., 2009. SUMOylation Attenuates the Function of PGC-1
alpha. J. Biol. Chem. 284, 26184–26193. doi:10.1074/jbc.M109.038943

Saccon, R.A., Bunton-Stasyshyn, R.K.A., Fisher, E.M.C., Fratta, P., 2013. Is SOD1
loss of function involved in amyotrophic lateral sclerosis? Brain 136, 2342–
2358. doi:10.1093/brain/awt097

Sajan, M., Hansen, B., Ivey, R., Sajan, J., Ari, C., Song, S., Braun, U., Leitges, M.,
Farese-Higgs, M., Farese, R.V., 2016. Brain Insulin Signaling Is Increased in
Insulin-Resistant States and Decreases in FOXOs and PGC-1α and Increases
in Aβ1-40/42 and Phospho-Tau May Abet Alzheimer Development. Diabetes 65,
1892–1903. doi:10.2337/db15-1428

Sakai, M., Matsumoto, M., Tujimura, T., Yongheng, C., Noguchi, T., Inagaki, K.,
Inoue, H., Hosooka, T., Takazawa, K., Kido, Y., Yasuda, K., Hiramatsu, R.,
Matsuki, Y., Kasuga, M., 2012. CITED2 links hormonal signaling to PGC-1α
acetylation in the regulation of gluconeogenesis. Nat. Med. 18, 612–617.
doi:10.1038/nm.2691

Sano, M., Tokudome, S., Shimizu, N., Yoshikawa, N., Ogawa, C., Shirakawa, K.,
Endo, J., Katayama, T., Yuasa, S., Ieda, M., Makino, S., Hattori, F., Tanaka, H.,
Fukuda, K., 2007. Intramolecular control of protein stability, subnuclear
compartmentalization, and coactivator function of peroxisome proliferator-
activated receptor gamma coactivator 1alpha. J. Biol. Chem. 282, 25970–
25980. doi:10.1074/jbc.M703634200

Santos, D., Cardoso, S.M., 2012. Mitochondrial dynamics and neuronal fate in
Parkinson's disease. Mitochondrion 12, 428–437.
doi:10.1016/j.mito.2012.05.002

Savkur, R.S., Burris, T.P., 2004. The coactivator LXXLL nuclear receptor recognition
motif. The journal of peptide research : official journal of the American Peptide

Society 63, 207–212. doi:10.1111/j.1399-3011.2004.00126.x

Sawada, N., Jiang, A., Takizawa, F., Safdar, A., Manika, A., Tesmenitsky, Y., Kang, K.-T., Bischoff, J., Kalwa, H., Sartoretto, J.L., Kamei, Y., Benjamin, L.E., Watada, H., Ogawa, Y., Higashikuni, Y., Kessinger, C.W., Jaffer, F.A., Michel, T., Sata, M., Croce, K., Tanaka, R., Arany, Z., 2014. Endothelial PGC-1α mediates vascular dysfunction in diabetes. Cell metabolism 19, 246–258. doi:10.1016/j.cmet.2013.12.014

Schapira, A.H., Cooper, J.M., Dexter, D., Clark, J.B., Jenner, P., Marsden, C.D., 1990. Mitochondrial complex I deficiency in Parkinson's disease. J. Neurochem. 54, 823–827.

Schapira, A.H.V., 2008. Mitochondria in the aetiology and pathogenesis of Parkinson's disease. Lancet Neurol. 7, 97–109. doi:10.1016/s1474-4422(07)70327-7

Sczelecki, S., Besse-Patin, A., Abboud, A., Kleiner, S., Laznik-Bogoslavski, D., Wrann, C.D., Ruas, J.L., Haibe-Kains, B., Estall, J.L., 2014. Loss of Pgc-1α expression in aging mouse muscle potentiates glucose intolerance and systemic inflammation. Am. J. Physiol. Endocrinol. Metab. 306, E157–67. doi:10.1152/ajpendo.00578.2013

Seytanoglu, A., Alsomali, N.I., Valori, C.F., McGown, A., Kim, H.R., Ning, K., Ramesh, T., Sharrack, B., Wood, J.D., Azzouz, M., 2016. Deficiency in the mRNA export mediator Gle1 impairs Schwann cell development in the zebrafish embryo. Neuroscience 322, 287–297. doi:10.1016/j.neuroscience.2016.02.039

Shan, P., Fan, G., Sun, L., Liu, J., Wang, W., Hu, C., Zhang, X., Zhai, Q., Song, X., Cao, L., Cui, Y., Zhang, S., Wang, C., 2017. SIRT1 Functions as a Negative Regulator of Eukaryotic Poly(A)RNA Transport. Current Biology 27, 2271–2284.e5. doi:10.1016/j.cub.2017.06.040

Shaw, G., Morse, S., Ararat, M., Graham, F.L., 2002. Preferential transformation of human neuronal cells by human adenoviruses and the origin of HEK 293 cells.

FASEB J. 16, 869–871. doi:10.1096/fj.01-0995fje

Shaw, P.J., 2005. Molecular and cellular pathways of neurodegeneration in motor neurone disease. J. Neurol. Neurosurg. Psychiatry 76, 1046–1057. doi:10.1136/jnnp.2004.048652

Sheng, Z.-H., 2014. Mitochondrial trafficking and anchoring in neurons: New insight and implications. J. Cell Biol. 204, 1087–1098. doi:10.1083/jcb.201312123

Shin, J.H., Ko, H.S., Kang, H., Lee, Y., Lee, Y.I., Pletinkova, O., Troconso, J.C., Dawson, V.L., Dawson, T.M., 2011. PARIS (ZNF746) repression of PGC-1alpha contributes to neurodegeneration in Parkinson's disease. Cell 144, 689–702. doi:10.1016/j.cell.2011.02.010

Shokouhi, S., Haghani, K., Borji, P., Bakhtiyari, S., 2015. Association between PGC-1alpha gene polymorphisms and type 2 diabetes risk: a case-control study of an Iranian population. Can J Diabetes 39, 65–72. doi:10.1016/j.jcjd.2014.05.003

Siddiqui, A., Bhaumik, D., Chinta, S.J., Rane, A., Rajagopalan, S., Lieu, C.A., Lithgow, G.J., Andersen, J.K., 2015. Mitochondrial Quality Control via the PGC1α-TFEB Signaling Pathway Is Compromised by Parkin Q311X Mutation But Independently Restored by Rapamycin. J. Neurosci. 35, 12833–12844. doi:10.1523/JNEUROSCI.0109-15.2015

Singh, G., Charlet-B, N., Han, J., Cooper, T.A., 2004. ETR-3 and CELF4 protein domains required for RNA binding and splicing activity in vivo. Nucleic Acids Res. 32, 1232–1241. doi:10.1093/nar/gkh275

Smith, C.A., Calabro, V., Frankel, A.D., 2000. An RNA-Binding Chameleon. Mol. Cell 6, 1067–1076. doi:10.1016/S1097-2765(00)00105-2

Smith, E.F., Shaw, P.J., De Vos, K.J., 2017. The Role of Mitochondria in Amyotrophic Lateral Sclerosis. Neurosci. Lett. doi:10.1016/j.neulet.2017.06.052

St-Pierre, J., Drori, S., Uldry, M., Silvaggi, J.M., Rhee, J., Jager, S., Handschin, C., Zheng, K., Lin, J., Yang, W., Simon, D.K., Bachoo, R., Spiegelman, B.M., 2006. Suppression of reactive oxygen species and neurodegeneration by the PGC-1

transcriptional coactivators. Cell 127, 397–408. doi:10.1016/j.cell.2006.09.024

Steele, J.W., Ju, S., Lachenmayer, M.L., Liken, J., Stock, A., Kim, S.H., Delgado, L.M., Alfaro, I.E., Bernales, S., Verdile, G., Bharadwaj, P., Gupta, V., Barr, R., Friss, A., Dolios, G., Wang, R., Ringe, D., Protter, A.A., Martins, R.N., Ehrlich, M.E., Yue, Z., Petsko, G.A., Gandy, S., 2013. Latrepirdine stimulates autophagy and reduces accumulation of α-synuclein in cells and in mouse brain. Mol. Psychiatry 18, 882–888. doi:10.1038/mp.2012.115

Strässer, K., Hurt, E., 2000. Yra1p, a conserved nuclear RNA-binding protein, interacts directly with Mex67p and is required for mRNA export. Embo J. 19, 410–420. doi:10.1093/emboj/19.3.410

Stroud, D.A., Maher, M.J., Lindau, C., Vögtle, F.N., Frazier, A.E., Surgenor, E., Mountford, H., Singh, A.P., Bonas, M., Oeljeklaus, S., Warscheid, B., Meisinger, C., Thorburn, D.R., Ryan, M.T., 2015. COA6 is a mitochondrial complex IV assembly factor critical for biogenesis of mtDNA-encoded COX2. Human molecular genetics 24, 5404–5415. doi:10.1093/hmg/ddv265

Stumvoll, M., Goldstein, B.J., van Haeften, T.W., 2005. Type 2 diabetes: principles of pathogenesis and therapy. Lancet 365, 1333–1346. doi:10.1016/s0140-6736(05)61032-x

Stutz, F., Bachi, A., Doerks, T., Braun, I.C., Séraphin, B., Wilm, M., Bork, P., Izaurralde, E., 2000. REF, an evolutionary conserved family of hnRNP-like proteins, interacts with TAP/Mex67p and participates in mRNA nuclear export. RNA 6, 638–650.

Su, X., Chu, Y., Kordower, J.H., Li, B., Cao, H., Huang, L., Nishida, M., Song, L., Wang, D., Federoff, H.J., 2015. PGC-1α Promoter Methylation in Parkinson's Disease. PloS one 10, e0134087. doi:10.1371/journal.pone.0134087

Sylvester, P.W., 2011. Optimization of the tetrazolium dye (MTT) colorimetric assay for cellular growth and viability. Methods Mol. Biol. 716, 157–168. doi:10.1007/978-1-61779-012-6_9

Szargel, R., Shani, V., Abd Elghani, F., Mekies, L.N., Liani, E., Rott, R., Engelender, S., 2016. The PINK1, synphilin-1 and SIAH-1 complex constitutes a novel mitophagy pathway. Human molecular genetics 25, 3476–3490. doi:10.1093/hmg/ddw189

Tacke, R., Manley, J.L., 1999. Determinants of SR protein specificity. Current Opinion in Cell Biology 11, 358–362. doi:10.1016/S0955-0674(99)80050-7

Taherzadeh-Fard, E., Saft, C., Andrich, J., Wieczorek, S., Arning, L., 2009. PGC-1alpha as modifier of onset age in Huntington disease. Molecular neurodegeneration 4, 10. doi:10.1186/1750-1326-4-10

Takacs, M., Petoukhov, M.V., Atkinson, R.A., Roblin, P., Ogi, F.-X., Demeler, B., Potier, N., Chebaro, Y., Dejaegere, A., Svergun, D.I., Moras, D., Billas, I.M.L., 2013. The asymmetric binding of PGC-1α to the ERRα and ERRγ nuclear receptor homodimers involves a similar recognition mechanism. PloS one 8, e67810. doi:10.1371/journal.pone.0067810

Takahashi, K., Yamanaka, S., 2006. Induction of pluripotent stem cells from mouse embryonic and adult fibroblast cultures by defined factors. Cell 126, 663–676. doi:10.1016/j.cell.2006.07.024

Tatsuta, T., Langer, T., 2008. Quality control of mitochondria: protection against neurodegeneration and ageing. Embo J. 27, 306–314. doi:10.1038/sj.emboj.7601972

Teyssier, C., Ma, H., Emter, R., Kralli, A., Stallcup, M.R., 2005. Activation of nuclear receptor coactivator PGC-1 alpha by arginine methylation. Genes Dev. 19, 1466–1473. doi:10.1101/gad.1295005

Thau, N., Knippenberg, S., Körner, S., Rath, K.J., Dengler, R., Petri, S., 2012. Decreased mRNA expression of PGC-1α and PGC-1α-regulated factors in the SOD1G93A ALS mouse model and in human sporadic ALS. J. Neuropathol. Exp. Neurol. 71, 1064–1074. doi:10.1097/NEN.0b013e318275df4b

Tintaru, A.M., Hautbergue, G.M., Hounslow, A.M., Hung, M.-L., Lian, L.-Y., Craven,

C.J., Wilson, S.A., 2007. Structural and functional analysis of RNA and TAP binding to SF2/ASF. EMBO reports 8, 756–762. doi:10.1038/sj.embor.7401031

Tiraby, C., Tavernier, G., Lefort, C., Larrouy, D., Bouillaud, F., Ricquier, D., Langin, D., 2003. Acquirement of brown fat cell features by human white adipocytes. J. Biol. Chem. 278, 33370–33376. doi:10.1074/jbc.M305235200

Trausch-Azar, J., Leone, T.C., Kelly, D.P., Schwartz, A.L., 2010. Ubiquitin proteasome-dependent degradation of the transcriptional coactivator PGC-1{alpha} via the N-terminal pathway. J. Biol. Chem. 285, 40192–40200. doi:10.1074/jbc.M110.131615

Trifunovic, A., Wredenberg, A., Falkenberg, M., Spelbrink, J.N., Rovio, A.T., Bruder, C.E., Bohlooly-Y, M., Gidlöf, S., Oldfors, A., Wibom, R., Törnell, J., Jacobs, H.T., Larsson, N.-G., 2004. Premature ageing in mice expressing defective mitochondrial DNA polymerase. Nature 429, 417–423. doi:10.1038/nature02517

Tsumoto, K., Ejima, D., Kumagai, I., Arakawa, T., 2003. Practical considerations in refolding proteins from inclusion bodies. Protein Expr. Purif. 28, 1–8.

Tsunemi, T., Ashe, T.D., Morrison, B.E., Soriano, K.R., Au, J., Roque, R.A.V., Lazarowski, E.R., Damian, V.A., Masliah, E., La Spada, A.R., 2012. PGC-1 Rescues Huntington's Disease Proteotoxicity by Preventing Oxidative Stress and Promoting TFEB Function. Science translational medicine 4, 142ra97–142ra97. doi:10.1126/scitranslmed.3003799

Valla, J., Schneider, L., Niedzielko, T., Coon, K.D., Caselli, R., Sabbagh, M.N., Ahern, G.L., Baxter, L., Alexander, G., Walker, D.G., Reiman, E.M., 2006. Impaired platelet mitochondrial activity in Alzheimer's disease and mild cognitive impairment. Mitochondrion 6, 323–330. doi:10.1016/j.mito.2006.10.004

Van Damme, P., Robberecht, W., Van Den Bosch, L., 2017. Modelling amyotrophic lateral sclerosis: progress and possibilities. Dis Model Mech 10, 537–549. doi:10.1242/dmm.029058

Varadi, M., Zsolyomi, F., Guharoy, M., Tompa, P., 2015. Functional Advantages of

Conserved Intrinsic Disorder in RNA-Binding Proteins. PloS one 10, e0139731. doi:10.1371/journal.pone.0139731

Venkateshappa, C., Harish, G., Mahadevan, A., Srinivas Bharath, M.M., Shankar, S.K., 2012. Elevated oxidative stress and decreased antioxidant function in the human hippocampus and frontal cortex with increasing age: implications for neurodegeneration in Alzheimer's disease. Neurochem. Res. 37, 1601–1614. doi:10.1007/s11064-012-0755-8

Verwer, R.W., Jansen, K.A., Sluiter, A.A., Pool, C.W., Kamphorst, W., Swaab, D.F., 2000. Decreased hippocampal metabolic activity in Alzheimer patients is not reflected in the immunoreactivity of cytochrome oxidase subunits. Exp. Neurol. 163, 440–451. doi:10.1006/exnr.2000.7385

Viphakone, N., Cumberbatch, M.G., Livingstone, M.J., Heath, P.R., Dickman, M.J., Catto, J.W., Wilson, S.A., 2015. Luzp4 defines a new mRNA export pathway in cancer cells. Nucleic Acids Res. 43, 2353–2366. doi:10.1093/nar/gkv070

Viphakone, N., Hautbergue, G.M., Walsh, M., Chang, C.-T., Holland, A., Folco, E.G., Reed, R., Wilson, S.A., 2012. TREX exposes the RNA-binding domain of Nxf1 to enable mRNA export. Nature communications 3, 1006. doi:10.1038/ncomms2005

Volpicelli-Daley, L.A., Abdelmotilib, H., Liu, Z., Stoyka, L., Daher, J.P.L., Milnerwood, A.J., Unni, V.K., Hirst, W.D., Yue, Z., Zhao, H.T., Fraser, K., Kennedy, R.E., West, A.B., 2016. G2019S-LRRK2 Expression Augments α-Synuclein Sequestration into Inclusions in Neurons. J. Neurosci. 36, 7415–7427. doi:10.1523/JNEUROSCI.3642-15.2016

Walsh, M.J., Cooper-Knock, J., Dodd, J.E., Stopford, M.J., Mihaylov, S.R., Kirby, J., Shaw, P.J., Hautbergue, G.M., 2015. Invited review: decoding the pathophysiological mechanisms that underlie RNA dysregulation in neurodegenerative disorders: a review of the current state of the art. Neuropathol. Appl. Neurobiol. 41, 109–134. doi:10.1111/nan.12187

Walsh, M.J., Hautbergue, G.M., Wilson, S.A., 2010. Structure and function of mRNA export adaptors. Biochemical Society transactions 38, 232–236. doi:10.1042/BST0380232

Wang, T., Wu, H., Li, Y., Szulwach, K.E., Lin, L., Li, X., Chen, I.-P., Goldlust, I.S., Chamberlain, S.J., Dodd, A., Gong, H., Ananiev, G., Han, J.W., Yoon, Y.-S., Rudd, M.K., Yu, M., Song, C.-X., He, C., Chang, Q., Warren, S.T., Jin, P., 2013. Subtelomeric hotspots of aberrant 5-hydroxymethylcytosine-mediated epigenetic modifications during reprogramming to pluripotency. Nat. Cell Biol. 15, 700–711. doi:10.1038/ncb2748

Wang, W., Li, L., Lin, W.-L., Dickson, D.W., Petrucelli, L., Zhang, T., Wang, X., 2013. The ALS disease-associated mutant TDP-43 impairs mitochondrial dynamics and function in motor neurons. Human molecular genetics 22, 4706–4719. doi:10.1093/hmg/ddt319

Wang, W., Wang, L., Lu, J., Siedlak, S.L., Fujioka, H., Liang, J., Jiang, S., Ma, X., Jiang, Z., da Rocha, E.L., Sheng, M., Choi, H., Lerou, P.H., Li, H., Wang, X., 2016. The inhibition of TDP-43 mitochondrial localization blocks its neuronal toxicity. Nat. Med. 22, 869–878. doi:10.1038/nm.4130

Wang, X., Su, B., Siedlak, S.L., Moreira, P.I., Fujioka, H., Wang, Y., Casadesus, G., Zhu, X., 2008. Amyloid-beta overproduction causes abnormal mitochondrial dynamics via differential modulation of mitochondrial fission/fusion proteins. Proc. Natl. Acad. Sci. U.S.A. 105, 19318–19323. doi:10.1073/pnas.0804871105

Webster, C.P., Smith, E.F., Bauer, C.S., Moller, A., Hautbergue, G.M., Ferraiuolo, L., Myszczynska, M.A., Higginbottom, A., Walsh, M.J., Whitworth, A.J., Kaspar, B.K., Meyer, K., Shaw, P.J., Grierson, A.J., De Vos, K.J., 2016. The C9orf72 protein interacts with Rab1a and the ULK1 complex to regulate initiation of autophagy. Embo J. 35, 1656–1676. doi:10.15252/embj.201694401

Wernig, M., Meissner, A., Cassady, J.P., Jaenisch, R., 2008. c-Myc Is Dispensable for Direct Reprogramming of Mouse Fibroblasts. Cell Stem Cell 2, 10–12.

doi:10.1016/j.stem.2007.12.001

Wernig, M., Meissner, A., Foreman, R., Brambrink, T., Ku, M., Hochedlinger, K.,
Bernstein, B.E., Jaenisch, R., 2007. In vitro reprogramming of fibroblasts into a
pluripotent ES-cell-like state. Nature 448, 318–324. doi:10.1038/nature05944

Weydt, P., Soyal, S.M., Gellera, C., Didonato, S., Weidinger, C., Oberkofler, H.,
Landwehrmeyer, G.B., Patsch, W., 2009. The gene coding for PGC-1alpha
modifies age at onset in Huntington's Disease. Molecular neurodegeneration 4,
3. doi:10.1186/1750-1326-4-3

Weydt, P., Soyal, S.M., Landwehrmeyer, G.B., Patsch, W., European Huntington
Disease Network, 2014. A single nucleotide polymorphism in the coding region
of PGC-1α is a male-specific modifier of Huntington disease age-at-onset in a
large European cohort. BMC Neurol 14, 1. doi:10.1186/1471-2377-14-1

Williams, B.J.L., Boyne, J.R., Goodwin, D.J., Roaden, L., Hautbergue, G.M., Wilson,
S.A., Whitehouse, A., 2005. The prototype gamma-2 herpesvirus
nucleocytoplasmic shuttling protein, ORF 57, transports viral RNA through the
cellular mRNA export pathway. Biochem. J. 387, 295–308.
doi:10.1042/BJ20041223

Wisnovsky, S., Jean, S.R., Kelley, S.O., 2016. Mitochondrial DNA repair and
replication proteins revealed by targeted chemical probes. Nat. Chem. Biol. 12,
567–573. doi:10.1038/nchembio.2102

Wrann, C.D., White, J.P., Salogiannnis, J., Laznik-Bogoslavski, D., Wu, J., Ma, D.,
Lin, J.D., Greenberg, M.E., Spiegelman, B.M., 2013. Exercise Induces
Hippocampal BDNF through a PGC-1 alpha/FNDC5 Pathway. Cell metabolism
18, 649–659.

Wu, Z., Puigserver, P., Andersson, U., Zhang, C., Adelmant, G., Mootha, V., Troy,
A., Cinti, S., Lowell, B., Scarpulla, R., 1999. Mechanisms Controlling
Mitochondrial Biogenesis and Respiration through the Thermogenic Coactivator
PGC-1. Cell 98, 115–124. doi:10.1016/s0092-8674(00)80611-x

Xiong, S., Patrushev, N., Forouzandeh, F., Hilenski, L., Alexander, R.W., 2015. PGC-1α Modulates Telomere Function and DNA Damage in Protecting against Aging-Related Chronic Diseases. Cell Rep 12, 1391–1399. doi:10.1016/j.celrep.2015.07.047

Yamaguchi, H., Miyazaki, M., 2014. Refolding techniques for recovering biologically active recombinant proteins from inclusion bodies. Biomolecules 4, 235–251. doi:10.3390/biom4010235

Yang, Y., Mahaffey, C.L., Bérubé, N., Maddatu, T.P., Cox, G.A., Frankel, W.N., 2007. Complex seizure disorder caused by Brunol4 deficiency in mice. PLoS Genet. 3, e124. doi:10.1371/journal.pgen.0030124

Yang, Y., Mo, X., Chen, S., Lu, X., Gu, D., 2011. Association of peroxisome proliferator-activated receptor gamma coactivator 1 alpha (PPARGC1A) gene polymorphisms and type 2 diabetes mellitus: a meta-analysis. Diabetes/metabolism research and reviews 27, 177–184. doi:10.1002/dmrr.1158

Yoon, J.C., Puigserver, P., Chen, G.X., Donovan, J., Wu, Z.D., Rhee, J., Adelmant, G., Stafford, J., Kahn, C.R., Granner, D.K., Newgard, C.B., Spiegelman, B.M., 2001. Control of hepatic gluconeogenesis through the transcriptional coactivator PGC-1. Nature 413, 131–138. doi:10.1038/35093050

Yoshihara, M., Hayashizaki, Y., Murakawa, Y., 2017. Genomic Instability of iPSCs: Challenges Towards Their Clinical Applications. Stem Cell Rev 13, 7–16. doi:10.1007/s12015-016-9680-6

Yuan, Y., Cruzat, V.F., Newsholme, P., Cheng, J., Chen, Y., Lu, Y., 2016. Regulation of SIRT1 in aging: Roles in mitochondrial function and biogenesis. Mech. Ageing Dev. 155, 10–21. doi:10.1016/j.mad.2016.02.003

Zarei, S., Carr, K., Reiley, L., Diaz, K., Guerra, O., Altamirano, P.F., Pagani, W., Lodin, D., Orozco, G., Chinea, A., 2015. A comprehensive review of amyotrophic lateral sclerosis. Surg Neurol Int 6, 171. doi:10.4103/2152-

7806.169561

Zhang, X.-M., Yin, M., Zhang, M.-H., 2014. Cell-based assays for Parkinson's disease using differentiated human LUHMES cells. Acta Pharmacol. Sin. 35, 945–956. doi:10.1038/aps.2014.36

Zhao, W., Varghese, M., Yemul, S., Pan, Y., Cheng, A., Marano, P., Hassan, S., Vempati, P., Chen, F., Qian, X., Pasinetti, G.M., 2011. Peroxisome proliferator activator receptor gamma coactivator-1alpha (PGC-1alpha) improves motor performance and survival in a mouse model of amyotrophic lateral sclerosis. Molecular neurodegeneration 6, 51. doi:10.1186/1750-1326-6-51

Zheng, B., Liao, Z., Locascio, J.J., Lesniak, K.A., Roderick, S.S., Watt, M.L., Eklund, A.C., Zhang-James, Y., Kim, P.D., Hauser, M.A., Gruenblatt, E., Moran, L.B., Mandel, S.A., Riederer, P., Miller, R.M., Federoff, H.J., Wuellner, U., Papapetropoulos, S., Youdim, M.B., Cantuti-Castelvetri, I., Young, A.B., Vance, J.M., Davis, R.L., Hedreen, J.C., Adler, C.H., Beach, T.G., Graeber, M.B., Middleton, F.A., Rochet, J.-C., Scherzer, C.R., Global, P.D.G.E.G., 2010a. PGC-1 alpha, A Potential Therapeutic Target for Early Intervention in Parkinson's Disease. Science translational medicine 2. doi:10.1126/scitranslmed.3001059

Zheng, B., Liao, Z., Locascio, J.J., Lesniak, K.A., Roderick, S.S., Watt, M.L., Eklund, A.C., Zhang-James, Y., Kim, P.D., Hauser, M.A., Grunblatt, E., Moran, L.B., Mandel, S.A., Riederer, P., Miller, R.M., Federoff, H.J., Wullner, U., Papapetropoulos, S., Youdim, M.B., Cantuti-Castelvetri, I., Young, A.B., Vance, J.M., Davis, R.L., Hedreen, J.C., Adler, C.H., Beach, T.G., Graeber, M.B., Middleton, F.A., Rochet, J.C., Scherzer, C.R., Global, P.D.G.E.C., 2010b. PGC-1alpha, a potential therapeutic target for early intervention in Parkinson's disease. Science translational medicine 2, 52ra73. doi:10.1126/scitranslmed.3001059

Zhou, Z., Luo, M.J., Straesser, K., Katahira, J., Hurt, E., Reed, R., 2000. The protein

Aly links pre-messenger-RNA splicing to nuclear export in metazoans. Nature 407, 401–405. doi:10.1038/35030160

Zhu, G., Zhang, Y., Xu, H., Jiang, C., 1998. Identification of endogenous outward currents in the human embryonic kidney (HEK 293) cell line. J. Neurosci. Methods 81, 73–83.

Zuccato, C., Tartari, M., Crotti, A., Goffredo, D., Valenza, M., Conti, L., Cataudella, T., Leavitt, B.R., Hayden, M.R., Timmusk, T., Rigamonti, D., Cattaneo, E., 2003. Huntingtin interacts with REST/NRSF to modulate the transcription of NRSE-controlled neuronal genes. Nature Genet. 35, 76–83. doi:10.1038/ng1219

8. Appendix 1

Standard curves for qRT-PCR primers used in this doctoral work have been produced using total RNA from HEK293T cells.

For each primer, efficiency (in percentage) and R^2 were assessed.

Table 8.1 qRT-PCR primers optimisation details.

Gene ID	Efficiency (%)	R^2
U1 snRNA	104	0.999
PGC-1[alpha] 3'UTR	181.4	0.927
mtTFAM	111.4	0.975
NRF-1	95.3	0.991
COX2	111	0.998